BioMed Research International

# Biomass and Wastes for Bioenergy: Thermochemical Conversion and Biotechnologies

Lead Guest Editor: Ningbo Gao
Guest Editors: Zhang Lei and Chun-Fei Wu

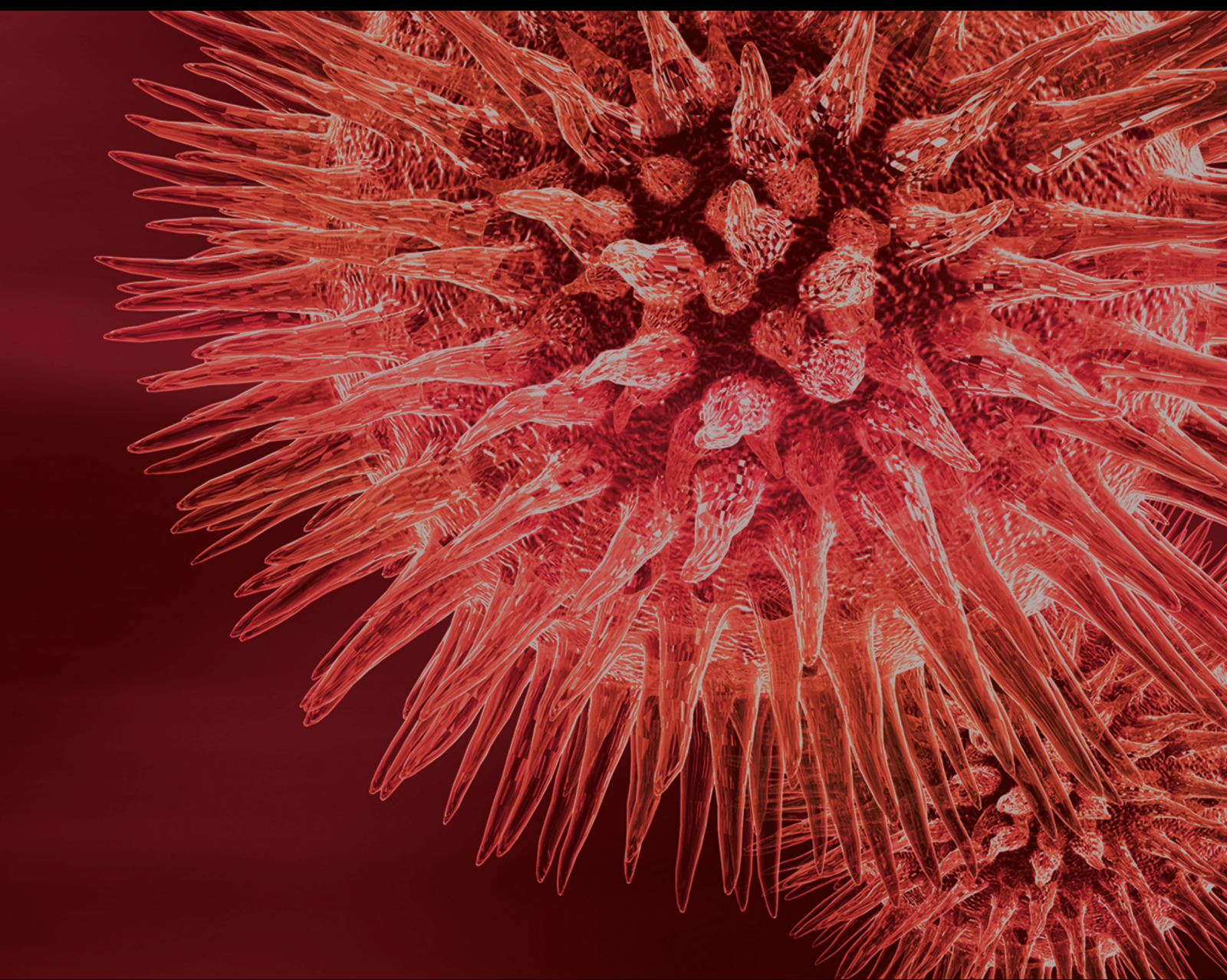

# Biomass and Wastes for Bioenergy: Thermochemical Conversion and Biotechnologies

BioMed Research International

# Biomass and Wastes for Bioenergy: Thermochemical Conversion and Biotechnologies

Lead Guest Editor: Ningbo Gao
Guest Editors: Zhang Lei and Chun-Fei Wu

# Contents

Hindawi
BioMed Research International
Volume 2018, Article ID 9638380, 2 pages
https://doi.org/10.1155/2018/9638380

*Editorial*

# Biomass and Wastes for Bioenergy: Thermochemical Conversion and Biotechnologies

**Ningbo Gao**,[1] **Lei Zhang**,[2] **and Chunfei Wu**[3]

[1]*School of Energy and Power Engineering, Xi'an Jiaotong University, Xi'an 710049, China*
[2]*School of Environmental Science & Technology, Dalian University of Technology, Dalian 116024, China*
[3]*School of Chemistry and Chemical Engineering, Queen's University Belfast, Belfast BT7 1NN, UK*

Correspondence should be addressed to Ningbo Gao; nbogao@xjtu.edu.cn

Received 17 October 2018; Accepted 17 October 2018; Published 1 November 2018



In response to the global environmental pollution and energy resource issues, biomass and wastes have obtained a widespread attention to be used for fuel and energy production. Now it is evident that wastes that could cause risks to the environment could be converted into useful energy via some realistic technologies. Using biomass and wastes as an energy resource not only solves environmental pollution problems, but also reduces the dependency on fossil fuels. Thermochemical and biological conversion of biomass and wastes are the two most important bioenergy conversion methods.

In order to pursue the latest developments of bioenergy and keep the global academic communities up to date to the current advances in the Biomass and Wastes for Bioenergy, the applications of biomass in thermochemical conversion and biotechnologies have been discussed in 8 high-quality papers published in this special issue. The brief introduction for these works is listed as follows.

The paper titled "Energy Analysis of a Complementary Heating System Combining Solar Energy and Coal for a Rural Residential Building in Northwest China" by X. Zhen et al. designed a work on energy efficiency of the system and the determination of thermal efficiency of a coal stove by using a prototype model. In this study, multiple linear regression was adopted to present the dual function of multiple factors on the daily heat-collecting capacity of the solar water heater. Their results showed that the orientation and the shade of solar water heaters had profound influences on heat-collection capacity compared to the reference solar water heater. Additionally, the allocation of the radiation of solar energy projecting into the collecting area of the solar water heater was only effectively utilized by 28%. Moreover, the results also showed that the main factors that led to the high heat loss were the mismatch between the working temperature of the radiator, collecting temperature of the solar water heater and the location of storage tanks.

The paper titled "Experimental Study on Productivity Performance of Household Combined Thermal Power and Biogas System in Northwest China" by J. Kang et al. developed a method to create a heat, electricity, and biogas cogeneration system with low-temperature solar thermal collectors, photovoltaic solar power generators, and solar-powered thermostatic biogas digesters. The method was experimentally studied via two buildings in a farming village in northwestern China. Even though the ambient temperature reached down to −25°C, the temperature of the biogas digester was maintained at 27°C±2 for thermostatic fermentation. After optimization, the energy-saving rate was improved from 66.2% to 85.5%. This installation reduced $CO_2$ emissions by approximately 27.03 t, and the static payback period was 3.1 yr. The results indicated that the system was highly economical, energy efficient, and beneficial for the environment.

The paper titled "Neural Network Prediction of Corn Stover Saccharification Based on Its Structural Features" by L. Gao et al. developed a neural networks model, which was demonstrated for the prediction of the corn stover saccharification based on the features without enzymatic hydrolysis. By using this method, the predicted value of corn stover digestibility was very similar to the actual determined value of corn stover digestibility. A fast approach for bioenergy crops

selection could be offered by the neural network model. Thus, the neural network model is cost-effective and time-saving and it will have a good application for corn stover storage and evaluation.

The paper titled "Ni-Ru/$CeO_2$ Catalytic Hydrothermal Upgrading of Water-insoluble Biocrude from Algae Hydrothermal Liquefaction" by D. Xu et al. used hydrothermal liquefaction to convert wet algae into water-insoluble biocrude and other coproducts. By using Ni-Ru/$CeO_2$+$H_2$, the yield, HHV (higher heating value) and the best elemental compositions for quality of water-insoluble biocrude ($B_2$) were increased. The result indicated that the Ni-Ru/$CeO_2$ +$H_2$ technology was able to transform high-molecular-weight compounds into low-molecular-weight compounds and led $B_2$ to contain a series of abundant aliphatic saturated hydrocarbons such as pentadecane, tridecane, tetradecane, heptadecane, and dodecane. The results also showed that Ni-Ru/$CeO_2$+$H_2$ led to the largest fraction and the best light of light biocrude in $B_2$.

The paper titled "Second-Generation Bioethanol from Coconut Husk" by M. Bolivar-Telleria et al. discussed the methods that have been used to produce bioethanol from coconut husk and suggested ways to improve different aspects of the process. It was observed that the use of enzymes to perform hydrolysis was a good alternative. In this review, it has been confirmed that alkaline pretreatment is the best choice for delignification potential. Biorefining of this material for the production of ethanol and other molecules with greater added value would enable economically developing countries to create new jobs and boost income.

The paper titled "The Effect of Digested Manure on Biogas Productivity and Microstructure Evolution of Corn Stalks in Anaerobic Cofermentation" written by Z. Lv et al. explored the effect of mixing corn stalk with cow dung at five different fermentation stages on the further cofermentation process. The straw microstructure evolution was investigated by the SEM and XRD methods to identify the optimal conditions for the straw biodegradation process enhancement. The authors proved that the mesophilic codigestion of corn stalk with cow dung improved the biogas production, enhanced the degradation efficiency of organic matter, and reduced the anaerobic fermentation cycle. The results of this study were quite instrumental to the further optimization of the corn stalk anaerobic digestion by inoculation with digested manure for lignocellulose degradation enhancement and biogas productivity improvement.

The paper titled "The Effects of Different Oxytetracycline and Copper Treatments on the Performance of Anaerobic Digesters and the Dynamics of Bacterial Communities" by Y. Zhang et al. evaluated the performance of anaerobic digesters and discussed the dynamics of bacterial communities under the different treatments of oxytetracycline and copper during the anaerobic digestion of cow manure. Methane production and pH value were measured and analyzed to reflect the performance of anaerobic digestion. PCR-DGGE method was used to discuss the dynamics of bacterial communities. It was found that the bacterial communities had significant differences under the different treatments of oxytetracycline and copper.

The paper titled "The Migration and Transformation of Heavy Metals in Sewage Sludge during Hydrothermal Carbonization Combined with Combustion" by M. Liu et al. investigated the migration and transformation behaviors of heavy metals (Cr, Mn, Ni, Cu, Zn, As, Cd, and Pb) during the hydrothermal carbonization of sewage sludge. In this work, the authors considered the effects of HTC reaction temperatures and residence times on the distribution and chemical speciation transformation behaviors of HMs in the HTC of sewage sludge. The results indicated that most of the HMs accumulated in the Solid residue (SR) during HTC and combustion process. The authors also concluded that the HTC process promoted the immobilization of HMs in the combustion process.

## Conflicts of Interest

We declare that there are no conflicts of interest or private agreements with companies regarding our work for this special issue. We have no financial relationships through employment, consultancies, either stock ownership, or honoraria, with industry.

*Ningbo Gao*
*Lei Zhang*
*Chunfei Wu*

Hindawi
BioMed Research International
Volume 2018, Article ID 4916497, 20 pages
https://doi.org/10.1155/2018/4916497

*Review Article*

# Second-Generation Bioethanol from Coconut Husk

**Maria Bolivar-Telleria**,[1] **Cárita Turbay**,[1] **Luiza Favarato**,[1] **Tarcio Carneiro**,[1] **Ronaldo S. de Biasi**,[2] **A. Alberto R. Fernandes**,[1] **Alexandre M. C. Santos**,[1] **and Patricia M. B. Fernandes**[1]

[1]*Biotechnology Core, Federal University of Espírito Santo, Vitória, ES, Brazil*
[2]*Military Institute of Engineering, Rio de Janeiro, RJ, Brazil*

Correspondence should be addressed to Patricia M. B. Fernandes; patricia.fernandes@ufes.br

Received 2 March 2018; Revised 12 August 2018; Accepted 3 September 2018; Published 27 September 2018

Guest Editor: Zhang Lei



Coconut palm (*Cocos nucifera*) is an important commercial crop in many tropical countries, but its industry generates large amounts of residue. One way to address this problem is to use this residue, coconut husk, to produce second-generation (2G) ethanol. The aim of this review is to describe the methods that have been used to produce bioethanol from coconut husk and to suggest ways to improve different steps of the process. The analysis performed in this review determined that alkaline pretreatment is the best choice for its delignification potential. It was also observed that although most reported studies use enzymes to perform hydrolysis, acid hydrolysis is a good alternative. Finally, ethanol production using different microorganisms and fermentation strategies is discussed and the possibility of obtaining other added-value products from coconut husk components by using a biorefinery scheme is addressed.

## 1. Introduction

Modern life demands high mobility and, as a result, transport is one of the largest and fastest growing energy demanding sectors [1]. Also, increase in competitive agribusiness automatization leads to a high energy demand [2]. However, due to concern on the negative impact of fossil fuels on the environment, the use of biofuels emerges as a promising alternative that is gradually becoming technically and economically feasible [3].

Modern ethanol industry began in the 1970s when petroleum-based fuel became expensive and environmental concerns arose. In 1975, the Brazilian government launched a pioneer program known as "Proálcool" (Pro-Alcohol) with two main objectives: to reduce the impact caused by oil price increases and, at the same time, mitigate the fall of sugar price in the international market [4, 5]. Between 1980 and 2002, over five billion dollars were invested on sugarcane agriculture and industry to expand alcohol fuel production [5]. "Proálcool" is known worldwide for its positive effect on biofuel promotion [6]. Nowadays, in Brazil, 20 to 25% of anhydrous ethanol is used as an additive in gasoline. Moreover, since 2003, flex-fuel vehicles, which can use alcohol, gasoline or gasoline+alcohol, are on the market [5].

Ethanol is the leading liquid biofuel used for transportation. First-generation ethanol has a simple production process using sugar or grain as raw material (sugarcane juice in Brazil and corn in the USA and EU, for example), while 2G ethanol (bioethanol) has more complex steps of production and uses lignocellulosic material as a substrate [7]. Among the major byproducts generated by agroindustries, lignocellulosic biomass is one of the most abundant, conflict-free with food production and is available throughout the year at low prices [8, 9]. All of these characteristics show that lignocellulose waste might be considered the most feasible option for fossil fuel replacement, having a significant potential for bioethanol productivity while giving a destination for an environmental liability.

In Brazil, GranBio and Raízen are pioneering companies that utilize sugarcane coproducts as a substrate, enhancing ethanol production without increasing the cultivated area [10, 11]. In 2003, Raízen was able to produce more than 40 million liters per year [11]. In the USA, three companies produce cellulosic ethanol in commercial scale: POET-DSM

Advanced Biofuels, DuPont, and ABENGOA [12]. There are many projects around the world focusing on the use of lignocellulosic residues for biofuel production [13]. These residues can come from homes or city dumps: companies in Canada are investing in the construction and operation of a renewable fuel plant using local residential kitchen and yard waste; Phuket's Provincial Administration Organization, in Thailand, is building a waste-to-biofuel facility that will use the municipal solid waste of the entire island as feedstock [14]. China's State Development & Investment Corporation began the construction of its first ethanol plant in the Liaoning province with 300,000 tons capacity and is planning to build five ethanol plants in other provinces [15]. Nowadays, biofuels have an important part in the global liquid fuel market and over a hundred companies in different countries base their production on various types of 2G biofuels [13]. Coconut husk is a very promising substrate that can be used as raw material for 2G ethanol production, since coconut palm plays an important role in the economy of several tropical countries [16]. The food industry uses coconuts to obtain various products leaving the husk as waste. It is important to note that coconut husk has a high lignin content that during husk decomposition penetrates the soil and can reach the water table imposing a great environmental risk. Since it is discarded in high volumes (coconut husk encompasses 80 to 85% of the weight of the fruit [17, 18], while sugarcane bagasse corresponds only to 27 to 28% dry weight), it is mandatory to find a safe destination for this waste. Therefore, the use of coconut husk for 2G ethanol production may be a solution to reduce the environmental impact. Moreover, if the technology is cheap and simple enough it can be used by small producers.

The three main components of a biomass (cellulose, hemicellulose, and lignin) form a recalcitrant structure, making it difficult for enzymes to have complete access to cellulose for conversion to monosaccharides. To make this feasible, the first major step in bioethanol production is biomass pretreatment (biological, physical or chemical), in which the lignin content is reduced to release the fermentable sugars from the rigid structure and, therefore, prepare the biomass for enzymatic conversion [19]. Different types of biomasses have different amounts and types of sugars (hemicellulose and cellulose) and lignin, so knowing its composition is crucial for the process. Moreover, the abundance of the residue must be taken into account so that the whole process is economically feasible.

The second major step in 2G ethanol production is the hydrolysis that unlocks and saccharifies the polysaccharides that are present in the biomass to fermentable sugars [20]. Generally, enzyme cocktails are used to catalyze reactions to obtain simple sugars such as glucose and mannose for further fermentation by microorganisms. This process, also called saccharification, is very important and the requirements of these enzyme complexes, which act synergistically, add major costs to the overall process. The main challenge is to obtain a cost-effective technology of enzymatic hydrolysis for economically viable biofuels [20].

The fermentation process is the next step, in which a microorganism such as the yeast *Saccharomyces cerevisiae* ferments the sugars that are present in the treated biomass and produces ethanol [21]. To increase the economic feasibility of this process, industries show great interest in using yeast strains that are more tolerant and resistant to various kinds of stresses and that are also able to use pentoses that come from hemicellulose degradation, such as xylose, as most strains naturally only consume hexoses.

Currently, the process for 2G bioethanol production in large scale is being improved, since it still has cost production issues that derive from the procedures needed to overcome the recalcitrance of the lignocellulose (pretreatment and enzymatic hydrolysis) in order to obtain fermentable sugars [22]. To transform the bioethanol production into a sustainable and economically viable process, it is important to integrate it in a biorefinery, which is a great supporter of a biobased economy. In a biorefinery, almost all types of biomass residues can be converted to different classes of biofuels, biomaterials and other marketable bioproducts through jointly applied conversion technologies [23].

Although many articles address the use of coconut husk as a raw material for bioethanol production, few of them compare the results obtained using different methods. This work intends to give an overview on different approaches already tested to obtain ethanol from coconut husk to facilitate the development of a process that can effectively produce ethanol from coconut residue.

## 2. The Coconut Plant and Industry

Coconut palm tree is a perennial crop grown in tropical climate countries which present ideal conditions for its cultivation, such as soil with proper water capacity and drainage and warm ambient temperatures [24, 25]. Due to the coconut structure, many valuable products can be obtained from it, such as meat (copra), oil, water, milk, and fibers [25]; therefore, this fruit is of great economic importance. There are two major varieties, the tall (Typica), mainly used to obtain coconut meat and milk, and the dwarf (Nana), the most cultivated in Brazil, used for coconut water extraction [24, 25].

Coconut harvesting time is determined by its purpose and is usually carried out in two stages of ripening. The green fruits are destined to the coconut water market, while mature fruits are destined to the dry coconut market (for meat, milk and oil) [26]. Therefore, depending on the plantation site, the residue is made of green or mature coconut husks, which have different compositions (Table 1).

The coconut fruit has a smooth green epidermis (epicarp), a medium region with bundles of fibers (mesocarp), and a stony layer that surrounds its edible part (endocarp) (Figure 1).

The estimated annual worldwide coconut production in 2015 was around 55 million tons and the main producing countries are Brazil, India, Indonesia, the Philippines, and Sri Lanka [16, 17]. Indonesia is responsible for 33.1% of the total world production [24], and the coconut industry plays a significant economic role in this country as well as in other tropical countries. However, as mentioned before, 80

Table 1: Chemical composition of green and mature coconut husk (%).

| Substrate | Reference | Cellulose | Hemicellulose | Lignin |
|---|---|---|---|---|
| Green coconut husk | [27] | 39.31 | 16.15 | 29.79 |
| | [28] | 43.40 | 19.90 | 45.80 |
| | [29] | 32.80 | 15.90 | n.a. |
| | [30] | 33.23 | 29.14 | 25.44 |
| Mature coconut husk | [31] | 30.47 | 25.42 | 33.15 |
| | [32] | 29.58 | 27.77 | 31.04 |
| | [33] | 32.18 | 27.81 | 25.02 |
| | [30] | 29.58 | 27.77 | 31.04 |

n.a.: not available or present.


(a) (b)

Figure 1: Green coconut and its structures. (a) Green coconut. (b) Green coconut without epicarp and liquid albumen. i, epicarp; ii, mesocarp; iii, endocarp; iv, solid albumen.

to 85% of the weight of the fruit is not used and is simply discarded, resulting in large amount of waste [17, 18]. Also, the coconut husk is rich in phenolic compounds, which are toxic to humans and animals and are released in the environment as a result of natural deterioration [39]. Actually, only a small percentage of the total fiber residue is designated for the production of fertilizers and handmade products like mats, nets, and brooms [17, 40], and, unfortunately, the traditional process to obtain the coir fiber is highly polluting as it is performed in surface waters and, again, liberates polyphenols [17, 40]. Due to high residue volumes and the husk slow decomposition, the coconut industry turns into an environmental and handling problem [41]. A possible and sustainable solution for the coconut husk residue is the production of 2G bioethanol.

Currently, around 20 published scientific papers describe the study of coconut husk as raw material for bioethanol. This means that it is an interesting opportunity to contribute to this field of study, allowing, hopefully in a near future, that small and local producers to produce biofuels for their personal use and for the development of a sustainable coconut chain production. As mentioned earlier, coconut producing countries are part of the third-world economy; in this way, turning trash into jobs and income generation is a very important matter.

## 3. Methods Used in Coconut Conversion to Ethanol

*3.1. Coconut Husk Pretreatment for Bioethanol Production.* The three main components of lignocellulosic biomass, cellulose, hemicellulose, and lignin, form a strong matrix, which gives it recalcitrance, meaning low enzyme digestibility [42]. Biomass used for bioethanol production has to undergo a pretreatment to remove lignin and hemicellulose and overcome recalcitrance by increasing porosity and reducing cellulose crystallinity making it available for biological or chemical hydrolysis. An effective pretreatment must return high sugar concentration but always avoiding their loss and degradation; also it has to minimize formation of inhibitors

and be able to undergo fermentation without detoxification, to reduce process steps, water, and energy consumption in order to decrease costs [43–45]. The pretreatment is a very important step as it has an impact on the next stages, such as hydrolysis, fermentation, and downstream processing [43]. Since biomass composition varies from one substrate to another, different pretreatments have to be tested to find the best for each specific substrate.

The first step in the pretreatment is the substrate preparation to make the enzymatic hydrolysis more effective by mechanically reducing cellulose crystallinity [45]. In the case of coconut husk, it is dried, ground, and sieved to obtain a powder [31].

The most used pretreatment for coconut husk is alkaline, followed by acid, but there are also other methods being tested that will be discussed in this section (Table 2).

Depending on biomass composition and the type and conditions of the pretreatment, products that inhibit enzymatic hydrolysis and fermentation, such as weak acids, furfural, 5-hydroxymethyl furfural (HMF) and phenolic compounds are formed [42]. After the pretreatment, most authors wash the pretreated coconut husk to extract inhibitors from the biomass [27–29, 46, 47]. This approach might not be the best as it increases the number of process steps and uses more water which affect the cost, and, moreover, a high content of sugars are lost during these washes [29, 48].

*3.1.1. Alkaline Pretreatment.* The main effect of alkaline pretreatment is delignification of the biomass and reduction of crystallinity [29, 43–45]. For these pretreatments, sodium, potassium, calcium, and ammonium hydroxides and ammonia are used [44, 45]. All revised studies that used alkaline pretreatment in coconut husk used NaOH and most of them use high temperatures [27–29, 33, 46, 48–50].

Soares et al. [50] proposed a pretreatment with dilute NaOH (1% (w/v)) at room temperature to decrease the formation of inhibitors, using high-solid loadings (18% (w/v)) and no detoxification of the pretreated biomass to obtain higher sugar concentration. In a later work, Soares et al. [48] suggest the use of a fed-batch pretreatment and saccharification with higher solid loadings (25 and 30% (w/v)).

*3.1.2. Acid Pretreatment.* Acid pretreatment is a widely used and effective method for obtaining high yields of sugars from lignocellulosic biomass. Fatmawati and Agustriyanto [47] and da Costa Nogueira et al. [29] pretreated coconut husks with diluted acid (1.5% and 3% (w/v) of $H_2SO_4$) and autoclaved at 121°C. De Araújo et al. [51] tried an acid pretreatment followed by an alkaline treatment of the washed neutralized fibers, both at high temperature.

*3.1.3. Other Pretreatment Approaches.* Pretreatments using alkaline conditions combined with other techniques have been tested for coconut husk. One approach consists of presoaking the coconut husks in a NaOH solution and then microwaving them [52, 53]. Other pretreatments use a combination of alkaline and oxidative conditions [31, 51], where an $H_2O_2$ solution is adjusted to pH 11.5 with NaOH.

Gonçalves et al. [30] used a two-step method to remove different components from the husk. First, they utilized oxidative conditions ($NaClO_2$–$C_2H_4O_2$) to remove the lignin. Then, they performed autohydrolysis to extract the hemicellulose.

Other pretreatments reported for coconut husk are the use of high temperature for autohydrolysis [29, 32, 53], use of aqueous glycerol and acidified aqueous glycerol at 130°C [54], and use of the surfactant Tween® 80 during acid, alkaline, and hydrothermal pretreatment to increase enzymatic hydrolysis [29].

*3.2. Hydrolysis.* The next step in bioethanol production is breaking cellulose and hemicellulose into simple sugar monomers that can be fermented. Cellulose is hydrolyzed to glucose, while hemicellulose hydrolysis releases a mixture of pentoses and hexoses [44]. There are different hydrolysis strategies like dilute and concentrated acid, alkaline, hot-compressed water, and enzymatic [55]. Enzymatic hydrolysis is the most widely used as it is the most ecofriendly, has no formation of inhibitors, requires less energy, and is operated at mild conditions (40-50°C and pH 4-5) so there are no corrosion problems [20, 44, 56]. On the other hand, alkaline and acid hydrolysis present high toxicity, high utility cost, lower sugar yields, and corrosion, along with the formation of inhibitors [44, 56].

A cocktail of enzymes composed of cellulases and hemicellulases that work in synergy is needed to effectively hydrolyze the cellulose and hemicellulose (Figure 2) [34, 44, 56]. These enzymes are naturally produced by various fungi and bacteria. The fungus *Trichoderma reesei* is one the most used industrially to produce cellulases [57]. These strains have been engineered to produce a large amount of chosen cellulases (native, homologous, or engineered) so they have a high specific activity on crystalline cellulose [58, 59]. Currently, the most advanced cocktails in the market are Cellic® CTec3 from Novozymes (Bagsværd, Denmark) and Accellerase® TRIO™ from DuPont Genencor (CA, USA) [58].

Enzymatic hydrolysis is the economic bottleneck of lignocellulosic bioethanol production because of its high cost. Enzyme production costs comprise 25 to 50% of bioethanol production cost [60]. Efforts have been made to decrease enzyme price and it has dropped from US$ 5 per gallon or US$ 0.75 per liter of bioethanol to US$ 0.10–0.18 per gallon or US$ 0.027 per liter of bioethanol [34].

Producing better enzymes with higher efficiency using lower doses are important to make lignocellulosic bioethanol economically feasible. There are many factors that affect the efficiency of enzymatic hydrolysis including temperature, pH, mixing rate, enzyme loading, pretreatment, present inhibitors, substrate type and concentration (can lead to inhibition), and end-product inhibition (glucose) [44, 56]. As a result, the development of enzymes with (i) stability at higher temperatures and pH, (ii) increased tolerance to pretreatment inhibitors and end-product inhibition, (iii) better efficiency, (iv) higher adsorption, and (v) catalytic efficiency is highly needed [20]. For example, new thermophilic strains such as *M. thermophila* C1 are used to produce cellulases with

Table 2: Comparison of pretreatment methods and inhibitors formed during pretreatment.

| Reference | Substrates | Type | Conditions | Reported inhibitors |
|---|---|---|---|---|
| [52] | Coconut husk | Microwave-assisted-alkaline | 2450 MHz | n.a. |
| [27] | Young coconut husk | Step 1: NaOH 20-30% (w/v)<br>Step 2: NaOH 25% (w/v) | Step 1: 100°C, 2 and 3 h<br>Step 2: 170°C, 3 h | n.a. |
| [53] | Coconut husk | Microwave-assisted-alkaline<br>Autohydrolysis<br>$H_2SO_4$ 1% (v/v)<br>NaOH 5% (w/v) | 2450 MHz, 20 min<br>121°C, 1.043 bar, 15 min<br>40°C, 150 rpm, 24 h, TS 2%<br>40°C, 150 rpm, 24 h, TS 2% | n.a. |
| [31] | Green coconut shell, mature coconut fiber, mature coconut shell and cactus | Alkaline hydrogen peroxide ($H_2O_2$ 7.35% (v/v), pH 11.5) followed by alkaline delignification (NaOH 4% (w/v)) | $H_2O_2$: 25°C, 1 h<br>NaOH: 100 rpm, 100°C, 1 h | n.a. |
| [61] | Coconut husk, defatted grape seed and pressed palm fiber | No pretreatment. Direct non-enzymatic hydrolysis with subcritical water | | Furfural, HMF, 4-hydroxybenzoic acid and vanillin |
| [47] | Coconut husk | $H_2SO_4$ 1% (v/v) | 121°C, 1 h, TS 7.5% | n.a. |
| [32] | Green coconut shell, mature coconut fiber, mature coconut shell and cactus | Autohydrolysis | 160-200°C, 10-50 min, TS 10% | Acetic acid, furfural and HMF |
| [28] | Coconut fiber | NaOH 3% (w/v) | 121°C, 90 min | n.a. |
| [46] | Coconut husk | NaOH 2.5 mol·$L^{-1}$ | Soaking in NaOH: 30 min<br>Autoclaved: 125°C, 30 min | Phenolic compounds |
| [49] | Green coconut husks | NaOH 5% | 121°C, 40 min, TS 5% | Acetic acid |

Table 2: Continued.

| Reference | Substrates | Type | Conditions | Reported inhibitors |
|---|---|---|---|---|
| [33] | Mature coconut fiber | Hydrothermal catalyzed with NaOH | 160-200°C, 10-50 min | Phenolic compounds, HMF, furfural and acetic acid |
| [50] | Green coconut mesocarp | NaOH 1-4% (w/v) | 25°C, 200 rpm, 1-24 h, TS 18% | Acetic acid, formic acid, phenolic compounds (various). NO levulinic acid, furfural or HMF detected |
| [51] | Green coconut husk | Acid-alkaline ($H_2SO_4$ 0.6 mol·$L^{-1}$ and NaOH 4% (w/v))<br>Alkaline hydrogen peroxide ($H_2O_2$ 7.35% (v/v), pH 11.5) | Acid: 121°C, 15 min, TS 20%<br>Alkaline: 121°C, 30 min<br>Room temperature, 100 rpm, 1 h, TS 4% | n.a. |
| [54] | Coconut coir fibers | Acidified aqueous glycerol<br>Aqueous glycerol | 130°C, 400 rpm, 30 and 60 min, TS 3.3 and 5% | n.a. |
| [62] | Coconut husk, defatted grape seed, sugarcane bagasse and pressed palm fiber | No pretreatment. Direct non-enzymatic hydrolysis with subcritical water + $CO_2$ | | Furfural, HMF, 4-hydroxybenzoic and vanillin |
| [48] | Green coconut husk | NaOH 1-2% (w/v) | 200 rpm, 25°C, 1 h | Acetic acid, formic acid, phenolic compounds (various) and fatty acids. NO levulinic acid, furfural or HMF detected |
| [29] | Coconut fiber | NaOH 1 and 2% (w/v) -/+ Tween® 80<br>$H_2SO_4$ 1.5 and 3% (w/v) -/+ Tween® 80<br>Autohydrolysis -/+ Tween ® 80 | 121°C, 10-30 min, TS 10%<br>121°C, 10-60 min, TS 15%<br>121°C, 10-60 min, TS 10 and 15% | Acetic acid and phenolic compounds. NO furfural or HMF detected |
| [30] | Green coconut shell, mature coconut fiber, mature coconut shell and cactus | $NaClO_2$ (0.93% (w/v)) - $C_2H_4O_2$ (0.31% (v/v)) followed by autohydrolysis | $NaClO_2$-$C_2H_4O_2$: 75°C, 1-4 h, TS 3.1%<br>Autohydrolysis: 200°C, 50 min, TS 10% | Phenolic compounds, HMF, furfural and acetic acid |

TS: total solids loadings (w/v); n.a.: not available or not present.

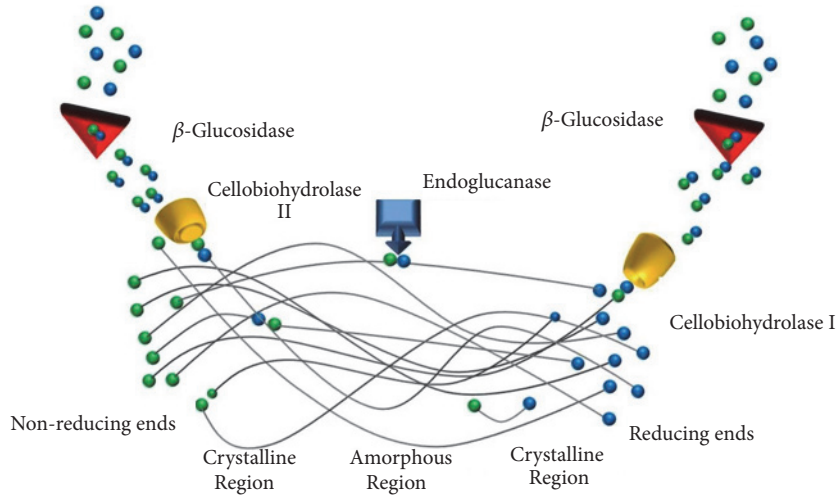


Figure 2: Hydrolysis mechanism of cellulose by cellulase cocktail components. Endoglucanases cleave the inner region of cellulose, the reducing and non-reducing regions are hydrolyzed by cellobiohydrolases (I and II) and the cellobiose is hydrolyzed to glucoses by β-glucosidase [34]. Adapted from Wang et al. [35].

broader pH and temperature ranges that also contain richer hemicellulases [58].

In the case of bioethanol production from coconut husk, most studies use enzymatic hydrolysis, where the use of commercial cocktails is the most common approach [27, 29, 31–33, 46–54]. Another method is to isolate fungi from the substrate to be used for bioethanol production hoping to find a microorganism with high specificity for that biomass as was done by Albuquerque et al. [46] for fresh and rotting coconut husk. The best isolates (*Penicillium variable* and *Trichoderma* sp.) were used to produce enzymes by submerged fermentation.

Some studies have been made to test the use of surfactants to improve enzymatic hydrolysis in coconut husk but using different approaches. Da Costa Nogueira et al. [29] used Tween® 80 during different pretreatments, while de Araújo et al. [51] used rhamnolipids produced by *Pseudomonas aeruginosa* during enzymatic hydrolysis. Rhamnolipids are biosurfactants that, unlike chemical surfactants, are biodegradable and that makes them an environmentally friendly option.

Non-enzymatic hydrolysis methods have also been tested for coconut husk. Acid hydrolysis using sulfuric acid 1, 2, 3, and 4% (v/v) and high temperature after an alkaline pretreatment was performed by Jannah and Asip [28]. Moreover, Prado et al. [61, 62] employed subcritical water hydrolysis, which utilizes pressure to maintain the water in a liquid state using coconut husk without any pretreatment.

*3.3. Fermentation.* Microbial fermentation is the next step in the production of lignocellulosic bioethanol in which the fermentable sugars, such as glucose and mannose, obtained in the saccharification, are converted to ethanol [63].

*Saccharomyces cerevisiae* has traditionally been used to produce alcohol in brewing and wine industries [21]. This yeast produces high yields of ethanol with high productivity [64, 65]. Nowadays, other yeasts and bacteria are also used for bioethanol production [9]. Using other microorganisms with different characteristics from *S. cerevisiae* or a combination of microorganisms (cofermentation) can increase ethanol yield. For example, using yeasts that naturally ferment pentoses, such as the xylose consuming *Pichia (Scheffersomyces) stipitis*, *Candida shehatae* and *Pachysolen tannophilus* [66], or bacteria such as *Zymomonas mobilis,* which presents fermentation under anaerobic conditions, high ethanol tolerance, and high ethanol-producing capacity [67], can increase the final ethanol concentration.

Another approach to overcome the challenges in lignocellulosic bioethanol production is the development of genetically engineered microorganisms that are capable of fermenting pentoses and hexoses. Engineered yeast strains with these characteristics are more economically viable for industrial production of bioethanol [68]. With development of new DNA editing technology, the metabolic potentials of microorganisms are being explored and harnessed in plenty new ways. The development of strains that can ferment xylose, the main pentose in coconut husk, is done by inserting genes related to the degradation pathway of this pentose, like overexpressing genes related to the pentose phosphate pathway (such as TKL1 and TAL1) [69, 70]. Other strategies are decreasing the formation of xylitol as it is a harmful derivative for the complete fermentation of the pentoses and preventing the ubiquitination of hexose transporters, since they also act to carry pentoses, but suffer degradation when the concentration (or absence) of glucose decreases [71, 72]. Ethanol production can also be improved by preventing the formation of glycerol, another fermentation product. It has been shown that the deletion of genes in this pathway like GPD2 and FPS1 is related to an improvement in the final ethanol production, since they redirect the metabolic flow to the alcoholic fermentation [73, 74]. Another approach is the interruption of the ADH2 gene, related to the transformation of ethanol into aldehyde, as it has higher affinity for ethanol

compared to other isoenzymes [75]. Genetic engineering can also be used to obtain microorganisms that are more tolerant to stresses like inhibitors produced during the pretreatment and a high ethanol concentration that is present at the end of the process. This can be done by inserting genes, such as *Saccharomycopsis fibuligera* TPS1 (6-phosphate-trehalose synthase) into *Saccharomyces cerevisiae*, or fine-tuned proteins such as RNA pol2 responsible for mRNA expression [76, 77]. Genetic engineering offers the advantage over traditional methods of increasing molecular diversity in a direct, specific, and faster way.

*3.4. Hydrolysis and Fermentation Strategies.* There are three main strategies for hydrolysis and fermentation: separate hydrolysis and fermentation (SHF), simultaneous hydrolysis and fermentation (SSF), and semi-simultaneous hydrolysis and fermentation (SSSF). In SHF the hydrolysis is done at a higher temperature which is optimal for the enzymes and later the fermentation is performed at a lower temperature optimal for the microorganism. On the other hand, in SSF the enzymatic hydrolysis and the fermentation are executed at the same time at an intermediate temperature. This strategy helps to reduce processing times, sugar inhibition, and equipment cost, since only one vessel is needed [78]. The major problem is that the temperature is not optimal for the enzymes and sometimes for the microorganisms (the use of microorganisms with higher optimal temperature solves this last problem).

A way to obtain the advantages of both SHF and SSF is to include a prehydrolysis step before inoculation, which is performed at an optimal temperature for the enzyme, followed by an SSF. This method is called SSSF. Some of the advantages of using SSSF are no carbon deficiency in early stages as presented during SSF [78], higher enzymatic activity during prehydrolysis because of optimal enzyme temperature, and reduction of slurry viscosity, which enables higher solid loadings and easier stirring and pumping [79].

## 4. Results and Discussion

*4.1. Coconut Husk Pretreatment for Bioethanol Production.* A strategy to evaluate the effectiveness of a pretreatment is to compare the composition of the biomass before and after the procedure. This is a key parameter to know whether the technique removes the lignin, degrades the hemicellulose, and conserves the cellulose. However, since the sugar concentration after hydrolysis depends on many factors, the biomass with the most changes will not yield necessary the highest sugar turnout. Therefore, both the coconut husk composition after pretreatment and the sugar concentration after hydrolysis should be taken into account in any study.

Alkaline pretreatment seems to be the best approach to obtain sugars from coconut husk probably because it helps to remove the lignin from the substrate. The results of delignification with NaOH are reported by Gonçalves et al. [33] and Jannah and Asip [28]. As for hemicellulose content, two studies show an increase [27, 29], while other two show a decrease [33, 49]. This is probably due to the conditions used on each work. The highest increase in cellulose content was observed by Gonçalves et al. [33] and Cabral et al. [49]. Of the studies with composition analysis after pretreatment, Gonçalves et al. [33] obtained the best results using NaOH pretreatment, with high cellulose increase and high delignification. On the other hand, Vaithanomsat et al. [27] and da Costa Nogueira et al. [29] observed only a small increase in cellulose content and delignification in comparison with other methods.

Also, the studies that presented highest sugar concentrations after hydrolysis used alkaline pretreatment with NaOH (the results will be discussed in the hydrolysis section) [27–29, 48, 50]. It was observed that higher NaOH concentrations, temperature, and processing time produce more inhibitors, which may affect the next steps of the process [33, 48].

Soares et al. [50] selected mild alkaline conditions (1% NaOH (w/v), room temperature, and shorter reaction time) to decrease the formation of inhibitors. They also proposed no detoxification of the pretreated biomass and the use of high-solid loadings (18% (w/v)), which improved sugar release over most of the other studies, and consequently ethanol concentration. In a later study, Soares et al. [48] used the same mild conditions but did a fed-batch pretreatment and saccharification increasing the solid loadings to 25 and 30% (w/v), which increased the final sugar and ethanol concentration. However, rising the solids loading up to 30% also led to a diminution in the yield (g ethanol/g sugar) but also showed one of highest sugar concentrations.

The use of high-solid loadings (≥ 15% solids, (w/v)) during the pretreatment and/or hydrolysis stages brings economic benefits such as less energy consumption during the processes, including distillation, and use of smaller vessels and equipment, which translates to lower capital cost [80]. Unfortunately, it also implies many setbacks, including a higher concentration of inhibitors, mass transfer limitations and reduction of ethanol yield as solid loadings rise [80, 81]. As solid loadings increase, free water decreases and viscosity rises; as a result, there is a reduction in the effectiveness of the pretreatment and enzymatic efficiency because of poor diffusion and solubilization [80–83]. High viscosity also brings handling problems, as mixing, pumping, and pouring become harder [82]. There are different approaches to reduce viscosity such as the use of surfactants [84] and employing a fed-batch process, which unfortunately shows a decline in conversion when more solids are introduced [81] as observed by Soares et al. [48].

Da Costa Nogueira et al. [29] compared alkaline, acid, and autohydrolysis pretreatments and the alkaline pretreatment showed the highest final sugars concentration. The composition of the husk was almost unchanged by the autohydrolysis pretreatment and the composition after acid pretreatment was not shown. They also showed that adding Tween® 80 during alkaline pretreatment can increase final sugars concentration by obtaining a higher digestibility during the enzymatic hydrolysis, but no difference was seen when acid and autohydrolysis pretreatments were performed with or without the surfactant [29].

Ding et al. [53] showed best results for microwave-assisted-alkaline pretreatment, followed by alkaline, then

acid and lastly autohydrolysis. Unfortunately, all pretreatments in this study led to a low sugars concentration. The delignification obtained by microwave-assisted-alkaline pretreatment was significant and led to a significant increase in cellulose and hemicellulose concentration. Other works that used autohydrolysis also obtained better results using other pretreatments [29, 32].

The studies that used $H_2O_2$ in alkaline conditions showed a large difference in the sugars concentration. This might be due to the delignification with NaOH performed by Gonçalves et al. [31] after the pretreatment, which resulted in higher delignification and increased cellulose and sugar concentration relative to the values reported by de Araújo et al. [51].

On the other hand, it was observed that dilute acid pretreatment is not the best strategy for obtaining sugars from green coconut fibers [29]. A possible explanation for dilute acid pretreatment not being the best strategy for obtaining sugars from green coconut fibers is that coconut husk has a high lignin content. Studies have shown that acidic pretreatment at high temperature forms lignin droplets that adhere to the biomass interfering with the enzymatic hydrolysis [85]. De Araújo et al. [51] reported no significant removal of lignin using acid pretreatment followed by an alkaline treatment at high temperature, which agrees with the low delignification reported by Fatmawati and Agustriyanto [47].

Another interesting pretreatment proposed by Gonçalves et al. [30] for coconut husk is the use of oxidative conditions ($NaClO_2$- $C_2H_4O_2$) for delignification and autohydrolysis for hemicellulose removal. The authors obtained a high sugar content after hydrolysis, a high delignification, and a reduction of hemicellulose as desired, but most lignin was conserved. In terms of lignin removal and cellulose increase, their results are similar to those of Gonçalves et al. [33] with NaOH at high temperature, but they also obtained a higher hemicellulose elimination. They also reported a higher difference in crystallinity than in other studies [29, 31–33].

*4.2. Inhibitors of the Enzymatic Hydrolysis and Fermentation.* The main inhibitors found in pretreated coconut husk are HFM, furfural, phenolic compounds, formic acid, and acetic acid, the last one in the highest concentrations (Table 2) [29, 33, 46, 48–50]. Soares et al. [50] showed a relationship between an increase in NaOH concentration in the pretreatment and the inhibitor concentration. After alkaline pretreatment, acetic and formic acids and phenolic compounds are the main inhibitors produced, but no HMF or furfural were detected [29, 50]. On the other hand, Gonçalves et al. [33] showed a rise of HMF, furfural and total phenolic compounds with increasing pH. These differences seen in the inhibitors found are due to differences in the pretreatment. Also, pretreated coconut husks that still have solid albumen present very high levels of fatty acids that act as strong inhibitors [48].

*4.3. Hydrolysis.* Table 3 presents a compilation of the results published so far. As it can be observed, each work uses a different approach, making it difficult to determine the best methodology for enzymatic hydrolysis. Different pretreatments (which affect the type and concentration of inhibitors), amount of total solid loadings, and type of enzymatic cocktail and doses are used in each study (Table 3). Nevertheless, it is expected that the enzymatic hydrolysis efficiency will be affected by the pretreatment method. It has been shown that mature coconut fiber has the highest enzymatic conversion yield after NaOH pretreatment at high temperatures (90.72%)[33], followed by autohydrolysis pretreatment (84.10%) [32] and, at last, the alkaline hydrogen peroxide pretreatment with a posterior NaOH delignification (76.21%) (Table 3)[31]. Interestingly, the highest glucose concentration was reported for the pretreatment with the lowest hydrolysis yield [31] and the lowest glucose concentration was determined for the pretreatment with the highest yield [33] (Table 3). This might be explained by a difference in initial cellulose composition for the enzymatic hydrolysis after the pretreatment and by the cellobiose concentration after hydrolysis, which is not reported.

There are also differences in the enzymatic performance depending on the severity of the pretreatment conditions. For example, coconut husk pretreated with 4% (w/v) NaOH gives lower sugar titers than with 1% (w/v) NaOH due to enzymatic inhibition. Also, the longer the pretreatment, the lowest the final sugar concentration [50].

Other factors might also influence enzymatic activity. As an example, Albuquerque et al. [46] used different hydrostatic pressures to improve the performance of fungi cellulases isolated from coconut husk in comparison to industrial cellulases. Actually, coconut fungi cellulases displayed better enzymatic activity on filter paper and on coconut husk hydrolysis than commercial cellulases at atmospheric pressure and at 300 MPa. These findings show that isolating native strains from the biomass can lead to highly specific cellulases, which lead to better results than commercial enzymes. They also demonstrated that high pressure can be used as pretreatment of cellulosic fibers as it promoted ruptures in the coconut fibers that helped in the later saccharification process. High hydrostatic pressure establishes interesting physical and consequently biological changes that can be used in biomass pretreatment and fermentation areas on biofuels synthesis and in the use of residual lignocellulosic materials with greater efficiency.

In the end, the main objective is to have the highest sugars concentration with the highest conversion yield possible. Some authors report very low total reducing sugars after hydrolysis of coconut husk like Fatmawati and Agustriyanto ($1.2\ g{\cdot}L^{-1}$) [47] and Ding et al. ($2.8\ g{\cdot}L^{-1}$) [53] (Table 3), which are far from the 8% (w/w) of glucose minimum required to make the distillation economical [81]. Nevertheless, three studies achieved over 8% (w/w) of sugars and all of them used alkaline pretreatment [28, 48, 50]. While two of the studies used enzymatic hydrolysis [48, 50], Jannah and Asip [28] performed an acid hydrolysis showing the highest sugars concentration with 4% (v/w) sulfuric acid but no information about inhibitors was reported (Table 3). Soares et al. [48] reached the highest sugars concentration using high-solids loadings in a fed-batch pretreatment and enzymatic

Table 3: Comparison of hydrolysis methods and maximum final sugar concentrations.

| Reference | Pretreatment | Hydrolysis strategy | Enzymes | Enzyme concentration | Conditions | Maximum Sugars concentration |
|---|---|---|---|---|---|---|
| [52] | Microwave-assisted-alkaline | SSF | Cellusclast® 1.5 L and Pectinex® Ultra SP-L | n.a. | 30°C, 150 rpm, 96 h, TS 2.5% | n.p. |
| [27] | 2 steps with NaOH | SHF | Celluclast ®1.5L and Novozyme 188 (Novozymes A/S; Denmark) | 15 FPU·(g substrate)$^{-1}$ and 15 IU·(g substrate)$^{-1}$ | 50°C, 140 rpm, 72 h, pH 4.8, TS 5% | 22.8 g glucose·L$^{-1}$ |
| | | SSF | | | 37°C, 72 h, pH 5.5, TS 5% | n.p. |
| [53] | Microwave-assisted-alkaline<br>Autohydrolysis<br>$H_2SO_4$<br>NaOH | Only hydrolysis | Cellusclast ®1.5 L and Pectinex ® Ultra SP-L | 0.5% (v/v) each | 35°C, 150 rpm, 5 days, TS 1% | 2.8 g TRS ·L$^{-1}$<br>Aprox 0.7 g TRS ·L$^{-1}$<br>Aprox 0.7 g TRS ·L$^{-1}$<br>Aprox 1.4 g TRS ·L$^{-1}$ |
| [31] | Alkaline hydrogen peroxide + alkaline delignification | SSF mature coconut fiber<br>SSSF mature coconut fiber | Cellic®CTec2 and HTec2 | 30 FPU·(g substrate)$^{-1}$, 75 CBU·(g substrate)$^{-1}$ and 130 IU·(g substrate)$^{-1}$ | 30°C, 48 h, TS 4%<br>Prehydrolysis: 50°C, 8 h<br>SSF: 30°C, 40 h<br>TS 4% | Aprox 19 g glucose·L$^{-1}$ * |
| [61] | No pretreatment. | Only hydrolysis | Non-enzymatic hydrolysis with subcritical water | | | 3.4 g monosaccharides ·(100 g substrate)$^{-1}$ |
| [47] | $H_2SO_4$ | Only hydrolysis | Celluclast ® and Novozyme 188 (Novozymes A/S; Denmark) | 0.33 mL of each | 50°C, 150 rpm, 72 h, pH 4.8, TS 0.1-2% | 1.2 g TRS ·L$^{-1}$ |
| [32] | Autohydrolysis TS 10% | SSF green coconut shell<br>SSSF green coconut shell | Cellic® CTec2 and HTec2 | 30 FPU·(g substrate)$^{-1}$, 75 CBU·(g substrate)$^{-1}$ and 130 IU·(g substrate)$^{-1}$ | 30°C, 48 h, TS 4%<br>Prehydrolysis: 50°C, 12 h<br>SSF: 30°C, 36 h,<br>TS 4% | Aprox 13 g glucose·L$^{-1}$ * |
| [28] | NaOH | SHF | Non-enzymatic hydrolysis with 1-4% (v/w) $H_2SO_4$, 121°C, 2 h | | | 8.4% (w/v) glucose |
| [46] | NaOH | SHF | Cellulase® 26921, Novozyme188 (Novozymes A/S; Denmark) and enzymes from coconut husk isolated fungi | 7.5 FPU·(g substrate)$^{-1}$ | 50°C, 96 h, pH 5 | 50 mM TRS |
| [49] | NaOH | SHF | Accelerase® 1500 | 2% (v/v) | 50°C, 150 rpm, 72 h. TS 1% | 8.7 g TRS ·L$^{-1}$ |

Table 3: Continued.

| Reference | Pretreatment | Hydrolysis strategy | Enzymes | Enzyme concentration | Conditions | Maximum Sugars concentration |
|---|---|---|---|---|---|---|
| [33] | Hydrothermal catalyzed with NaOH | SSF<br>SSSF | Cellic® CTec2 and HTec2 | 30 FPU·(g substrate)$^{-1}$, 75 CBU·(g substrate)$^{-1}$ and 130 IU·(g substrate)$^{-1}$ | 30°C, 48 h, TS 4%<br>Pre-hydrolysis: 50°C, 12 h<br>SSF: 30°C, 36 h, TS 4% | Aprox 16 g glucose·L$^{-1}$ ∗ |
| [50] | NaOH | SHF | AlternaFuel® CMAX | 3.75, 7.5 and 15 FPU·(g substrate)$^{-1}$ | 50°C, 200 rpm, 96 h, pH 6, TS 17% | 8.7% (w/v) sugars |
| [51] | Acid-alkaline<br>Alkaline hydrogen peroxide TS 4% | Only hydrolysis | Celluclast ®1.5 L | 20.0 FPU·(g substrate)$^{-1}$, 20.0 CBU·(g substrate)$^{-1}$ and 10.0 XU·(g substrate)$^{-1}$ | 50°C, 150 rpm, 72 h, TS 5% | Aprox 9 g TRS ·L$^{-1}$<br>Aprox 11 g TRS ·L$^{-1}$ |
| [54] | Acidified aqueous glycerol<br>Aqueous glycerol | SSF | Enzyme from *T. reseei* | 10 FPU·(g substrate)$^{-1}$ | 37°C, 120 rpm, 96 h | n.p. |
| [62] | No pretreatment. | Only hydrolysis | Non-enzymatic hydrolysis with subcritical water + $CO_2$ | | | 1.7 g monosaccharides ·(100 g substrate)$^{-1}$ |
| [48] | NaOH | SHF | AlternaFuel® CMAX | 15 FPU·(g substrate)$^{-1}$ each time | 50°C, 200 rpm, 96 h, pH 6, TS 24 and 29% | 9.7% (w/v) sugars |
| [29] | NaOH + Tween® 80<br>Autohydrolysis | Only hydrolysis | *T. reesei* ATCC 26921, $\beta$-glucosidases and xylanases | 20.0 FPU·(g substrate)$^{-1}$, 20.0 CBU·(g substrate)$^{-1}$ and 10.0 FXU/·(g substrate)$^{-1}$ | 50°C, 150 rpm, 96 h, TS 5% | 0.5 g TRS ·(g substrate)$^{-1}$<br>0.1 g TRS ·(g substrate)$^{-1}$ |
| [30] | $NaClO_2$- $C_2H_4O_2$/ autohydrolysis | Only hydrolysis | Cellic® CTec2 and HTec2 | 10 FPU·(g substrate)$^{-1}$, 30 CBU·(g substrate)$^{-1}$ and 40 IU·(g substrate)$^{-1}$ | 50°C, 150 rpm, 96 h, TS 4% | Aprox 24 g glucose·L$^{-1}$ |

n.a.: not available or present; TS: total solids loadings (w/v); n.p.: not present because of SSF or SSSF; ∗ values obtained from liquor after enzymatic hydrolysis but not used for fermentation (SSF and SSSF).

saccharification, but they also observed a decrease of the conversion yield, which is characteristic of this kind of conditions.

As for the use of surfactants to enhance hydrolysis, da Costa Nogueira et al. [29] only obtained higher digestibility when using Tween® 80 during the alkaline pretreatment, whereas de Araújo et al. [51] found that adding rhamnolipids during hydrolysis improved cellulose conversion. Comparing both studies, da Costa Nogueira et al. [29] showed a higher hydrolysis yield in all conditions, presenting the best results for the coconut husk pretreated with NaOH and Tween® 80.

While using subcritical water hydrolysis, Prado et al. [61] obtained best results at 250°C and 20 MPa but observed an increase in the concentration of inhibitors (HMF and furfural) relative to processes at lower temperatures, where only hemicellulose is degraded. In this study, three different substrates were used and the results showed that coconut husk and palm fiber have similar final sugars concentrations (11.7 and 11.9%, respectively), but a defatted grape seed displays a much lower concentration (6.4%). On the other hand, using $CO_2$ during the subcritical water hydrolysis resulted in a lower concentration of monosaccharides for coconut husk [62], which is detrimental for ethanol production. The advantages of subcritical water hydrolysis are the absence of polluting reagents, a reduction of process steps, no corrosion, less residue generation, and lower sugar degradation [61]. As a downside, high temperature and pressure are necessary.

Up to now, enzymatic hydrolysis has been the preferred method for coconut husk hydrolysis, but after reviewing all results it is evident that further investigation of the use of acid hydrolysis is necessary. An important factor that must be taken in account is the concentration of inhibitors after acid hydrolysis. It must be observed that the substances that are considered inhibitors of enzymatic hydrolysis may not be important in the case of acid hydrolysis if they do not affect the fermentation process. Measuring the concentration of other sugars would also be interesting to evaluate the real potential of acid hydrolysis compared to enzymatic hydrolysis. Other factors to take into account are the costs and the handling complexity of the process of acid hydrolysis, including corrosion due to acid conditions.

*4.4. Fermentation.* Results on which hydrolysis and fermentation approach is best for ethanol production differ as it is affected by many factors such as the enzymatic loading used, substrate, solid loadings, pretreatment, inhibitors, the microorganism used, and prehydrolysis time in SSSF [78].

Ebrahimi et al. [54] used a SSF approach and obtained a much higher ethanol concentration (similar to Gonçalves et al. [31]) when using acidified aqueous glycerol compared to the just aqueous glycerol (Table 4). Gonçalves et al. [31–33] compared SSF and SSSF for different pretreatments with coconut husk using three microorganisms. In all three studies, SSSF presented higher ethanol yield, final sugars concentration, and productivity (Table 4). They also proved that *S. cerevisiae, P. stipitis*, and *Z. mobilis* are suitable for fermenting the coconut husk hydrolysates showing similar sugar consumption patterns and kinetic parameters (ethanol yield, concentration, and productivity) for each separate pretreatment. For sequential alkaline hydrogen peroxide-sodium hydroxide [31] and autohydrolysis [32] pretreatments, *P. stipitis* showed slightly higher ethanol concentration and ethanol productivity than the other microorganisms but the ethanol yield was a bit lower. The highest ethanol concentrations (11-12 $g \cdot L^{-1}$), yield (84-92%), and productivity (0.23-0.32) for all strains were achieved with the NaOH pretreatment using high temperature with very little differences between microorganisms [33]. It is important to point out that the sugars concentration after hydrolysis reported on Table 3 for these three studies might not be of the same quantity as the one produced by SSF and SSSF as many interactions modify the enzymatic activity, so direct comparison of the ethanol produced with the glucose concentration obtained by hydrolysis is not recommended.

Soares et al. [50] compared ethanol production of coconut husk hydrolysate with two different *S. cerevisiae* strains, a commercial strain, Ethanol Red, and a genetically modified strain, GSE16-T18. This engineered strain can ferment xylose and resists fermentation inhibitors, leading to enhanced ethanol production (Table 4).

Once again, the largest concentrations of ethanol were obtained in processes that used alkaline pretreatment and used SFH [28, 48, 50], but only two [28, 48] are above the 4% (w/w), considered as the minimum ethanol concentration for an economically feasible production [81]. Soares et al. [48] obtained the highest sugars concentration using a fed-batch pretreatment and hydrolysis approach, but the ethanol concentration was smaller than that obtained by Jannah and Asip [28]. This is probably due to the fact that the sugars concentration reported by Jannah and Asip [28] is just glucose, while Soares et al. [48] used the total sugars concentration. This shows the importance of the way data are presented, since Jannah and Asip [28] are probably presenting less sugars than the ones that can be fermented and Soares et al. [48, 50] are showing a mix of sugars that may include some that are nonfermentable. The best way to report sugar concentration would be by showing separately the concentration of glucose, since it is the main sugar in the liquor, and that of total fermentable sugars (which varies depending on the microorganism used). Soares et al. [48, 50] determine ethanol yield based on the concentration of fermentable sugars, while Jannah and Asip [28] do not calculate the conversion yield. For coconut husk, all reported ethanol yields are based on the relationship between the mass of ethanol produced divided by the mass of fermentable sugars detected by HPLC, ignoring the ambiguity of using total reducing sugars as a parameter [27, 31–33, 50]. TRS is the easiest way to measure sugars but includes nonfermentable sugars, making it difficult to compare different processes and to evaluate the real efficiency of fermentation.

Vaithanomsat et al. [27] and Cabral et al. [49] showed an initial sugar concentration for fermentation higher than that reported after hydrolysis with no further explanation on how that increase occurred.

Currently, the use of genetically modified organisms and the use of microorganisms other than *Saccharomyces cerevisiae* or a mix of them (coculture) have been scarcely

Table 4: Comparison of fermentation conditions, ethanol concentration, and yield.

| Reference | Pretreatment | Fermentation strategy | Microorganisms | Conditions | Maximum Ethanol concentration (g/L or %) | Ethanol yield (g ethanol/ g sugars or %) |
|---|---|---|---|---|---|---|
| [53] | Microwave-assisted-alkaline | SSF | *S. cerevisiae* ATCC 36858 | 30°C, 150 rpm, 96 h | 0.09% (w/w) | n.a. |
| [27] | 2 steps with NaOH | SHF<br>SSF | *S. cerevisiae* | 37°C, 72 h, pH 5.5. | 2.28% (w/v)∗<br>1.03% (w/v) | Approx 85% |
| [31] | Alkaline hydrogen peroxide + alkaline delignification | SSF | *S. cerevisiae*, *P. stipitis* and *Z.mobilis* | 30°C, agitation depending on microorganism, 48 h | *S. cerevisiae* 8.44 g·L$^{-1}$<br>*P.stipitis* 9.12 g·L$^{-1}$<br>*Z. mobilis* 8.27 g·L$^{-1}$ | *S. cerevisiae* 0.43<br>*P.stipitis* 0.40<br>*Z. mobilis* 0.42 |
| | | SSSF | | 30°C, agitation depending on microorganism, 40 h | *S. cerevisiae* 9.32 g·L$^{-1}$<br>*P.stipitis* 10.17 g·L$^{-1}$<br>*Z. mobilis* 8.91 g·L$^{-1}$ | *S. cerevisiae* 0.45<br>*P.stipitis* 0.43<br>*Z. mobilis* 0.44 |
| [32] | Autohydrolysis | SSF | *S. cerevisiae*, *P. stipitis* and *Z.mobilis* | 30°C, agitation depending on microorganism, 48 h | *S. cerevisiae* 7.44 g·L$^{-1}$<br>*P.stipitis* 8.47 g·L$^{-1}$<br>*Z. mobilis* 7.30 g·L$^{-1}$ | *S. cerevisiae* 0.44<br>*P.stipitis* 0.43<br>*Z. mobilis* 0.43 |
| | | SSSF | | 30°C, agitation depending on microorganism, 40 h | *S. cerevisiae* 7.71 g·L$^{-1}$<br>*P.stipitis* 8.78 g·L$^{-1}$<br>*Z. mobilis* 7.63 g·L$^{-1}$ | *S. cerevisiae* 0.45<br>*P.stipitis* 0.44<br>*Z. mobilis* 0.45 |
| [28] | NaOH | SHF | *S. cerevisiae* | 150 rpm, 11 days, pH 4.5-5 | 5.9% | n.a. |
| [49] | NaOH | SHF | *S. cerevisiae* | 30°C, 100 rpm, 9 h | 7 g·L$^{-1+}$ | n.a. |
| [33] | Hydrothermal catalyzed with NaOH | SSF | *S. cerevisiae*, *P. stipitis* and *Z.mobilis* | 30°C, agitation depending on microorganism, 48 h | *S. cerevisiae* 10.91 g·L$^{-1}$<br>*P.stipitis* 10.96 g·L$^{-1}$<br>*Z. mobilis* 10.81 g·L$^{-1}$ | *S. cerevisiae* 0.44<br>*P.stipitis* 0.45<br>*Z. mobilis* 0.43 |
| | | SSSF | | 30°C, agitation depending on microorganism, 36 h | *S. cerevisiae* 11.65 g·L$^{-1}$<br>*P.stipitis* 11.29 g·L$^{-1}$<br>*Z. mobilis* 11.64 g·L$^{-1}$ | *S. cerevisiae* 0. 47<br>*P.stipit*is 0.46<br>*Z. mobilis* 0.47 |
| [50] | NaOH | SHF | *S. cerevisiae* strains Ethanol Red and GSE16- T18 | 35°C, 100 rpm, 103 h, pH 5.5 | 3.73% (v/v) | 0.43 |
| [54] | Acidified aqueous glycerol | SSF | *S. cerevisiae* Hansen 2055 | 37°C, 150 rpm, 72 h | 8.97 g·L$^{-1}$ | n.a. |
| | Aqueous glycerol | | | | 2.66 g·L$^{-1}$ | n.a. |
| [48] | NaOH | SHF | *S. cerevisiae* GSE16- T18 | 35°C, 100 rpm, 72 h, pH 5.5 | 4.33% (v/v) | 0.41 |

n.a.: not available or not present; ∗ with 50 g·L$^{-1}$ of initial glucose instead of the 22.8 g·L$^{-1}$ reported from the hydrolysis. No explanation for the rise of sugar concentration was found. $^{+}$ with aprox 16 g·L$^{-1}$ of initial glucose instead of the 8.7 g·L$^{-1}$ reported from the hydrolysis. No explanation for the rise of sugar concentration was found.

studied in the case of ethanol made from coconut husk. Since this biomass has a high hemicellulose content, the use of microorganisms that are able to ferment pentoses may help to increase the ethanol production.

*4.5. Comparison with Other Biomasses.* Bioethanol production conditions analyzed in studies similar to the present one (where various works about a biomass are compared), but for sugarcane bagasse [86, 87], wheat straw [88], and corn stover [89] were examined.

Zhao et al. [89] did a profound analysis of the literature for articles published during the last 10 years that used corn stover as a raw material for bioethanol production. By analyzing a high number of works on the subject (474), they were able to draw some conclusions that are hard to do when analyzing a much smaller sample and confirmed some of the observations obtained on this study. Regarding the pretreatment, they saw that two-thirds of the papers used acid, steam explosion, ammonia-based, and alkaline processes. In the beginning acid and steam explosion were the most popular but their use is declining, while solvent-based and combined techniques are gaining ground. Compared to coconut husk, which presented best results with alkaline pretreatment, corn stover showed highest ethanol production with alkaline, solvents, and ammonia pretreatment (19-22%) and lowest with fungi (11%). This low effectiveness with biological pretreatment was also reported for sugarcane bagasse [86].

The best results found by Cardona et al. [86] in 2010 for sugarcane bagasse were using acid hydrolysis (48% (w/w) TRS and 19 g etanol·$L^{-1}$), but Bezerra and Ragauskas [87] in 2016 found the highest sugar and concentration with steam explosion (57.7 g glucose·$L^{-1}$ and 25.6 g ethanol·$L^{-1}$). Even though Cardona et al. [86] saw a higher glucose concentration when using alkaline pretreatment, they argue that costs are too high for the process to be viable at large scale. Talebnia et al. [88] reported steam explosion as the most suitable pretreatment for wheat straw because it has a lower reaction time, higher solid loadings, and a minimum use of chemicals. The best results for wheat straw were obtained with native non-adapted *S. cerevisiae* (31.2 g ethanol·$kg^{-1}$, 99% ethanol yield).

As pointed out in this study for coconut husk, Zhao et al. [89] also remarks that most of the studies for corn stover are focused on the pretreatment. Fermentation is only reported in half of the studies and most use yeasts (92%) and the rest bacteria (8%). Also purification is usually not described and when it is they mostly use distillation.

Equal to the findings for coconut husk, enzymatic hydrolysis is used in most of the studies [86–89]. Zhao et al. [89] report that 95% of the articles for corn stover used enzymatic hydrolysis and, as also seen on this work, the enzyme doses differ significantly from study to study.

Parallel to the findings of this study, Zhao et al. [89] confirm that ethanol production varies greatly from one study to another even when using similar processes. For corn stover, ethanol conversion for most studies ranged between 80 and 100% with no significant difference while using different microorganisms for fermentation [89]. They also observed that xylose fermentation was a key factor for higher ethanol production, confirming the importance of not extracting the hemicellulose for fermentation and the need to use microorganisms that can ferment these sugars.

Most studies analyzed for this kind of technology are done in laboratory scale (98% for corn stover [89]), including coconut husk. Zhao et al. [89] observed that, in the case of corn stover, some pilot scale processes used smaller concentrations of chemicals than the concentration used in laboratory studies. No full scale plants for this kind of work are reported on the articles analyzed [86–89]. This is probably because it is not in the interest of industry to report its know-how and results.

*4.6. Techno-Economic Overview on Bioethanol Production.* Since there are no published data on the costs of bioethanol production from coconut husk, an extrapolation based on results from other biomasses was performed. Most of the techno-economic analyses on the production of biofuels were simulations for a few lignocellulosic feedstock, pretreatments, and enzymatic hydrolysis [19, 90–94]. Eggeman and Elander [90] made the economic analysis using different pretreatments for corn stover and found a similar minimum ethanol selling prices (MESPs) using dilute acid, hot water, ammonia fiber explosion (AFEX), ammonia recycle percolation (ARP), and lime pretreatments. Similar results were found by da Silva et al. [19] for hot water and AFEX pretreatment, but a higher MESP was obtained using dilute acid pretreatment. On the other hand, Chovau et al. [92] find dilute acid pretreatment as the best option.

The main factors that affect the MESP are plant size [91, 95], feedstock price and transportation [91, 93, 95–98], composition of the feedstock [91], pretreatment [94], enzyme cost and loading [91, 93, 96–98], conversion from cellulose to glucose [91, 93], ethanol yield [95], fermentation of pentoses [93], investment costs [93, 95], and energy cost [96–98]. Ethanol yield is relevant, since a higher yield means that less feedstock is required and overhead costs are smaller [95].

The MESP is also significantly affected by the location of the production, not only due to the availability, price, and transportation cost of the feedstock but because of the local technology, the cost of raw material (especially enzyme), the cost of energy, and the local policies. Zhao et al. [93] compared the MESP of a process using the technology available in China, which included using local enzymes with lower activity, so that higher loadings were needed and only hexoses were fermented, and technology from the United States of America using economic parameters from China. They observed that the MESP for their process with Chinese technology was above the local price of fuel ethanol, while the MESP obtained using more advanced technology was lower than the local price of fuel ethanol.

As observed by Chouvau et al. [92] the MESP reported by different authors varies greatly (from \$0.21/L to \$1.21/L) according to the assumptions involved. Most authors use a future expected cost for the enzymes that is much lower than the present cost and leads to a significant decrease of MESP [90–92]. Chovau et al. [92] observed an increase in reported

MESP with higher enzyme cost when comparing various studies. They also estimated from these studies that about 13% of the MESP is due to enzyme cost. Some studies propose producing enzymes at the plant [92, 95], but Chovau et al. [92] reported higher costs for enzymes produced in-site due to energy consumption, higher investment, and lower plant capacity. As an alternative to enzyme use, acid hydrolysis, may be used, but recycling of acid is expensive and rises the costs [95].

Feedstock price also greatly affects the MESP, representing between 30 and 40% of it [92]. Corn stover price includes the grower payment, which is a compensation to the farmer for the fertilizers that he will use to recover the nutrients that would have been obtained from decomposition of the corn stover on the field [92]. This makes corn stover expensive and its price can vary greatly as fertilizer prices change annually and regionally. In addition, to reduce the transportation cost, which is significant, the plant has to be close to the source. Since feedstock price has a large impact on the MESP, it is important to use a realistic approach to this item when performing an economic simulation.

Macrelli et al. [97] studied the costs of using sugarcane to produce 1G and 2G (bagasse and leaves) in the same plant using steam pretreatment and enzymatic hydrolysis. By doing so, they achieved a lower MESP than when producing just 2G ethanol. This kind of scheme is already used by Raízen, as they produce sugar and later use the bagasse to produce 2G ethanol [11]. Therefore, they use the whole sugarcane and they do not have the extra transportation cost that most 2G ethanol plants have.

Duque et al. [98] and Quintero et al. [99] made an analysis using Aspen Plus™ for plants using agricultural residues from Colombia using acid pretreatment, enzymatic hydrolysis, and purification. Quintero et al. [99] added an energy generation facility powered mostly by lignin, while Duque et al. [98] did not include any heat exchange networks. Later Duque et al. [98] proposed to add such facility as their utilities represented 45.3% of the variable cost. Quintero et al. [99] also show the importance of including an energy generation system by comparing the MESP with and without this system. They obtained a lower MESP for all the biomasses when generating their own energy.

## 5. Future Perspectives

Bioethanol production from coconut husk might be a way to benefit rural development as it is mainly obtained by small producers. This way producers or cooperatives in rural areas might obtain a fuel for personal use enhancing energy security [1] and reducing waste volume, hence the environmental impact that the husks discarding brings. In order to make this possible it is crucial to have a simple and low-cost process by developing an appropriate pretreatment and access to cheaper enzymes. Since coconut husk is an agroindustrial residue, it should enhance competitiveness and social acceptance [8], as well as not presenting the ethical issue found when food crops are used to produce biofuels.

Producing bioethanol from coconut husk still has many challenges starting from the low concentration of sugars achieved in most of the studies, less than the 8% (w/w) of glucose needed to get a minimum of 4% (w/w) of ethanol to have an economically viable process [81]. After surpassing these sugar and ethanol concentrations the scale-up of the process must be done, where new challenges await, such as the decrease of sugar and ethanol yield due to physical differences between scales [100, 101], along with other technical and financial issues that may arise.

For now, most of the studies for bioethanol production from coconut husk have focused on the pretreatment and hydrolysis steps; less than half of the articles have addressed the fermentation to ethanol. It is important to include fermentation data because even hydrolysates with high sugar concentration may present problems when put to fermentation due to the presence of inhibitors.

It would be helpful to standardize the way research data are reported in order to facilitate the comparison of different processes and steps, but this is not always possible. In the case of the pretreatment step, one should include the biomass composition before and after pretreatment. As for the hydrolysis, as commented before, stating the glucose concentration in the hydrolysate as well as the total fermentable sugars that can be consumed by the microorganism used would help to determine the effectiveness of the hydrolysis and the fermentation. Stating the ethanol yield based on fermentable sugars also helps to compare the fermentation with other studies and may be useful to alert to a possible problem due to inhibitors. It is always helpful to report the concentration of inhibitors to determine if the simple sugars are being further degraded. Moreover, it is important to report the amount of sugar and ethanol obtained from a given mass of coconut husk so that the efficiency of the process may be determined.

Nowadays, the most economical way to produce 2G bioethanol is the biorefinery scheme, which is important for strengthening and supporting the growing biobased economy.

*5.1. Biorefinery.* The world is entering a new scenario where many countries are taking substantial steps towards a biobased economy. New bioproducts are beginning to replace fossil based products, greenhouse gas emissions are decreasing and innovative policies are emerging to support these changes [102]. To establish the foundation of a biobased economy, the use of biomass resources must be efficient and sustainable. That goal can be achieved by biorefinery systems.

In an energy driven biorefinery system, the biomass is primarily used to produce energy (biofuel, power and/or heat), and other byproducts are upgraded to more added-value products to optimize the economic and ecological performance of the whole production process [103]. Larragoiti-Kuri et al. [104] propose a biorefinery using corn cob as a substrate that produces bioethanol and lactic acid from the cellulose fraction, xylitol and succinic acid from xylose (hemicellulose) and lignosulfonates from lignin. They optimized product distribution by using economic potential, specific energy intensity, and safety indexes as criteria.

Advances in biorefineries allow the development of alternative products to avoid the accumulation of different residues (Figure 3). As an example, 1,3-propanediol obtained

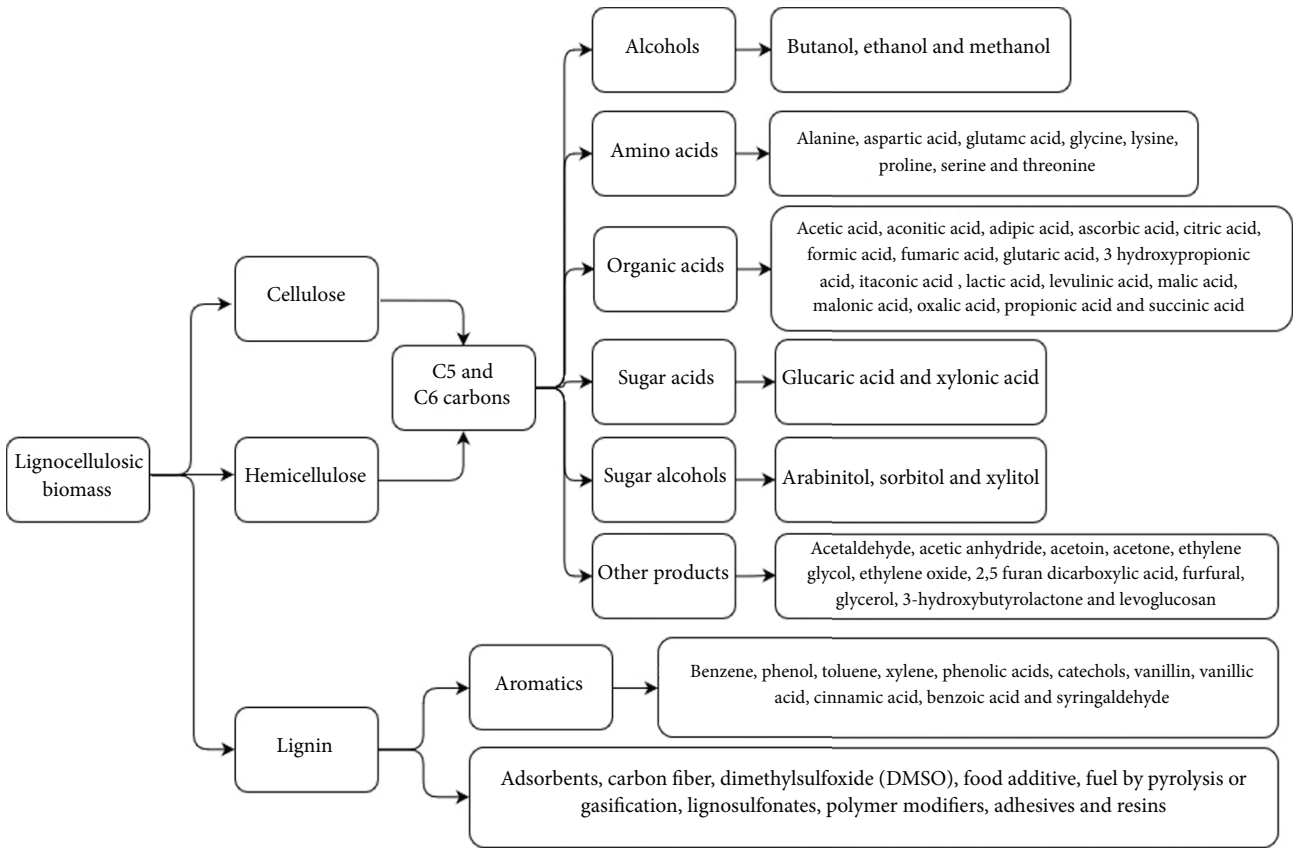


Figure 3: Possible products obtained in a biorefinery [36–38].

from maize residues is important in the formation of polymers. Also, succinic acid removed from various lignocellulosic residues is used in the chemical and pharmaceutical industries. An important alternative to polyethylene is the use of ether amylose derived from various wastes such as sugarcane, potato, and corn [105–108]. From an economic point of view, Gnansounou and Dauriat [95] propose producing a lower diversity of products with stable markets instead of offering a larger number of products, some of which may be unprofitable.

Up to now, all studies of the use of coconut husk for bioethanol production have been made in a small scale and only three studies mention the use of coconut husk as substrate for a biorefinery [30, 32, 33]. These works only discuss the possibility of using byproducts of ethanol production to obtain other substances but no tests to obtain other products have been reported. Gonçalves et al. [33] only suggested the use of sugars, acetic acid, phenolic compounds, and lignin found in the coconut hydrolysate to obtain different products using a biorefinery scheme with no further detail. Later, Gonçalves et al. [30] proposed using their process to make ethanol from coconut husk to obtain also value-added products. They propose that the phenolic compounds obtained during pretreatment and autohydrolysis be used as food additives, since they are antioxidants, while lignin can be used to produce pharmaceutical and veterinarian bioactive compounds and thermoplastic polymers, as well as for energy production through gasification or pyrolysis. They also suggest that xylans obtained from hemicellulose undergo another autohydrolysis to obtain xylooligosaccharide that can be employed in food and pet feed. They suggest that other substances present in the liquors can be used to obtain further products but no specific applications are mentioned. On the other hand, studies not focused on ethanol production show the potential of coconut husks to produce furfural, levulinic acid, formic acid, and acetic acid [109, 110].

Other applications for coconut husks different from ethanol production and possible byproducts were found, such as polymer composites [111, 112] and adsorbents to remove a wide range of water pollutants [113]. As the focus of this work is ethanol production, further studies should be made to see if the biomass remaining after the chosen process to obtain ethanol can still be used for these purposes and analyze if this strategy is economically viable.

## 6. Conclusion

Lignocellulosic ethanol production is a multistep process with many factors that can greatly affect its efficiency. The published coconut husk studies were performed in different conditions throughout the ethanol production process, so it is important to analyze various parameters to define which procedure as a whole has the best results. The final objective is

to obtain the highest ethanol concentration per mass of initial substrate for the lowest price, which translates to simpler processes with less energy consumption (lower temperature, pressure, and process time) and less reagents that at the same time have to be low-cost.

Using the concentration of sugars after hydrolysis as a comparison parameter to determine the best method to produce bioethanol is not the best strategy, since studies that use SSF and SSSF do not show the obtained sugars because they are consumed as they are produced. Additionally, most of the works report sugars concentration as total reducing sugars but not all these sugars are fermentable, so estimates of ethanol production may not reflect reality. On the other hand, ethanol yield is related to the transformation of those sugars into ethanol, so comparing these results reflects the ability of the microorganism to ferment the sugars that are present in the hydrolysate. This study showed that alkaline pretreatment is the best method in the case of coconut husk. The highest ethanol yields using coconut husk as a substrate were obtained by Gonçalves et al. [33] using SSSF. The highest ethanol concentration was obtained by Jannah and Asip [28] using an alkaline pretreatment and acid hydrolysis, achieving yields above the 4% (w/w) of ethanol required for an economically feasible distillation.

Finally, the most significant coconut producers are economically developing nations and the industrial residues generated by this culture impose a serious environmental problem. Biorefining this material for the production of ethanol and other molecules with greater added value would enable these countries to create new jobs and boost income.

## Conflicts of Interest

The authors declare that there are no conflicts of interest regarding the publication of this paper.

## Acknowledgments

This work was supported by the Fundação de Amparo à Pesquisa do Estado do Espírito Santo, FAPES, Grants [48497231] and [59899549/12]. P.M.B. Fernandes was granted the research productivity award from the Conselho Nacional de Desenvolvimento Científico e Tecnológico, CNPq, Grant [304719/2014-5]. M. Bolivar-Telleria, C. Turbay, and T. Carneiro acknowledge the Coordenação de Aperfeiçoamento de Pessoal de Nível Superior, CAPES, and L. Favarato acknowledge CNPq for their scholarships.

## References

[1] L. R. Lynd, "The grand challenge of cellulosic biofuels," *Nature Biotechnology*, vol. 35, no. 10, pp. 912–915, 2017.

[2] R. Sims, A. Flammini, M. Puri, and S. Bracco, "Opportunities for Agri-Food Chains to become Energy-Smart," *FAO USAID*, 2015.

[3] B. Hahn-Hägerdal, M. E. Himmel, C. Somerville, and C. Wyman, "Welcome to Biotechnology for Biofuels," *Biotechnology for Biofuels*, vol. 1, 2008.

[4] R. C. Leite and L. A. B. Cortez, "O Etanol Combustível no Brasil," *Biocombustíveis no Bras. Real. e Perspect. Ministério das Relações Exteriores*, 2008.

[5] M. A. A. de Mendonça, F. R. Edivaldo, A. O. P. Dos Santos, A. S. Pereira, and R. C. Da Costa, "Expansão da produção de álcool combustível no Brasil: uma análise baseada nas curvas de aprendizagem," in *Proceedings of the 46th Congress*, Rio Branco , Acre, Brazil, 2008.

[6] M. G. da Cruz, E. Guerreiro, and A. P. Raiher, "A Evolução da Produção de Etanol no Brasil, no Período de 1975 a 2009," *Revista Econômica do Nordeste*, vol. 43, no. 4, pp. 141–160, 1975.

[7] K. Saha, U. M. R, J. Sikder, S. Chakraborty, S. S. da Silva, and J. C. dos Santos, "Membranes as a tool to support biorefineries: Applications in enzymatic hydrolysis, fermentation and dehydration for bioethanol production," *Renewable & Sustainable Energy Reviews*, vol. 74, pp. 873–890, 2017.

[8] A. Scoma, L. Bertin, M. A. M. Reis, M. Kornaros, and M. Coma, "Multipurpose, Integrated 2nd Generation Biorefineries," *BioMed Research International*, vol. 2016, 2016.

[9] M. Tabatabaei, K. Karimi, R. Kumar, and I. S. Horváth, "Renewable Energy and Alternative Fuel Technologies," *BioMed Research International*, vol. 2015, Article ID 245935, 2 pages, 2015.

[10] GranBio Investimento SA, "GranBio," http://www.granbio .com.br/en/.

[11] Raízen, "Tecnologia em energia renovável: Etanol de segunda geração," https://www.raizen.com.br/energia-do-futuro-tecnologia-em-energia-renovavel/etanol-de-segunda-geracao.

[12] M. Peplow, "Cellulosic ethanol fights for life," *Nature*, vol. 507, no. 7491, pp. 152-153, 2014.

[13] UNCTAD, "Second generation biofuel market: State of play, trade and developing country perspectives," http://unctad.org/en/pages/PublicationWebflyer.aspx?publicationid=1455.

[14] J. Lane, "Biofuels Mandates Around the World: 2016," http://www.biofuelsdigest.com/bdigest/.

[15] J. Lane, "Biofuels Mandates Around the World: 2017," http://www.biofuelsdigest.com/.

[16] FAOSTAT, "Coconut production in 2013," http://faostat3 .fao.org/browse/Q/*/E.

[17] J. E. G. Van Dam, "Coir processing technologies: improvement of drying, softening, bleaching and dyeing coir fibre/yarn and printing coir floor coverings," *Common Fund Commod*, 2002.

[18] M. de Freitas, F. J. Rosa, A. A. T. Montenegro et al., "Caracterização Do Pó Da Casca De Coco Verde Usado Como Substrato Agrícola," *Embrapa Agroindústria Tropical Comunication Técnicon*, 2001.

[19] A. R. G. da Silva, C. E. Torres Ortega, and B.-G. Rong, "Techno-economic analysis of different pretreatment processes for lignocellulosic-based bioethanol production," *Bioresource Technology*, vol. 218, pp. 561–570, 2016.

[20] S. Mohanram, D. Amat, J. Choudhary, A. Arora, and L. Nain, "Novel perspectives for evolving enzyme cocktails for lignocellulose hydrolysis in biorefineries," *Sustainable Chemical Processes*, vol. 1, no. 1, p. 15, 2013.

[21] S. H. Mohd Azhar, R. Abdulla, S. A. Jambo et al., "Yeasts in sustainable bioethanol production: A review," *Biochemistry and Biophysics Reports*, vol. 10, pp. 52–61, 2017.

[22] L. R. Lynd, X. Liang, M. J. Biddy et al., "Cellulosic ethanol: status and innovation," *Current Opinion in Biotechnology*, vol. 45, pp. 202–211, 2017.

[23] F. Cherubini, "The biorefinery concept: Using biomass instead of oil for producing energy and chemicals," *Energy Conversion and Management*, vol. 51, no. 7, pp. 1412–1421, 2010.

[24] J. M. N. Marikkar and W. S. Madurapperuma, "Coconut," *Tropical and Subtropical Fruits: Postharvest Physiology, Processing and Packaging*, pp. 159–177, 2012.

[25] S. A. C. N. Perera, H. D. M. A. C. Dissanayaka, H. M. N. B. Herath, M. G. M. K. Meegahakumbura, and L. Perera, "Quantitative Characterization of Nut Yield and Fruit Components in Indigenous Coconut Germplasm in Sri Lanka," *International Journal of Biodiversity*, vol. 2014, Article ID 740592, 5 pages, 2014.

[26] H. Martins, R. Fontes, and W. M. Aragπo, "A Cultura do Coqueiro," https://www.spo.cnptia.embrapa.br/.

[27] P. Vaithanomsat, W. Apiwatanapiwat, N. Chumchuent, W. Kongtud, and S. Sundhrarajun, "The potential of coconut husk utilization for bioethanol production," *Kasetsart Journal - Natural Science*, vol. 45, no. 1, pp. 159–164, 2011.

[28] A. M. Jannah and F. Asip, "Bioethanol production from coconut fiber using alkaline pretreatment and acid hydrolysis method," *International Journal on Advanced Science, Engineering and Information Technology*, vol. 5, no. 5, pp. 320–322, 2015.

[29] C. da Costa Nogueira, C. E. de Araújo Padilha, A. L. de Sá Leitão, P. M. Rocha, G. R. de Macedo, and E. S. dos Santos, "Enhancing enzymatic hydrolysis of green coconut fiber—Pretreatment assisted by tween 80 and water effect on the post-washing," *Industrial Crops and Products*, vol. 112, pp. 734–740, 2018.

[30] F. A. Gonçalves, H. A. Ruiz, E. S. Dos Santos, J. A. Teixeira, and G. R. de Macedo, "Valorization, Comparison and Characterization of Coconuts Waste and Cactus in a Biorefinery Context Using NaClO2–C2H4O2 and Sequential NaClO2–C2H4O2/Autohydrolysis Pretreatment," *Waste and Biomass Valorization*, pp. 1–14, 2018.

[31] F. A. Gonçalves, H. A. Ruiz, C. D. C. Nogueira, E. S. D. Santos, J. A. Teixeira, and G. R. De Macedo, "Comparison of delignified coconuts waste and cactus for fuel-ethanol production by the simultaneous and semi-simultaneous saccharification and fermentation strategies," *Fuel*, vol. 131, pp. 66–76, 2014.

[32] F. A. Gonçalves, H. A. Ruiz, E. S. Dos Santos, J. A. Teixeira, and G. R. De Macedo, "Bioethanol production from coconuts and cactus pretreated by autohydrolysis," *Industrial Crops and Products*, vol. 77, pp. 1–12, 2015.

[33] F. A. Gonçalves, H. A. Ruiz, E. Silvino dos Santos, J. A. Teixeira, and G. R. de Macedo, "Bioethanol production by Saccharomyces cerevisiae, Pichia stipitis and Zymomonas mobilis from delignified coconut fibre mature and lignin extraction according to biorefinery concept," *Journal of Renewable Energy*, vol. 94, pp. 353–365, 2016.

[34] M. Taha, M. Foda, E. Shahsavari, A. Aburto-Medina, E. Adetutu, and A. Ball, "Commercial feasibility of lignocellulose biodegradation: Possibilities and challenges," *Current Opinion in Biotechnology*, vol. 38, pp. 190–197, 2016.

[35] M. Wang, Z. Li, X. Fang, L. Wang, and Y. Qu, "Cellulolytic enzyme production and enzymatic hydrolysis for second-generation bioethanol production," *Advances in Biochemical Engineering/Biotechnology*, vol. 128, pp. 1–24, 2012.

[36] T. Werpy and G. Petersen, "Top Value Added Chemicals from Biomass: Volume I – Results of Screening for Potential Candidates from Sugars and Synthesis Gas," Tech. Rep. DOE/GO-102004-1992, 2004.

[37] J. E. Holladay, J. F. White, J. J. Bozell, and D. Johnson, "Top Value-Added Chemicals from Biomass - Volume II—Results of Screening for Potential Candidates from Biorefinery Lignin," Tech. Rep. PNNL-16983, 2007.

[38] R. Arora, N. K. Sharma, and S. Kumar, "Valorization of By-Products Following the Biorefinery Concept: Commercial Aspects of By-Products of Lignocellulosic Biomass," in *Advances in Sugarcane Biorefinery*, pp. 163–178, Elsevier, 2018.

[39] W. M. A. M. Anku, M. A. Mamo, and P. P. Govender, "Phenolic Compounds in Water: Sources, Reactivity, Toxicity and Treatment Methods," in *Phenolic Compounds in Water: Sources, Reactivity, Toxicity and Treatment Methods. , Phenolic Compounds - Natural Sources, Importance and Applications*, Phenolic Compounds - Natural Sources, Importance and Applications, 2017.

[40] L. M. Divya, G. K. Prasanth, and C. Sadasivan, "Potential of the salt-tolerant laccase-producing strain Trichoderma viride Pers. NFCCI-2745 from an estuary in the bioremediation of phenol-polluted environments," *Journal of Basic Microbiology*, vol. 54, no. 6, pp. 542–547, 2014.

[41] O. A. Carrijo, R. S. Liz, and N. Makishima, "Fibra da casca do coco verde como substrato agrícola," *Horticultura Brasileira*, vol. 20, no. 4, pp. 533–535, 2002.

[42] S. Sun, S. Sun, X. Cao, and R. Sun, "The role of pretreatment in improving the enzymatic hydrolysis of lignocellulosic materials," *Bioresource Technology*, vol. 199, pp. 49–58, 2016.

[43] M. Galbe and G. Zacchi, "Pretreatment: the key to efficient utilization of lignocellulosic materials," *Biomass & Bioenergy*, vol. 46, pp. 70–78, 2012.

[44] N. Sarkar, S. K. Ghosh, S. Bannerjee, and K. Aikat, "Bioethanol production from agricultural wastes: an overview," *Journal of Renewable Energy*, vol. 37, no. 1, pp. 19–27, 2012.

[45] Y. Sun and J. Cheng, "Hydrolysis of lignocellulosic materials for ethanol production: a review," *Bioresource Technology*, vol. 83, no. 1, pp. 1–11, 2002.

[46] E. D. Albuquerque, F. A. G. Torres, A. A. R. Fernandes, and P. M. B. Fernandes, "Combined effects of high hydrostatic pressure and specific fungal cellulase improve coconut husk hydrolysis," *Process Biochemistry*, vol. 51, no. 11, pp. 1767–1775, 2016.

[47] A. Fatmawati and R. Agustriyanto, "Kinetic study of enzymatic hydrolysis of acid-pretreated coconut coir," in *Proceedings of the 2nd International Conference of Chemical and Material Engineering: Green Technology for Sustainable Chemical Products and Processes, ICCME 2015*, Indonesia, September 2015.

[48] J. Soares, M. M. Demeke, M. Van de Velde et al., "Fed-batch production of green coconut hydrolysates for high-gravity second-generation bioethanol fermentation with cellulosic yeast," *Bioresource Technology*, vol. 244, pp. 234–242, 2017.

[49] M. M. S. Cabral, A. K. D. S. Abud, C. E. D. F. Silva, and R. M. R. G. Almeida, "Bioethanol production from coconut husk fiber," *Ciência Rural*, vol. 46, no. 10, pp. 1872–1877, 2016.

[50] J. Soares, M. M. Demeke, M. R. Foulquié-Moreno et al., "Green coconut mesocarp pretreated by an alkaline process as raw material for bioethanol production," *Bioresource Technology*, vol. 216, pp. 744–753, 2016.

[51] C. K. C. de Araújo, A. de Oliveira Campos, C. E. de Araújo Padilha et al., "Enhancing enzymatic hydrolysis of coconut husk through Pseudomonas aeruginosa AP 029/GLVIIA rhamnolipid preparation," *Bioresource Technology*, vol. 237, pp. 20–26, 2017.

[52] T.-Y. Ding, S.-L. Hii, L.-G.-A. Ong, and T.-C. Ling, "Investigating the Potential of Using Coconut Husk as Substrate for

Bioethanol Production," in *Proceedings of the 2011 International Conference on Biotechnology and Environment Management (ICBEM 2011)*, Singapore, 2011.

[53] T. Y. Ding, S. L. Hii, and L. G. A. Ong, "Comparison of pretreatment strategies for conversion of coconut husk fiber to fermentable sugars," *Bioresources*, vol. 7, no. 2, pp. 1540–1547, 2012.

[54] M. Ebrahimi, A. R. Caparanga, E. E. Ordono, and O. B. Villaflores, "Evaluation of organosolv pretreatment on the enzymatic digestibility of coconut coir fibers and bioethanol production via simultaneous saccharification and fermentation," *Journal of Renewable Energy*, vol. 109, pp. 41–48, 2017.

[55] Y. Yu, X. Lou, and H. Wu, "Some recent advances in hydrolysis of biomass in hot-compressed water and its comparisons with other hydrolysis methods," *Energy & Fuels*, vol. 22, no. 1, pp. 46–60, 2008.

[56] A. K. Chandel, G. Chandrasekhar, M. B. Silva, and S. Silvério Da Silva, "The realm of cellulases in biorefinery development," *Critical Reviews in Biotechnology*, vol. 32, no. 3, pp. 187–202, 2012.

[57] I. S. Druzhinina and C. P. Kubicek, "Genetic engineering of Trichoderma reesei cellulases and their production," *Microbial Biotechnology*, vol. 10, no. 6, pp. 1485–1499, 2017.

[58] A. V. Gusakov, "Cellulases and hemicellulases in the 21st century race for cellulosic ethanol," *Biofuels*, vol. 4, no. 6, pp. 567–569, 2013.

[59] D. B. Wilson, "Cellulases and biofuels," *Current Opinion in Biotechnology*, vol. 20, no. 3, pp. 295–299, 2009.

[60] J. Zhuang, M. A. Marchant, S. E. Nokes, and H. J. Strobel, "Economic Analysis of Cellulase Production Methods for Bio-Ethanol," *Applied Engineering in Agriculture*, vol. 23, no. 5, pp. 679–687, 2007.

[61] J. M. Prado, T. Forster-Carneiro, M. A. Rostagno, L. A. Follegatti-Romero, F. Maugeri Filho, and M. A. A. Meireles, "Obtaining sugars from coconut husk, defatted grape seed, and pressed palm fiber by hydrolysis with subcritical water," *The Journal of Supercritical Fluids*, vol. 89, pp. 89–98, 2014.

[62] J. M. Prado, R. Vardanega, G. C. Nogueira et al., "Valorization of Residual Biomasses from the Agri-Food Industry by Subcritical Water Hydrolysis Assisted by CO2," *Energy & Fuels*, vol. 31, no. 3, pp. 2838–2846, 2017.

[63] P. Vaithanomsat, W. Apiwatanapiwat, N. Chumchuent, W. Kongtud, and S. Sundhrarajun, "Possibility of Ethanol Production from Coconut Husk Using Separate Hydrolysis and Fermentation and Simultaneous Saccharification and Fermentation," in *Proceedings of the 48th University Annual Conference*, Kasetsart University, Bangkok, Thailand, 2010.

[64] C. Kasavi, I. Finore, L. Lama et al., "Evaluation of industrial *Saccharomyces cerevisiae* strains for ethanol production from biomass," *Biomass & Bioenergy*, vol. 45, pp. 230–238, 2012.

[65] J. C. Fay and J. A. Benavides, "Evidence for domesticated and wild populations of saccharomyces cerevisiae," *PLoS Genetics*, vol. 1, no. 1, pp. 0066–0071, 2005.

[66] N. Fu and P. Peiris, "Co-fermentation of a mixture of glucose and xylose to ethanol by Zymomonas mobilis and Pachysolen tannophilus," *World Journal of Microbiology and Biotechnology*, vol. 24, no. 7, pp. 1091–1097, 2008.

[67] S. H. Cho, R. Lei, T. D. Henninger, and L. M. Contreras, "Discovery of ethanol-responsive small RNAs in Zymomonas mobilis," *Applied and Environmental Microbiology*, vol. 80, no. 14, pp. 4189–4198, 2014.

[68] M. M. Demeke, F. Dumortier, Y. Li, T. Broeckx, M. R. Foulquié-Moreno, and J. M. Thevelein, "Combining inhibitor tolerance and D-xylose fermentation in industrial Saccharomyces cerevisiae for efficient lignocellulose-based bioethanol production," *Biotechnology for Biofuels*, vol. 6, no. 1, 2013.

[69] T. W. Jeffries and Y.-S. Jin, "Metabolic engineering for improved fermentation of pentoses by yeasts," *Applied Microbiology and Biotechnology*, vol. 63, no. 5, pp. 495–509, 2004.

[70] Y. Kobayashi, T. Sahara, T. Suzuki et al., "Genetic improvement of xylose metabolism by enhancing the expression of pentose phosphate pathway genes in Saccharomyces cerevisiae IR-2 for high-temperature ethanol production," *Journal of Industrial Microbiology and Biotechnology*, vol. 44, no. 6, pp. 879–891, 2017.

[71] J. G. Nijland, E. Vos, H. Y. Shin, P. P. De Waal, P. Klaassen, and A. J. M. Driessen, "Improving pentose fermentation by preventing ubiquitination of hexose transporters in Saccharomyces cerevisiae," *Biotechnology for Biofuels*, vol. 9, no. 1, 2016.

[72] D. Moysés, V. Reis, J. Almeida, L. Moraes, and F. Torres, "Xylose Fermentation by Saccharomyces cerevisiae: Challenges and Prospects," *International Journal of Molecular Sciences*, vol. 17, no. 3, p. 207, 2016.

[73] H. Valadi, C. Larsson, and L. Gustafsson, "Improved ethanol production by glycerol-3-phosphate dehydrogenase mutants of Saccharomyces cerevisiae," *Applied Microbiology and Biotechnology*, vol. 50, no. 4, pp. 434–439, 1998.

[74] C. Navarrete, J. Nielsen, and V. Siewers, "Enhanced ethanol production and reduced glycerol formation in fps1△ mutants of Saccharomyces cerevisiae engineered for improved redox balancing," *AMB Express*, vol. 4, no. 1, pp. 1–8, 2014.

[75] W. Ye, W. Zhang, T. Liu, G. Tan, H. Li, and Z. Huang, "Improvement of Ethanol Production in Saccharomyces cerevisiae by High-Efficient Disruption of the ADH2 Gene Using a Novel Recombinant TALEN Vector," *Frontiers in Microbiology*, vol. 7, 2016.

[76] T.-S. Cao, Z. Chi, G.-L. Liu, and Z.-M. Chi, "Expression of TPS1 gene from Saccharomycopsis fibuligera A11 in Saccharomyces sp. W0 enhances trehalose accumulation, ethanol tolerance, and ethanol production," *Molecular Biotechnology*, vol. 56, no. 1, pp. 72–78, 2014.

[77] Z. Qiu and R. Jiang, "Improving Saccharomyces cerevisiae ethanol production and tolerance via RNA polymerase II subunit Rpb7," *Biotechnology for Biofuels*, vol. 10, no. 1, 2017.

[78] L. Paulová, P. Patáková, M. Rychtera, and K. Melzoch, "High solid fed-batch SSF with delayed inoculation for improved production of bioethanol from wheat straw," *Fuel*, vol. 122, pp. 294–300, 2014.

[79] K. Öhgren, J. Vehmaanperä, M. Siika-Aho, M. Galbe, L. Viikari, and G. Zacchi, "High temperature enzymatic prehydrolysis prior to simultaneous saccharification and fermentation of steam pretreated corn stover for ethanol production," *Enzyme and Microbial Technology*, vol. 40, no. 4, pp. 607–613, 2007.

[80] A. A. Modenbach and S. E. Nokes, "The use of high-solids loadings in biomass pretreatment-a review," *Biotechnology and Bioengineering*, vol. 109, no. 6, pp. 1430–1442, 2012.

[81] A. A. Modenbach and S. E. Nokes, "Enzymatic hydrolysis of biomass at high-solids loadings - A review," *Biomass & Bioenergy*, vol. 56, pp. 526–544, 2013.

[82] H. Jørgensen, J. B. Kristensen, and C. Felby, "Enzymatic conversion of lignocellulose into fermentable sugars: challenges and opportunities," *Biofuels, Bioproducts and Biorefining*, vol. 1, no. 2, pp. 119–134, 2007.

[83] J. B. Kristensen, C. Felby, and H. Jørgensen, "Yield-determining factors in high-solids enzymatic hydrolysis of lignocellulose," *Biotechnology for Biofuels*, vol. 2, article 11, 2009.

[84] X. Ma, G. Yue, J. Yu, X. Zhang, and T. Tan, "Enzymatic hydrolysis of cassava bagasse with high solid loading," *Journal of Biobased Materials and Bioenergy*, vol. 5, no. 2, pp. 275–281, 2011.

[85] M. J. Selig, S. Viamajala, S. R. Decker, M. P. Tucker, M. E. Himmel, and T. B. Vinzant, "Deposition of lignin droplets produced during dilute acid pretreatment of maize stems retards enzymatic hydrolysis of cellulose," *Biotechnology Progress*, vol. 23, no. 6, pp. 1333–1339, 2007.

[86] C. A. Cardona, J. A. Quintero, and I. C. Paz, "Production of bioethanol from sugarcane bagasse: status and perspectives," *Bioresource Technology*, vol. 101, no. 13, pp. 4754–4766, 2010.

[87] T. L. Bezerra and A. J. Ragauskas, "A review of sugarcane bagasse for second-generation bioethanol and biopower production," *Biofuels, Bioproducts and Biorefining*, vol. 10, no. 5, pp. 634–647, 2016.

[88] F. Talebnia, D. Karakashev, and I. Angelidaki, "Production of bioethanol from wheat straw: an overview on pretreatment, hydrolysis and fermentation," *Bioresource Technology*, vol. 101, no. 13, pp. 4744–4753, 2010.

[89] Y. Zhao, A. Damgaard, and T. H. Christensen, "Bioethanol from corn stover – a review and technical assessment of alternative biotechnologies," *Progress in Energy and Combustion Science*, vol. 67, pp. 275–291, 2018.

[90] T. Eggeman and R. T. Elander, "Process and economic analysis of pretreatment technologies," *Bioresource Technology*, vol. 96, no. 18, pp. 2019–2025, 2005.

[91] A. Aden and T. Foust, "Technoeconomic analysis of the dilute sulfuric acid and enzymatic hydrolysis process for the conversion of corn stover to ethanol," *Cellulose*, vol. 16, no. 4, pp. 535–545, 2009.

[92] S. Chovau, D. Degrauwe, and B. Van Der Bruggen, "Critical analysis of techno-economic estimates for the production cost of lignocellulosic bio-ethanol," *Renewable & Sustainable Energy Reviews*, vol. 26, pp. 307–321, 2013.

[93] L. Zhao, X. Zhang, J. Xu, X. Ou, S. Chang, and M. Wu, "Techno-economic analysis of bioethanol production from lignocellulosic biomass in china: Dilute-acid pretreatment and enzymatic hydrolysis of corn stover," *Energies*, vol. 8, no. 5, pp. 4096–4117, 2015.

[94] H. Chen and X. Fu, "Industrial technologies for bioethanol production from lignocellulosic biomass," *Renewable & Sustainable Energy Reviews*, vol. 57, pp. 468–478, 2016.

[95] E. Gnansounou and A. Dauriat, "Techno-economic analysis of lignocellulosic ethanol: A review," *Bioresource Technology*, vol. 101, no. 13, pp. 4980–4991, 2010.

[96] J. Littlewood, L. Wang, C. Turnbull, and R. J. Murphy, "Techno-economic potential of bioethanol from bamboo in China," *Biotechnology for Biofuels*, vol. 6, no. 1, 2013.

[97] S. Macrelli, J. Mogensen, and G. Zacchi, "Techno-economic evaluation of 2nd generation bioethanol production from sugar cane bagasse and leaves integrated with the sugar-based ethanol process," *Biotechnology for Biofuels*, vol. 5, no. 1, 2012.

[98] S. H. Duque, C. A. Cardona, and J. Moncada, "Techno-economic and environmental analysis of ethanol production from 10 agroindustrial residues in Colombia," *Energy & Fuels*, vol. 29, no. 2, pp. 775–783, 2015.

[99] J. A. Quintero, J. Moncada, and C. A. Cardona, "Techno-economic analysis of bioethanol production from lignocellulosic residues in Colombia: A process simulation approach," *Bioresource Technology*, vol. 139, pp. 300–307, 2013.

[100] F. R. Schmidt, "Optimization and scale up of industrial fermentation processes," *Applied Microbiology and Biotechnology*, vol. 68, no. 4, pp. 425–435, 2005.

[101] L. R. Formenti, A. Nørregaard, A. Bolic et al., "Challenges in industrial fermentation technology research," *Biotechnology Journal*, vol. 9, no. 6, pp. 727–738, 2014.

[102] E. de Jong and G. Jungmeier, "Biorefinery Concepts in Comparison to Petrochemical Refineries," *Industrial Biorefineries White Biotechnology*, p. 33, 2015.

[103] F. Cherubini, G. Jungmeier, M. Wellisch et al., "Toward a common classification approach for biorefinery systems," *Biofuels, Bioproducts and Biorefining*, vol. 3, no. 5, pp. 534–546, 2009.

[104] J. Larragoiti-Kuri, M. Rivera-Toledo, J. Cocho-Roldán, K. Maldonado-Ruiz Esparza, S. Le Borgne, and L. Pedraza-Segura, "Convenient Product Distribution for a Lignocellulosic Biorefinery: Optimization through Sustainable Indexes," *Industrial & Engineering Chemistry Research*, vol. 56, no. 40, pp. 11388–11397, 2017.

[105] R. Parajuli, T. Dalgaard, U. Jørgensen et al., "Biorefining in the prevailing energy and materials crisis: A review of sustainable pathways for biorefinery value chains and sustainability assessment methodologies," *Renewable & Sustainable Energy Reviews*, vol. 43, pp. 244–263, 2015.

[106] T. M. Carole, J. Pellegrino, and M. D. Paster, "Opportunities in the industrial biobased products industry," *Applied Biochemistry and Biotechnology—Part A Enzyme Engineering and Biotechnology*, vol. 115, no. 1–3, pp. 871–885, 2004.

[107] A. A. Koutinas, C. Du, R. H. Wang, and C. Webb, "Production of Chemicals from Biomass," *Introduction to Chemicals from Biomass*, pp. 77–101, 2008.

[108] C. R. Somerville and D. Bonetta, "Plants as factories for technical materials," *Plant Physiology*, vol. 125, no. 1, pp. 168–171, 2001.

[109] M. K. D. Rambo, F. L. Schmidt, and M. M. C. Ferreira, "Analysis of the lignocellulosic components of biomass residues for biorefinery opportunities," *Talanta*, vol. 144, pp. 696–703, 2015.

[110] K. Ding, Y. Le, G. Yao et al., "A rapid and efficient hydrothermal conversion of coconut husk into formic acid and acetic acid," *Process Biochemistry*, 2018.

[111] G. E. Gopi E , Saleem M, "Experimental Results of Coconut Shell Polymer Matrix Composites," *International Journal of Mechanical and Production Engineering Research and Development*, vol. 7, no. 6, pp. 163–170, 2017.

[112] S. Kocaman, M. Karaman, M. Gursoy, and G. Ahmetli, "Chemical and plasma surface modification of lignocellulose coconut waste for the preparation of advanced biobased composite materials," *Carbohydrate Polymers*, vol. 159, pp. 48–57, 2017.

[113] A. Bhatnagar, V. J. P. Vilar, C. M. S. Botelho, and R. A. R. Boaventura, "Coconut-based biosorbents for water treatment-A review of the recent literature," *Advances in Colloid and Interface Science*, vol. 160, no. 1-2, pp. 1–15, 2010.

Hindawi
BioMed Research International
Volume 2018, Article ID 9167508, 7 pages
https://doi.org/10.1155/2018/9167508

*Research Article*

# Neural Network Prediction of Corn Stover Saccharification Based on Its Structural Features

**Le Gao, Shulin Chen, and Dongyuan Zhang**

*Tianjin Key Laboratory for Industrial Biological Systems and Bioprocessing Engineering, Tianjin Institute of Industrial Biotechnology, Chinese Academy of Sciences, Tianjin, China*

Correspondence should be addressed to Dongyuan Zhang; zhang_dy@tib.cas.cn

Received 16 January 2018; Revised 4 April 2018; Accepted 31 May 2018; Published 12 August 2018

Academic Editor: Ningbo Gao



The classic assay for a large population biomass is time-consuming, labor intensive, and chemically expensive. This paper would find out a rapid assay for predicting biomass digestibility from biomass structural features without hydrolysis. We examined the 62 representative corn stover accessions that displayed a diverse cell-wall composition and varied biomass digestibility. Correlation analysis was firstly to detect effects of cell-wall compositions and wall polymer features on corn stover digestibility. Based on the dependable relationship of structural features and digestibility, a neural networks model has been developed and successfully predicted the corn stover saccharification based on the features without enzymatic hydrolysis. The actual measured and net-simulated predicted corn stover saccharification had good results as mean square error of 1.80E-05, coefficient of determination of 0.942 and average relative deviation of 3.95. The trained networks satisfactorily predicted the saccharification results based on the features of corn stover. Predicting the corn stover saccharification without hydrolysis will reduce capital and operational costs for corn stover purchasing and storage.

## 1. Introduction

Bioethanol production from lignocellulosic materials has drawn worldwide attention due to the concern about depletion of fossil fuel. In China, corn stover is one of the most common agricultural residues and can be used as feedstock to produce fuel ethanol because of its abundance, high carbohydrate content, and low cost.

As the second generation of biofuels, corn stover conversion into bioethanol principally involves three major steps: physical and chemical pretreatments for cell-wall disassociation, enzymatic digestion towards soluble sugar release, and yeast fermentation resulting in ethanol production [1]. In this process, corn stover saccharification is the critical step due to its complex structures and recalcitrance [2]. Many factors such as cell-wall compositions, wall network styles, and wall polymer features affect the corn stover digestibility [3]. For example, plant cell walls are mainly composed of cellulose, hemicelluloses, and lignin. Cellulose is a long chain of glucose molecules linked to one another primarily by glycosidic bonds [4]. Cellulose makes up about 30% of the dry mass of primary cell walls and up to 40% of the secondary cell walls. The hydrogen bonds between different layers of polysaccharides and the van der Waals forces between the parallel chains contribute to the crystalline structure of cellulose. The cellulose crystalline regions alternate with amorphous regions [5, 6]. The crystalline index (CrI) and hydrogen-bond intensity (HBI) have been characterized as the major features that affect biomass enzymatic hydrolysis in plants [7]. Lignin is associated with cellulose or hemicellulose to form a cell-wall network that is extremely recalcitrant for enzyme penetration and degradation [8]. Lignin is composed of three major phenolic components: *p*-coumaryl alcohol (H), coniferyl alcohol (G), and sinapyl alcohol (S) [9]. The efficiency of biomass saccharification during biofuel production is strongly affected not only by the total amount of lignin but also by the lignin monomer composition in plants [10].

Because of the heterogeneous nature of corn stover and many factors affecting corn stover hydrolysis, corn stover digestibility only can be measured by saccharification with a high enzyme loading for at least 72 h. It would require a significant resource investment in order to analyze a large

number of samples. Therefore, the classic assay for corn stover digestibility is time-consuming, labor intensive, and chemically expensive and appears to be unsuitable for screening of large population samples [11]. Therefore, development of a rapid prediction of corn stover digestibility based on cell-wall features became more imperative. Understanding lignocellulosic features and their effects on corn stover saccharification is scientifically important for the prediction model development. This study exploited the relationship between the key determinants of plant walls and corn stover enzymatic digestion. In this paper, an artificial neural network (ANN) has been developed and successfully predicted the corn stover saccharification based on the corn stover features without enzymatic hydrolysis. This was accomplished by supplying the networks with both inputs (i.e., biomass structural features) and outputs (i.e., experimental measured saccharification from 62 corn stover samples). Successfully predicting biomass digestibility from structural features is highly valuable for the rapid assessment corn stovers, thus reducing the saccharification cost. This work will provide a way for the pricing of corn stover purchasing and storage in the future of biomass energy industry.

## 2. Material and Method

*2.1. Plant Materials.* The corn stover samples were typically selected from accessions collected in China. The samples were harvested from an experimental field in Jinan. The mature stem tissues were collected and dried tissues were ground through a 60-mesh screen and stored in a dry container until use.

*2.2. Plant Cell-Wall Components Analysis.* The cellulose and hemicelluloses contents of corn stover were quantitatively analyzed according to the NREL Laboratory Analytical Procedures (NREL, 2006) for biomass using a two-step acid method [12]. Glucan and xylan contents were calculated according to (1) and (2), where factors of 0.9 and 0.88 reflect the weight loss in converting glucose into glucan and xylose into xylan, respectively [13]. Acid-soluble lignin and acid-insoluble lignin were determined according to Chinese standard methods [13].

$$\text{Glucan content (\%)} = \frac{\text{Glucose released from acid hydrolysis (mg)} \times 0.9}{\text{Samples weight (mg)}} \times 100\%. \quad (1)$$

$$\text{Xylan content (\%)} = \frac{\text{Xylose released from acid hydrolysis (mg)} \times 0.88}{\text{Samples weight (mg)}} \times 100\% \quad (2)$$

*2.3. FT-IR Spectroscopy and X-Ray Diffraction (XRD) Analysis.* The sample was dried at -20°C at 24 h by vacuum dryer (FD-IC-50, Beijing). Infrared spectra were determined using an FT-IR 710 infrared spectrophotometer (Nicolet, Madison, WI). A total of 100 scans with a 2 $cm^{-1}$ resolution were signal-averaged and stored; the wave number range scanned was 4000-400 $cm^{-1}$.The ratio of absorbance at 4000-2995 $cm^{-1}$ to those at 1337 $cm^{-1}$ of C-OH in-plane stretching was introduced as empirical criterion of hydrogen-bond intensity (HBI) [13].

$$\text{HBI} = \frac{\text{Absorbance (4000 - 2995 cm-1)}}{\text{Absorbance (1337cm-1)}}. \quad (3)$$

The crystallinity of samples was examined by XRD measurements performed on a Bruker D8 Advance Diffractometer using Cu K$\alpha$ radiation ($\lambda$=0.1541 nm) at 30 kV and 30 mA. The sample was scanned, and the intensity was recorded in 2$\theta$ range from 10 to 80°.

To compare the intensity difference and determine the pretreatment effect, the CrI of the corn stover was calculated by referring to the diffraction intensities of the crystalline area and amorphous region using the following:

$$\text{CrI} = \frac{I_{002} - I_{am}}{I_{002}}. \quad (4)$$

*2.4. Fourier Transform Raman (FT-Raman) Spectroscopy.* To evaluate S/G ratios by FT-Raman spectroscopy, a recently developed spectral deconvolution method was used [14]. Raman spectra were collected from samples using a Bruker MultiRAM FT-Raman spectrometer with 1064 nm excitation (Bruker Optics, Inc., Billerica, MA). Laser power of 50 mW and scan number of 256 were used at a spectral resolution of 4 $cm^{-1}$. The acquired spectra were mildly smoothed and the spectral range of 1220–1530 $cm^{-1}$ was selected and baseline corrected using OPUS software (Bruker Optics, Inc.). The spectra were then deconvoluted at medium sensitivity using OMNIC software (Thermo Fisher Scientific, Inc., Waltham, MA). For each spectrum, S/G and H/G ratios were calculated as intensity ratio of the resolved target peaks (1331 $cm^{-1}$ for S, 1270 $cm^{-1}$ for G, and 1215 $cm^{-1}$ for H) [14, 15].

*2.5. Analysis of Biomass Enzymatic Digestibility.* The biomass was subjected to the enzymatic hydrolysis by cellulase at 50°C for 72 h in triplicate. Hydrolysis experiments were conducted in 50 mL Erlenmeyer flasks with a total working volume of 20 mL while maintaining the substrate concentration of 5% (w/v). The enzyme loading was 20 FPU/g substrate. 0.5% $NaN_3$ was added To the reaction mixtures to prevent microbial contamination. The samples were removed at regular intervals, and the supernatants were boiled to denature the enzyme activity and filtered through a 0.22 $\mu$m filter for glucose content analysis. After hydrolysis was completed, the residues were separated from liquid by centrifugation, decantation, and filtration. Glucose in enzymatic-hydrolysis liquor was measured by high performance liquid chromatography (HPLC) (Shimadzu, Kyoto, Japan) with a refractive index detector (Shimadzu) on an Aminex HPX-87H column (Bio-Rad, Hercules, CA, USA) run at a flow rate of 0.6 mL/min at 60°C, with 5 mM $H_2SO_4$ as mobile phase [13].

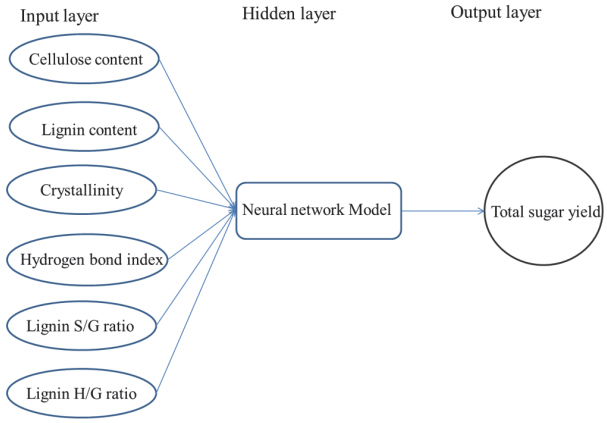


Figure 1: General framework of the model-based approach used in neural network model and to optimize the enzymatic-hydrolysis results of corn stover.

*2.6. Statistical Calculation of Correlation Coefficients.* Correlation coefficients were generated by performing regression analysis for all pairs of measured traits across the whole population. The analysis used average values calculated from all original determinations for a given traits pair.

*2.7. Artificial Neural Network.* An artificial neural network, analogous to the behavior of biological neural structure, is an effective empirical modeling tool in approximating nonlinear functions, pattern recognition, and classification problems [16]. Neural networks perform the correlation without requiring a mathematical description of how the output depends on the input, which gives neural networks a key advantage over traditional approaches to function estimation. Instead, neural networks learn from examples of input-output data sets supplied to them [17].

The fitting of the experimental data was performed in MATLAB using the neural network toolbox available in MATLAB (MathWorks, Natick, MA, USA). A multilayer feed-forward backpropagation neural network was the framework chosen for 18 networks. A neural network is an array of nodes linked by connections. The neural network model in this paper was the general regression neural network (GRNN). GRNN was a form of ANN. This GRNN creates a multilayer network. The first layer has radbas neurons and calculates weighted inputs with dist and net input with netprod. The second layer has purelin neurons and calculates weighted input with normprod and net inputs with netsum. There are six neurons in the input layer, namely, cellulose content, lignin content, CrI, HBI, S/G, and H/G. Hidden layers are employed to perform complex and nonlinear functions on the network (Figure 1). The neurons number in the hidden layer was the sample number. The relative weight of each input factor was the transposition of each input value. Lower values of MSE indicate better suitability of the model. After correct simulation on test points based on the MSE and correlation coefficient ($R^2$), training was then performed on all data. After training the ANN using the training data set, validation data was used to evaluate the performance of the training based on the ability to correctly predict/simulate the validation data. The total sugar yield released from corn stover was used in the output layer. The data set used for training the GRNN model contains 62 input/output patterns. We simplified the modeling process. 76% of all samples are taken up for training and 24% of all samples for testing the model. The goal of training a network is to minimize the error between the actual outputs and the network outputs, called a training algorithm. The network outputs are compared to the actual target values until the square error is satisfied.

The mean square error (MSE) was minimized by making adjustments to the network parameters, namely, error goal, maximum number of iterations, validation checks, etc. In order to further evaluate the prediction performance, mean square error (MSE) coefficient of determination ($R^2$) and average relative deviation (ARD) were utilized as the index of the prediction error of a batch:

$$\begin{aligned} MSE &= \frac{1}{n} \\ &\quad \cdot \sum_{i=1}^{n} \left(actual\ determined\ value_i - predicted\ value_i\right)^2. \\ ARD &= \frac{100}{n} \\ &\quad \times \sum_{i=1}^{n} \left| \frac{predicted\ value_i - actual\ determined\ value_i}{actual\ determined\ value_i} \right| \\ R^2 &= 1 \\ &\quad - \frac{\sum_{i=1}^{n} \left(predicted\ value_i - actual\ determined\ value_i\right)^2}{\sum_{i=1}^{n} \left(predicted\ value_i - \overline{actual\ determined\ value}\right)^2} \end{aligned} \tag{5}$$

Lower values of MSE indicate better suitability of the model. Figure 1 shows the general framework of the neural network model used in this study. The cellulose content, lignin content, CrI, HBI, S/G, and H/G were taken as the input vectors to the model, whereas the total sugar yield released from corn stover were the output vectors. The purpose of developing such a model is to obtain the optimum sugar yield upon varying input parameters.

## 3. Results and Discussion

*3.1. Analysis of Cell-Wall Composition in Corn Stover.* Considering natural corn stover accessions include various ecological types and genetic germplasms, 62 representative corn stover samples that showed a large variation of plant cell-wall composition were selected. The cell-wall polymer composition of corn stover was analyzed (Figure 2). A diverse cell-wall composition (cellulose, hemicellulose, and lignin) was observed between different corn stover samples. The coefficient of variation (CV) values for cellulose, hemicellulose, and lignin were 21.67%, 11.47%, and 8.53%, respectively. The cellulose content of 62 corn stover samples were ranging from 23.50% to 45.17% (% dry matter), hemicellulose ranging from 19.86% to 31.33%, lignin ranging from 6.29% to 14.82%. The contents of cellulose, hemicellulose, and lignin also were

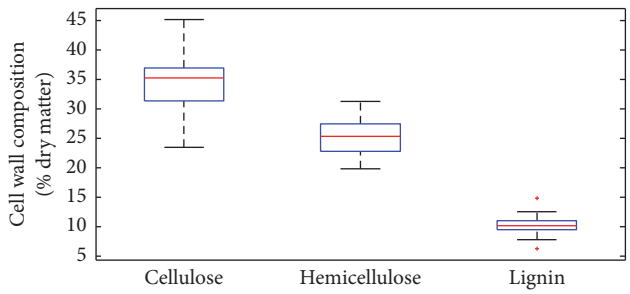


Figure 2: Variation of cell-wall composition of corn stover samples (n=62). The line and square in the box presented the median and mean values of all data; the bottom and top edges of the box indicated 25 and 75 percentiles of all data, respectively; and the bottom and top bars presented maximum and minimum values of all data, respectively.

significantly different. The large variation on cell-wall polymer composition offers a possibility of analyzing correlation of cell-wall composition with biomass saccharification. A previously described [18] biomass saccharification was defined by accounting the total sugar yield (hexose and pentose / dry weight) from enzymatic hydrolysis. In this current study, we determined the total sugar yield released from enzymatic hydrolysis in the total 62 corn stover accessions. The selected corn stover samples showed a great variation of biomass saccharification. The diversity of corn stover and saccharification can provide the possibility for analysis of the effects of cellulose features on biomass saccharification.

*3.2. Effects of Cell-Wall Composition on Corn Stover Enzymatic Digestibility.* Due to the diverse compositions of plant cell walls, the 62 corn stover samples exhibited largely varied biomass digestibility. Correlation analysis was performed between cellulose and lignin content from 62 corn stover samples and enzymatic saccharification rate (Figure 3). As a result, the cellulose level showed positive correlation with the glucose yield from 62 corn stovers. The correlation $R^2$ value between the cellulose content and corn stover saccharification was 0.4219, while the correlation $R^2$ value between the lignin content and corn stover saccharification was 0.4068.

*3.3. Effects of Wall Polymers on Corn Stover Enzymatic Digestibility.* The cellulose microfibrils have both crystalline and amorphous regions, and the crystallinity is given by the relative amounts of these two regions. The major part of cellulose (around 2/3 of the total cellulose) is in the crystalline form. It was shown that cellulase readily hydrolyzes the more accessible amorphous portion of cellulose, while the enzyme is not so effective in degrading the less accessible crystalline portion. The 62 corn stover samples exhibited largely varied crystalline. A correlation analysis was performed to ascertain the distinct impacts of biomass features on biomass saccharification. CrI is customarily detected using raw biomass materials and has briefly been reported as a negative factor on biomass digestibility [19]. The correlation $R^2$ values between the CrI and corn stover saccharification was 0.7072, which suggested that CrI showed a significantly negative correlation (Figure 3). Decreasing the crystallinity of corn stover could result in the increase of digestibility of lignocelluloses. Lower CrI would offer favorable access of cellulase to the substrate and higher biomass digestibility (Pei et al., 2016). This finding is consistent with several reports [20]. However, there has been also opposite results on correlation between crystallinity and enzymatic hydrolysis. Grethlein [21] pretreated hardwood and softwood by mild acid hydrolysis and determined their pore size distribution. It was shown that the crystallinity index has no relationship to the rate of hydrolysis. Kim and Holtzapple [22] found that the degree of crystallinity of corn stover slightly increased from 43% to 60% through delignification with calcium hydroxide, which was related to removal of amorphous components (lignin and hemicellulose). However, an increase in crystallinity of pretreated materials did not negatively affect the yield of enzymatic hydrolysis. Fan et al. [23] studied the effect of ball milling on surface area and crystallinity of cellulose. They observed an increase in crystallinity of cellulose by reducing the size of cellulose by milling. It is believed that recrystallization during water swelling may increase the crystallinity of highly ball-milled cellulose. There are two conflicting opinions that are caused by analytical methods for crystallinity. The crystallinity of pretreated biomass increased relatively by decrease in amorphous portion, e.g., lignin and hemicellulose. Maybe the most significant limitation is that they did not address the potential cross effects between structural features that may have occurred during pretreatment. Most pretreatments alter several structural features simultaneously. Studies that alter targeted structural features while ignoring the effect on nontargeted features may result in misleading information. Therefore the correlation between crystallinity and enzymatic hydrolysis could not be explained just by relative crystalline index. In this paper, it may be more correct to analyze the correlation between crystallinity and corn stover saccharification which was analyzed for raw corn stover.

The hydrogen-bond intensity (HBI) is a property specific to cellulose, considering the chain mobility and bond distance; the HBI of cellulose is closely related to the crystal system and degree of intermolecular regularity, *i.e.*, crystallinity [24]. The correlation $R^2$ values between the HBI and corn stover CrI was 0.55. Therefore, the correlation $R^2$ values between the HBI and corn stover saccharification was 0.6969, which suggested that HBI, like the CrI, showed a significantly negative correlation (Figure 3). Decreasing the HBI of corn stover could result in the increase of digestibility of lignocelluloses.

*3.4. Correlation of Monolignin with Corn Stover Saccharification.* Given the structural diversity and chemical heterogeneity of lignin, evaluation lignin effect on biomass digestibility could be difficult [25]. The efficiency of corn stover saccharification is strongly affected not only by the total amount of lignin but also by the lignin monomer composition in plants. Determination of the relative abundance of the lignin

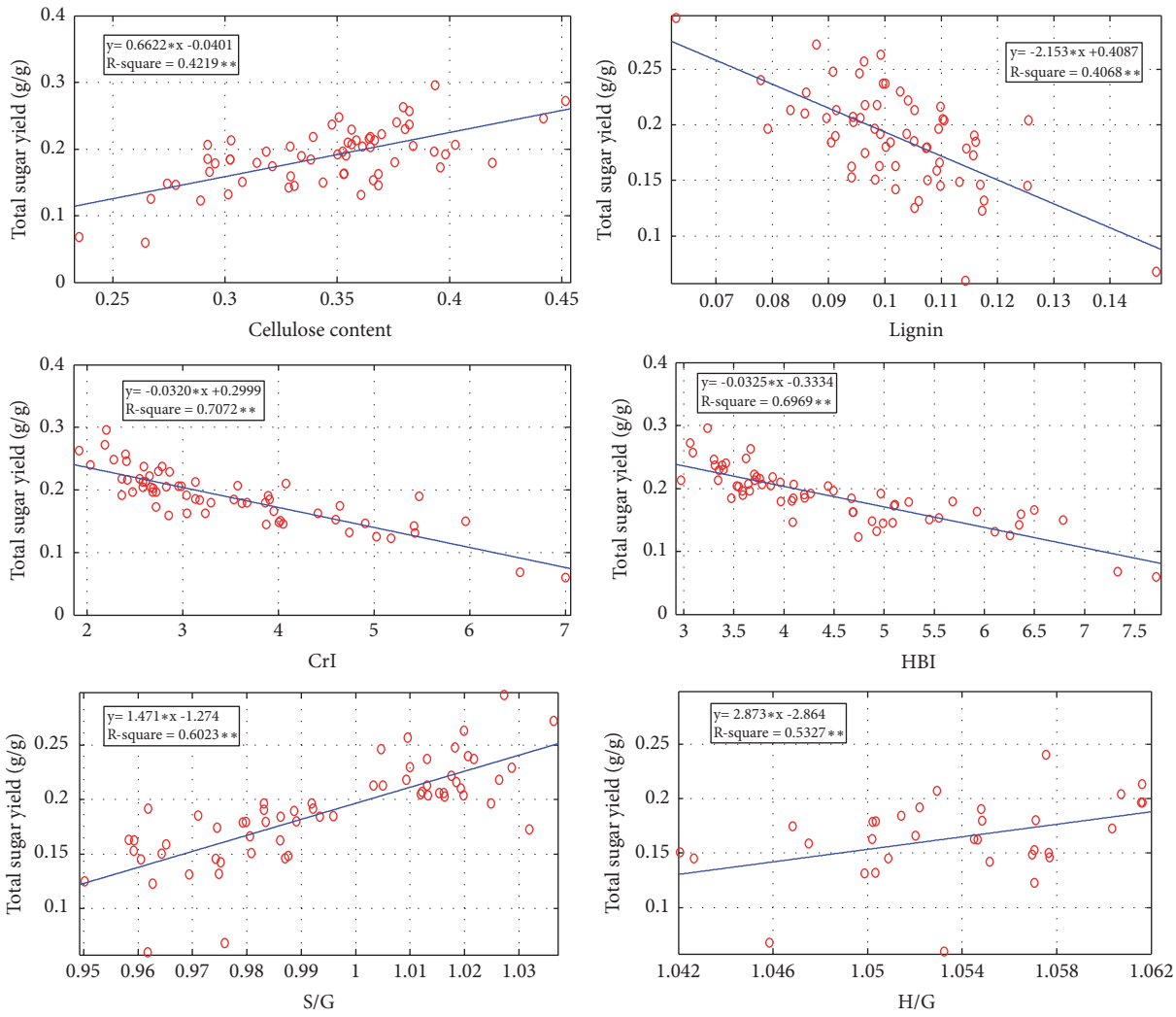


FIGURE 3: Correlation analysis between cell-wall composition (cellulose content, lignin content) / cell-wall features (CrI, HBI, S/G, H/G) of corn stover and enzymatic saccharification (n=62).

monomers, particularly the S/G ratio and H/G ratio, is very important to fundamentally elucidate lignin structure [11]. The S/G and H/G have been determined by FT-Raman spectroscopy. The corn stover samples with high saccharification displayed relatively higher H/G values. The correlation $R^2$ values between the H/G and corn stover saccharification was 0.5327, which suggested that H/G ratio had a possible positive correlation with corn stover saccharification (Figure 3). This result was consistent with the previous report that is the first time report of H/G as a positive factor in biomass enzymatic saccharification in wheat and rice [3]. On the other hand, although S/G has been reported as a negative factor in *Miscanthus* and other plants [18], the corn stover samples in this paper exhibited different result. The correlation $R^2$ value between the S/G and corn stover saccharification was 0.6023, which suggested that S/G showed a possible positive correlation in corn stover saccharification. To understand the positive effect of S/G on corn stover saccharification, we further performed correlation analyses between S/G and CrI in the 62 corn stover accessions. Surprisingly, the corn stovers with high S/G ratios were found to have relatively higher cellulose CrI values. The possible negative correlation $R^2$ value between the S/G and corn stover CrI was 0.4623. It suggested that S monomer may have a different interlinking with wall polymers. The exact crossing network between cellulose, hemicellulose, and lignin is far from clear [26]. With the knowledge now we could only tentatively speculate that the lignin monomers might be more important for cellulose-hemicellulose-lignin network and secondary cell-wall recalcitrance. The S monomer may have a different interlinking with wall polymers [18], which could reduce cellulose network.

*3.5. Building the Neutral Network Model for Predicting.* The 62 corn stover samples contained the following structural features: cellulose content, lignin content, crystallinity, HBI, S/G ratio, and H/G ratio, respectively. The wide spectrum of

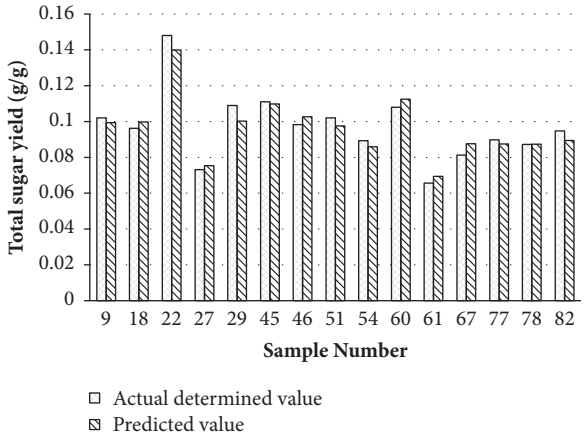


Figure 4: Comparison of the predicted value with the actual determined value of corn stovers saccharification.

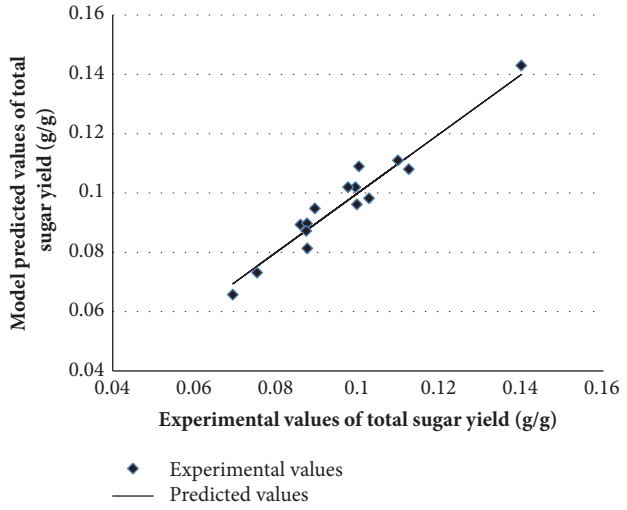


Figure 5: Experimental validation of model predicted total sugar yields. Comparison of neural network model predicted and experimental total sugar yields.

structural features made it possible to develop reliable empirical models to predict biomass digestibility from structural features. The neutral network model has been trained and built on the features of 62 corn stover samples through rolling learning-prediction approach. The selection of the most appropriate parameters for ANN modeling is considered of paramount importance for prediction of the hydrolysis process [27]. In the present work, to test the prediction capabilities of the neural network model, the predicted values obtained from the model are compared with the experimental values. The coefficient of determination ($R^2$) and the average relative deviation (ARD) were 0.942 and 3.95, respectively (Table 1). The average of MSE of the net-simulated outputs of glucose released from corn stover samples features is 1.80E-05, which lies near zero. The $R^2$ value of testing set was found to approach unity which confirms the reliability of the model in predicting the total sugar yield. Net-simulated outputs of total sugars released from 15 corn stover samples

Table 1: Performance of neural network model.

| Statistical parameter | Value |
|---|---|
| $R^2$ | 0.942 |
| MSE | 1.80E-05 |
| ARD | 3.95 |

features were compared with measured values as shown in Figure 4. It is evident that the relative error between experimentally observed and model predicted values is very low. Performance of the model in describing the correlation between experimental and predicted total sugar yield are shown in Figure 5. The results showed that the neural network model has predictions that are closer to the line of perfect prediction. The agreement in measured and net-simulated slopes and intercepts indicated the trained networks satisfactorily predicted the saccharification results based on the features of corn stover. It has been reported in literature that ANNs are flexible as new data can be added anytime giving fitting [27].

## 4. Conclusions

Based on the structural features and saccharification of a large number of corn stover samples, a neural networks model has been developed and was demonstrated applicable for the prediction of the corn stover saccharification based on the features without enzymatic hydrolysis. The predicted value of corn stover digestibility via this model was very similar with the actual determined value of corn stover saccharification. This neural network model could offer the fast approach for bioenergy crops selection. In the future, the neural network model will have good application for corn stover storage and evaluation, which will be cost-effective and time-saving.

## Data Availability

The data used to support the findings of this study are available from the corresponding author upon request.

## Conflicts of Interest

The authors declare that they have no conflicts of interest regarding the publication of this paper.

## Acknowledgments

This work was supported by the National Key Research and Development Program of China (2016YFD0501405).

## Supplementary Materials

**Supplemental Table.1**: the compositions and wall polymer features of the samples for training. **Supplemental Table.2**: the compositions and wall polymer features of the samples for testing. *(Supplementary Materials)*

## References


[1] E. M. Rubin, "Genomics of cellulosic biofuels," *Nature*, vol. 454, no. 7206, pp. 841–845, 2008.

[2] M. E. Himmel, S. Ding, D. K. Johnson et al., "Biomass recalcitrance: engineering plants and enzymes for biofuels production," *Science*, vol. 315, no. 5813, pp. 804–807, 2007.

[3] Z. Wu, M. Zhang, L. Wang et al., "Biomass digestibility is predominantly affected by three factors of wall polymer features distinctive in wheat accessions and rice mutants," *Biotechnology for Biofuels*, vol. 6, no. 1, p. 183, 2013.

[4] T. Arioli, L. C. Peng, A. S. Betzner et al., "Molecular analysis of cellulose biosynthesis in *Arabidopsis*," *Science*, vol. 279, no. 5351, pp. 717–720, 1998.

[5] P. Bansal, M. Hall, M. J. Realff, J. H. Lee, and A. S. Bommarius, "Multivariate statistical analysis of X-ray data from cellulose: A new method to determine degree of crystallinity and predict hydrolysis rates," *Bioresource Technology*, vol. 101, no. 12, pp. 4461–4471, 2010.

[6] J.-Y. Park, M. Kang, J. S. Kim, J.-P. Lee, W.-I. Choi, and J.-S. Lee, "Enhancement of enzymatic digestibility of Eucalyptus grandis pretreated by NaOH catalyzed steam explosion," *Bioresource Technology*, vol. 123, pp. 707–712, 2012.

[7] Y.-H. P. Zhang and L. R. Lynd, "Toward an aggregated understanding of enzymatic hydrolysis of cellulose: noncomplexed cellulase systems," *Biotechnology and Bioengineering*, vol. 88, no. 7, pp. 797–824, 2004.

[8] K. E. Achyuthan, A. M. Achyuthan, P. D. Adams et al., "Supramolecular self-assembled chaos: Polyphenolic lignin's barrier to cost-effective lignocellulosic biofuels," *Molecules*, vol. 15, no. 12, pp. 8641–8688, 2010.

[9] J. Ralph, K. Lundquist, G. Brunow et al., "Lignins: Natural polymers from oxidative coupling of 4-hydroxyphenyl-propanoids," *Phytochemistry Reviews*, vol. 3, no. 1-2, pp. 29–60, 2004.

[10] M. Baucher, M. A. Bernard-Vailhé, B. Chabbert et al., "Down-regulation of cinnamyl alcohol dehydrogenase in transgenic alfalfa (*Medicago sativa* L.) and the effect on lignin composition and digestibility," *Plant Molecular Biology*, vol. 39, no. 3, pp. 437–447, 1999.

[11] J. Huang, T. Xia, A. Li et al., "A rapid and consistent near infrared spectroscopic assay for biomass enzymatic digestibility upon various physical and chemical pretreatments in Miscanthus," *Bioresource Technology*, vol. 121, pp. 274–281, 2012.

[12] B. H. A. Sluiter, R. Ruiz, and C. Scarlata, "Determination of structural carbohydrates and lignin in biomass," *NREL/TP-510-42618*, pp. 510–42618, 2008.

[13] L. Gao, D. Li, F. Gao et al., "Hydroxyl radical-aided thermal pretreatment of algal biomass for enhanced biodegradability," *Biotechnology for Biofuels*, vol. 8, no. 1, 2015.

[14] L. Sun, P. Varanasi, F. Yang, D. Loqué, B. A. Simmons, and S. Singh, "Rapid determination of syringyl: Guaiacyl ratios using FT-Raman spectroscopy," *Biotechnology and Bioengineering*, vol. 109, no. 3, pp. 647–656, 2012.

[15] G. Papa, P. Varanasi, L. Sun et al., "Exploring the effect of different plant lignin content and composition on ionic liquid pretreatment efficiency and enzymatic saccharification of Eucalyptus globulus L. mutants," *Bioresource Technology*, vol. 117, pp. 352–359, 2012.

[16] O. Giustolisi, "Sparse solution in training artificial neural networks," *Neurocomputing*, vol. 56, no. 1-4, pp. 285–304, 2004.

[17] J. P. O'Dwyer, L. Zhu, C. B. Granda, V. S. Chang, and M. T. Holtzapple, "Neural network prediction of biomass digestibility based on structural features," *Biotechnology Progress*, vol. 24, no. 2, pp. 283–292, 2008.

[18] N. Xu, W. Zhang, S. Ren et al., "Hemicelluloses negatively affect lignocellulose crystallinity for high biomass digestibility under NaOH and H2SO4 pretreatments in Miscanthus," *Biotechnology for Biofuels*, vol. 5, no. 1, p. 58, 2012.

[19] W. Zhang, Z. Yi, J. Huang et al., "Three lignocellulose features that distinctively affect biomass enzymatic digestibility under NaOH and H2SO4 pretreatments in Miscanthus," *Bioresource Technology*, vol. 130, pp. 30–37, 2013.

[20] K. Grohmann, D. J. Mitchell, M. E. Himmel, B. E. Dale, and H. A. Schroeder, "The role of ester groups in resistance of plant cell wall polysaccharides to enzymatic hydrolysis," *Applied Biochemistry and Biotechnology*, vol. 20-21, no. 1, pp. 45–61, 1989.

[21] H. E. Grethlein, "The effect of pore size distribution on the rate of enzymatic hydrolysis of cellulosic substrates," *Bio/Technology*, vol. 3, no. 2, pp. 155–160, 1985.

[22] S. Kim and M. T. Holtzapple, "Effect of structural features on enzyme digestibility of corn stover," *Bioresource Technology*, vol. 97, no. 4, pp. 583–591, 2006.

[23] M.-Q. Fan, F. Xu, and L.-X. Sun, "Studies on hydrogen generation characteristics of hydrolysis of the ball milling Al-based materials in pure water," *International Journal of Hydrogen Energy*, vol. 32, no. 14, pp. 2809–2815, 2007.

[24] R. Gaur, R. Agrawal, R. Kumar et al., "Evaluation of recalcitrant features impacting enzymatic saccharification of diverse agricultural residues treated by steam explosion and dilute acid," *RSC Advances*, vol. 5, no. 75, pp. 60754–60762, 2015.

[25] Y. Pei, Y. Li, Y. Zhang et al., "G-lignin and hemicellulosic monosaccharides distinctively affect biomass digestibility in rapeseed," *Bioresource Technology*, vol. 203, pp. 325–333, 2016.

[26] H. V. Scheller and P. Ulvskov, "Hemicelluloses," *Annual Review of Plant Biology*, vol. 61, no. 1, pp. 263–289, 2010.

[27] R. Gama, J. S. Van Dyk, M. H. Burton, and B. I. Pletschke, "Using an artificial neural network to predict the optimal conditions for enzymatic hydrolysis of apple pomace," *3 Biotech*, vol. 7, no. 2, 2017.

Hindawi
BioMed Research International
Volume 2018, Article ID 1897280, 6 pages
https://doi.org/10.1155/2018/1897280

*Research Article*

# The Effects of Different Oxytetracycline and Copper Treatments on the Performance of Anaerobic Digesters and the Dynamics of Bacterial Communities

**Yun Zhang,[1] Xin Ke,[2] Wei Sun,[2] Guangcai Zhang,[1] Xiaodan Gao,[1] Haijun Zhang,[2] and Weiyun Wang[2]**

[1]*Northeast Key Laboratory of Arable Land Conservation and Improvement, Ministry of Agriculture, National Engineering Laboratory for Efficient Utilization of Soil and Fertilizer Resources, College of Land and Environment, Shenyang Agricultural University, Shenyang 110866, China*
[2]*College of Energy and Environment, Shenyang Aerospace University, Shenyang 110136, China*

Correspondence should be addressed to Guangcai Zhang; guangcaizhang@syau.edu.cn and Weiyun Wang; cathywwy@sau.edu.cn

Received 24 October 2017; Revised 27 April 2018; Accepted 21 May 2018; Published 5 July 2018

Academic Editor: Zhang Lei



Oxytetracycline and copper are the common residues in animal manures. Meanwhile, anaerobic digestion is considered as a clean biotechnology for the disposal of animal manures. In this paper, the performance of anaerobic digesters and the dynamics of bacterial communities under the different treatments of oxytetracycline and copper were discussed. The parameters of methane production and pH values were studied to reflect the performance of anaerobic digester. Results showed that the changes of methane production and pH values were not obvious compared with the control. This means that the treatments of oxytetracycline and copper almost have no effects on the performance of anaerobic digesters. This phenomenon might be due to the chelation reaction between oxytetracycline and copper. This chelation reaction might reduce the toxicity of oxytetracycline. The study on the dynamics of bacterial communities was based on the polymerase chain reaction-denaturing gradient gel electrophoresis (PCR-DGGE) method. Results indicated that the bacterial communities had significant differences under the different treatments of oxytetracycline and copper. Uncultured *Bacteroidetes* bacterium (CU922272.1) and uncultured *Bacteroidetes* bacterium (AB780945.1) showed adaptability to the different treatments of oxytetracycline and copper and were the dominant bacterial communities.

## 1. Introduction

With the development of livestock, the residual antibiotics and heavy metals in animal manure have attracted more and more world-wide attention. This residual phenomenon is due to the low bioavailability of antibiotics and heavy metals which are widely added to the feeds in order to control diseases and enhance the growth of livestock animals [1–4]. Heuer et al. [5] found that 30–90% of the antibiotics as feeding additives were excreted through urine and manures. The residual metals in manure were also considerable [6, 7]. Oxytetracycline and copper are the common residues in animal manures. It was found that the residual oxytetracycline in cow manure ranged from 0.32 mg/kg to 59.59 mg/kg [8]. The residual copper could reach up to 481.5 mg/kg in cattle manures [9]. These residual antibiotics and heavy metals can cause the potential threats to environment. Therefore, it is necessary to find appropriate methods to solve the problems of residual oxytetracycline and copper in animal manure.

Animal manures belong to the organic wastes. The common methods of the disposal of manure include aerobic composting and anaerobic digestion [10–12]. Compared to other methods, anaerobic digestion belongs to a clean biotechnology which can produce biogas [13]. Meanwhile, the use of biogas can reduce the consumption of fossil fuels and the emissions of greenhouse gases [14, 15]. The residual digestate after anaerobic digestion can be used as an improved fertilizer [16].

Table 1: Different treatments of oxytetracycline and copper in the laboratory-scale anaerobic digesters.

| Treatments | Oxytetracycline dry weight (mg/kg) | Copper (dose as $CuSO_4$) dry weight (mg/kg) |
|---|---|---|
| A1 | 20 | 100 |
| A2 | 20 | 200 |
| A3 | 20 | 300 |
| B1 | 50 | 100 |
| B2 | 50 | 200 |
| B3 | 50 | 300 |
| C1 | 100 | 100 |
| C2 | 100 | 200 |
| C3 | 100 | 300 |
| Control | 0 | 0 |

The performance of anaerobic digester can be reflected by methane production and pH values [17, 18]. Furthermore, anaerobic digestion is considered to be a biological process which involves many classes of bacteria. It consists of four stages: hydrolysis, acidogenesis, acetogenesis, and methanogenesis [19, 20]. Bacterial communities show dynamics during the process of anaerobic digestion. Bouallagui et al. [21] studied the dynamics of bacterial communities in a two-phase anaerobic bioreactor. They found that the species composition of bacterial communities had very significant changes during the process of anaerobic digestion. Patil et al. [22] studied the dynamics of microbial community via polymerase chain reaction-denaturing gradient gel electrophoresis (PCR-DGGE) and found that *Firmicutes* and uncultured bacteria were the dominant genera in the mesophilic digesters treating with piggery wastewater. However, there is still short of the study on the dynamics of bacterial communities under the treatments of oxytetracycline and copper during anaerobic digestion.

The objectives of this study were to evaluate the performance of anaerobic digesters and discuss the dynamics of bacterial communities under the treatments of oxytetracycline and copper during the anaerobic digestion of cow manure. Methane production and pH values were measured and analyzed to reflect the performance of anaerobic digestion. Furthermore, the PCR-DGGE method was used to discuss the dynamics of bacterial communities.

## 2. Materials and Methods

*2.1. Experimental Set-Up and Analytical Methods.* Cow manure samples were taken from the surrounding countryside Shenyang City, China. Then the samples were stored in a refrigerator at 4°C before used. The physical and chemical properties of samples were as follows: total solids, 25.67%; pH value, 8.26; volatile organic acids, 878.4 mg $l^{-1}$; and organic carbon, 42.75%. Laboratory-scale anaerobic digesters (1 L) were prepared. Then each digester was added with 200 g cow manure. Different amounts of oxytetracycline and copper (dose as $CuSO_4$) were added to each digester (Table 1). In this experiment, the fermentation broth of digested cow manure was used as the inoculum. Each anaerobic digester was inoculated with 200 ml inoculum, then continuously stirred, and maintained at a mesophilic condition of 37°C in a water bath. All the experiments were performed in triplicate. Methane production was measured by gas chromatography (GC-14B, Shimadzu, Japan). The pH values were determined using a hand-held pH meter.

*2.2. DNA Extraction and PCR-DGGE.* Total genomic DNA of manure samples was extracted on days 1, 15, and 50, respectively. In this experiment, the primers 341F with 40 bp GC-clamps and 907R were used for the polymerase chain reaction amplification [23]. The operations of DNA extraction and PCR-DGGE were carried out as the previous study [24], but with some modifications that the electrophoresis was performed in a 7 L 1×TAE buffer at 60°C for 6 h at 180 V in this experiment.

*2.3. Sequencing and Phylogenetic Analysis.* The selected DGGE bands were reamplified and electrophoresed to confirm the mobility and then transported to Beijing Huada Gene Company (Beijing, China) for sequencing. Through the CLUSTAL X and MEGA 4.0, the phylogenetic tree was built via the neighbor-joining method [25].

*2.4. Nucleotide Sequence Accession Numbers.* Nucleotide sequences were deposited in the NCBI nucleotide sequence databases to get the accession numbers: KM491540-KM491545.

## 3. Results and Discussion

*3.1. The Performance of Anaerobic Digesters*

*3.1.1. Methane Production.* Methane production under the different treatments of oxytetracycline and copper is present in Figure 1. The highest methane production under treatments A1, A2, A3, B1, B3, B4, C1, C2, C3, and the control was 331.9 ml (day 15), 399.5 ml (day 10), 556.2 ml (day 10), 371.7 ml (day 15), 510.5 ml (day 10), 360.5 ml (day 10), 399.5 ml (day 10), 460.3 ml (day 10), 516.8 ml (day 10),

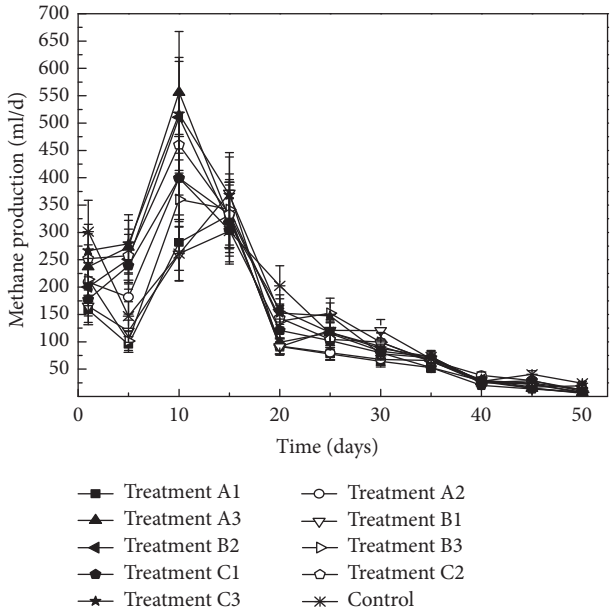


Figure 1: Variations of methane production with time under different oxytetracycline and copper treatments.

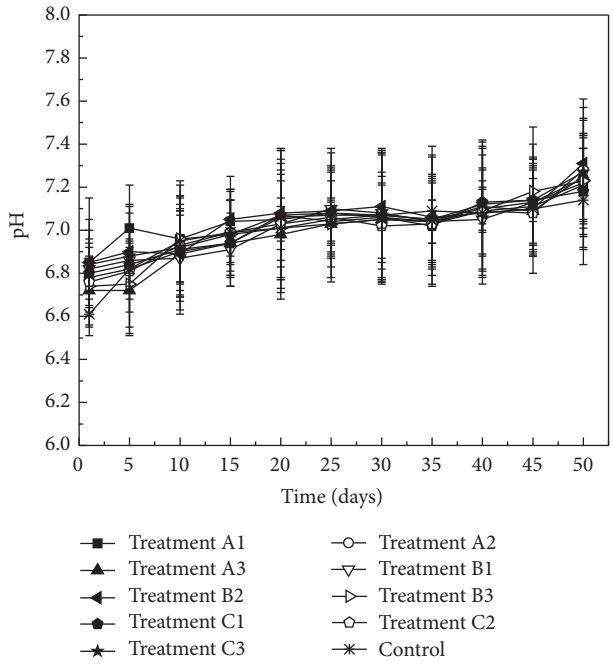


Figure 2: Variations of pH value with time under different oxytetracycline and copper treatments.

and 302.7 ml (day 15), respectively. At the first five days, the process of anaerobic digestion was not stable. Then the methane production increased until the 10th day. Compared with the control, the curve of methane production had nonsignificant differences after the 25th day. This might be caused by the chelation reaction between oxytetracycline and copper. Pouliquen and Le Bris [26] found that oxytetracycline was likely to form complexes with mineral cations. Moreover, Hassan et al. [27] reported that oxytetracycline could form the copper-oxytetracycline chelates. Previous studies had found that oxytetracycline had inhibition on methane production during the anaerobic digestion [28, 29]. However, the chelation reaction between oxytetracycline and copper might reduce the toxicity of oxytetracycline. Therefore, the treatments of oxytetracycline and copper had little effect on the methane production.

*3.1.2. The pH Values.* The changes of pH values during the anaerobic digestion are shown in Figure 2. The pH values under all treatments ranged from 6.61 to 7.31. This range belongs to the optimal pH values to produce maximal biogas yield. Throughout the process of anaerobic digestion, pH values gradually increased. This might be due to the continuous stirring which could make cow manure continued dissolution. The highest pH values which were all present at the end of the anaerobic digestion were 7.21 (treatment A1), 7.24 (treatment A2), 7.25 (treatment A3), 7.22 (treatment B1), 7.31 (treatment B2), 7.23 (treatment B3), 7.18 (treatment C1), 7.28 (treatment C2), 7.27 (treatment C3), and 7.14 (control). As is shown in Figure 2, the pH values under all treatments did not present significant differences compared with the control. This means that the treatments of oxytetracycline and copper almost have no significant effects on the pH values during the process of anaerobic digestion of cow manure.

*3.2. Dynamics of Bacterial Communities.* Dynamics of bacterial communities under the different treatments of oxytetracycline and copper are present via the DGGE fingerprints in Figure 3. The DGGE band patterns showed significant differences and clear changes under different treatments. Bands H1, H2, and H4 were detected at day 10. However, they disappeared at day 50. Band H3 could only be observed at day 50. Bands H5 and H6 were present under all the treatments of oxytetracycline and copper during the whole process of anaerobic digestion. They were the dominant bacterial communities.

Although band H5 was not shown at the control DGGE bands of day 1, it appeared at the control DGGE bands of day 10 and day 50. In contrast, band H6 was shown at all DGGE bands. This indicated that band H6 seemed to play as the functional bacteria. Through the sequence similarity analysis by the BLAST program, these six bacterial sequences were conducted by homology comparison (Table 2). The phylogenetic tree was established in Figure 4. Results showed that Band H2 had 98% similarity to uncultured bacterium (KJ853330.1). Band 4 was closely related to *Acidovorax* sp. (JQ912595.1). Hoshino et al. [30] found that *Acidovorax* sp. played an important role in denitrification. Band 3 had high similarity to uncultured *Cytophagales* bacterium (HQ692035.1). Band H1 shared 95% similarity with *Porphyromonadaceae* bacterium (HQ133063.1). These three kinds of bacteria all could be detected in the anaerobic digestion [31, 32]. Band H5 had 99% similarity to uncultured *Bacteroidetes* bacterium (CU922272.1). Band H6 was closely related to uncultured *Bacteroidetes* bacterium (AB780945.1). Riviere et al. [33] reported that uncultured *Bacteroidetes* bacterium (CU922272.1) existed in the mesophilic anaerobic digestion

Table 2: Closest relatives of the bacterial 16S-rRNA gene sequences.

| DGGE band | Closest GenBank Relative (accession number) | Sequence homology (%) | Accession Number |
|---|---|---|---|
| H1 | *Porphyromonadaceae* bacterium (HQ133063.1) | 95% | KM491540 |
| H2 | Uncultured bacterium (KJ853330.1) | 98% | KM491541 |
| H3 | Uncultured *Cytophagales* bacterium (HQ692035.1) | 90% | KM491542 |
| H4 | *Acidovorax* sp. (JQ912595.1) | 99% | KM491543 |
| H5 | Uncultured *Bacteroidetes* bacterium (CU922272.1) | 99% | KM491544 |
| H6 | Uncultured *Bacteroidetes* bacterium (AB780945.1) | 98% | KM491545 |

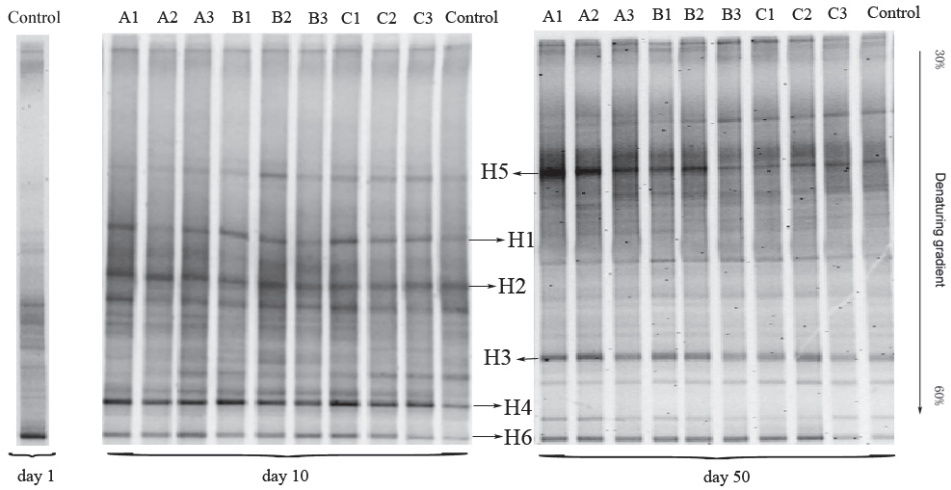


Figure 3: Denaturing gradient gel electrophoresis (DGGE) fingerprints of bacterial 16S-rRNA gene fragments of cow manure samples under different oxytetracycline and copper treatments at day 1, day 10, and day 50.

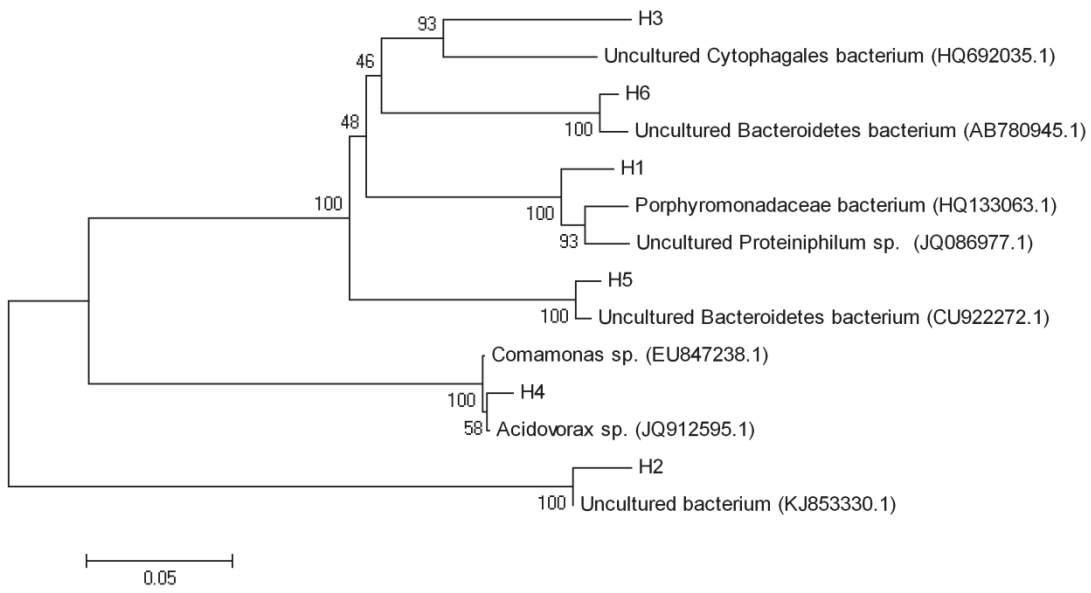


Figure 4: Phylogenetic tree of the bacterial 16S-rRNA gene sequences compared with known sequences from Genbank.

of municipal sewage sludge. Uncultured *Bacteroidetes* bacterium (AB780945.1) could be found in a full-scale mesophilic anaerobic completely stirred tank reactor during the anaerobic digestion of untreated corn straw [34].

In this experiment, it could be concluded that uncultured *Bacteroidetes* bacterium (CU922272.1) and uncultured *Bacteroidetes* bacterium (AB780945.1) showed adaptability to the different treatments of oxytetracycline and copper and were the dominant bacterial communities during the anaerobic digestion under the treatments of oxytetracycline and copper.

## 4. Conclusions

This study discussed the performance of anaerobic digesters and the dynamics of bacterial communities under different treatments of oxytetracycline and copper. Results indicated that methane production and pH values were hardly affected compared with the control. This might be due to the chelation reaction between oxytetracycline and copper. The reaction might reduce the toxicity of oxytetracycline. Meanwhile, uncultured *Bacteroidetes* bacterium (CU922272.1) and uncultured *Bacteroidetes* bacterium (AB780945.1) were the dominant bacterial communities during the anaerobic digestion under the treatments of oxytetracycline and copper. This research can help to optimize the performance of anaerobic digestion and the structure of bacterial community for increasing the biogas production and reducing the pollution of residues.

## Conflicts of Interest

The authors declare that there are no conflicts of interest.

## Acknowledgments

This study was supported by Agro-Scientific Research in the Public Interest (201503118-10), National Natural Science Foundation of China (41601230), and Postdoctoral Science Foundation (2017M611265).

## References

[1] M.-O. Aust, F. Godlinski, G. R. Travis et al., "Distribution of sulfamethazine, chlortetracycline and tylosin in manure and soil of Canadian feedlots after subtherapeutic use in cattle," *Environmental Pollution*, vol. 156, no. 3, pp. 1243–1251, 2008.

[2] N. Kemper, "Veterinary antibiotics in the aquatic and terrestrial environment," *Ecological Indicators*, vol. 8, no. 1, pp. 1–13, 2008.

[3] A. Bielicka, I. Bojanowska, and A. Wisniewski, "Two faces of chromium-pollutant and bioelement," *Polish Journal of Environmental Studies*, vol. 14, no. 5, 2005.

[4] Y.-G. Zhu, T. A. Johnson, J.-Q. Su et al., "Diverse and abundant antibiotic resistance genes in Chinese swine farms," *Proceedings of the National Acadamy of Sciences of the United States of America*, vol. 110, no. 9, pp. 3435–3440, 2013.

[5] H. Heuer, H. Schmitt, and K. Smalla, "Antibiotic resistance gene spread due to manure application on agricultural fields," *Current Opinion in Microbiology*, vol. 14, no. 3, pp. 236–243, 2011.

[6] J. Dach and D. Starmans, "Heavy metals balance in Polish and Dutch agronomy: Actual state and previsions for the future," *Agriculture, Ecosystems & Environment*, vol. 107, no. 4, pp. 309–316, 2005.

[7] M. Irshad, A. H. Malik, S. Shaukat, S. Mushtaq, and M. Ashraf, "Characterization of heavy metals in livestock manures," *Polish Journal of Environmental Studies*, vol. 22, no. 4, pp. 1257–1262, 2013.

[8] L. Zhao, Y. H. Dong, and H. Wang, "Residues of veterinary antibiotics in manures from feedlot livestock in eight provinces of China," *Science of the Total Environment*, vol. 408, no. 5, pp. 1069–1075, 2010.

[9] X. Ji, Q. Shen, F. Liu et al., "Antibiotic resistance gene abundances associated with antibiotics and heavy metals in animal manures and agricultural soils adjacent to feedlots in Shanghai; China," *Journal of Hazardous Materials*, vol. 235-236, pp. 178–185, 2012.

[10] A. Khalid, M. Arshad, M. Anjum, T. Mahmood, and L. Dawson, "The anaerobic digestion of solid organic waste," *Waste Management*, vol. 31, no. 8, pp. 1737–1744, 2011.

[11] R. Yazdani, M. A. Barlaz, D. Augenstein, M. Kayhanian, and G. Tchobanoglous, "Performance evaluation of an anaerobic/aerobic landfill-based digester using yard waste for energy and compost production," *Waste Management*, vol. 32, no. 5, pp. 912–919, 2012.

[12] R. Kulcu, "Composting of greenhouse tomato plant residues, wheat straw, and separated dairy manure, and the effect of free air space on the process," *Polish Journal of Environmental Studies*, vol. 23, no. 4, pp. 1341–1346, 2014.

[13] R. Kothari, V. V. Tyagi, and A. Pathak, "Waste-to-energy: A way from renewable energy sources to sustainable development," *Renewable & Sustainable Energy Reviews*, vol. 14, no. 9, pp. 3164–3170, 2010.

[14] K.-H. Kim, S. A. Jahan, and E. Kabir, "A review of diseases associated with household air pollution due to the use of biomass fuels," *Journal of Hazardous Materials*, vol. 192, no. 2, pp. 425–431, 2011.

[15] K. Starr, X. Gabarrell, G. Villalba, L. Talens, and L. Lombardi, "Life cycle assessment of biogas upgrading technologies," *Waste Management*, vol. 32, no. 5, pp. 991–999, 2012.

[16] P. Weiland, "Biogas production: current state and perspectives," *Applied Microbiology and Biotechnology*, vol. 85, no. 4, pp. 849–860, 2010.

[17] P. Illmer and G. Gstraunthaler, "Effect of seasonal changes in quantities of biowaste on full scale anaerobic digester performance," *Waste Management*, vol. 29, no. 1, pp. 162–167, 2009.

[18] M. N. Young, R. Krajmalnik-Brown, W. Liu, M. L. Doyle, and B. E. Rittmann, "The role of anaerobic sludge recycle in improving anaerobic digester performance," *Bioresource Technology*, vol. 128, pp. 731–737, 2013.

[19] P. V. Rao and S. S. Baral, "Attribute based specification, comparison and selection of feed stock for anaerobic digestion using MADM approach," *Journal of Hazardous Materials*, vol. 186, no. 2-3, pp. 2009–2016, 2011.

[20] F. Xu, J. Shi, W. Lv, Z. Yu, and Y. Li, "Comparison of different liquid anaerobic digestion effluents as inocula and nitrogen sources for solid-state batch anaerobic digestion of corn stover," *Waste Management*, vol. 33, no. 1, pp. 26–32, 2013.

[21] H. Bouallagui, M. Torrijos, J. J. Godon et al., "Microbial monitoring by molecular tools of a two-phase anaerobic bioreactor treating fruit and vegetable wastes," *Biotechnology Letters*, vol. 26, no. 10, pp. 857–862, 2004.

[22] S. S. Patil, M. S. Kumar, and A. S. Ball, "Microbial community dynamics in anaerobic bioreactors and algal tanks treating piggery wastewater," *Applied Microbiology and Biotechnology*, vol. 87, no. 1, pp. 353–363, 2010.

[23] G. Muyzer, E. C. de Waal, and A. G. Uitterlinden, "Profiling of complex microbial populations by denaturing gradient gel electrophoresis analysis of polymerase chain reaction-amplified genes coding for 16S rRNA," *Applied and Environmental Microbiology*, vol. 59, no. 3, pp. 695–700, 1993.

[24] X. Ke, C. Wang, R. Li, Y. Zhang, H. Zhang, and S. Gui, "Biomethane production and dynamics of microflora in response to copper treatments during mesophilic anaerobic digestion," *Waste Management & Research*, vol. 32, no. 8, pp. 726–732, 2014.

[25] K. Tamura, J. Dudley, M. Nei, and S. Kumar, "MEGA4: molecular evolutionary genetics analysis (MEGA) software version 4.0," *Molecular Biology and Evolution*, vol. 24, no. 8, pp. 1596–1599, 2007.

[26] H. Pouliquen and H. Le Bris, "Sorption of oxolinic acid and oxytetracycline to marine sediments," *Chemosphere*, vol. 33, no. 5, pp. 801–815, 1996.

[27] S. S. M. Hassan, M. M. Amer, and S. A. Ahmed, "Composition and stability constants of iron- and copper-oxytetracycline chelates," *Microchimica Acta*, vol. 84, no. 3-4, pp. 165–175, 1984.

[28] O. A. Arikan, L. J. Sikora, W. Mulbry, S. U. Khan, C. Rice, and G. D. Foster, "The fate and effect of oxytetracycline during the anaerobic digestion of manure from therapeutically treated calves," *Process Biochemistry*, vol. 41, no. 7, pp. 1637–1643, 2006.

[29] N. Beneragama, S. A. Lateef, M. Iwasaki, T. Yamashiro, and K. Umetsu, "The combined effect of cefazolin and oxytertracycline on biogas production from thermophilic anaerobic digestion of dairy manure," *Bioresource Technology*, vol. 133, pp. 23–30, 2013.

[30] T. Hoshino, T. Terahara, S. Tsuneda, A. Hirata, and Y. Inamori, "Molecular analysis of microbial population transition associated with the start of denitrification in a wastewater treatment process," *Journal of Applied Microbiology*, vol. 99, no. 5, pp. 1165–1175, 2005.

[31] H. D. Ariesyady, T. Ito, and S. Okabe, "Functional bacterial and archaeal community structures of major trophic groups in a full-scale anaerobic sludge digester," *Water Research*, vol. 41, no. 7, pp. 1554–1568, 2007.

[32] N. Krakat, S. Schmidt, and P. Scherer, "Potential impact of process parameters upon the bacterial diversity in the mesophilic anaerobic digestion of beet silage," *Bioresource Technology*, vol. 102, no. 10, pp. 5692–5701, 2011.

[33] D. Rivière, V. Desvignes, E. Pelletier et al., "Towards the definition of a core of microorganisms involved in anaerobic digestion of sludge," *The ISME Journal*, vol. 3, no. 6, pp. 700–714, 2009.

[34] J.-T. Qiao, Y.-L. Qiu, X.-Z. Yuan, X.-S. Shi, X.-H. Xu, and R.-B. Guo, "Molecular characterization of bacterial and archaeal communities in a full-scale anaerobic reactor treating corn straw," *Bioresource Technology*, vol. 143, pp. 512–518, 2013.

Hindawi
BioMed Research International
Volume 2018, Article ID 1913848, 11 pages
https://doi.org/10.1155/2018/1913848

*Research Article*

# The Migration and Transformation of Heavy Metals in Sewage Sludge during Hydrothermal Carbonization Combined with Combustion

**Meng Liu**,[1,2] **Yufeng Duan**,[1] **Kagiso Bikane**,[2] **and Liang Zhao**[3]

[1]*Key Laboratory of Energy Thermal Conversion and Control of Ministry of Education, Southeast University, Nanjing 210096, China*
[2]*Department of Chemical Engineering, Imperial College London, SW7 2AZ, UK*
[3]*College of Materials Science and Engineering, Nanjing Forestry University, Nanjing 210037, China*

Correspondence should be addressed to Meng Liu; lmubear@seu.edu.cn

Received 27 January 2018; Revised 16 April 2018; Accepted 5 June 2018; Published 27 June 2018

Academic Editor: Zhang Lei



The migration and transformation behaviors of heavy metals (HMs), including Cr, Mn, Ni, Cu, Zn, As, Cd, and Pb, during the hydrothermal carbonization (HTC) of sewage sludge (SS) were investigated. The immobilization of HMs during the combustion of solid residual (SR) produced from HTC of SS was also analyzed. With increasing HTC temperature and residence time, the majority of HMs (except As) accumulated in the SR. The residual rate of As in the SR decreased from 73.95% to 56.74% when the residence time was increased from 1h to 3h and reduced significantly from 73.95% to 37.48% when the temperature increased from 220∘C to 280∘C, implying that numerous arsenic compounds dissolved into liquid phase products. Although the HTC process has a positive influence on the transformation of HMs from weakly bound fractions to the more stable fractions, the exchangeable and reducible fractions of Mn, Zn, As, and Cd in the SR were still high. In addition, the leached amounts of Zn and As were high (14.61 and 6.16 mg/kg, respectively) and showed a high leaching risk to the environment. An increase in HTC temperature and residence time led to an increase of the residual rate of HMs in the combustion residual of SR, implying that the HTC process promotes the stabilization of HMs in the combustion process.

## 1. Introduction

Sewage sludge (SS) is a great potential energy resource and has attracted wide attention as a subject of research. However, it contains high concentrations of pollutants, including pathogenic bacteria, heavy metals (HMs), and toxic organic compounds [1, 2]. Various sludge-to-energy technologies, such as fertilization, anaerobic digestion, carbonization, pyrolysis, gasification, and combustion, have been developed for the recovery of useful energy from SS [3–6]. From the energetic, economic, and environmental points of view, combustion or co-combustion of SS with other solid waste using present equipment is a viable technique of dealing with the sludge instead of land-filling disposal [7]. However, the SS must be dehydrated to improve the net energy input during the combustion process. The dehydration process requires substantial amounts of heat, thereby increasing the economic burden. Hydrothermal carbonization (HTC) is a process whereby sludge can be converted into high-density solid fuel under mild temperatures and pressures [8–10]. In addition, waste heat from the HTC process can be used to preheat the raw materials and improve the recovery of energy [11, 12]. Zhao et al. [11] demonstrated that, under mild conditions (200°C, 30 min), energy recovery from sludge via the HTC process is more than 50%, showing better performance than the mechanical dewatering technology. During the HTC process, copious amounts of toxicity organics are decomposed and the contents of S, N, and Cl are reduced. Moreover, some HMs are stabilized in the solid residual (SR) [2, 13–18]. Therefore, HTC of SS for high-density and clean solid fuel preparation is a promising technology.

Influences of the HTC reaction conditions, including reaction time, temperature, and dewatering time, on the physicochemical properties of solid, liquid, and gas phase products have been widely investigated to explore the HTC

Table 1: Physicochemical characteristic of SS before and after HTC.

| Samples | Ultimate analysis/wt.% | | | | | Proximate analysis/wt.% | | | | HHV[2] (kJ/kg) | Moisture content of SR[3] (wt.%) | pH (WL) | $NH_4^+$-N (mg/L) (WL) |
|---|---|---|---|---|---|---|---|---|---|---|---|---|---|
| | $C_{ad}$ | $H_{ad}$ | $N_{ad}$ | $S_{ad}$ | $O_{ad}$[1] | $M_{ad}$ | $V_{ad}$ | $FC_{ad}$ | $A_{ad}$ | | | | |
| SS | 20.13 | 4.61 | 4.68 | 1.73 | 12.41 | 9.54 | 39.66 | 3.90 | 46.90 | 10.11 | - | ND | ND |
| SS-220-1h | 23.87 | 3.45 | 3.49 | 1.12 | 7.71 | 1.95 | 32.74 | 6.90 | 58.41 | 10.31 | 64.90 | 8.70 | 1734 |
| SS-220-2h | 23.21 | 3.06 | 2.95 | 1.44 | 5.57 | 1.86 | 28.86 | 7.37 | 61.91 | 9.78 | 62.50 | 8.90 | 1773 |
| SS-220-3h | 23.65 | 3.14 | 2.82 | 1.82 | 5.28 | 1.59 | 29.37 | 7.34 | 61.70 | 10.06 | 59.35 | 9.00 | 1825 |
| SS-250-1h | 25.26 | 2.93 | 2.32 | 1.36 | 1.85 | 1.54 | 26.61 | 7.11 | 64.74 | 10.67 | 52.30 | 9.20 | 2005 |
| SS-280-1h | 26.69 | 2.64 | 2.16 | 0.87 | 0.28 | 1.34 | 25.07 | 7.47 | 66.02 | 11.28 | 48.50 | 9.50 | 2245 |

[1] O(%)=100%-(C%+N%+H%+S+%M%+A%); ad-air dry basis.

[2] HHV, higher heating value. Calculated was according to Channiwala and Parikh [25].

[3] Moisture content of SR after filtration and before drying.

mechanism of SS [7–15]. Furthermore, the optimized operation conditions were also obtained from previous studies. In recent years, several researchers have studied the migration and transformation behaviors of HMs during the HTC of SS [2, 16–21]. They mainly focused on the three aspects of the transformation of HMs. (1) The redistribution of HMs in the solid and liquid phase products: after HTC process, most HMs in the SS accumulate in the SR whilst minute amounts of HMs are released into liquid phase products. Additionally, as the temperature is increased, the quantity of HMs released into liquid products increases due to the extraction and decomposition effects of organics and minerals materials. Shi et al. [17] demonstrated that the quantity of HMs released into liquid was only 1.3%, with Cr, Ni, and Cu constituting the largest portion of the released HMs at 200°C. However, Wang et al. [19] found that the quantity of HMs released into liquid phase products was lower than 19%. (2) The chemical fractions and speciation of HMs: although different HMs show different transformation behaviors of chemical fractions, the HTC process may have a positive effect on the migration of HMs from bioavailable fractions into the more stable fractions. Shi et al. [17] found that the concentrations of acid soluble/exchangeable and reducible fractions of HMs (Zn, Cd, Pb, Cr, Ni, and Cu) in the SR decreased whilst the residual fraction increased when the HTC temperature was increased. This suggested that the weaker bound fraction of HMs was transformed into the more stable bound fraction. However, Wang et al. [19] found that the acid soluble/exchangeable and reducible fractions of Zn, Ni, and Cd in the SR were high, presenting potential risk to the environment. (3) The changes in the leaching characteristics of HMs: after the HTC process, the leachable amounts and leaching rate of HMs were reduced, indicating a reduction of the leaching toxicity of HMs in the SR. However, the leaching percentages of Zn, Ni, and Cd in the SR were still high and showed a considerable risk to the environment [19]. From the aforementioned works, the HTC process reduces the toxicity and improves the stabilization of HMs in the SR, but the transformation behaviors of HMs is significantly different, even some HMs still pose a high risk to the environment after HTC process. Considering the difference in the properties of SS and the effect of operation conditions on the transformation of HMs, the detailed mechanism of HTC influences the distribution and chemical speciation transformation of HMs in the SS requires further investigation.

Combustion of SR produced from the HTC of SS is considered a promising approach to convert sludge to energy, particularly the cocombustion with other solid fuels [22–24]. After the HTC process, SR showed a lower activation energy and preexponential factor. More than 60% of nitrogen and sulfur within SS can be removed, making it suitable for use in the combustion equipment [14, 22]. The transformation and immobilization behaviors of HMs during the combustion of SR produced from HTC of SS are crucial for the reduction of HMs emissions in the combustion process. However, no related studies were reported. Researchers [19] have only investigated the transformation behaviors of HMs in the pyrolysis of SR produced from HTC of SS. They found that the ecotoxicity of HMs in the pyrolysis residual reduced and the HMs could be migrated from bioavailable fractions to the more stable fractions.

In this work, the HTC reaction temperatures and residence times are considered systematically to investigate the distribution and chemical speciation transformation behaviors of HMs in the HTC of SS. Additionally, the immobilization characteristics of HMs during the combustion of SR produced from HTC of SS were analyzed.

## 2. Experimental

*2.1. Materials.* Dewatered municipal SS with the moisture content of 84.5 wt.% was obtained from a wastewater treatment plant in Nanjing, China. All the samples were sealed in a glass beaker and kept in a refrigerator at 4°C. The fuel characteristics of air dry basis raw SS are shown in Table 1. Raw SS has a high ash content (46.9 wt.%), low fixed carbon content (3.9wt.%), and an HHV (10.11kJ/kg). Additionally, the elemental contents of C, H, N, S, and O are 20.13, 4.16, 4.68, 1.73, and 12.41 wt.%, respectively.

*2.2. Experiment Procedure of HTC.* All HTC experiments were carried out in a batch-type reactor with a volume of 1 L. The schematic of reactor is shown in Figure 1. The reactor was heated by an electric furnace and the reaction

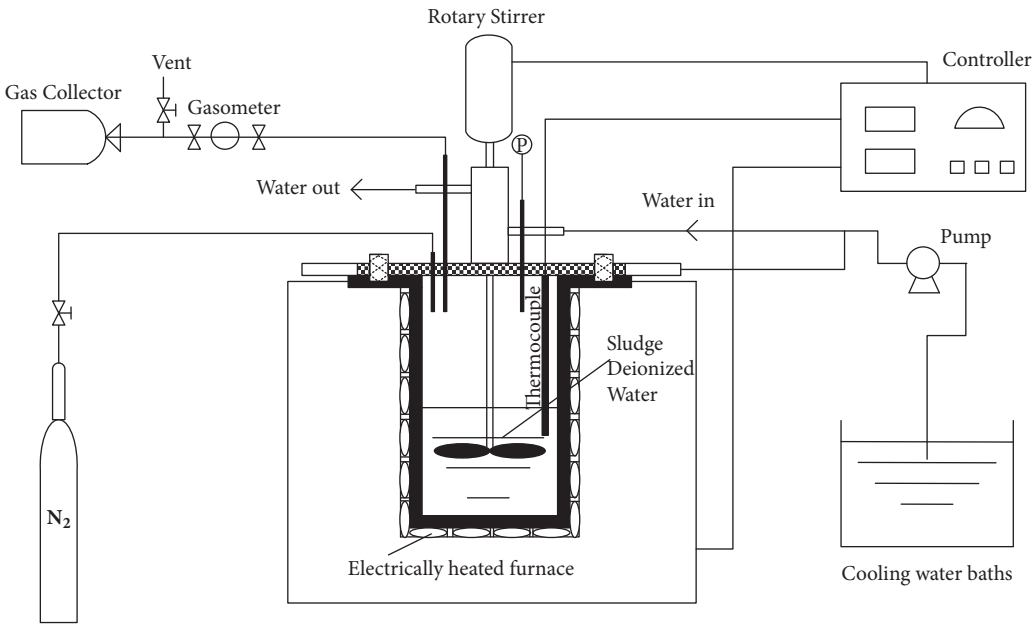


Figure 1: Schematic figure of hydrothermal batch-type reactor.

temperature was controlled by a PID control unit. During each experiment, 500 g of SS and 100 g of deionized water were fed to the reactor, and the air in the reactor was discharged using high-pressure pure nitrogen. The reaction temperature (i.e., 220, 250, and 280°C) was attained at a heating rate of 5°C/min and the residence times investigated were 1, 2, and 3 h, respectively. The mixer was stirred at 700 rpm to maintain the homogeneity of the reaction. After the reaction, the reactor was rapidly cooled to room temperature using running water. The waste liquid (WL) and SR were collected from the reactor and subsequently separated by suction filtration. When the filtration step was complete, the SR was dried at 105°C for 2 h and ground into fine particles (less than 200 $\mu$m) for further analysis. The WL was then placed in a refrigerator at 4°C. All HTC experiments were carried out three times to ensure the accuracy of data. Operating conditions were labeled using a format of "SS-xxx-xx", where "xxx" is the reaction temperature and "xx" is the reaction time. For example, "SS-220-1h" represents the HTC of SS at 220°C for 1 h.

*2.3. Fractionation Procedure of HMs.* Speciation of HMs in SS and SR was investigated using the three-step BCR sequential extraction procedure [26]. Four fractions of HMs were extracted, including an acid soluble/exchangeable fraction (F1), a reducible fraction (F2), an oxidizable fraction (F3), and the residual fraction (F4). Detailed steps of the BCR method are reported in the previous studies [26]. For F1~F3, the suspension was collected after the centrifugation step at 10000 rpm for 20 min and diluted to a constant volume with 2% $HNO_3$. Fine particles were removed by filtration and dissolved organics were degraded by digestion using $H_2O_2$ and concentrated $HNO_3$. The F4 fraction and the total amounts of HMs in SS and SR were extracted by digestion with aqua regia solution and subsequently heated on a hot plate. All digestion solutions were filtered and stored in a refrigerator at 4°C prior to ICP-MS analysis.

*2.4. Leaching Test.* The toxicity characteristic leaching procedure (TCLP) has been widely used to evaluate the leach ability of HMs in the SS and SR [27]. TCLP leachates of SR were conditioned using the acetic acid solution (pH 2.88, liquid/solid ratio=20:1) and were subsequently shook at 200 rpm for 18 h. After centrifugation and filtration, the samples were digested with $H_2O_2/HNO_3$ to remove dissolved organics.

*2.5. Analysis.* The ultimate and proximate analysis of the SS and SR were determined using Elemental Analyzer (LECO-CHNS 932, USA) and an Infrared Rapid Analyzer (5E-MACIII, China), respectively. The samples' calorific value was determined using the adiabatic bomb calorimetric method. The HMs content was measured using an ICP-MS (PerkinElmer Elan 9000, LabX, Canada). The composition of elements and minerals in the SS and SR was analyzed by XRF (ARL QUANTX, Thermo Fisher, USA) and XRD (Smartlab 3, Japan), respectively. The ammonia nitrogen in the WL was analyzed with a continuous flow analyzer (AutoAnalyzer3, SEAL).

*2.6. Combustion Condition.* The combustion process of SS and SR was conducted in a Thermo Gravimetric Analyzer (SETSYS-1750CSEvol, France). The reaction temperature and heating rate were set at 900°C and 20°C/min, respectively. $O_2/N_2$ (volume 1:4) was used to simulate air atmosphere, and the total flow rate was 50 ml/min. The mass of solid samples was accurately kept at 10 mg for each experiment. The combustion residual was collected for digestion using

HCl, $HNO_3$, HF, and $HClO_4$, successively. After digestion, the liquid samples were sent to an ICP-MS to measure the content of HMs. Each combustion experiment was carried out three times to obtain accuracy data.

## 3. Results and Discussion

*3.1. Physicochemical Properties of SR after HTC.* Table 1 shows the physicochemical properties of SS before and after HTC. After the HTC process, the moisture content and volatile matter reduced significantly whilst the fixed carbon and ash content increased, implying that the HTC process has a positive effect on the fuel characteristics of SS. In addition, the moisture and oxygen content of SR reduced from 1.95 wt.% and 8.83 wt.% to 1.34 wt.% and 0.35 wt.%, respectively, when the temperature was increased from 220 to 280°C. This suggests that the dehydration of sludge significantly occurs during the HTC process. The characteristics presented above led to a slight increase of the HHV of SR. After filtration and before drying, the moisture of SR reduced from 64.9 wt% to 48.5% when the reaction temperature was increased from 220 to 280°C. This observation is associated with the decomposition of protein, polysaccharide, and other macromolecule organic compounds [25, 28]. Moreover, an increase in the reaction temperature from 220 to 280°C led to an increase of the WL pH value from 8.7 to 9.5. During the HTC of SS, the concentration of ammonium nitrogen organics in the WL increased significantly when the reaction temperature increased. This was attributed to the breakage of N-containing functional groups [29]. This is consistent with the concentration of $NH_4^+$-N in the WL shown in Table 1. It can be observed that the concentration of $NH_4^+$-N in the WL increased significantly from 1734 to 2245 mg/L when the temperature was increased from 220 to 280°C. Based on the results of Table 1, the influence of reaction temperature on the fuel quality improvement of HTC of SS is greater than that of the reaction residence time.

*3.2. HMs Concentrations and Redistribution in the SR and WL.* It is well known that hydrothermal treatment, including hydrothermal carbonization [17–19], hydrothermal liquefaction [30–32], and hydrothermal gasification [33], has a significant effect on the transformation of HMs in the SS. The total concentrations of Cr, Mn, Ni, Cu, Zn, As, Cd, and Pb in the SS and SR are shown in Figure 2. As seen from Figure 2, the considerable amounts of Mn and Zn were present; however, relatively low concentrations of Cr, Cu, As, and Pb were observed in the SS. After the HTC process, nearly all the HMs concentrations increased with an increase in reaction temperature and residence time, particularly for Mn and Zn. In addition, there was a significant increase for Cu at 280°C. However, the concentration of As decreased slightly with an increase in temperature and residence time, suggesting that some of the arsenic compounds were dissolved into liquid phase products after the HTC process. From Figure 2, HMs seems to be effectively accumulated in the SR after the HTC process, which is closely related to the physical structures of heavy metal crystal and the condition of HMs under certain temperatures and pressures.

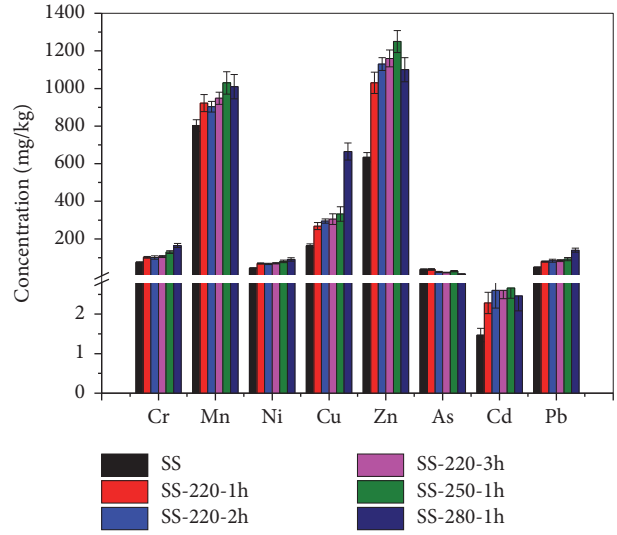


Figure 2: Concentrations of HMs in SS and SR.

Since the HTC of sludge is always conducted at low temperature (less than 350°C), the concentration of HMs in the gas phase products is extremely low and is usually not analyzed. The transformation and stabilization effects of HMs exist simultaneously during the HTC process, resulting in the redistribution of HMs in the solid and liquid phase products. The residual rate of HMs is a parameter that determines the distribution behaviors of HMs during the HTC or combustion process. It can be calculated using the flowing equation:

$$R_c = \frac{C2_x \times m_2}{C1_x \times m_1} \times 100\% \quad (1)$$

where $Rc$ is the residual rate of HMs in the HTC/combustion SR; x is the type of heavy metal; $C2_x$ is the total concentration of x in the SR; $m_2$ is the mass of solid residual (kg); $C1_x$ is the total concentration of x in the raw samples (mg/kg); $m_1$ is the mass of raw samples (kg).

The residual rate of HMs in the SR and WL is presented in Table 2. The results indicate that HTC process seems to have some positive effect on the release of HMs from the solid into liquid phase products. This might be due to the decomposition of extracellular polymeric substances, resulting in breakage of weaker bonded of HMs [17, 19, 21]. As seen from Table 2, different HMs show different released behaviors based on the reaction temperature and residence time. The residual rates of HMs in the SR products, Mn, Ni, Zn, and As, reduced with an increase in the reaction temperature and residence time. The residual rate of As in the SR decreased significantly from 73.95% to 37.48% when the temperature was increased from 220 to 280°C and reduced from 73.95% to 56.74% when the residence time was increased from 1h to 3h. This indicated that many arsenic compounds were released into the liquid phase products and posed a substantial risk to the environment. The effect of reaction temperature on the dissolution of HMs into liquid phase products is greater than that of residence time. In general, elevated temperature

Table 2: Residual rates of HMs in the SR and WL after HTC process.

| Samples | Percentage (%) | | | | | | | | | | | | | | | |
|---|---|---|---|---|---|---|---|---|---|---|---|---|---|---|---|---|
| | Cr | | Mn | | Ni | | Cu | | Zn | | As | | Cd | | Pb | |
| | SR | WL | SR | WL | SR | WL | SR | WL | SR | WL | SR | WL | SR | WL | SR | WL |
| SR-220-1h | 87.12 | 12.88 | 86.10 | 13.90 | 99.70 | 0.30 | 90.10 | 9.90 | 95.53 | 4.47 | 73.95 | 26.05 | 80.88 | 19.12 | 97.46 | 2.54 |
| SR-220-2h | 81.71 | 18.29 | 80.08 | 19.92 | 91.48 | 8.52 | 94.16 | 5.84 | 90.27 | 9.73 | 63.78 | 36.22 | 86.68 | 13.32 | 97.62 | 2.38 |
| SR-220-3h | 83.42 | 16.58 | 81.83 | 18.17 | 93.79 | 6.21 | 94.89 | 5.11 | 90.30 | 9.70 | 56.74 | 43.26 | 84.51 | 15.49 | 97.94 | 2.06 |
| SR-250-1h | 91.29 | 8.71 | 79.26 | 20.74 | 95.19 | 4.81 | 92.00 | 8.00 | 80.17 | 19.83 | 46.83 | 53.17 | 77.79 | 22.21 | 99.06 | 0.94 |
| SR-280-1h | 94.51 | 5.49 | 71.93 | 28.07 | 93.44 | 6.56 | 99.62 | 0.38 | 85.29 | 14.71 | 37.48 | 62.52 | 66.40 | 33.60 | 99.19 | 0.81 |

can enhance the extraction effects of HMs and improve the degradation and transformation of organic compounds and minerals, resulting in an increase in the release rate of HMs from solid into liquid phase products [21, 34]. However, the residual rate of Cu and Pb in the SR increased from 90.10% and 97.46% to 99.62% and 99.19% when the temperature was increased from 220°C to 280°C. During the HTC process, Cu prefers to be bound to organic matter and form the Cu-sulfide substance with high stability [17, 19, 20, 35–37]. In addition, Pb is easily combined with the primary minerals, such as Ca, Mg, and Fe, through the ion exchange [38, 39]. In the case of Cr and Cd, the temperature and residence time have a different effect on the residual rate in the SR. When the temperature was increased from 220°C to 280°C, the residual rate of Cr was enhanced from 87.12% to 94.51% whilst that of Cd reduced from 80.88% to 66.40%. In addition, as the residence time increased from 1h to 3h, the residual rate of Cr reduced from 87.12% to 83.42%, but that of Cd increased from 80.88% to 84.51%.

As described above, the minerals in the SS have a great influence on the absorption, precipitation, and complexation of HMs. Therefore, the minerals compositions of SS before and after the HTC process need to be investigated. The experimental results are shown in Figure 3. It can be deducted that the SS and SR were mainly composed of crystalline compounds, particularly Si, Cu, and Al compounds. After the HTC process, the intensity at 20° to 35° increased significantly, indicating that the crystalline phenomenon of the HMs increased. In addition, the HMs in the SR after the HTC of SS is mainly in the form of complex compounds, and parts of their crystal structures have a resemblance [40]. According to the literature [21, 41, 42], Fe/Al oxide and some inorganic minerals (clay, carbonate and phosphate, et al.) can combine and absorb the HMs through ion exchange and the surface complexation. Additionally, some organic functional groups (carboxyl and phenolic groups) and S, N-containing groups can reduce the migration of HMs in the SR via the complexation and adsorption [43]. The transformation and immobilization behaviors of HMs during the HTC process can be associated with some complicated physical-chemical processes, such as adsorption, precipitation complexation, and recombination, occurring between the HMs and the crystal lattices of SR [21, 36, 37, 44, 45]. However, detailed mechanisms of how the hydrothermal treatment affects the migration and transformation of HMs in sludge is extremely complex and still needs further investigation.

### 3.3. Fractions of HMs and Environment Risk Analysis of SR

*3.3.1. Fractions and Migration Behavior of HMs during the HTC Process.* Evaluation of environmental ecotoxicity of HMs predominantly depends on the chemical speciation of HMs. With reference to the bioavailability and ecotoxicity of HMs, F1 and F2 are identified as directly toxic fraction; F3 and F4 are considered as potentially toxic and nontoxic fractions, respectively. The transformation behaviors of the chemical speciation of HMs in the SS and SR after the HTC process are shown in Figure 4. The main fractions of HMs in the SS were found to be very different. Cr and Pb were mainly present in the F4 fraction (80.7% and 95.45%). More than 60% Ni and Cu were in the F3 and F4 fractions, respectively. The F1 fraction of Ni, Zn, and Cd was 17.7%, 16.2%, and 9.43%, respectively, whilst they almost have no F2 fraction. Mn and As had the high concentrations in the F1 fraction, with As having more than 50% of the total, implying that there exists high potential bioavailability and ecotoxicity. From Figure 4, Cr, Cu, and Pb are exceptionally low at the exchangeable (F1 <5%) fraction. Ni, Zn, and Cd are also low at the exchangeable (F1 <20%) fraction. However, Mn and As are high at the exchangeable (F1>40%) fraction.

At longer HTC residence times and higher temperatures, Cr and Pb showed no obvious changes in the F1 and F2 fraction but had a minute increase in the F3 fraction and slight decrease in the F4 fraction. Although Cu has a similar trend to Cr and Pb with regard to the change of F1 and F2 fractions, the F3 fraction of Cu sharply increased with residence time. There was also an observed initial increase followed a decrease when the temperature was increased from 220 to 280°C. An opposite trend was observed in the F4 fraction of Cu, indicating that the increase of the F3 fraction of Cu was mainly a result of migration from the F4 fraction. The Fe oxides composition favors the oxidation of copper and the combination of organic matters, resulting in the formation of Cu-oxide complexes during the HTC process [17, 19, 20, 35–37]. In the case of Mn, the HTC process showed a positive effect on the reduction of the F1 fraction when reaction temperature and residence time were increased, resulting in an increase in the F2 fraction. This suggests that the F1 fraction was converted into the F2 fraction. However, the directly toxic fractions (F1+F2) reduced with an increase in the reaction temperature and residence time. The percentage of Mn increased in the F3 fraction with increasing temperature and residence time. Contrastingly, it reduced in the F4 fraction with increasing residence time,

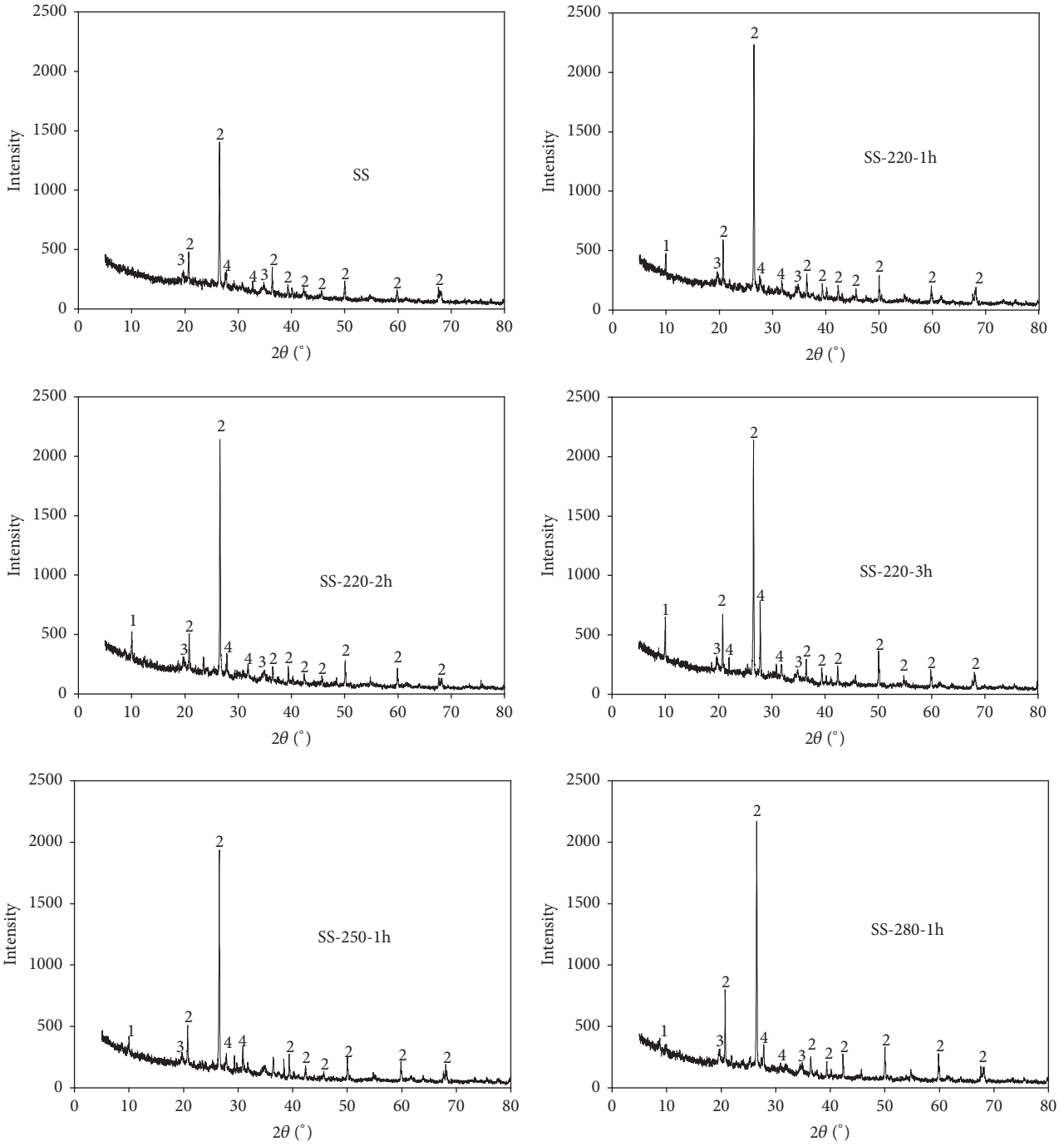


Figure 3: Minerals compositions of SS and SR. 1: $K_2Cu_3$+2O$(SO_4)_3$; 2: $SiO_2$; 3: $KAl_2Si_3AlO_{10}(OH)_2$; 4: $AlSO_4(OH)\cdot 5H_2O$.

indicating that some of the F4 fraction of Mn was converted into the F3 fraction and increased the potential bioavailability and ecotoxicity. Similar transformation behaviors of F1~F4 fraction were observed for Ni.

As for Zn and Cd, their F1 fractions reduced significantly whilst their F2 and F1+F2 fractions considerably decreased. The HMs F1+F2 fractions increased with the reaction residence time. When the temperature was increased from 220 to 280°C, there was an observed initial increase superseded by a reduction. The Zn and Cd F3 fractions increased whilst their F4 fraction reduced with an increase in the reaction residence time and temperature, indicating that most of the F4 fraction was converted to the F3 fraction. In addition, the F3+F4 fractions reduced significantly with an increase of the residence time. However, no pronounced changes with temperature were observed. From the results of Zn and Cd, the bioavailability and ecotoxicity increased after the HTC process, and the effect of residence time is greater than that of the reaction temperature. For As, the highest F1 fraction (64.6%) in the SR was obtained during the HTC of SS at 220°C

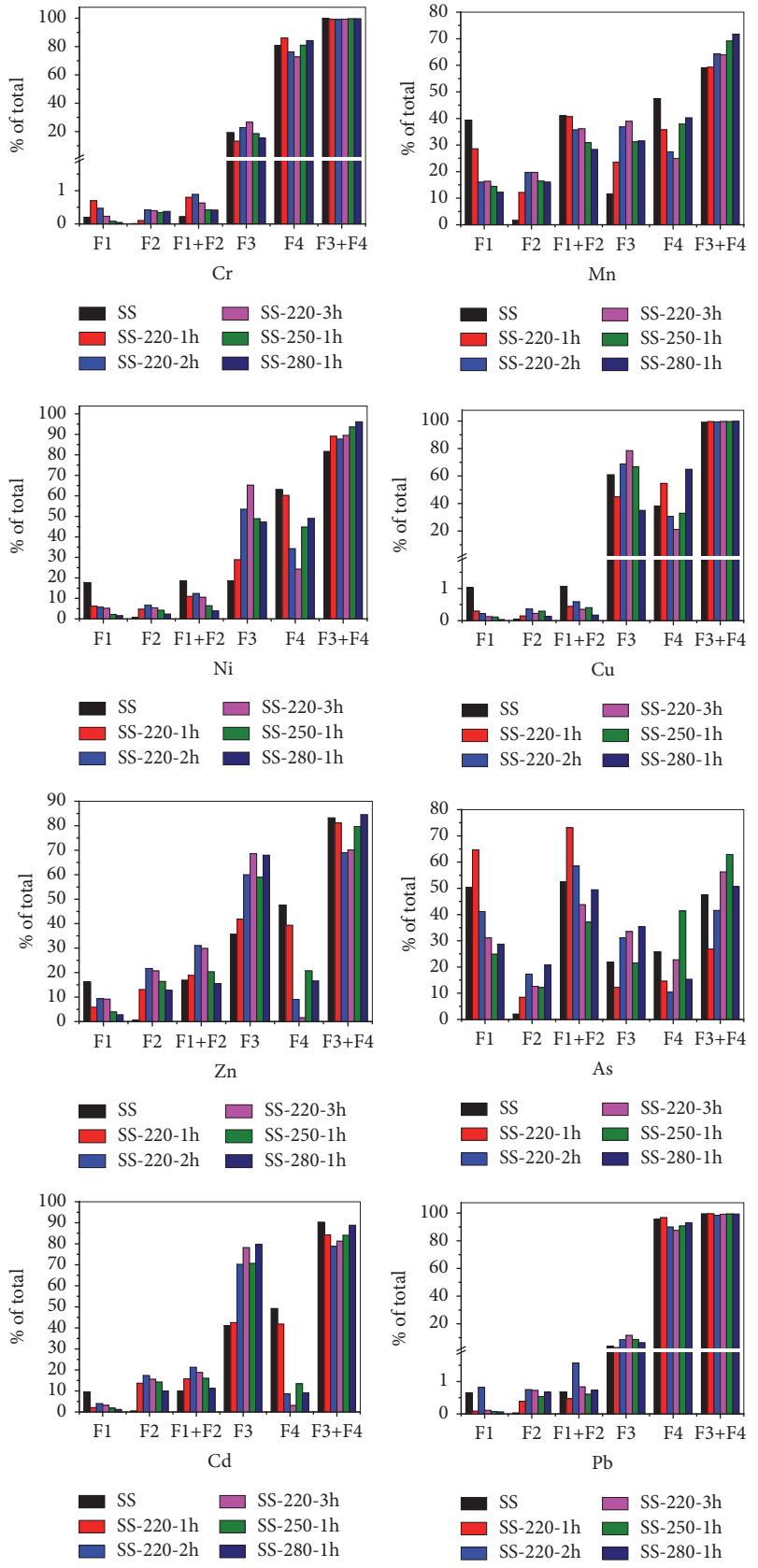


Figure 4: Speciation transformation behaviors of HMs in the SS before and after HTC.

Table 3: Concentrations of leachable HMs in the TCLP tests (mg/kg).

| HMs | Raw SS | SS-220-1h | SS-220-2h | SS-220-3h | SS-250-1h | SS-280-1h | Permissible limits[a] |
|---|---|---|---|---|---|---|---|
| Cr | 0.11±0.00 | 0.61±0.01 | 0.44±0.01 | 0.39±0.01 | 0.09±0.00 | 0.09±0.00 | 5.0 |
| Mn | 231.06±10.67 | 289.22±10.56 | 293.71±12.45 | 446.73±16.56 | 536.53±16.78 | 449.39±14.34 | —[b] |
| Ni | 5.41±0.23 | 6.73±0.25 | 1.53±0.07 | 1.10±0.05 | 0.68±0.01 | 0.72±0.01 | 5.0 |
| Cu | 1.42±0.06 | 0.41±0.01 | 0.18±0.01 | 0.09±0.00 | 0.12±0.01 | 0.04±0.00 | —[b] |
| Zn | 30.32±1.67 | 38.62±2.12 | 32.18±1.68 | 30.97±1.56 | 13.77±0.53 | 14.62±0.68 | 5.0 |
| As | 25.57±0.48 | 20.42±0.59 | 12.01±0.43 | 7.97±0.25 | 10.34±0.38 | 6.16±0.21 | 5.0 |
| Cd | 0.05±0.00 | 0.03±0.00 | 0.04±0.00 | 0.03±0.00 | 0.03±0.00 | 0.01±0.00 | 1.0 |
| Pb | 0.03±0.00 | 0.02±0.00 | 0.03±0.00 | 0.02±0.00 | 0.08±0.00 | 0.01±0.00 | 5.0 |

(1) a: USEPA, test methods for evaluating solid waste: physical/chemical methods (SW-846).
(2) b: Not titled.

for a residence time of 1h. Its F1 fraction reduced whilst its F2 fraction increased with an increase in the residence time and temperature. The F1+F2 fraction of As reduced with an increase in the residence time. With respect to increases in temperature, there was an observed increase in the F1+F2 fraction followed by a reduction. The As F3 fraction increased with residence time and temperature. These results indicate that there was practically no positive effect on the speciation transformation of As during the HTC process.

Basing on the preceding results, the weakly bound exchangeable fraction (F1) for HMs can be converted into F2 fraction as a result of the HTC process. However, HMs (Cr, Mn, Ni, Zn, Cd, and Pb) underwent a transformation from F4 fractions into F3 fractions. The F1+F2 fractions for Mn, Ni and Cu significantly reduced whilst those for Cr, Zn, As, and Cd increased. The F1 and F2 fractions of Mn, Zn, As, and Cd in the SR were high, suggesting a high potential bioavailability and ecotoxicity to the environment. As such, these results indicate that the HTC process has a positive effect on the chemical speciation transformation of HMs from weakly bound fractions to the more stable fractions.

*3.3.2. Leaching Characterization of SR.* The leaching characteristics of HMs in the SS and SR were determined using the TLCP method [27]. The results are shown in Table 3 and Figure 5. The leached amounts of HMs from SS were 0.11, 231, 5.41, 1.42, 30.32, 25.57, 0.05 and 0.03 mg/kg for Cr, Mn, Ni, Cu, Zn, As, Cd and Pb, respectively. The leached amounts of Ni, Zn and As were higher than the permissible limits (USEPA, SW-846) and therefore exhibited potential toxicity. When the reaction temperature and residence time were increased, the leached amounts of Ni, Cu, Zn and As reduced significantly. However, the amount of Mn highly increased and no obvious changes were observed for Cr, Cd and Pb. In addition, the concentrations of leachable HMs in SS-220-3h were higher than those in SS-280-1h, indicating that the influence of reaction temperature on the reduction of leachable HMs was greater than that of residence time. Higher reaction temperatures contribute to the combination of HMs with crystal lattices of SR and enhance the immobilization of HMs [21, 40, 44, 45]. Briefly, the HTC process exhibited a significant reduction of the leaching risk of HMs. In contrast, the leached amounts of Zn and As were still high (14.61mg/kg and 6.16 mg/kg, respectively) and therefore showed a high leaching risk to the environment.

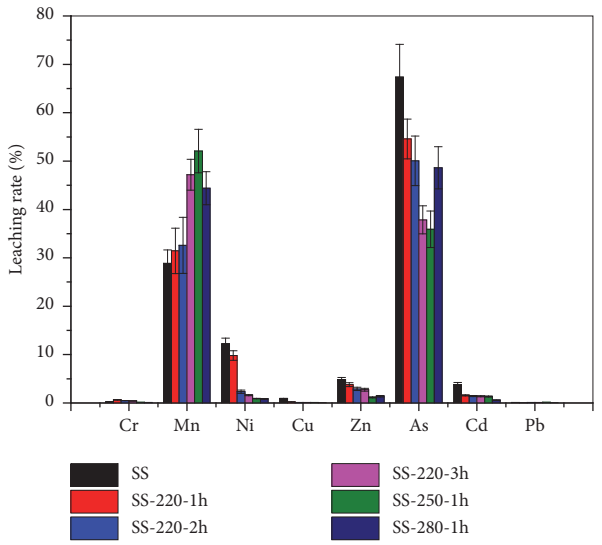


Figure 5: Leaching rates of HMs in the TCLP tests.

The leaching rate of HMs from SS and SR are shown in Figure 5. The leaching rate is defined as the ratio of the amount of a heavy metal in the leachate to the total amount of this heavy metal [17, 19, 46].

With an increase in the reaction temperature and residence time, the leaching rate of all HMs (except Mn and As) in the SR decreased significantly and almost exhibited no leaching rate. The leaching rate of As reduced when residence time was increased. However, the leaching rate of As first reduced and then increased when the temperature was increased from 220 to 280°C. The As leaching rate was close 50% at a reaction temperature of 280°C for a residence time of 1h. This exhibits a high leaching risk to the environment. As shown in Table 3 and Figure 5, the leachable fractions of HMs in the SR endured a significant reduction as a result of the HTC process. This observation however does not include As and Mn which had high leaching rates.

*3.4. Immobilization Behaviors of HMs in the Combustion Residual.* The immobilization behaviors of HMs during the

Table 4: Concentrations of HMs in the combustion residual (mg/kg).

| Samples | Cr | Mn | Ni | Cu | Zn | As | Cd | Pb |
|---|---|---|---|---|---|---|---|---|
| SS | 156.50±5.56 | 1160.75±65.87 | 88.61±4.89 | 382.20±15.67 | 1448.33±70.45 | 62.36±2.56 | 3.35±0.08 | 111.87±3.32 |
| SS-220-1h | 200.90±6.78 | 1338.55±77.34 | 126.63±7.45 | 580.82±18.56 | 2026.21±68.62 | 62.58±2.03 | 4.62±0.10 | 168.50±5.25 |
| SS-220-2h | 182.66±6.68 | 1345.87±72.56 | 118.05±6.45 | 505.83±12.05 | 1950.73±55.24 | 44.65±1.89 | 4.66±0.11 | 147.99±3.98 |
| SS-220-3h | 187.80±8.56 | 1425.18±65.45 | 125.41±5.23 | 531.88±10.78 | 2010.28±69.46 | 41.61±1.01 | 4.63±0.09 | 152.88±4.23 |
| SS-250-1h | 184.07±10.56 | 1350.55±75.78 | 118.88±6.54 | 531.64±11.34 | 1964.51±51.67 | 41.36±1.56 | 4.55±0.13 | 152.55±4.01 |
| SS-280-1h | 219.89±11.45 | 1356.32±68.67 | 124.50±5.45 | 580.29±15.67 | 1972.96±75.34 | 38.39±1.12 | 4.69±0.08 | 153.34±4.23 |

Table 5: Residual rates of HMs in the combustion residual (%).

| Samples | Cr | Mn | Ni | Cu | Zn | As | Cd | Pb |
|---|---|---|---|---|---|---|---|---|
| Raw SS | 87.36 | 74.97 | 90.69 | 72.16 | 88.47 | 85.09 | 91.72 | 75.31 |
| SS-220-1h | 90.15 | 84.84 | 91.70 | 79.13 | 86.65 | 87.57 | 91.87 | 79.59 |
| SS-220-2h | 91.12 | 92.29 | 92.39 | 80.07 | 88.60 | 85.02 | 92.23 | 80.96 |
| SS-220-3h | 90.09 | 92.78 | 92.95 | 79.26 | 90.12 | 88.22 | 91.13 | 81.13 |
| SS-250-1h | 92.53 | 84.80 | 95.95 | 75.14 | 90.31 | 91.50 | 92.08 | 76.81 |
| SS-280-1h | 93.88 | 88.46 | 93.28 | 78.51 | 92.03 | 92.86 | 92.61 | 72.23 |

combustion of SR produced from the HTC of SS were analyzed. The concentrations of HMs in the combustion residual are shown in Table 4. Compared to the combustion of SS, the respective amounts of HMs (except As) in the combustion residual of SR increased. In addition, the amounts of HMs in the combustion residual are higher than that in the SS and SR (Figure 2). This indicates that most of HMs accumulated in the combustion residual. However, as for As, the concentration changed considerably from 62.58 mg/kg to 38.39 mg/kg when the HTC SR changed from "SS-220-1h" to "SS-280-1h". Arsenic has a low boiling point and therefore exhibits volatile and gasification properties [47]. Consequently, it can easily be gasified during the combustion process. In addition, some inorganic compounds (Ca, Al, and Fe compounds) can provide chemical reactive sites of arsenic and enhance the complexation and absorption of arsenic by forming various arsenates in the fly ash and solid residual [48–51]. From Table 4, the concentrations of HMs in the combustion residual have minimal pronounced changes even when the HTC reaction temperature and residence time were varied. Although the HTC process was carried out at different reaction conditions, the chemical compositions of SR tend to be stable and the crystal lattices of HMs are similar [40]. The residual rates of HMs after the combustion of SR produced from the HTC of SS are presented in Table 5. As seen from Table 5, the residual rates of all HMs were more than 70%, particularly for Cr, Ni, Zn, and Cd which had more than 90% residual rates. With increasing HTC reaction temperature and residence time, the residual rates of HMs (except Pb) in the combustion residual of SR increased, indicating that the HTC process promotes the immobilization of HMs in the combustion solid residual.

## 4. Conclusions

The transformation behaviors of Cr, Mn, Ni, Cu, Zn, As, Cd, and Pb in the SS during the HTC process combined with combustion were investigated. Most of the HMs accumulated in the SR during HTC and combustion process, respectively. However, the concentration and residual rate of As in the SR reduced with an increase in the HTC reaction temperature and residence time, implying that many arsenic compounds are released into the liquid phase products. After the HTC process, the weakly bonded fractions of HMs migrated to the more stable fraction. However, the exchangeable and reducible fractions of Mn, Zn, As, and Cd in SR were remarkably high and presented an elevated risk to the environment. The leaching characteristics of HMs in the SR showed a significant improvement. Contrastingly, the leached amounts of Zn and As were still high and exceeded the permissible limits. The contents of HMs in the combustion residual were higher than those in the SS and SR. The residual rates of almost all the HMs in the combustion residual of SR produced from the HTC of SS increased with increasing HTC temperature and residence time, indicating that the HTC process promotes the immobilization of HMs in the combustion process.

## Data Availability

The data used to support the findings of this study are available from the corresponding author upon request.

## Conflicts of Interest

There are no conflicts of interest regarding the publication of this paper.

## Acknowledgments

The authors would like to thank Dr. Marcos Millan, Department of Chemical Engineering, Imperial College London, UK, for his good suggestion and professional advice. This work was supported by the National Natural Science Foundation of China (51606103 and 51206028).

## References


[1] I. Fonts, G. Gea, M. Azuara, J. Ábrego, and J. Arauzo, "Sewage sludge pyrolysis for liquid production: a review," *Renewable & Sustainable Energy Reviews*, vol. 16, no. 5, pp. 2781–2805, 2012.

[2] Y. Zhai, X. Liu, Y. Zhu et al., "Hydrothermal carbonization of sewage sludge: The effect of feed-water pH on fate and risk of heavy metals in hydrochars," *Bioresource Technology*, vol. 218, pp. 183–188, 2016.

[3] N. Gao, C. Quan, B. Liu, Z. Li, C. Wu, and A. Li, "Continuous Pyrolysis of Sewage Sludge in a Screw-Feeding Reactor: Products Characterization and Ecological Risk Assessment of Heavy Metals," *Energy & Fuels*, vol. 31, no. 5, pp. 5063–5072, 2017.

[4] W. Rulkens, "Sewage sludge as a biomass resource for the production of energy: Overview and assessment of the various options," *Energy & Fuels*, vol. 22, no. 1, pp. 9–15, 2008.

[5] W. H. Rulkens and J. D. Bien, "Recovery of energy from sludge - Comparison of the various options," *Water Science and Technology*, vol. 50, no. 9, pp. 213–221, 2004.

[6] L. Wang, A. Li, and Y. Chang, "Hydrothermal treatment coupled with mechanical expression at increased temperature for excess sludge dewatering: Heavy metals, volatile organic compounds and combustion characteristics of hydrochar," *Chemical Engineering Journal*, vol. 297, pp. 1–10, 2016.

[7] G. Mininni, R. Di Bartolo Zuccarello, V. Lotito, L. Spinosa, and A. C. Di Pinto, "A design model of sewage sludge incineration plants with energy recovery," *Water Science and Technology*, vol. 36, no. 11, pp. 211–218, 1997.

[8] T. Namioka, Y. Morohashi, R. Yamane, and K. Yoshikawa, "Hydrothermal Treatment of Dewatered Sewage Sludge Cake for Solid Fuel Production," *Journal of Environment and Engineering*, vol. 4, no. 1, pp. 68–77, 2009.

[9] C. Areeprasert, D. Ma, P. Prayoga, and K. Yoshikawa, "A Review on Pilot-Scale Applications of Hydrothermal Treatment for Upgrading Waste Materials," *International Journal of Environmental Science and Development*, vol. 7, no. 6, pp. 425–430, 2016.

[10] M. Yan, B. Prabowo, Z. Fang, W. Chen, Z. Jiang, and Y. Hu, "Effect of hydrothermal treatment temperature on the properties of sewage sludge derived solid fuel," *International Journal of Renewable Energy Development (IJRED)*, vol. 4, no. 3, 2015.

[11] P. Zhao, Y. Shen, S. Ge, and K. Yoshikawa, "Energy recycling from sewage sludge by producing solid biofuel with hydrothermal carbonization," *Energy Conversion and Management*, vol. 78, pp. 815–821, 2014.

[12] M. Escala, T. Zumbühl, C. Koller, R. Junge, and R. Krebs, "Hydrothermal carbonization as an energy-efficient alternative to established drying technologies for sewage sludge: A feasibility study on a laboratory scale," *Energy & Fuels*, vol. 27, no. 1, pp. 454–460, 2013.

[13] J. H. Zhang, Q. Luo, Q. M. Lin, X. X. Zhao, G. T. Li, and G. F. Wu, "Characteristics of wastewater from municipal sludge after hydrothermal carbonization treatment," *Chinese Journal of Envionmental Engineering*, vol. 7, pp. 3363–3368, 2003.

[14] P. Zhao, H. Chen, S. Ge, and K. Yoshikawa, "Effect of the hydrothermal pretreatment for the reduction of no emission from sewage sludge combustion," *Applied Energy*, vol. 111, pp. 199–205, 2013.

[15] E. Danso-Boateng, G. Shama, A. D. Wheatley, S. J. Martin, and R. G. Holdich, "Hydrothermal carbonisation of sewage sludge: Effect of process conditions on product characteristics and methane production," *Bioresource Technology*, vol. 177, pp. 318–327, 2015.

[16] L. Appels, J. Degrève, B. Van der Bruggen, J. Van Impe, and R. Dewil, "Influence of low temperature thermal pre-treatment on sludge solubilisation, heavy metal release and anaerobic digestion," *Bioresource Technology*, vol. 101, no. 15, pp. 5743–5748, 2010.

[17] W. Shi, C. Liu, D. Ding et al., "Immobilization of heavy metals in sewage sludge by using subcritical water technology," *Bioresource Technology*, vol. 137, pp. 18–24, 2013.

[18] W. Shi, C. Liu, Y. Shu, C. Feng, Z. Lei, and Z. Zhang, "Synergistic effect of rice husk addition on hydrothermal treatment of sewage sludge: Fate and environmental risk of heavy metals," *Bioresource Technology*, vol. 149, pp. 496–502, 2013.

[19] X. Wang, C. Li, B. Zhang, J. Lin, Q. Chi, and Y. Wang, "Migration and risk assessment of heavy metals in sewage sludge during hydrothermal treatment combined with pyrolysis," *Bioresource Technology*, vol. 221, pp. 560–567, 2016.

[20] X. Xu and E. Jiang, "Treatment of urban sludge by hydrothermal carbonization," *Bioresource Technology*, vol. 238, pp. 182–187, 2017.

[21] H.-J. Huang and X.-Z. Yuan, "The migration and transformation behaviors of heavy metals during the hydrothermal treatment of sewage sludge," *Bioresource Technology*, vol. 200, pp. 991–998, 2016.

[22] C. He, A. Giannis, and J.-Y. Wang, "Conversion of sewage sludge to clean solid fuel using hydrothermal carbonization: Hydrochar fuel characteristics and combustion behavior," *Applied Energy*, vol. 111, pp. 257–266, 2013.

[23] G. K. Parshetti, Z. Liu, A. Jain, M. P. Srinivasan, and R. Balasubramanian, "Hydrothermal carbonization of sewage sludge for energy production with coal," *Fuel*, vol. 111, pp. 201–210, 2013.

[24] C. Areeprasert, P. Chanyavanich, D. Ma, Y. Shen, and K. Yoshikawa, "Effect of hydrothermal treatment on co-combustion of paper sludge with coal: thermal behavior, NO emissions, and slagging/fouling tendency," *Biofuels*, vol. 8, no. 2, pp. 187–196, 2017.

[25] J. Yu, M. Guo, X. Xu, and B. Guan, "The role of temperature and CaCl2 in activated sludge dewatering under hydrothermal treatment.," *Water Research*, vol. 50, pp. 10–17, 2014.

[26] G. Rauret, J. F. López-Sánchez, A. Sahuquillo et al., "Improvement of the BCR three step sequential extraction procedure prior to the certification of new sediment and soil reference materials," *Journal of Environmental Monitoring*, vol. 1, no. 1, pp. 57–61, 1999.

[27] A. Nair, A. A. Juwarkar, and S. Devotta, "Study of speciation of metals in an industrial sludge and evaluation of metal chelators for their removal," *Journal of Hazardous Materials*, vol. 152, no. 2, pp. 545–553, 2008.

[28] L. Wang, L. Zhang, and A. Li, "Hydrothermal treatment coupled with mechanical expression at increased temperature for excess sludge dewatering: Influence of operating conditions and the process energetics," *Water Research*, vol. 65, pp. 85–97, 2014.

[29] A. Funke and F. Ziegler, "Hydrothermal carbonization of biomass: a summary and discussion of chemical mechanisms for process engineering," *Biofuels, Bioproducts and Biorefining*, vol. 4, no. 2, pp. 160–177, 2010.

[30] X. Yuan, H. Huang, G. Zeng et al., "Total concentrations and chemical speciation of heavy metals in liquefaction residues of sewage sludge," *Bioresource Technology*, vol. 102, no. 5, pp. 4104–4110, 2011.

[31] L. Leng, X. Yuan, H. Huang, H. Jiang, X. Chen, and G. Zeng, "The migration and transformation behavior of heavy metals during the liquefaction process of sewage sludge," *Bioresource Technology*, vol. 167, pp. 144–150, 2014.

[32] H.-J. Huang and X.-Z. Yuan, "Recent progress in the direct liquefaction of typical biomass," *Progress in Energy and Combustion Science*, vol. 49, pp. 59–80, 2015.

[33] L. Li, Z. R. Xu, C. Zhang, J. Bao, and X. Dai, "Quantitative evaluation of heavy metals in solid residues from sub- and super-critical water gasification of sewage sludge," *Bioresource Technology*, vol. 121, pp. 169–175, 2012.

[34] N. Peng, Y. Li, T. Liu, Q. Lang, C. Gai, and Z. Liu, "Polycyclic Aromatic Hydrocarbons and Toxic Heavy Metals in Municipal Solid Waste and Corresponding Hydrochars," *Energy & Fuels*, vol. 31, no. 2, pp. 1665–1671, 2017.

[35] M. R. Lasheen and N. S. Ammar, "Assessment of metals speciation in sewage sludge and stabilized sludge from different Wastewater Treatment Plants, Greater Cairo, Egypt," *Journal of Hazardous Materials*, vol. 164, no. 2-3, pp. 740–749, 2009.

[36] Y. Zhou, Z. Zhang, J. Zhang, and S. Xia, "Understanding key constituents and feature of the biopolymer in activated sludge responsible for binding heavy metals," *Chemical Engineering Journal*, vol. 304, pp. 527–532, 2016.

[37] J. Laurent, M. Casellas, H. Carrère, and C. Dagot, "Effects of thermal hydrolysis on activated sludge solubilization, surface properties and heavy metals biosorption," *Chemical Engineering Journal*, vol. 166, no. 3, pp. 841–849, 2011.

[38] M. N. Islam and J.-H. Park, "Immobilization and reduction of bioavailability of lead in shooting range soil through hydrothermal treatment," *Journal of Environmental Management*, vol. 191, pp. 172–178, 2017.

[39] J. W. C. Wong, K. Li, K. Fang, and D. C. Su, "Toxicity evaluation of sewage sludges in Hong Kong," *Environment International*, vol. 27, no. 5, pp. 373–380, 2001.

[40] R. Ma, Y. Zhou, and L. Fang, "International Conference on Advances in Energy and Environmental Science (ICAEES," in *Proceedings of the International Conference on Advances in Energy and Environmental Science (ICAEES*, Zhuhai , China, 2015.

[41] D. S. Apul, K. H. Gardner, T. T. Eighmy, A.-M. Fällman, and R. N. J. Comans, "Simultaneous application of dissolution/precipitation and surface complexation/surface precipitation modeling to contaminant leaching," *Environmental Science & Technology*, vol. 39, no. 15, pp. 5736–5741, 2005.

[42] A. A. Rouff, E. J. Elzinga, R. J. Reeder, and N. S. Fisher, "X-ray Absorption Spectroscopic Evidence for the Formation of Ph(II) Inner-Sphere Adsorption Complexes and Precipitates at the Calcite-Water Interface," *Environmental Science & Technology*, vol. 38, no. 6, pp. 1700–1707, 2004.

[43] L. K. Koopal, T. Saito, J. P. Pinheiro, and W. H. Van Riemsdijk, "Ion binding to natural organic matter: General considerations and the NICA-Donnan model," *Colloids and Surfaces A: Physicochemical and Engineering Aspects*, vol. 265, no. 1-3, pp. 40–54, 2005.

[44] C. Wang, N. Zhu, Y. Wang, and F. Zhang, "Co-detoxification of transformer oil-contained PCBs and heavy metals in medical waste incinerator fly ash under sub- and supercritical water," *Environmental Science & Technology*, vol. 46, no. 2, pp. 1003–1009, 2012.

[45] H. Pan, "Effects of liquefaction time and temperature on heavy metal removal and distribution in liquefied CCA-treated wood sludge," *Chemosphere*, vol. 80, no. 4, pp. 438–444, 2010.

[46] H. Huang, X. Yuan, G. Zeng et al., "Quantitative evaluation of heavy metals' pollution hazards in liquefaction residues of sewage sludge," *Bioresource Technology*, vol. 102, no. 22, pp. 10346–10351, 2011.

[47] S. Van Wesenbeeck, W. Prins, F. Ronsse, and M. J. Antal, "Sewage sludge carbonization for biochar applications. Fate of heavy metals," *Energy & Fuels*, vol. 28, no. 8, pp. 5318–5326, 2014.

[48] Y. Zhao, Q. Ren, and Y. Na, "Speciation transformation of arsenic during municipal sewage sludge incineration with cotton stalk as additive," *Fuel*, vol. 202, pp. 541–546, 2017.

[49] H. Yao and I. Naruse, "Control of trace metal emissions by sorbents during sewage sludge combustion," *Proceedings of the Combustion Institute*, vol. 30, pp. 3009–3016, 2005.

[50] Y. Zhao, J. Zhang, W. Huang et al., "Arsenic emission during combustion of high arsenic coals from Southwestern Guizhou, China," *Energy Conversion and Management*, vol. 49, no. 4, pp. 615–624, 2008.

[51] H. Liu, C. Wang, C. Zou, Y. Zhang, and J. Wang, "Simultaneous volatilization characteristics of arsenic and sulfur during isothermal coal combustion," *Fuel*, vol. 203, pp. 152–161, 2017.

Hindawi
BioMed Research International
Volume 2018, Article ID 7420656, 9 pages
https://doi.org/10.1155/2018/7420656

*Research Article*

# Experimental Study on Productivity Performance of Household Combined Thermal Power and Biogas System in Northwest China

**Jian Kang**[1,2,3,4] **Jinping Li**[1,3,4] **Xiaofei Zhen**,[1,3,4] **Yassir Idris Abdalla Osman**,[1,3,4] **Rong Feng**,[5] **and Zetian Si**[1,3,4]

[1] *Western China Energy & Environment Research Center, Lanzhou University of Technology, Lanzhou 730050, China*
[2] *School of Material Science and Engineering, Lanzhou University of Technology, Lanzhou 730050, China*
[3] *Key Laboratory of Complementary Energy System of Biomass and Solar Energy, Lanzhou, Gansu Province 730050, China*
[4] *Collaborative Innovation Center of Key Technology for Northwest Low Carbon Urbanization, Lanzhou 730050, China*
[5] *Shaanxi Key Laboratory of Industrial Automation, Shaanxi University of Technology, Hanzhong 723000, China*

Correspondence should be addressed to Jinping Li; lijinping77@163.com

Received 10 December 2017; Revised 6 March 2018; Accepted 11 April 2018; Published 13 May 2018

Academic Editor: Ningbo Gao



Ample quantities of solar and local biomass energy are available in the rural regions of northwest China to satisfy the energy needs of farmers. In this work, low-temperature solar thermal collectors, photovoltaic solar power generators, and solar-powered thermostatic biogas digesters were combined to create a heat, electricity, and biogas cogeneration system and were experimentally studied through two buildings in a farming village in northwestern China. The results indicated that the floor heater had the best heating effect. And the fraction of the energy produced by the solar elements of the system was 60.3%. The photovoltaic power-generation system achieved photovoltaic (PV) conversion efficiencies of 8.3% and 8.1% during the first and second season, respectively. The intrinsic power consumption of the system was 143.4 kW·h, and 115.7 kW·h of electrical power was generated by the system in each season. The average volume of biogas produced daily was approximately 1.0 $m^3$. Even though the ambient temperature reached −25°C, the temperature of the biogas digester was maintained at 27°C ± 2 for thermostatic fermentation. After optimization, the energy-saving rate improved from 66.2% to 85.5%. The installation reduced $CO_2$ emissions by approximately 27.03 t, and the static payback period was 3.1 yr. Therefore, the system is highly economical, energy efficient, and beneficial for the environment.

## 1. Introduction

Nonrenewable energy production and utilization prevail in rural regions of northwest China due to restrictions imposed by geographical location, costs associated with clean energy implementation, and insufficient knowledge of deployment and operation of clean energy systems. The majority of these rural communities still rely on coal energy, and households have been found to be significant energy consumers [1]. In fact, $CO_2$ emissions in rural residential areas have grown at higher per-capita rates than those of urban areas [2]. Notwithstanding these challenges, agricultural communities in northwest China are rich in renewable resources, especially solar energy and organic biomass, and sustainable generation of clean energy for rural communities has been found to be feasible [3]. In fact, harnessing these sources has been deemed necessary to achieve China's goals of carbon emission reduction and transition to clean energy, as well as eliminating rural energy poverty [4].

Several studies have investigated the performance of solar and biomass systems for energy production [4–11]. Bhattarai et al. [5] found that tank capacity has a significant effect on thermal efficiency and economic performance of photovoltaic and thermal solar (PV/T) collectors. Esen and Yuksel [6] used solar, geothermal energy, and biogas to heat a model greenhouse (6 m × 4 m × 2.10 m) in Turkey,

successfully attaining a plant-friendly temperature of 23°C. Jenssen et al. [7] analyzed a model municipality in Germany that uses biomass energy to understand the balance between the reduction in $CO_2$ emissions and the increase in land-use competition and energy supply costs. The findings of Jenssen et al. indicate that heat and power demand can be easily met with biomass, but transport fuel necessitates a different source. Aguilar et al. [12] assessed and implemented a pilot-scale, closed-loop system that combined a solar thermal collector, an anaerobic digester, and a constructed wetland treatment system that used organic wastes for energy production, in which the wastes were subsequently treated prior to their release into the environment. The implemented system showed that organic wastes can be efficiently used to produce energy, while protecting the environment. O. Ozgener and L. Ozgener [9] utilized a driveway as a solar thermal panel to enhance the efficiency of a solar-assisted geothermal heat pump system. The results are reported as a 68% energy replacement for the product/fuel of the entire system and for the driveway that is used as the solar collector. Chen et al. [10] performed experiments and numerical simulations to study a combined solar system consisting of a solar collector and a $CO_2$ heat pump. The simulated results indicated that the optimized system could reduce electricity expenditure by 14.2% and improve solar energy production by 8%. The solar portion of the optimized system was 71.1%. Wu et al. [11] proposed an optimal energy management system for a grid-connected PV-battery hybrid system for optimal harnessing of solar energy to meet consumer demand.

The scale of energy supply systems based on renewable energy at home and abroad and that can meet the needs of multiple levels of energy use is often too large to be suitable for the highly dispersed characteristics of residential properties still existing in rural China. Photovoltaic power generation, low-temperature heat collection, and biomass anaerobic fermentation and production of biogas, as three mature technologies for renewable energy use, can meet the energy needs of rural households in northwest China, such as household electricity, thermal energy, and domestic gas. However, the single-technology renewable energy utilization devices have great limitations in terms of energy supply stability and meet the needs of multiple levels of energy use and are severely constrained by environmental factors; therefore, they can be integrated with current solar photovoltaic power-generation technologies and solar energy cryogenic sets. Thermal technology and solar-powered constant-temperature biogas digester technology are used to construct a household heat and electricity cogeneration system that uses solar energy and biomass energy as input and can meet the needs of farmers in multiple levels in northwest cold regions. The literature shows that the potential for a 100%-renewable energy supply using solar energy, biomass energy, or a combination thereof has been either predicted or observed in different settings. However, verification by complete deployment of said technologies in real scenarios and analyses of measurements of relevant energy parameters to assess efficiency and cost remain scarce. Here, we report findings from an experimental study that was conducted under actual operating conditions over two winter seasons. We studied a heating-electricity-gas cogeneration system for use in two inhabited buildings located in Zhangma village (Gansu Province, Minqin County, China), each covering an area of 117 $m^2$. Radiator heaters were used during the first season and low-temperature floor heaters during the second season. Comparative analysis was performed of the power-generation performance of this system using different heating terminals. In addition, a comprehensive evaluation of the resulting energy savings and emission reductions was performed, together with an assessment of economic viability.

## 2. Materials and Methods

*2.1. Experimental Energy-Generation System.* The experimental heating-electricity-gas cogeneration system was installed in a single-block building in Zhangma village. The system comprised three subsystems: a combined heating subsystem using both solar energy and a coal-fired boiler, a PV solar-power-generation subsystem, and a solar-heated thermostatic biogas digester. The heating system comprised a coal-fired boiler, heat-dissipating terminals, a water-circulating pump, valves, pipes, and six sets of evacuated-tube solar collectors. The heat-dissipating terminals consisted of radiator heaters that were subsequently replaced by low-temperature floor heaters. Each set of solar collectors comprised 40 evacuated tubes of length 1.8 m and diameter 0.058 and a collector with a surface area of 3.85 $m^2$. The solar collectors were connected in series. The power-generation subsystem consisted of an array of solar cells, a controlled inverter, and battery cells. The PV array consisted of 10 single-crystal silicon PV cells divided into five parallel sets (each set having two solar cells connected in parallel).

The system included four batteries divided into two parallel sets, each set having two batteries connected in series. The total output power of this system was 1000 kW. The solar-heated thermostatic biogas digester subsystem was composed of a single set of evacuated-tube solar collectors, a biogas digester, heating coil, water-circulating pump, valves, and a red mud soft-matter biogas bag. Some of the power generated by the PV array was used to power the circulation pumps that drive hot water from the water tank into the building and into the biogas digester to provide heat. The remaining power supplied electricity for household usage. A photograph and schematic of the heat-electricity-gas cogeneration system are shown in Figures 1 and 2, respectively.

*2.2. Experimental Parameters and Measuring Instruments.* The two experimental periods were from December 1, 2014, to March 31, 2015, and from December 1, 2015, to March 31, 2016. The measurements and measuring instruments are shown in Table 1. All the parameters were automatically acquired and recorded using an Agilent 34970A data-acquisition device at a scanning interval of 10 s. An extraction pump was used at a fixed time each day to transfer the biogas produced within the fermentation bag into the gas storage bag. Daily gas production was measured by a G16

Table 1: Types and technical parameters of the measuring instruments.

| Measured parameters | Measuring instruments | Technical parameters |
|---|---|---|
| Solar radiation on the collector face of solar water heater and PV array | TBQ-2 Pyranometer (Jinzhou Sunshine Technology, Jinzhou, Liaoning) | Range: 0–2,000 $Wm^{-2}$<br>Sensitivity: 8.963 $\mu V = Wm^{-2}$<br>Precision: 2% |
| Output voltage of PV array | DC voltmeter (Chujing Electric, Wenzhou, Zhejiang) | Range: 0–50 V<br>Precision: 0.5% |
| Output current of PV array | DC ammeter (Chujing Electric, Wenzhou, Zhejiang) | Range: 0–50 A<br>Precision: 0.5% |
| Inlet water temperature for space heating<br>Outlet water temperature for space heating<br>Inlet water temperature for digester heating<br>Outlet water temperature for digester heating<br>Ambient temperature | pt100 temperature sensor (Beijing Sailing Technology, Beijing) | Range: −50°C to 100°C<br>Precision: -0.10°C |
| Flow rate for space heating | LWGY-20 turbine flowmeter (Shanghai Huaman Industrial, Shanghai) | Range: 0.7–7.0 $m^3 = h$<br>Precision: -0.45% |
| Flow rate for digester heating | LWGY-15 turbine flowmeter (Shanghai Huaman Industrial, Shanghai) | Range: 0.4–4.0 $m^3 = h$<br>Precision: -0.45% |
| Quantity of daily consumed coal | Platform balance (Shanghai Shuoheng Electronic Technology, Shanghai) | Minimum scale: 0.2 kg |
| Daily biogas production | G16 gas meter (Zhejiang Xinlong Instrument, Yongkang, Zhijiang) | Precision: -1.5% |
| Biogas contents | Gas600 portable biogas analysis (Geotech Instruments, Leamington, UK) | Precision: -2% |
| Electricity consumed by pumps | Electric energy meter (Wenzhou Libajia Technology, Wenzhou, Zhejiang) | Minimum scale: 0.1 kW·h |


Figure 1: Photograph of the heat-electricity-biogas cogeneration system.

gas meter, and its composition was analyzed using a Gas 600 portable biogas analyzer. A DDS1531 single-phase electronic electricity meter was used to measure daily electricity consumption, which was then scaled to obtain daily coal consumption.

## 3. Methods

(1) Power generated by the PV array is expressed as

$$E = \sum UIt. \quad (1)$$

This equation represents the power generated by the PV array, $E$ (expressed in J). $U$ is the PV array's output voltage (V), $I$ is the array's output current (A), and $t$ is the time (s).

(2) The quantity of heat provided to the building by the solar collectors is expressed as

$$Q = \sum cm\left(t_{in} - t_{out}\right)t. \quad (2)$$

In (2), $Q$ is the heat provided to the building by the solar collectors (J), $c$ is the heat capacity of water (4200 J/kg·°C), $m$ is the flow of the circulated water (kg/s), $t_{in}$ is the supply water temperature (°C), $t_{out}$ is the return water temperature (°C), and $t$ is the time (s).

(3) The energy-saving rate ($\eta$) due to the energy-conserving measures taken by a user [13] is expressed as

$$\eta = \frac{W_1 - W_2}{W_1} \times 100\%, \quad (3)$$

where $W_1$ and $W_2$ represent energy consumption before and after adopting energy-saving measures, respectively. For this system, the energy-saving rate occurs by reducing consumption of standard coal.

## 4. Results and Discussion

*4.1. Performance Analysis: Heating Stability of Solar-Powered Heating Subsystem.* Winters in the northwestern regions of China are cold and dry, with significant diurnal temperature differences. Periods of extreme rain/snow are common. Therefore, auxiliary coal-fired boilers are required as a heating source in addition to a solar heater, to ensure the continuity and stability of the power-generation system. The

Table 2: Number of heating days for each mode of heating.

| Period | Solar heating (d) | Boiler heating (d) | Solar and boiler heating (d) |
|---|---|---|---|
| 2014-2015 | 55 | 13 | 53 |
| 2015-2016 | 90 | 18 | 14 |

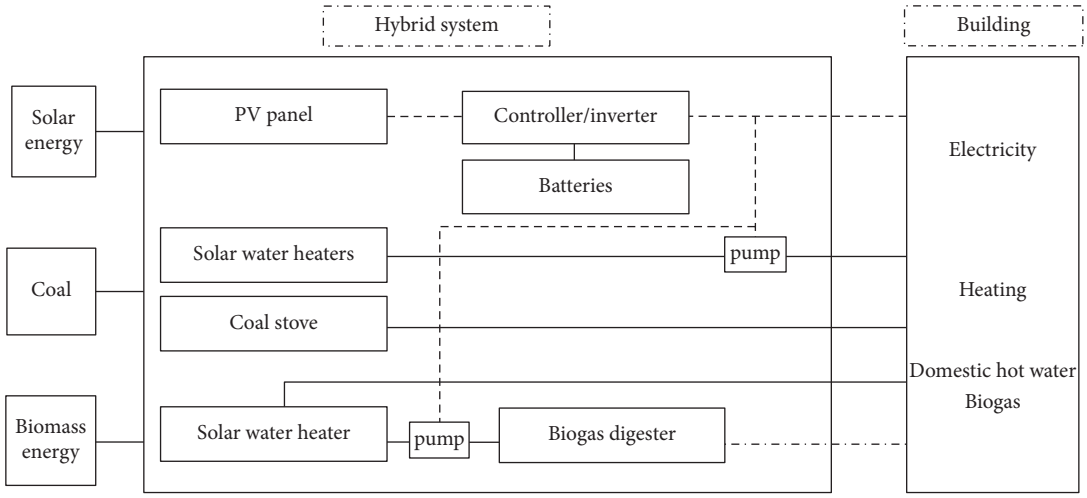


Figure 2: Integration schematic of the hybrid system.

heating system has three different heating modes that are used according to the availability of solar radiation: (1) with adequate sunlight, all heat is obtained from solar energy; (2) with weak sunlight, heating is provided by solar energy and the coal-fired boiler in combination; and (3) during rain, snow, and extreme weather events, all heat is provided by the coal-fired boiler. During the first winter (2014-2015), there were 82 d of clear weather, 26 d of cloudy weather, and 13 d of extreme rainy/snowy weather, compared with 70, 34, and 18 d, respectively, during the second winter (2015-2016). The numbers of days for each heating mode during both seasons are shown in Table 2. This comparison shows that the weather over the course of the second cool season was generally poorer, but that solar-powered heating alone was used on significantly more days than those requiring boiler usage. This indicates that, when the heating system was switched from radiators to low-temperature floor heating, the system showed greater resistance to weather-induced interference. In addition, the power-generation stability of the system improved significantly during these periods.

*4.2. Indoor Temperatures.* To compare the effectiveness of the three heating modes, 4 d with similar ambient temperatures were selected from each of the heating seasons, and the temperature data acquired from the building's living room were evaluated. There was ample solar radiation on those days, so solar energy was used to heat the experimental building, while a coal-fired boiler heated the reference building. Heating was provided between 16:00 h and 24:00 h each day. Indoor and ambient temperatures for the experimental and reference buildings on December 30 and 31, 2014, are shown in Figure 3(a). Ambient temperature ranged between −10.4°C and 3.8°C. The average living-room temperature was 14°C (range 7.3°C, minimum 11°C) in the experimental building, compared with 12°C (range 10.4°C, minimum 8°C) in the reference building. Figure 3(b) illustrates the indoor and ambient temperatures of the experimental and reference buildings on December 2 and 3, 2015, during which time the ambient temperature ranged between −10.8°C and 3.2°C. The average living-room temperature was 14.3°C (minimum 12.4°C, range 4.4°C) in the experimental building, compared with 12.4°C (minimum 8.1°C, range 9.8°C) in the reference building. The living-room temperature of 14.3°C in the experimental building, which had been modified to conserve energy, met the requirements of the Design Standard for Energy Efficiency of Rural Residential Buildings (GBT50824-2013). In addition, the use of low-temperature floor heating resulted in the highest average indoor temperature and a smooth temperature-variation curve with minimal fluctuation. This mode of heating provided the greatest stability among the observed cases.

*4.3. Indoor Relative Humidity.* Figure 4 shows relative humidity in the living room of the experimental building on December 30 and 31, 2014, and December 2 and 3, 2015. When the building was heated with solar-driven radiators, the relative humidity was 47–65%, compared with 51–60% when using solar-driven low-temperature floor heating. Both heaters were able to provide a comfortable range of relative humidity during the winter, ranging between 40% and 60% [14, 15]. However, the low-temperature floor heater resulted in more consistent humidity levels and was more stable and provided greater comfort than the solar-driven radiator.

Table 3: Results of data analysis.

| $R^2$ | Standard error | Partial regression coefficient 1 ($\beta_1$) | Partial regression coefficient 2 ($\beta_2$) | Intercept |
|---|---|---|---|---|
| 0.633 | 0.332 | 2.32 | −0.30 | 5.75 |

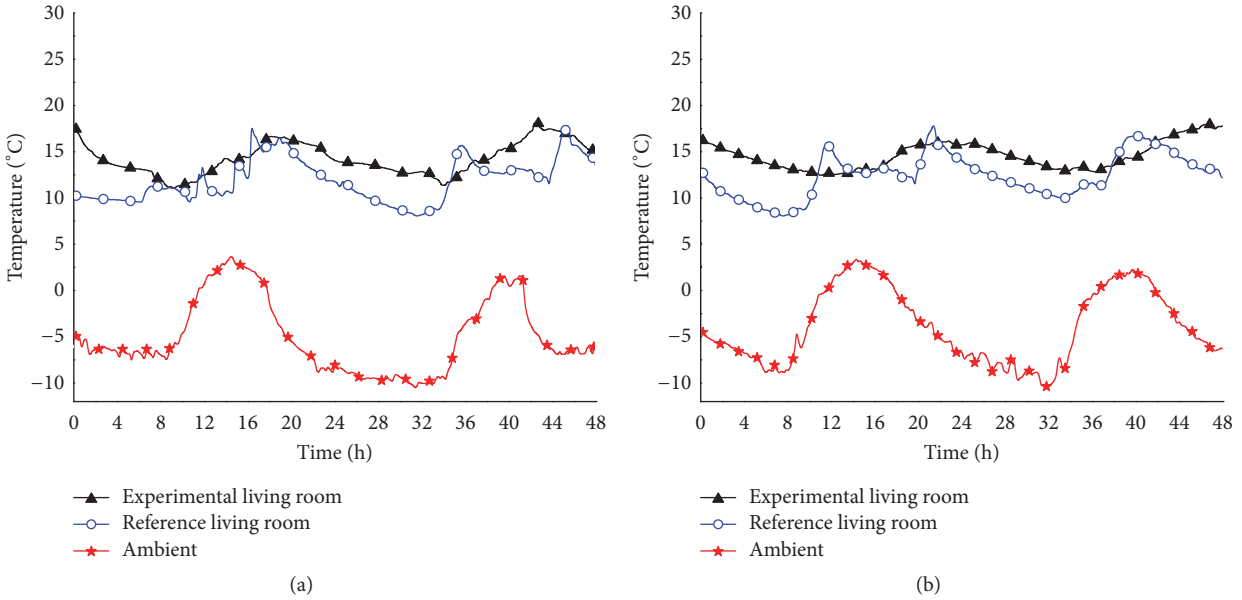


Figure 3: Ambient and indoor temperatures: (a) December 30 and 31, 2014; (b) December 2 and 3, 2015.

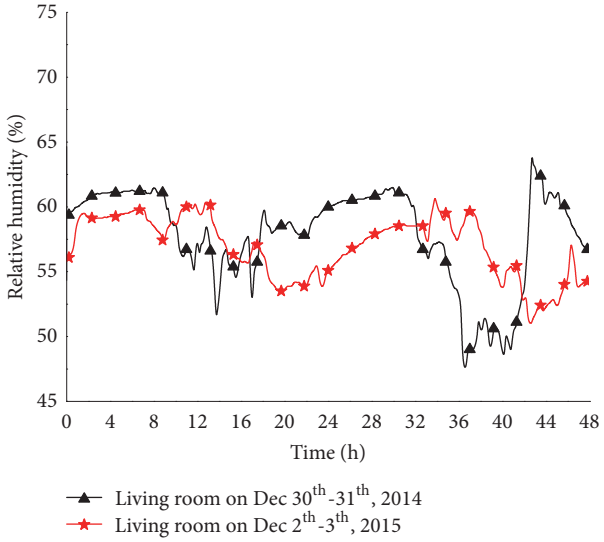


Figure 4: Relative humidity in the living room (experimental building) during December 30 and 31, 2014, and December 2 and 3, 2015.

*4.4. Efficiency of Solar Collector.* The efficiency of solar collectors is determined mainly by the quantity of solar radiation, temperature of the water tank, and ambient temperature. The average daily difference between the water tank temperature and ambient temperature and the cumulative solar radiation were treated as independent variables; the heat collected over the course of 1 d was treated as the dependent variable. The following equation was obtained using multiple linear regressions to describe the quantity of heat collected by a single solar collector over the course of 1 d:

$$Q_s = 2.32E - 0.30\left(\overline{T_s} - \overline{T_e}\right) + 5.75, \quad (4)$$

where $Q_s$ is the quantity of heat collected by a single solar collector over the course of 1 d (expressed in MJ), $E$ is the cumulative solar radiation (MJ/m$^2$), $T_s$ is the average daily temperature of the water tank (°C), and $T_e$ is the average daily ambient temperature (°C).

The results of the data analysis are shown in Table 3. The multiple determination coefficient ($R^2$ = 0.633) indicates a moderate fit, which is reasonable for the expected level of uncertainty in the observed process. The standard error was 0.332, representing an average error of 0.322 MJ in predicting the average daily difference between the water tank temperature and ambient temperature, the heat collected by the solar collector over the course of 1 d, and cumulative solar radiation. This error might be due to environmental factors that were not accounted for in this study, such as dust and wind speed. The regression coefficient $\beta_1$ was 2.32, indicating that the quantity of heat collected by a collector over the course of 1 d will increase by 2.32 MJ for every 1-MJ increase in cumulative solar radiation, assuming that the difference between average water tank temperature and ambient temperature remains constant. The regression coefficient

Table 4: Calculation of heat consumption by building footprint.

| Building footprint | HYC[a]/W ($m^2$·K) | CF[b] | Area | $t_n - t_w$ (°C) | HC[c] (W) |
|---|---|---|---|---|---|
| External wall | 0.36 | 0.9 | 120 | 16.6 | 645.4 |
| External window | 2 | 0.9 | 12 | 16.6 | 358.6 |
| Door | 3 | 1.1 | 5.2 | 16.6 | 284.8 |
| Ground | 0.47 | 1 | 64 | 16.6 | 499.3 |
| Roof | 1.45 | 1 | 64 | 16.6 | 1540.5 |
| Total | | | | | 3328.6 |

[a]Heat-transfer coefficient. [b]Correction factor. [c]Heat consumption.

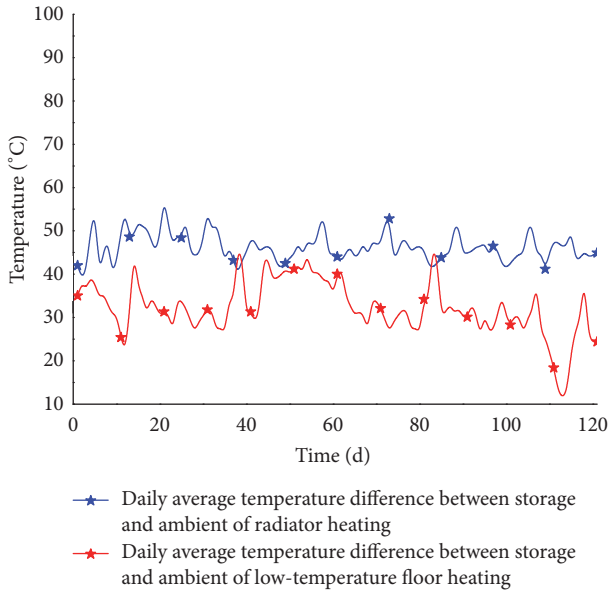


Figure 5: Daily average temperature difference between water tank temperature and ambient temperature during two heating seasons.

$\beta 2$ was −0.30, which indicates that the heat collected by a collector over the course of 1 d decreases by 0.30 MJ for each 1°C increase in the average difference between water tank temperature and ambient temperature, assuming that cumulative solar radiation remains unchanged.

By dividing both sides of (4) by $A_1E$ (where $A_1$ is the area of a single solar collector, 3.85 $m^2$), we then obtain the equation for calculating the collector's daily average collection efficiency,

$$\overline{\eta} = 0.60 - \frac{0.078\left(\overline{T_s} - \overline{T_e}\right) - 1.494}{E}, \quad (5)$$

from which it can be shown that decreases in the average difference between the water tank temperature and ambient temperature will increase the collector's daily average collection efficiency, if cumulative solar radiation remains unchanged. Figure 5 shows that this difference was generally smaller when using the floor heater compared with the radiator heater. Therefore, the use of floor heaters is beneficial for increasing the average daily collection efficiency.

## 5. Analysis of Solar Fraction of Solar-Powered Heating System

The solar fraction $f$ refers to the ratio of heat provided by the solar energy system versus the required heating load. Using (2), the total heat supplied by solar energy during the two heating seasons was calculated as 11619 MJ and 22715 MJ, respectively. The required heating load of the system was calculated as follows.

(1) The experimental building had a total footprint of 117 $m^2$; the radiator and floor heaters were located in the three bedrooms and living room, giving an effective heating area of 64 $m^2$. The heat consumption of the building envelope, $Q_{HT}$, calculated using (6), was 3328.6 W. The details of this calculation are shown in Table 4.

(2) The heat loss by infiltration can be calculated as follows:

$$Q_{INF} = 0.28 \times 1.293 \times 0.5 \times 173 \times (14 + 2.6) = 519.9\,\text{W}. \quad (6)$$

(3) The indoor heating of the building is given by

$$Q_{IH} = 64.4 \times 3.8 = 244.7\,\text{W}. \quad (7)$$

Based on (5), the heat consumption of the building, $Q_H$, was 3603.8 W. Therefore, the required heating load for a single heating season (121 d) for the experimental building was

$$q = 3603.8 \times 121 \times 24 \times 3600 = 37676\,\text{MJ}. \quad (8)$$

The solar fraction of the system during the first heating season was

$$f_1 = \frac{11619}{37676} \times 100\% = 30.8\%. \quad (9)$$

The solar fraction of the system during the second heating season was

$$f_2 = \frac{22715}{37676} \times 100\% = 60.3\%. \quad (10)$$

Therefore, the system provided considerably more heat to the building after the dissipating terminals of the solar-powered heating system were changed from radiators to low-temperature floor heaters. This significantly increased the solar fraction and solar utilization efficiency, resulting in substantial energy savings.

## 6. Performance of PV Subsystem

The power-generation subsystem has a PV array covering 6.44 $m^2$. During the first heating season, the cumulative solar radiation per unit area of the array was 1901 $MJ/m^2$, corresponding to a total solar input of 12242 MJ. Based on (1), the total power generated by the solar array was 1010 MJ, which is equivalent to 280.7 kW·h of power. The intrinsic power consumption of the system was 137.3 kW·h, leaving 143.4 kW·h for household usage. Therefore, the actual PV conversion efficiency of the PV arrays was 8.3%.

During the second heating season, the cumulative solar radiation per unit area of the PV array was 1817 $MJ/m^2$, corresponding to a total solar input of 11702 MJ. The total energy generated by the solar array was 942.1 MJ, equivalent to 261.7 kW·h. The intrinsic power consumption of the system was 146 kW·h, leaving 115.7 kW·h for household usage. Therefore, the actual PV conversion efficiency of the PV arrays was 8.1%.

It is clear that the PV conversion efficiency of the system began to decline during the second heating season, mainly reflecting gradually declining output of the PV components. The second reason was that the weather was noticeably poorer during the second heating season, as there were more days of extreme snowy/rainy weather with lower levels of solar radiation. The energy generated by the PV system was greater than the system's intrinsic power consumption. Hence, the system was able to sustain its own power requirements and supply power for household usage, which demonstrated that the system had excellent power-generation performance.

## 7. Biogas-Production Performance

The biogas system uses solar energy and biomass as inputs and produces biogas chemical energy and heat as outputs. This subsystem included evacuated-tube solar collectors, a temperature-controlled chamber, red mud soft-matter biogas bag, heating coil, controller, measurement devices, and data-acquisition device. The evacuated-tube solar collector used in the experiment had an area of 3.85 $m^2$ (40 tubes, each 1.8 m long, with an effective solar collector length of 1.66 m and diameter 0.058 m). The angle between the collector's surface and the ground was 45°. The hot water storage tank capacity was 400 L. The temperature-controlled chamber was a 1.9 m × 1.9 m × 2.6 m cuboid. The sides of the chamber were made of coated steel plates sandwiching a 7.5-cm-thick polystyrene board on the outside and 6-cm-thick extruded polystyrene boards on the inside. The bottom of the chamber consisted of a 12-cm-thick extruded polystyrene board, and the top of the chamber was made of coated steel plates sandwiching a 7.5-cm-thick polystyrene board. The chamber was placed on a horizontal surface and was fixed in place using a welded steel frame. The red mud soft-matter biogas bag had an effective storage capacity of 6.4 $m^3$ (1.6 m × 1.6 m × 2.5 m). The bag was fitted with feed inlets and gas outlets and was installed inside the temperature-controlled chamber. During operation, feed materials were loaded into the bottom of the bag, while gas accumulated at the top. The feed inlet on the outside of the temperature-controlled chamber was located 1.2 m from the bottom of the biogas bag, and the maximum quantity of feed that could be loaded into the bag was 3.0 $m^3$. Aluminum tubes (inner diameter 16 mm, outer diameter 20 mm) were attached to the solar-powered water heater and then secured to the extruded polystyrene boards on the bottom half of the temperature-controlled chamber (inside). The heating coils inside the temperature-controlled chamber had a total length of 40 m, while the aluminum and plastic pipes outside the chamber were insulated with a 3-cm-thick layer of polyethylene insulation.

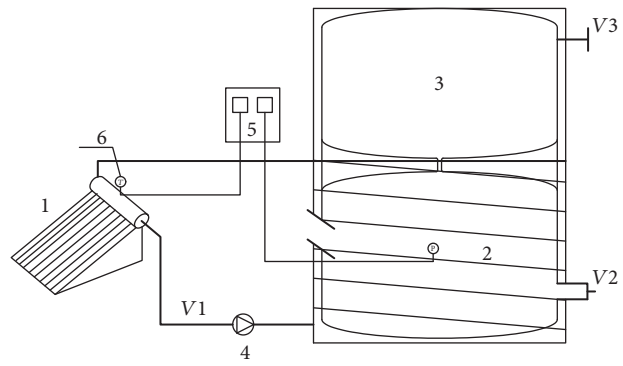


Figure 6: Schematic of solar-heated, thermostatically controlled anaerobic fermentation system for household usage.

In this system, raw materials for fermentation, as specified by the Western China Energy and Environment Research Center (Lanzhou University of Technology, China), were mixed with water at specific ratios. The resulting mixture was then poured into the red mud fermentation bag for soft feed (2 in Figure 6). The evacuated-tube solar collector (1 in Figure 6) absorbs solar radiation and converts this into thermal energy; this is used to heat water, which the water-circulating pump then forces through the coils on the bottom of the fermentation bag and the spiral coils around the chamber (4 in Figure 6). This process transmits the heat from the hot water, via heat radiation and convection, to the fermenting feed slurry, thus maintaining a thermostatic environment that will sustain the anaerobic digestion of biomass. After the fermenting feed slurry has been heated to a specified temperature, the automated temperature control box (5 in Figure 6) turns off the water-circulating pump. If the temperature sensor inside the fermentation bag records that the feed slurry has cooled below the temperature range specified for fermentation, the pump is reactivated to continue heating the feed slurry. In Figure 6, $V_1$ is a shut-off valve, while $V_2$ and $V_3$ are ball valves.

Figure 7 shows the temperature-variation curves of the water tank, feed slurry, and ambient temperature for both winter seasons (242 d). The results show that the biogas digester maintained a temperature within 27 ± 2°C even when the ambient temperature reached its minimum of −25°C. Thus, this system is capable of thermostatic fermentation during the coldest local winter conditions. During the first heating season, cumulative gas production was 114.7 $m^3$, with 54.6% average methane content (62.6 $m^3$) giving an average

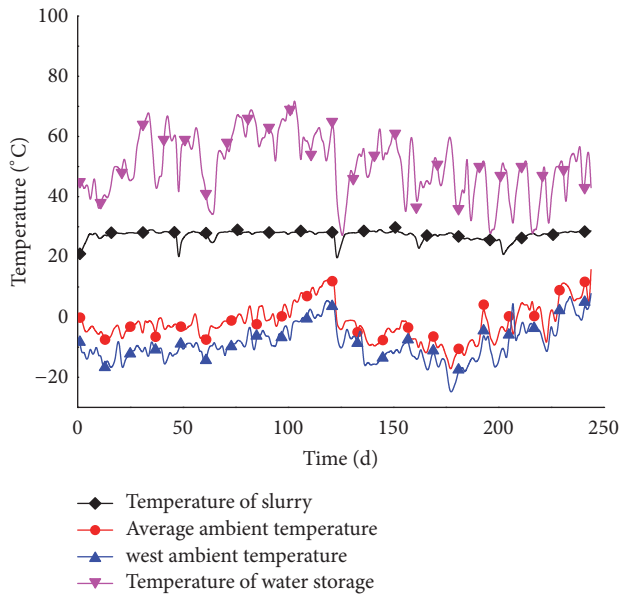


FIGURE 7: Feed slurry temperature, ambient temperature, and water tank temperature over two heating seasons.

daily biogas production of 0.96 $m^3$. During the second heating season, cumulative gas production was 120.5 $m^3$, with 55.0% average methane content (66.3 $m^3$) giving an average daily biogas production of 1.0 $m^3$. Therefore, the quantity of biogas produced by this system was sufficient to meet the cooking-gas requirements of a family of four to five members.

## 8. Analysis of Energy Savings

The residents of the experimental home throughout the experimental period primarily consumed energy supplied by the heating-electricity-gas cogeneration system, electrical power from the national power grid, and heat energy generated by the burning of coal. The cogeneration system provided energy from the solar collectors, the PV solar array, and biogas from the solar-powered digester. This combined energy provision was derived solely from solar energy and biomass and was therefore equivalent to the total quantity of fossil fuel energy that was conserved. The energy-saving rate of this system during the first season was calculated using (3), as follows.

(1) The heating provided by the solar collector, $q_1$, was 11619 MJ. The efficiency of a coal-fired boiler was calculated to be 32% [15], given that the calorific value of standard coal is 29.308 MJ/kg. The energy provided by the solar collector was then equivalent to $m_1 = 11619 \div (0.32 \times 29.308) = 1239$ kg of standard coal.

(2) The standard coal consumption of the auxiliary boiler was $m_2 = 680$ kg.

(3) The power generated by the PV array was $q_2 = 280.7$ MJ, given that the standard coal coefficient for electrical power is 0.404 kg/kW·h. Therefore, the equivalent amount of coal required to produce this power is $m_3 = 113$ kg.

(4) Based on local electric power requirements, the average electric power usage of each household was 3.3 kW·h, and the electrical power needed during the heating season was 396 kW·h. Since the heating-electricity-gas cogeneration system was able to supply 143.4 kW·h of power for daily usage, the household still consumed 253 kW·h of power from the national power grid, which is equivalent to consuming 102 kg of standard coal.

(5) The total quantity of biogas produced by the system was 114.7 $m^3$, of which 62.6 $m^3$ was methane. Given that the calorific value of methane is 35.9 MJ/$m^3$ and the heating efficiency of the biogas stove was 75%, the heat released by the burning of biogas was $q_3 = 62.6 \times 35.9 \times 0.75 = 1686$ MJ, which is equivalent to $m_5 = 1686 \div (0.32 \times 29.308) = 180$ kg of standard coal. The energy saved by the household was then $W_1 = m_1 + m_3 + m_5 = 1239 + 113 + 180 = 1532$ kg, while the energy consumed by the household was $W_2 = m_1 + m_2 + m_3 + m_4 + m_5 = 1239 + 680 + 113 + 102 + 180 = 2314$ kg.

The energy-saving rate of the system during the first heating season was therefore

$$\eta = \frac{W_1}{W_2} \times 100\% = \frac{1532}{2314} \times 100\% = 66.2\%. \quad (11)$$

Based on the same calculations, the energy saved during the second winter was 2718 kg, while the energy consumed by the household was 3178 kg. This results in an energy-saving rate of 85.5%. Therefore, the energy-saving rate of the system was significantly improved following optimization. This was mainly because the low-temperature floor heaters provided much more heat to the building than did the previous radiator heaters.

## 9. Economic and Environmental Benefits

The system costs comprised the PV power-generation subsystem, including PV arrays; a power inverter; and battery cells (total cost 16000 CNY). The heating subsystem consists of six sets of solar collectors (total cost 11400 CNY). The gas-production subsystem included a thermostatic chamber, a set of solar collectors, and the biogas bag for soft feed (total cost 6900 CNY). Therefore, the initial cost of the system was 34300 CNY. The cogeneration system supplied the low-temperature floor heaters, cooking gas, hot water, winter heating, and electricity and saved an equivalent of 7364 kg in coal a year. If each kg of coal releases 3.67 kg of $CO_2$, the reduction in emissions is equivalent to 27.03 t of $CO_2$. Based on a coal price of 1500 CNY/t, the savings accumulated over a year would be 11046 CNY, which gives a static payback period of 3.1 yr for this system. Therefore, the heating-electricity-gas cogeneration system studied here is economically viable, energy efficient, and environmentally beneficial.

## 10. Conclusions

The following conclusions were drawn from the operational tests performed on the proposed cogeneration system over two heating seasons under actual working conditions.

(1) After the system was optimized, the average indoor temperature was able to reach 14°C. Average indoor relative humidity was 47% and only fluctuated over a small range.

(2) During the first heating season, the total energy generated by the power-generation subsystem was 280.7 kW·h, of which 137.3 kW·h was consumed by the system's intrinsic power needs, leaving 143.4 kW·h for household usage. Therefore, the actual solar power conversion efficiency of the PV array was 8.3%. During the second heating season, total energy generated by the power-generation subsystem was 261.7 kW·h, with 146 kW·h consumed by the system, leaving 115.7 kW·h for household usage. Therefore, the actual solar power conversion efficiency of the PV array was 8.1%.

(3) Over both heating seasons, the solar-powered thermostatic biogas-generation subsystem was able to maintain a temperature of 27 ± 2°C for thermostatic fermentation inside the biogas digester, even when the ambient temperature reached a minimum of −25°C. Furthermore, the daily biogas production was maintained at approximately 1.0 $m^3$ throughout both heating seasons.

(4) After optimizing the system, the energy-saving rate increased from 66.2% to 85.5%. This was primarily because the low-temperature floor heaters provided substantially more heat to the building than the previous radiators. The system was able to save a total of 7,364 kg of standard coal each year, had a static payback period of 3.1 yr, and reduced $CO_2$ emissions by 27.03 t each year.

## Conflicts of Interest

The authors declare that they have no conflicts of interest.

## Acknowledgments

This work was funded by the National Natural Science Foundation of China (51676094), Natural Science Foundation of China (51706128), International S&T Cooperation Projects of Gansu Province (1604WKCA009), Scientific Research Program Funded by Shanxi Provincial Education Department (Program no. 17JS018), and the Natural Science Foundation of Gansu Province (1508RJYA097).

## References

[1] Q. Ding, W. Cai, C. Wang, and M. Sanwal, "The relationships between household consumption activities and energy consumption in china—an input-output analysis from the lifestyle perspective," *Applied Energy*, vol. 207, pp. 520–532, 2017.

[2] C. Yao, C. Chen, and M. Li, "Analysis of rural residential energy consumption and corresponding carbon emissions in China," *Energy Policy*, vol. 41, pp. 445–450, 2012.

[3] Y. Chen, W. Hu, P. Chen, and R. Ruan, "Household biogas CDM project development in rural China," *Renewable & Sustainable Energy Reviews*, vol. 67, pp. 184–191, 2017.

[4] C. Wang, A. Engels, and Z. Wang, "Overview of research on China's transition to low-carbon development: The role of cities, technologies, industries, and the energy system," *Renewable & Sustainable Energy Reviews*, vol. 81, no. 1, pp. 1350–1364, 2017.

[5] S. Bhattarai, G. K. Kafle, S.-H. Euh, J.-H. Oh, and D. H. Kim, "Comparative study of photovoltaic and thermal solar systems with different storage capacities: performance evaluation and economic analysis," *Energy*, vol. 61, pp. 272–282, 2013.

[6] M. Esen and T. Yuksel, "Experimental evaluation of using various renewable energy sources for heating a greenhouse," *Energy and Buildings*, vol. 65, pp. 340–351, 2013.

[7] T. Jenssen, A. König, and L. Eltrop, "Bioenergy villages in Germany: bringing a low carbon energy supply for rural areas into practice," *Journal of Renewable Energy*, vol. 61, pp. 74–80, 2014.

[8] H. Dagdougui, R. Minciardi, A. Ouammi, M. Robba, and R. Sacile, "Modeling and optimization of a hybrid system for the energy supply of a 'green' building," *Energy Conversion and Management*, vol. 64, pp. 351–363, 2012.

[9] O. Ozgener and L. Ozgener, "Modeling of driveway as a solar collector for improving efficiency of solar assisted geothermal heat pump system: a case study," *Renewable & Sustainable Energy Reviews*, vol. 46, pp. 210–217, 2015.

[10] J. F. Chen, Y. J. Dai, and R. Z. Wang, "Experimental and theoretical study on a solar assisted CO2 heat pump for space heating," *Journal of Renewable Energy*, vol. 89, pp. 295–304, 2016.

[11] Z. Wu, H. Tazvinga, and X. Xia, "Demand side management of photovoltaic-battery hybrid system," *Applied Energy*, vol. 148, pp. 294–304, 2015.

[12] A. R. E. Aguilar, M. B. Roman, D. Kirk et al., "Technical and economic feasibility of a solar-bio-powered waste utilization and treatment system in Central America," *Journal of Environmental Management*, vol. 184, no. 2, pp. 371–379, 2016.

[13] B. Zou, J. Dong, Y. Yao, and Y. Jiang, "An experimental investigation on a small-sized parabolic trough solar collector for water heating in cold areas," *Applied Energy*, vol. 163, pp. 396–407, 2016.

[14] Y. Wang, F. Wang, and H. Wang, "Heating energy consumption questionnaire and statistical analysis of rural buildings in China," *Procedia Engineering*, vol. 146, pp. 380–385, 2016.

[15] B. Lin and H. Liu, "China's building energy efficiency and urbanization," *Energy and Buildings*, vol. 86, pp. 356–365, 2015.

[16] M. Hu, G. Pei, Q. Wang, J. Li, Y. Wang, and J. Ji, "Field test and preliminary analysis of a combined diurnal solar heating and nocturnal radiative cooling system," *Applied Energy*, vol. 179, pp. 899–908, 2016.

Hindawi
BioMed Research International
Volume 2018, Article ID 8376127, 9 pages
https://doi.org/10.1155/2018/8376127

*Research Article*

# Ni-Ru/$CeO_2$ Catalytic Hydrothermal Upgrading of Water-Insoluble Biocrude from Algae Hydrothermal Liquefaction

**Donghai Xu, Shuwei Guo, Liang Liu, Hui Hua, Yang Guo, Shuzhong Wang, and Zefeng Jing**

*Key Laboratory of Thermo-Fluid Science & Engineering, Ministry of Education, School of Energy and Power Engineering, Xi'an Jiaotong University, Xi'an, Shaanxi Province 710049, China*

Correspondence should be addressed to Donghai Xu; haidongxu93346423@aliyun.com

Received 22 November 2017; Accepted 28 March 2018; Published 8 May 2018

Academic Editor: Chun-Fei Wu



Hydrothermal liquefaction (HTL) of algae is a promising crude bio-oil (biocrude) production technology, which can convert wet algae into water-insoluble biocrude and other coproducts. In this work, algae HTL at 350°C and 20 min was conducted to obtain water-insoluble biocrude ($B_1$), which was then hydrothermally upgraded at 450°C, 60 min, or with added $H_2$ and/or homemade catalyst (i.e., Ni-Ru/$CeO_2$ or Ni/$CeO_2$) for the first time. The characteristics (e.g., yield, elemental component, energy recovery, and molecular and functional group compositions) of upgraded water-insoluble biocrude ($B_2$) as well as light biocrude thereof were analyzed comprehensively. The results show that Ni-Ru/$CeO_2$+$H_2$ led to the highest yield and HHV (higher heating value), the best elemental compositions quality of $B_2$, and the largest fraction and the best light of light biocrude in $B_2$. Ni-Ru/$CeO_2$+$H_2$ had good catalytic desulfurization effect and could transform high-molecular-weight compounds into low-molecular-weight compounds in $B_1$ upgrading. At the condition above, 46.2% of chemical energy in the initial algae could be recovered by $B_2$, while average 54.9% of chemical energy in $B_2$ was distributed in its light biocrude (hexane-soluble) portion. On the whole, Ni-Ru/$CeO_2$+$H_2$ can be considered as the optimal additive in all tested cases.

## 1. Introduction

Hydrothermal liquefaction (HTL) of algae for crude bio-oil (biocrude) production has increasingly drawn much attention due to its benign raw material properties, high bio-oil yield, avoidance of drying step, and so on. It can chemically convert high moisture algae into water-insoluble biocrude and coproducts (i.e., gases, aqueous phase, and solids) in hot compressed water. However, the obtained biocrude does not meet biodiesel standards in some aspects such as heteroatoms content and heating value, so it requires further biorefinery via proper approaches. An effective method is hydrothermal upgrading, in which biocrude reacts in water, either thermally or with added $H_2$ and/or catalyst to remove heteroatoms and improve heating value, and so on [1].

Typically, after algae HTL of 1–4 h at around 350°C, total biocrude (both water-insoluble and water-soluble biocrudes) is collected by organic solvent (e.g., dichloromethane) extraction from all postreaction products and followed hydrothermal upgrading with 2–6 h at a supercritical temperature [2–7]. Notably, the water-insoluble biocrude can spontaneously separate from aqueous phase by gravity upon cooling after algae HTL and commonly accounts for more than 85 wt% of the total biocrude and has remarkably distinct characteristics in comparison to the water-soluble biocrude extracted from the aqueous phase by organic solvent [8, 9]. Due to pollution and cost restrictions of extraction solvent, it is more feasible to adopt solvent-free method to collect and upgrade the water-insoluble biocrude (as the majority of the total biocrude) in actual industrial production. On the other hand, it is convenient and economic to directly use the aqueous phase instead of water in hydrothermal upgrading, because it is easy to separate part of the aqueous phase after algae HTL and to use the rest for following

hydrothermal upgrading. However, relevant investigation about water-insoluble biocrude upgrading with the aqueous phase and catalyst is very scarce now, except for our latest research about catalytic hydrothermal upgrading of water-insoluble biocrude in supercritical water at 400°C, 60 min with commercial catalysts (i.e., $Mo_2C$, Ru/C, and Pt/C ) [1].

As an extension, this work conducted 20 min of algae HTL at 350°C to obtain water-insoluble biocrude and then upgraded it at the higher temperature of 450°C, 60 min with added $H_2$ and/or Ni-Ru bimetallic catalyst homemade for the first time. The yields, elemental components, energy recoveries, and molecular and functional group compositions of the upgraded water-insoluble biocrudes at various conditions were analyzed systematically. The characteristics concerning the light biocrude in the upgraded biocrude and gaseous products were examined as well. This information is valuable for optimizing processes design and operation parameters of the hydrothermal upgrading of the water-insoluble biocrude from algae HTL.

## 2. Experimental Section

*2.1. Experimental Procedures.* The adopted algae (*Nannochloropsis* sp.) slurry had 30.5 ± 2.5 wt% of biomass content, which was determined by drying three separate samples at 65°C in an oven for 48 h. The dry basis algae (about 23.30 MJ/kg) contained approximately 52.85, 7.43, 8.78, and 0.62 wt% of C, H, N, and S contents, respectively. High purity solvents (i.e., dichloromethane (DCM), n-hexane, and deuterated chloroform ($CDCl_3$)) were obtained from commercial sources. High purity (≥99.999%) hydrogen and helium were purchased from Baoguang Gas Co., Ltd. Several 4.1 ml mini-batch reactors were assembled for the HTL experiments by using 1/2-in. 316 stainless steel Swagelok port connectors and caps. Subsequent biocrude upgrading experiments were conducted in the same reactors, but upgrading reactions with added $H_2$ or with gas analysis were implemented by additionally equipping each reactor with a length of stainless steel tubing and a high-pressure gas valve.

First of all, one set of experiments were carried out to obtain water-insoluble biocrude from algae HTL at 350°C, 20 min, and 14.1 wt% of algae loading in the reactor (corresponding to 1.2354 g algae slurry and 1.3990 g deionized water). After being sealed, the reactor was placed in a Techne fluidized sand bath (Model SBL-2) preheated up to 350°C for the desired residence time (20 min). Herein, the corresponding reaction pressure was about 16.5 MPa and the reactor heating-up time was 2-3 min. The postreaction reactor was removed from the sand bath and quenched in an ambient-temperature water bath for 15 min and then equilibrated at room temperature for at least 1 h before products collection and analysis. The reactor was kept in a vertical position as it was cooled so that little biocrude would adhere to the inner surface of the reactor top cap. We then opened the reactor and removed 1.875 g aqueous phase via a pipette. The water-insoluble biocrude (about 0.1505 g) from algae HTL (with a little solids residue) and the aqueous phase residue (around 0.3750 g) in the reactor were never in contact with DCM and were used in situ for the following upgrading experiments. 0.0225 g catalyst (if necessary, about 15 wt% of $B_1$ mass) was loaded into the reactor, and then the reactor was vacuumed and filled either with helium (10 KPa) to eliminate the effect of reactor inside air in the test without $H_2$ addition or with $H_2$ to 2.0 MPa to check the effect of $H_2$ addition. The upgrading experiments were carried out in the sand bath at 450°C, 60 min under different conditions such as catalyst and/or $H_2$ addition, and the corresponding reaction pressure was approximately 22.5 MPa (based on steam tables). We then removed the reactor from the sand bath and cooled it and followed the previously described method 2 procedure [8] for products collection. In this procedure, the contact between the aqueous phase and DCM is avoided by removing the aqueous product via a pipette, prior to the recovery of the water-insoluble biocrude from the reactor. Eventually, water-insoluble biocrude ($B_2$) was obtained from $B_1$ upgrading products, and light biocrude in $B_2$ ($B_2^L$) could be further gained by n-hexane extraction.

The mainly used catalysts were 10 wt%Ni0.1Ru/$CeO_2$ and 10 wt%Ni/$CeO_2$, which were prepared in house and detailed procedures had been described by our previous report [10]. Herein, 10 wt% represents the mass percentage of active metal (Ni+Ru or Ni) in the catalyst, and 0.1 is the mass ratio of Ru/Ni. For simplification, Ni-Ru/$CeO_2$, Ni/$CeO_2$, and "none" were adopted to separately represent 10 wt%Ni0.1Ru/$CeO_2$, 10 wt%Ni/$CeO_2$, and the case without catalyst and $H_2$ in this work. Herein, the cases of Ni/$CeO_2$ and "none" were tested for comparison with that of Ni-Ru/$CeO_2$.

*2.2. Analysis Methods.* Elemental compositions (i.e., C, H, N, and S) of dry basis algae and all biocrude samples were determined by a cube CHNS elemental analyzer (Elementar Vario EL) with uncertainties of <3% of the reported value. Compound components of biocrude were identified via a gas chromatography-mass spectrometer (GC-MS, Agilent Technologies 6890N) equipped with an autosampler, an autoinjector, a mass spectrometric detector, and an Agilent HP-5 capillary column (50 m × 200 $\mu$m × 0.33 $\mu$m). Nuclear magnetic resonance (NMR) and Fourier transform infrared (FT-IR) spectroscopic analyses of biocrude were conducted to characterize functional group compositions. Detailed information on these instruments and procedures was introduced in our previous research [8]. Gaseous products were identified and quantified by an Agilent Technologies model 6890N gas chromatograph equipped with a thermal conductivity detector, following the method reported previously [11].

Biocrude yield and energy recovery were defined as follows:

$$\text{Biocrude yield} = \frac{\text{Mass of biocrude}}{\text{Mass of dry basis algae loaded into the reactor}} \times 100\% \quad (1)$$

$$\text{Energy recovery} = \frac{\text{HHV of biocrude} \times \text{the biocrude yield}}{\text{HHV of dry basis algae}} \times 100\%$$

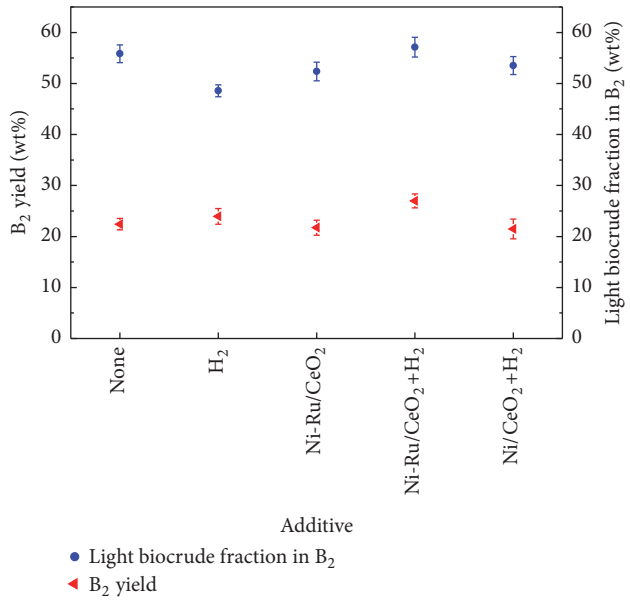


FIGURE 1: $B_2$ yield and light biocrude fraction in $B_2$ after $B_1$ (derived from algae HTL at 350°C, 20 min) upgrading at 450°C, 60 min with or without $H_2$ and/or catalyst.

The higher heating value (HHV) of dry basis algae or biocrude was estimated by the following Dulong formula:

$$\mathrm{HHV\,(MJ/kg)} = 0.338\mathrm{C} + 1.428\left(\mathrm{H} - \frac{\mathrm{O}}{8}\right) + 0.095\mathrm{S}, \quad (2)$$

where C, H, O, and S are the wt% composition of each element in the material. The O content was calculated by the differences from the C, H, N, and S values and reserving 1 wt% for other elements not assessed.

Three independent experiments were carried out at the same conditions to determine the uncertainties of experimental data. The results reported herein are mean values and their uncertainties are the sample standard deviations.

## 3. Results and Discussion

All experiments about algae HTL and biocrude upgrading produced water-insoluble biocrude, gases, aqueous phase, and solids, and total mass balance exceeded 91.0 wt% in products collection.

*3.1. Biocrude Yield.* Algae HTL at 350°C, 20 min, and 14.1 wt% of algae loading led to 37.5 ± 0.21 wt% of $B_1$ yield. Figure 1 shows $B_2$ properties after $B_1$ upgrading at 450°C, 60 min, with or without $H_2$ and/or catalyst. It can be found that Ni-Ru/$CeO_2$+$H_2$ led to the highest $B_2$ yield (27.0 wt%, corresponding to about 72.0 wt% of $B_1$ yield), likely due to catalytic hydrogenation effect during $B_1$ upgrading. The much lower $B_2$ yield (21.72 wt%) appeared at the Ni-Ru/$CeO_2$ condition, and this might be attributed to a large amount of gases formation promoted by the catalyst in supercritical water [10]. Based on the $B_2$ yield (23.94 wt%) in the case of $H_2$ addition, there seemingly was synergetic effect between $H_2$ and Ni-Ru/$CeO_2$ on $B_2$ yield improvement because their coexistence probably inhibits gases formations. Light biocrude fraction in biocrude, which was defined as the measured mass of light biocrude (hexane-soluble) divided by the biocrude mass, is a proxy for biocrude quality because these hexane-soluble compounds are less polar and of moderate boiling point and thus more desirable for fuel use, compared with heavy biocrude (hexane-insoluble) compounds [9]. As indicated in Figure 1, Ni-Ru/$CeO_2$+$H_2$ could obviously increase the light biocrude fraction in $B_2$ and led to the highest value (57.14 wt%), meaning the remarkable improvement of $B_2$ quality. Herein, similar synergetic effect between $H_2$ and Ni-Ru/$CeO_2$ on the promotion of the light biocrude fraction in $B_2$ was found as well, probably due to the conversion of hexane-insoluble biocrude to hexane-soluble biocrude in hydrothermal upgrading at the Ni-Ru/$CeO_2$+$H_2$ condition. Thereby, we could adopt the Ni-Ru/$CeO_2$ catalyst together with $H_2$ to regulate the properties of the upgraded water-insoluble biocrude. It is worthy noticing that the upgrading without $H_2$ and catalyst (i.e., none) rendered considerably high $B_2$ yield and light biocrude fraction in $B_2$, so it may be considered as a pre-upgrading process of $B_1$ in actual large scale production.

*3.2. Elemental Composition and HHV.* Table 1 indicates elemental compositions and HHVs of $B_2$ and $B_2{}^{L}$ after $B_1$ upgrading under different conditions. It can be observed that hydrothermal upgrading could increase the C content and simultaneously reduce S and O contents. Deoxygenation can be realized by forming $CO_2$, $H_2O$, and CO through complex reactions such as decarboxylation and dehydration [12, 13]. Note that the Ni-Ru/$CeO_2$ catalyst had the best catalytic desulfurization effect and Ni-Ru/$CeO_2$+$H_2$ was also much better for sulfur removal. This has good agreement with the findings that the S content in bio-oil by Ni/$SiO_2$-$Al_2O_3$ catalytic upgrading is below detection limit [14] and Ru/C has good desulfurization performance [15]. Ni-Ru/$CeO_2$+$H_2$ rendered the highest C content, the largest HHV, the lowest O content, and the second lowest N+S content, so totally exhibiting the best catalytic upgrading effect in all tested cases. Consistently, $H_2$ addition together with catalyst is desirable for hydrogenation and hydrodeoxygenation behaviors in biocrude upgrading [3, 4, 6]. Apparently, based on the higher C, H contents and HHV but lower heteroatoms (i.e., N, O, and S) contents, each $B_2{}^{L}$ had better quality than its corresponding $B_2$. Thus, the tested catalysts (i.e., Ni-Ru/$CeO_2$ and Ni/$CeO_2$) had substantially positive effect on the improvement of $B_2{}^{L}$ quality in $B_1$ upgrading in the presence of $H_2$, due to the increase of C, H contents, and HHVs and the decrease of N, S, and O contents. The combined Ni-Ru/$CeO_2$+$H_2$ led to the best $B_2{}^{L}$ quality with the highest C+H content, the largest HHV, and the lowest N+S+O content. Overall, the best catalytic effect of Ni-Ru/$CeO_2$+$H_2$ is likely attributed to positive reactions such as hydrogenation, deoxygenation, denitrogenation, and desulfurization in $B_1$ upgrading.

Energy recovery is a key indicator of the effectiveness of a hydrothermal process in capturing the chemical energy of initial algae in the produced biocrude [16]. Due to little

Table 1: Elemental compositions, HHVs, and energy recoveries of $B_1$ (derived from algae HTL at 350°C, 20 min) and $B_2$ and $B_2^L$ (obtained from $B_1$ upgrading at 450°C, 60 min with different additives).

| Additive | Biocrude | Element (wt%) | | | | | N/C | O/C | HHV (MJ/kg) | Energy recovery (%) |
|---|---|---|---|---|---|---|---|---|---|---|
| | | C | H | N | S | O | | | | |
| – | $B_1$ | 77.05 | 9.76 | 4.82 | 0.53 | 6.84 | 0.063 | 0.089 | 38.81 | 62.46 |
| None | $B_2$ | 79.74 | 9.44 | 4.24 | 0.37 | 5.21 | 0.053 | 0.065 | 39.54 | 38.03 |
| $H_2$ | $B_2$ | 79.19 | 9.59 | 4.37 | 0.41 | 5.44 | 0.055 | 0.069 | 39.53 | 40.61 |
| Ni-Ru/$CeO_2$ | $B_2$ | 79.63 | 9.55 | 4.03 | 0.19 | 5.6 | 0.051 | 0.070 | 39.57 | 36.89 |
| Ni-Ru/$CeO_2$+$H_2$ | $B_2$ | 80.23 | 9.57 | 4.12 | 0.22 | 4.86 | 0.051 | 0.061 | 39.94 | 46.24 |
| Ni/$CeO_2$+$H_2$ | $B_2$ | 79.27 | 8.87 | 4.55 | 0.45 | 5.86 | 0.057 | 0.074 | 38.46 | 37.80 |
| None | $B_2^L$ | 80.26 | 9.49 | 4.04 | 0.25 | 4.96 | 0.050 | 0.062 | 39.82 | 32.11 |
| $H_2$ | $B_2^L$ | 80.63 | 9.77 | 3.59 | 0.35 | 4.66 | 0.045 | 0.058 | 40.41 | 30.10 |
| Ni-Ru/$CeO_2$ | $B_2^L$ | 81.26 | 9.57 | 3.54 | 0.18 | 4.45 | 0.044 | 0.055 | 40.35 | 23.24 |
| Ni-Ru/$CeO_2$+$H_2$ | $B_2^L$ | 81.9 | 9.73 | 3.62 | 0.19 | 3.56 | 0.044 | 0.043 | 40.96 | 29.25 |
| Ni/$CeO_2$+$H_2$ | $B_2^L$ | 81.4 | 9.6 | 3.89 | 0.16 | 3.95 | 0.048 | 0.049 | 40.53 | 24.75 |

variation of biocrude HHVs under different conditions, the energy recovery is largely tracked with the biocrude yield, as displayed in Table 1. It can be noticed that the energy recovery of $B_1$ was 62.5% after algae HTL, but after $B_1$ upgrading at various conditions, the energy recoveries of $B_2$ ranged from 36.9 to 46.2% (average 39.9%) of the heating value of the algae initially loaded into the reactor. Ni-Ru/$CeO_2$+$H_2$ addition led to the high energy recovery of 46.2% owing to the largest $B_2$ yield in this case (see Figure 1). Moreover, the energy recoveries of $B_2^L$ ranged from 23.2 to 32.1% (average 27.9%) of the heating value of the algae loaded initially. Notably, it can be calculated that 49.7–58.6% (average 54.9%) of chemical energy in $B_2$ was distributed to $B_2^L$ (i.e., its light biocrude portion). Hence, taking into account the yields, elemental compositions, HHVs, and energy recoveries of both $B_2$ and $B_2^L$, Ni-Ru/$CeO_2$+$H_2$ can be regarded as the optimal additive in all tested cases.

*3.3. Gas Analysis.* Note that Ni-Ru/$CeO_2$ is favorable for organic matters gasification to produce a flammable gas mixture in supercritical water [10], so gaseous products are also concerned in this research. Table 2 provides gaseous products after hydrothermal upgrading of $B_1$ at different conditions, so major gases compositions included $H_2$, $CH_4$, $CO_2$, $C_2H_2$, $C_2H_6$, CO, and $C_2H_4$ at the condition in absence of $H_2$. Compared with the case without catalyst and $H_2$ (i.e., none), the Ni-Ru/$CeO_2$ catalyst could significantly improve $H_2$ mole fraction (from 29.6% to 41.1%), and meanwhile the postreaction pressure increased from about 2.2 to 3.5 bar. This suggests that Ni-Ru/$CeO_2$ led to much more $H_2$ and C-containing gases formation during $B_1$ upgrading probably mainly via promoting water-gas shift and decarbonation reactions. This outcome is in good accord with the findings that Ru/C [17] and Ni-Ru/$CeO_2$ [10] are effective for hydrothermal gasification and the relatively low $B_2$ yield in Figure 1 as well. Notably, it reminds us that these flammable gases formed in the water-insoluble biocrude upgrading should be disposed properly in large scale production processes. In the case of $H_2$ addition, major identified gaseous products were $CH_4$, $CO_2$, $C_2H_6$, $C_2H_4$, CO, and unreacted $H_2$, but there was no $C_2H_2$ due to hydrogenation effect. Similar gases compositions are also found in catalytic upgrading of duckweed biocrude in subcritical water [18]. The far high $H_2$ mole fraction (about 70%) is mainly attributed to initial $H_2$ addition (2.0 MPa). Nonetheless, the remarkable reduction of the postreaction pressure in contrast to that before reaction suggests a large amount of $H_2$ consumption for heteroatoms removal (likely in the forms of $H_2O$, $NH_3$, and $H_2S$) and hydrogenation in $B_1$ upgrading. Certainly, at the same time, there is also $H_2$ formation due to biocrude gasification in supercritical water (see the "none" group).

*3.4. GC-MS Analysis.* Biocrude is produced by complex reactions such as oligomerization, depolymerization, decomposition, and reformation reactions [19–21]. Its compounds compositions are mainly dependent on feedstock feature, since not only lipids but also proteins and carbohydrates are converted into biocrude in algae HTL [22]. Figure 2 exhibits total ion chromatograms of $B_1$ and $B_2$ derived from $B_1$ upgrading at the Ni-Ru/$CeO_2$+$H_2$ condition. The characteristics of the upgraded water-insoluble biocrude are explored here for the first time. In combination with Table 3 (tentative GC-MS analysis results), it can be confirmed that $B_1$ consisted of large amounts of complex compounds such as propanal, 2,2-dimethyl-, oxime; cycloheptasiloxane, tetradecamethyl-; cyclooctasiloxane, hexadecamethyl-; heptadecane; 2-hexadecene, 3,7,11,15-tetramethyl-, [R-[R*,R*-(E)]]-; 7,8-didehydro-4,5-epoxy-17-methyl-3,6-bis[(trimethylsilyl)oxy]-, (5.alpha.,6.alpha.)-; cycloheptasiloxane, tetradecamethyl-; cyclodecasiloxane, eicosamethyl-; and cyclotrisiloxane, hexamethyl-; 2-methyl-6-(5-methyl-2-thiazolin-2-ylamino)pyridine. Some of them contained N, O, and both them, which is consistent with high N and O contents in this material (see Table 1). Some existing cyclic nitrogenous compounds (e.g., 7,8-didehydro-4,5-epoxy-17-methyl-3,6-bis[(trimethylsilyl)oxy]-, (5.alpha.,6.alpha.)-; 2-methyl-6-(5-methyl-2-thiazolin-2-ylamino)pyridine) are likely produced

Table 2: Gaseous products compositions after $B_1$ upgrading at 450°C, 60 min with different additives.

| Additive | $H_2$ (%) | CO (%) | $CH_4$ (%) | $CO_2$ (%) | $C_2H_2$ (%) | $C_2H_4$ (%) | $C_2H_6$ (%) | Pressure after reaction (bar) |
|---|---|---|---|---|---|---|---|---|
| None | 29.6 ± 1.2 | 5.0 ± 0.8 | 18.7 ± 2.2 | 16.1 ± 1.1 | 12.2 ± 1.8 | 4.3 ± 0.4 | 12.5 ± 1.1 | 2.2 ± 0.2 |
| $H_2$ | 70.7 ± 6.9 | 2.8 ± 0.4 | 9.2 ± 2.4 | 6.6 ± 1.2 | – | 2.91 ± 0.3 | 6.5 ± 1.0 | 9.7 ± 0.4 |
| Ni-Ru/$CeO_2$ | 41.1 ± 2.7 | 3.2 ± 0.5 | 16.6 ± 1.9 | 21.8 ± 1.4 | 5.7 ± 1.0 | 2.7 ± 0.2 | 8.4 ± 1.5 | 3.5 ± 0.3 |
| Ni-Ru/$CeO_2$+$H_2$ | 70.4 ± 7.7 | 1.1 ± 0.6 | 9.0 ± 1.7 | 9.7 ± 1.3 | – | 1.8 ± 0.3 | 6.5 ± 0.9 | 8.8 ± 0.3 |
| Ni/$CeO_2$+$H_2$ | 69.8 ± 7.2 | 2.1 ± 0.4 | 8.75 ± 1.2 | 8.9 ± 1.1 | – | 1.9 ± 0.3 | 6.2 ± 0.8 | 8.2 ± 0.4 |

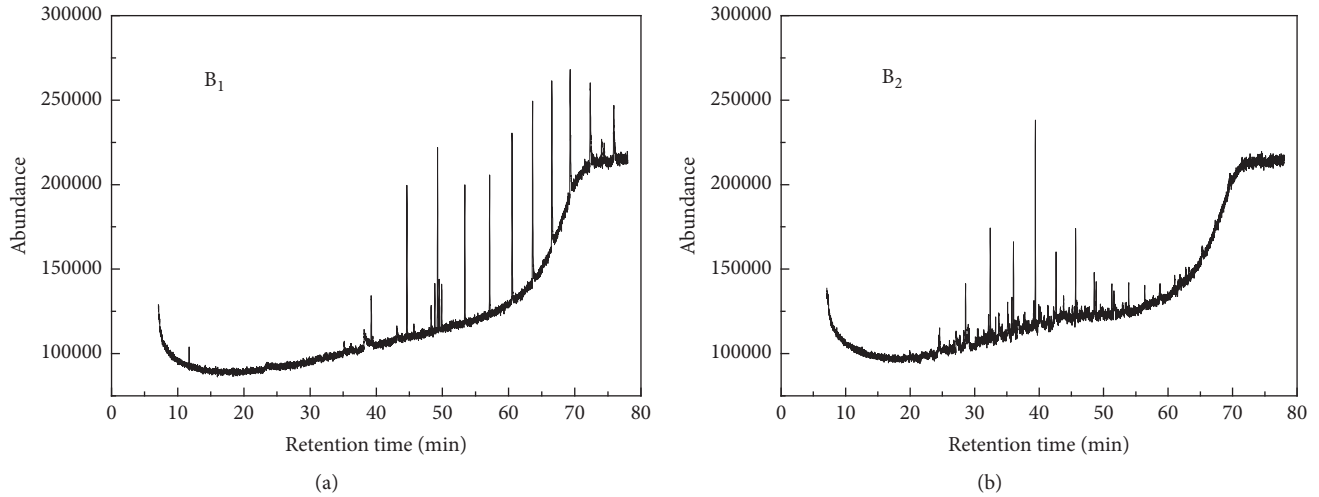


Figure 2: Total ion chromatograms of (a) $B_1$ derived from algae HTL at 350°C, 20 min, and (b) $B_2$ obtained from $B_1$ upgrading at 450°C, 60 min, Ni-Ru/$CeO_2$+$H_2$ conditions.

by Maillard reactions between amino acids and reducing sugars, which are separately formed by the hydrolysis of proteins and carbohydrates [20].

Apparently, the total ion chromatogram of $B_2$ looks completely different from that of $B_1$, because most compounds appearing in the range of 45–55 min in $B_1$ disappeared or reduced. Major compounds in $B_2$ appeared in the range of 28–55 min, where the peaks areas sum of all identified compounds took up 95.7% of the total peak area. Main compounds involved pentadecane, tridecane, tetradecane, heptadecane, and dodecane, in which pentadecane and tridecane seem to be the most abundant two species. Thus, hydrothermal upgrading of $B_1$ with Ni-Ru/$CeO_2$+$H_2$ is able to transform high-molecular-weight compounds into low-molecular-weight (i.e., low-boiling-point) compounds, meaning the quality improvement of the upgraded biocrude. More importantly, this catalytic upgrading helps to remove heteroatoms (e.g., O and N) in $B_1$ to form the upgraded biocrude with abundant presence of a series of aliphatic saturated hydrocarbons. Reactions such as decarboxylation, dehydroxylation, and deamination contribute to the heteroatoms removal, hydrocarbons formation, and so corresponding increase in carbon content and HHV after hydrothermal upgrading.

*3.5. NMR Analysis.* $^1$H-NMR and $^{13}$C-NMR analysis of biocrude was conducted to identify the types of functional groups. Chemical shift provides information concerning functional group identification, and corresponding peak area can roughly reflect its relative abundance.

*3.5.1. $^1$H NMR Analysis.* Figure 3 illustrates $^1$H NMR spectra of $B_1$ and $B_2$ derived from $B_1$ upgrading at the Ni-Ru/$CeO_2$+$H_2$ condition. The resonances at 0.8 and 1.2 ppm are characteristics of protons in terminal methyl groups and methylene groups in alkyl chains, respectively [23]. The peak at around 2.1 ppm is consistent with resonance expected from protons on carbon atoms $\alpha$ to an acyl group [15]. There was a peak near 7.2 ppm in $B_1$ and $B_2$, which arises from aromatic protons or conjugated dienes [15, 24], and herein the much smaller peak area in the $B_2$ spectrum suggests that the catalytic hydrothermal upgrading by Ni-Ru/$CeO_2$+$H_2$ can effectively reduce the compounds containing the functional groups above. This is consistent with the findings in the GC-MS analysis. Differently, in the $B_2$ spectrum, a clear peak emerged at around 5.2 ppm representing phenolic -OH [24], possibly due to the existence of hydroxyketone in the upgraded biocrude. The appearance of these peaks above reveals the

Table 3: Tentative products identifications by GC-MS analysis of $B_1$ and $B_2$ in Figure 2.

| Retention time (min) | Compound | Relative peak area (%) |
|---|---|---|
| 11.7223[a] | Propanal, 2,2-dimethyl-, oxime | 0.3283 |
| 38.1796[a] | Benzoic acid, 4-methyl-2-trimethylsilyloxy-, trimethylsilyl ester | 1.337 |
| 39.2486[a] | Cycloheptasiloxane, tetradecamethyl- | 3.2133 |
| 43.1274[a] | Diethyl phthalate | 0.0338 |
| 44.6316[a] | Cyclooctasiloxane, hexadecamethyl- | 7.5681 |
| 45.6930[a] | Heptadecane | 0.6365 |
| 48.2967[a] | 1-Dodecanol, 3,7,11-trimethyl- | 1.3641 |
| 48.8617[a] | Hexadecane, 2,6,10,14-tetramethyl- | 1.862 |
| 49.2741[a] | Cyclononasiloxane, octadecamethyl- | 7.8494 |
| 49.5718[a] | 2-Hexadecene, 3,7,11,15-tetramethyl-, [R-[R*,R*-(E)]]- | 5.1915 |
| 57.1387[a] | Cyclodecasiloxane, eicosamethyl- | 5.7078 |
| 60.5213[a] | Morphinan, 7,8-didehydro-4,5-epoxy-17-methyl-3,6-bis[(trimethylsilyl)oxy]-, (5.alpha.,6.alpha.)- | 8.6591 |
| 63.6290[a] | Cycloheptasiloxane, tetradecamethyl- | 10.5962 |
| 66.5381[a] | Cyclodecasiloxane, eicosamethyl- | 10.0725 |
| 69.3022[a] | Cyclotrisiloxane, hexamethyl- | 12.5258 |
| 69.7069[a] | Tetrasiloxane, decamethyl- | 0.5209 |
| 71.5088[a] | Arsenous acid, tris(trimethylsilyl) ester | 0.3042 |
| 72.3411[a] | (p-Methoxyphenyl)-acetonyl-dimethylsilane | 6.9254 |
| 72.5015[a] | 2-Methyl-6-(5-methyl-2-thiazolin-2-ylamino)pyridine | 1.0923 |
| 75.8993[a] | 2,4,6-Cycloheptatrien-1-one, 3,5-bis-trimethylsilyl- | 5.2647 |
| 24.5728 | Undecane | 2.7899 |
| 28.6044 | Dodecane | 6.3133 |
| 32.1702 | Benzene, 1-(2-butenyl)-2,3-dimethyl- | 4.0373 |
| 32.4222 | Tridecane | 10.9529 |
| 33.2621 | 2,4,6(1H,3H,5H)-Pyrimidinetrione, 5-butyl-5-ethyl-1,3-bis(trimethylsilyl)- | 3.2033 |
| 33.7432 | Spiro(9-methylenetricyclo[6.2.1.0(2,7)]undeca-2,4,6-triene)-11,1′-cyclopropane | 2.7049 |
| 35.1252 | Naphthalene, 1,2,3,4-tetrahydro-1,1,6-trimethyl- | 3.9456 |
| 35.7742 | 2-Tetradecene, (E)- | 3.7452 |
| 36.0338 | Tetradecane | 7.816 |
| 39.1873 | Cyclododecane | 3.3313 |
| 39.4240 | Pentadecane | 17.3115 |
| 39.9509 | 2H-1,2,5-Oxasilaborole, 5-tert-butyl-4-ethyl-2,2,3-trimethyl- | 3.3719 |
| 42.6309 | Hexadecane | 4.6292 |
| 45.6699 | Heptadecane | 7.1577 |
| 48.5485 | Octadecane | 5.014 |
| 48.8539 | Hexadecane, 2,6,10,14-tetramethyl- | 4.3843 |
| 51.2897 | Nonadecane | 3.2509 |
| 51.5951 | 3-Butyn-1-ol | 2.025 |
| 53.8934 | Eicosane | 2.5267 |
| 56.3826 | Heptadecane, 2,6,10,15-tetramethyl- | 1.4892 |

[a]The peaks are for Figure 2(a) and other peaks are for Figure 2(b).

existence of alkyl moieties, carbonyl functionalities, and aromatic or unsaturated molecules in the biocrudes, though in different amounts [9]. Overall, in $B_1$ and $B_2$ obtained from $B_1$ upgrading with Ni-Ru/$CeO_2$+$H_2$, alkane functionality (0.5–1.5 ppm) and aliphatic $\alpha$-to-heteroatom/unsaturated functionality (1.5–3.0 ppm) [25] were very abundant, due to the presence of alkanes and other compounds with aliphatic methylene and methyl groups.

*3.5.2. $^{13}C$ NMR Analysis.* Figure 4 displays $^{13}$C-NMR spectra of $B_1$ and $B_2$ (at the Ni-Ru/$CeO_2$+$H_2$ condition). They have larger chemical shift regions and thus provide more details

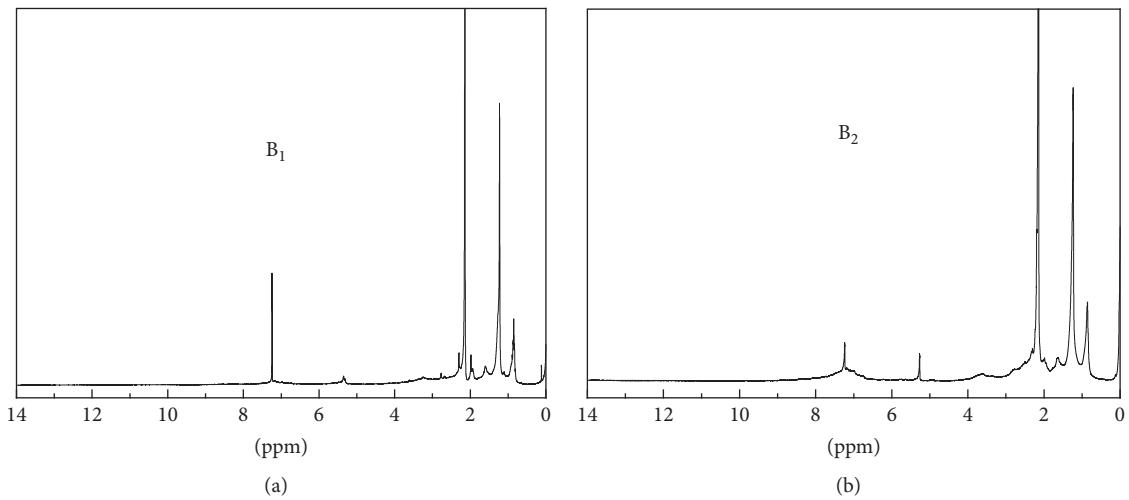


Figure 3: $^{1}$H-NMR spectra of (a) $B_1$ obtained from algae HTL at 350°C, 20 min, and (b) $B_2$ derived from $B_1$ upgrading at 450°C, 60 min, and Ni-Ru/$CeO_2$+$H_2$ conditions.

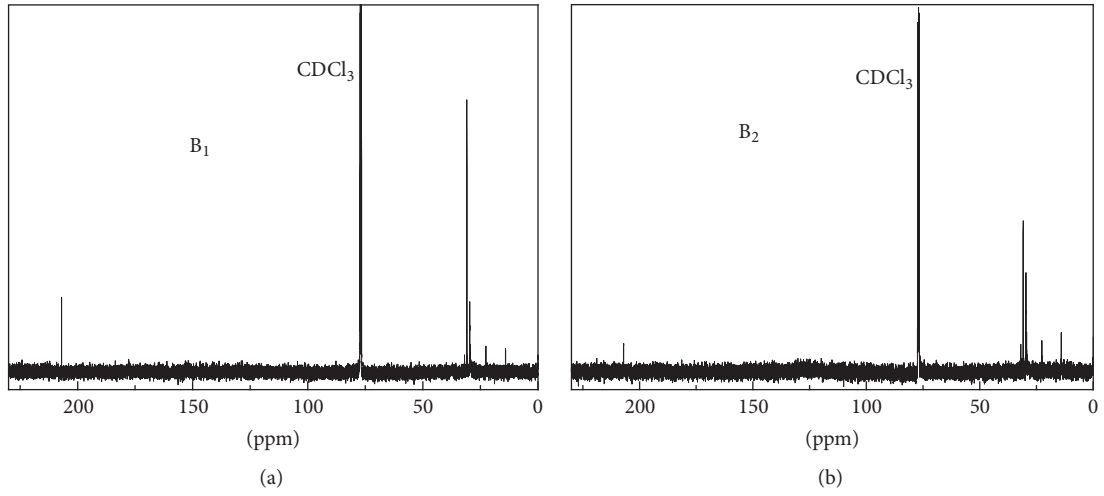


Figure 4: $^{13}$C-NMR spectra of (a) $B_1$ derived from algae HTL at 350°C, 20 min, and (b) $B_2$ obtained from $B_1$ upgrading at 450°C, 60 min, and Ni-Ru/$CeO_2$+$H_2$ conditions.

about C-related functional groups. The two spectra possessed some peaks in the 0–55 ppm region, where aliphatic methyl and methylene carbon (such as alkane carbons) atoms appear [4]. This suggests that aliphatic linkage variability lies with chain length or degree of branching within the linkers [24]. In detail, the region above can be divided into 0–28 ppm (short aliphatics) and 28–55 (long and branched aliphatics), and these aliphatic carbon atoms contribute significantly to energy content [25]. Except for the solvent peak at around 77 ppm, there was no signal in the 55–95 ppm region, where carbohydrate carbons appear [25]. Moreover, each biocrude also indicated a peak at about 207 ppm, where carbonyl carbons in ketones and aldehydes appear [8]. The drop of the peak area implies the content reduction of the O-containing compounds above after $B_1$ upgrading with Ni-Ru/$CeO_2$+$H_2$.

*3.6. FT-IR Analysis.* Figure 5 elucidates FT-IR spectra of $B_1$ from algae HTL and $B_2$ obtained from hydrothermal upgrading of $B_1$ with Ni-Ru/$CeO_2$+$H_2$. GC-MS and NMR analysis results show that the two biocrudes contained methylene groups in alkanes, which is proved by further FT-IR analysis herein. Asymmetrical and symmetrical C–H stretching vibrations in aliphatic methylene groups appear in the range of 2800–3000 $cm^{-1}$ [15]. The existence of carbonyl carbon (such as carboxylic acids and esters) is characterized by the bands at 1650–1760 $cm^{-1}$ [8]. The high intensity in these two regions is in accord with a significant amount of hydrogen in the biocrudes being aliphatic [15]. The spectrum of $B_2$ also exhibited strong absorbance at approximately 1450 $cm^{-1}$, where the scissoring band in methylene groups emerges [23]. This is probably attributed to some mononuclear

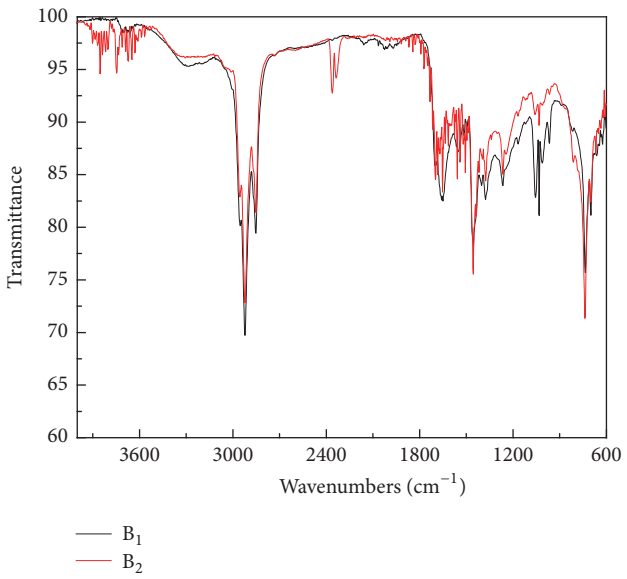


FIGURE 5: FT-IR spectra of $B_1$ derived from algae HTL at 350°C, 20 min, and $B_2$ obtained from $B_1$ upgrading at 450°C, 60 min, and Ni-Ru/$CeO_2$+$H_2$ conditions.

aromatic compounds (e.g., naphthalene, 1,2,3,4-tetrahydro-1,1,6-trimethyl- in Table 3) present in the biocrude. In addition, the two biocrudes also had other different functional groups such as methyl, methylene, aromatic, and alkyne groups appearing at ~1378, ~1271, ~1036, and ~735 cm$^{-1}$, respectively, and their different absorbance intensities imply content variations. Different from $B_1$, $B_2$ presented certain intensity of bands within 2000–2500 cm$^{-1}$ representing triple bonds or cumulative double bonds and large amounts of absorption peaks within 3600–3900 cm$^{-1}$ (e.g., O–H stretching vibrations in hydroxyketone [26]). Hence, hydrothermal upgrading of $B_1$ with Ni-Ru/$CeO_2$+$H_2$ led to obvious variations of functional groups compositions and contents in $B_2$.

## 4. Conclusions

In all tested hydrothermal upgrading (at 450°C, 60 min and with added $H_2$ and/or catalyst) of $B_1$ from algae HTL at 350°C, 20 min, Ni-Ru/$CeO_2$ had the best catalytic desulfurization effect and could significantly improve $H_2$ mole fraction and rendered much more $H_2$ and C-containing gases formation after $B_1$ upgrading. Ni-Ru/$CeO_2$+$H_2$ led to the highest $B_2$ yield (27.0 wt%), the best elemental compositions, and the largest HHV (39.94 MJ/kg), as well as the highest $B_2{}^L$ fraction in $B_2$ (57.1 wt%) and the best $B_2{}^L$ quality. At the Ni-Ru/$CeO_2$+$H_2$ condition, 46.2% of chemical energy in initial algae could be recovered in $B_2$, and average 54.9% of chemical energy in $B_2$ was in its light biocrude portion. Ni-Ru/$CeO_2$+$H_2$ was able to transform high-molecular-weight compounds into low-molecular-weight compounds and led $B_2$ to containing a series of abundant aliphatic saturated hydrocarbons such as pentadecane, tridecane, tetradecane, heptadecane, and dodecane. Overall, Ni-Ru/$CeO_2$+$H_2$ can be regarded as the optimal additive in all tested cases, and there seemingly was synergetic effect between Ni-Ru/$CeO_2$ and $H_2$ on $B_2$ yield and quality improvement after $B_1$ upgrading.

## Conflicts of Interest

The authors declare that they have no conflicts of interest.

## Acknowledgments

This work is supported by the Projects from the National Natural Science Foundation of China (21576219 and 21206132), the Fundamental Research Funds for the Central Universities (no. xjj2016116), the National Key Research and Development Program of China (nos. 2016YFC0801904 and 2017YFB0603604), the Special Financial Grant from the Shaanxi Province Postdoctoral Science Foundation, and the Special Financial Grant from the China Postdoctoral Science Foundation (2014T70922).

## References

[1] D. Xu and P. E. Savage, "Supercritical water upgrading of water-insoluble and water-soluble biocrudes from hydrothermal liquefaction of Nannochloropsis microalgae," *The Journal of Supercritical Fluids*, 2017.

[2] P. Duan and P. E. Savage, "Catalytic hydrotreatment of crude algal bio-oil in supercritical water," *Applied Catalysis B: Environmental*, vol. 104, no. 1-2, pp. 136–143, 2011.

[3] P. Duan and P. E. Savage, "Catalytic treatment of crude algal bio-oil in supercritical water: Optimization studies," *Energy & Environmental Science*, vol. 4, no. 4, pp. 1447–1456, 2011.

[4] P. Duan and P. E. Savage, "Upgrading of crude algal bio-oil in supercritical water," *Bioresource Technology*, vol. 102, no. 2, pp. 1899–1906, 2011.

[5] P. Duan, X. Bai, Y. Xu et al., "Catalytic upgrading of crude algal oil using platinum/gamma alumina in supercritical water," *Fuel*, vol. 109, pp. 225–233, 2013.

[6] P. Duan, B. Wang, and Y. Xu, "Catalytic hydrothermal upgrading of crude bio-oils produced from different thermo-chemical conversion routes of microalgae," *Bioresource Technology*, vol. 186, pp. 58–66, 2015.

[7] Z. Li and P. E. Savage, "Feedstocks for fuels and chemicals from algae: Treatment of crude bio-oil over HZSM-5," *Algal Research*, vol. 2, no. 2, pp. 154–163, 2013.

[8] D. Xu and P. E. Savage, "Characterization of biocrudes recovered with and without solvent after hydrothermal liquefaction of algae," *Algal Research*, vol. 6, pp. 1–7, 2014.

[9] D. Xu and P. E. Savage, "Effect of reaction time and algae loading on water-soluble and insoluble biocrude fractions from hydrothermal liquefaction of algae," *Algal Research*, vol. 12, pp. 60–67, 2015.

[10] Y. Guo, S. Wang, T. Yeh, and P. E. Savage, "Catalytic gasification of indole in supercritical water," *Applied Catalysis B: Environmental*, vol. 166-167, pp. 202–210, 2015.

[11] T. M. Brown, P. Duan, and P. E. Savage, "Hydrothermal liquefaction and gasification of Nannochloropsis sp," *Energy & Fuels*, vol. 24, no. 6, pp. 3639–3646, 2010.

[12] M. Balat, "Mechanisms of thermochemical biomass conversion processes. Part 3: Reactions of liquefaction," *Energy Sources,*

*Part A: Recovery, Utilization, and Environmental Effects*, vol. 30, no. 7, pp. 649–659, 2008.

[13] C. Tian, B. Li, Z. Liu, Y. Zhang, and H. Lu, "Hydrothermal liquefaction for algal biorefinery: A critical review," *Renewable & Sustainable Energy Reviews*, vol. 38, pp. 933–950, 2014.

[14] Y. Xu, P. Duan, and B. Wang, "Catalytic upgrading of pretreated algal oil with a two-component catalyst mixture in supercritical water," *Algal Research*, vol. 9, pp. 186–193, 2015.

[15] P. Duan and P. E. Savage, "Hydrothermal liquefaction of a microalga with heterogeneous catalysts," *Industrial & Engineering Chemistry Research*, vol. 50, no. 1, pp. 52–61, 2011.

[16] D. Xu and P. E. Savage, "Effect of temperature, water loading, and Ru/C catalyst on water-insoluble and water-soluble biocrude fractions from hydrothermal liquefaction of algae," *Bioresource Technology*, vol. 239, pp. 1–6, 2017.

[17] D. C. Elliott, "Catalytic hydrothermal gasification of biomass," *Biofuels, Bioproducts and Biorefining*, vol. 2, no. 3, pp. 254–265, 2008.

[18] C. Zhang, P. Duan, Y. Xu, B. Wang, F. Wang, and L. Zhang, "Catalytic upgrading of duckweed biocrude in subcritical water," *Bioresource Technology*, vol. 166, pp. 37–44, 2014.

[19] H. Li, Z. Liu, Y. Zhang et al., "Conversion efficiency and oil quality of low-lipid high-protein and high-lipid low-protein microalgae via hydrothermal liquefaction," *Bioresource Technology*, vol. 154, pp. 322–329, 2014.

[20] S. S. Toor, L. Rosendahl, and A. Rudolf, "Hydrothermal liquefaction of biomass: A review of subcritical water technologies," *Energy*, vol. 36, no. 5, pp. 2328–2342, 2011.

[21] D. R. Vardon, B. K. Sharma, G. V. Blazina, K. Rajagopalan, and T. J. Strathmann, "Thermochemical conversion of raw and defatted algal biomass via hydrothermal liquefaction and slow pyrolysis," *Bioresource Technology*, vol. 109, pp. 178–187, 2012.

[22] P. Biller, R. Riley, and A. B. Ross, "Catalytic hydrothermal processing of microalgae: Decomposition and upgrading of lipids," *Bioresource Technology*, vol. 102, no. 7, pp. 4841–4848, 2011.

[23] R. M. Silverstein, F. X. Webster, and D. J. Kiemle, *Spectrometric Identification of Organic Compounds*, Wiley, New York, NY, USA, 7TH edition, 2005.

[24] C. A. Mullen and A. A. Boateng, "Characterization of water insoluble solids isolated from various biomass fast pyrolysis oils," *Journal of Analytical and Applied Pyrolysis*, vol. 90, no. 2, pp. 197–203, 2011.

[25] C. A. Mullen, G. D. Strahan, and A. A. Boateng, "Characterization of various fast-pyrolysis bio-oils by NMR spectroscopy," *Energy & Fuels*, vol. 23, no. 5, pp. 2707–2718, 2009.

[26] R. M. Silverstein, F. X. Webster, and D. J. Kiemle, *Spectrometric Identification of Organic Compounds*, Wiley, New York, NY, USA, 7th edition, 1998.

Hindawi
BioMed Research International
Volume 2018, Article ID 5214369, 10 pages
https://doi.org/10.1155/2018/5214369

*Research Article*

# The Effect of Digested Manure on Biogas Productivity and Microstructure Evolution of Corn Stalks in Anaerobic Cofermentation

**Zongyan Lv,[1] Lei Feng,[1] Lijie Shao,[2] Wei Kou,[2] Peihan Liu,[2] Peng Gao,[1] Xiaoying Dong,[2] Meiling Yu,[2] Jiuzhang Wang,[3] and Dalei Zhang[2]**

[1]*College of Energy & Environment, Shenyang Aerospace University, Shenyang 110136, China*
[2]*Liaoning Institute of Energy Research Co., Ltd, Yingkou 115005, China*
[3]*Liaoning Haosheng Biogas Power Generation Co., Ltd, Shenyang 110400, China*

Correspondence should be addressed to Dalei Zhang; daleizhang@163.com

Received 4 December 2017; Accepted 13 March 2018; Published 23 April 2018

Academic Editor: Chun-Fei Wu



The anaerobic fermentation of crop straw and animal wastes is increasingly used for the biogas and green energy generation, as well as reduction of the environmental pollution. The anaerobic cofermentation of corn stalks inoculated by cow dung was found to achieve higher biogas production and cellulose biodegradation. In this study, the effect of mixing corn stalks with cow dung at five different fermentation stages (0, 7, 15, 23, and 31 days of the total fermentation cycle of 60 days) on the further cofermentation process was explored, in order to optimize the corn straw utilization rate and biogas production capacity. In addition, the straw microstructure evolution was investigated by the SEM and XRD methods to identify the optimal conditions for the straw biodegradation process enhancement. The five test groups exhibited nearly identical total biogas productivity values but strongly differed by daily biogas yields (the maximal biogas generation rate being 524.3 ml/d). Based on the degradation characteristics of total solids (TS), volatile solids (VS), and lignocellulose, groups #1 and #3 (0 and 15 days) had the most significant degradation rates of VS (43.73%) and TS (42.07%), respectively, while the largest degradation rates of cellulose (62.70%) and hemicellulose (50.49%) were observed in group #4 (23 days) and group #1 (0 days), respectively. The SEM analysis revealed strong microstructural changes in corn stalks after fermentation manifested by multiple cracks and striations, while the XRD results proved the decrease in peak intensity of cellulose ⟨002⟩ crystal surface and the reduced crystallinity after cofermentation. The results of this study are assumed to be quite instrumental to the further optimization of the corn stalk anaerobic digestion by inoculation with digested manure for lignocellulose degradation enhancement and biogas productivity improvement.

## 1. Introduction

Large agricultural countries, which produce food and livestock products, have to utilize the by-products, including crop straw and livestock manure. Thus, in China, the annual production of crop straw in 2015 amounted to about 810 million tons, the corn straw share being about 36% or 290 million tons, while the respective livestock manure annual production exceeded 2 billion ton [1]. Crop straw is a multipurpose renewable biological resource, which contains nutrient elements such as C, N, P, K, Ca, Mg, and many organic matters like cellulose, hemicellulose, and protein, but a large part of it is discarded or burned, which not only wastes biomass but also causes a serious environmental pollution. Manure also contains organic matters and nutrient elements, which makes it a good fertilizer, but it is not fully utilized as well. Since inappropriate treatment of crop stalks and livestock manure causes great stress to the environment, their comprehensive and efficient utilization is of great significance for saving bioresources, environmental protection, and agricultural development improvement.

Anaerobic digestion (AD) is one of the renewable energy production technologies, wherein wastes are efficiently treated and the residue (digestate) from the process

can be returned to farmland as a biofertilizer [2]. The anaerobic digestion technology can effectively solve the above problems and convert the renewable straw and livestock waste resources into energy substances, such as biogas and industrial ethanol [3–7]. More and more researchers address the anaerobic fermentation [8, 9], and many countries have already launched biogas projects [10, 11]. However, the anaerobic fermentation of pure waste materials exhibited many disadvantages, including nutritional imbalance, acidification, weak buffering capacity, high ammonia nitrogen content, and long chain fatty acid suppression [12, 13], which affect the stability of biogas-generating systems. Therefore, experts have combined various organic compounds to make anaerobic fermentation [14, 15] and revealed that their codigestion can not only avoid the limitation of single raw material fermentation but also improve the utilization efficiency of biomass resources and ensure the joint treatment of various wastes [10, 16–19]. In particular, Jang et al. [20] studied the mixed anaerobic fermentation of wastewater and activated sludge and reported the best organic removal rate and biogas yield when the wastewater and activated sludge ratio was 3 to 4. Zheng et al. [21] found that the anaerobic fermentation of mixed cow dung and switchgrass outperformed that of pure switchgrass by the buffering ability, anaerobic digestion efficiency, and the methane production (which increased by 39%). Codigestion has become an important development trend of anaerobic fermentation technology.

The crop straw structure is complex and includes lignocellulose (lignin, hemicellulose, and cellulose). In turn, the main components of cellulose and hemicellulose are hexose and pentose, respectively, where degradation occurs during the anaerobic fermentation, in contrast to lignin, as reported by Fernandes et al. [22]. A separate fermentation of straw exhibits easy acidification, long fermentation cycle, low degradation efficiency, yield and utilization of straw, and so on [23]. In contrast to straw, livestock dung has a lower carbon-nitrogen ratio and contains numerous nitrogenous substances, including protein, which are decomposed into ammonia nitrogen and exert a buffer effect on the pH drop caused by volatile fatty acids (VFA) [24]. Therefore, the codigestion of animal waste and straw can solve the above problems, improve their utilization rate, enhance the biogas yield, and shorten the fermentation cycle. In recent years, the codigestion of livestock manure and crop straw has attracted attention of international researchers, and some successful achievements were reported. Thus, Gebert and Groengroeft [25] revealed that the addition of 40% of wheat stalks and 100% of rice straw to cow dung increased the daily biogas production by 10.2% and 88.1%, respectively. Liu et al. studied the codigestive performance effect of varied proportions of pig dung and rice straw and reported the optimal ratio, which made the biogas peak appearance acceleration by 11 to 15 days and the maximum yield improvement by 85~265 mL compared to the separate fermentation.

Although the codigestion of crop straw and livestock manure improves the utilization rate of waste/raw materials, numerous nondegraded organic matters (mostly, straw residue) remain in the biogas slurry. This issue was addressed in this study on anaerobic cofermentation of cow dung and corn stalk. The former was fermented separately, and the resulting fermentation broth obtained at five different stages of the fermentation period was mixed with corn stalk to start the codigestion experiment. The comparative analysis of the respective five test groups, including their biogas production, organic matter degradation rate, and microstructural changes, made it possible to identify the optimal mixing conditions for the biogas yield and organic compound utilization efficiency improvement.

Table 1: Physicochemical properties of materials.

| Physicochemical properties | Corn straw | Cow dung |
|---|---|---|
| Total solids (TS), % | 94.51 | 10.28 |
| Volatile solids (VS), % | 95.21 | 79.01 |
| Cellulose, % | 39.77 | 20.15 |
| Hemicellulose, % | 26.63 | 18.13 |
| Lignin, % | 7.22 | 10.76 |

## 2. Materials and Methods

*2.1. Source and Description of Material.* The corn stalks and fresh cow dung (FCD) used in the test were taken from dairy farm in Yingkou, China. The stalks were treated by natural air drying and ground into fragments of 1–3 cm length. The physicochemical properties of the materials are listed in Table 1.

*2.2. Methods*

*2.2.1. Experimental Setup.* The test equipment consisted of anaerobic fermentation tank, thermostat device, and biogas-gathering device. As an anaerobic reactor, 500 ml serum bottle was used, which was sealed with a rubber stopper, and connected by the hose with a flowmeter to the biogas-gathering device. The constant-temperature water bath was used to maintain the fermentation temperature of $(37 \pm 1)^{\circ}$C.

*2.2.2. Experimental Design.* The experimental study involved a mixed anaerobic fermentation of corn straw and cow dung, wherein fresh or partly digested cow dung was added to corn straw, in order to enhance the joint fermentation process. According to the anaerobic fermentation curve of fresh cow dung (FCD) depicted in Figure 1, five terms were selected to add the straw: 0 days/immediate mixing (test group #1), 7 days (test group #2), 15 days (test #3), 23 days (test group #4), and 31 days (test group #5), respectively. These terms corresponded to respective peaks or kink points in the biogas production rate curve (see blue line in Figure 1), while the total fermentation cycle was 60 days.

The 500 ml serum bottle was used as an anaerobic tank, with the active volume of 400 ml. Cow dung and corn straw were mixed in proportion 3 : 1 at different fermentation stages (this is based on mass; strictly controlled mass of corn stalks is 29.17 g for each bottle), and then the completely digested biogas slurry (TS = 5%) was added for dilution (the total proportion of mixed fermentation broth components being

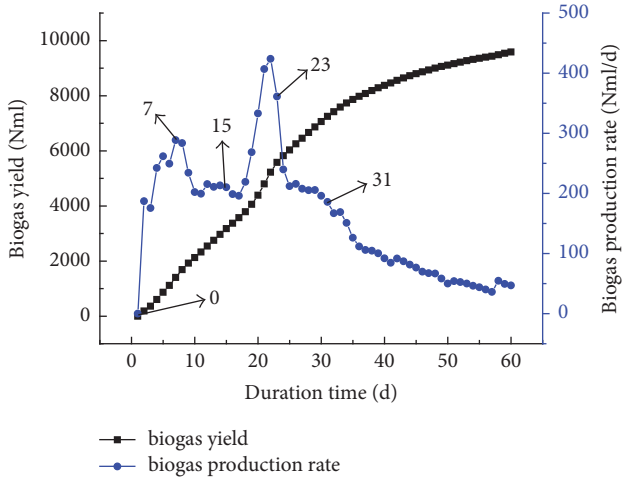


Figure 1: Anaerobic fermentation of fresh cow dung (FCD).

equal to 2/3), with the total mass of reactants being equal to 350 g. Each test was repeated twice.

*2.2.3. Analytical Methods.* The content of total solids (TS) and volatile solids (VS) was determined by the standard APHA methods [26]. Lignin, hemicellulose, and cellulose were determined according to the procedure of Van Soest [27] using a semiautomatic fiber analyzer (ANKOM 200i, Beijing ANKOM Science and Technology Ltd.), with differentiation of neutral detergent fibers (NDF) and acid detergent fibers (ADF). The system of biogas potential testing (AMPTS II bioprocess, Sweden) was used for the determination of biogas yield and production. The X-ray diffraction method was used for the determination of crystallinity (XRD-7000S by Shimadzu Corporation). The ultrahigh resolution field emission scanning electron microscopy (FE-SEM, Nova NanoSEM 450, FEI) was applied to microstructural analysis before and after the fermentation.

## 3. Results and Discussion

*3.1. Biogas Generation Characteristics.* Biogas production rates and accumulated biogas yields for various test groups of mixed corn stalk and cow dung fermentation filtrate are depicted in Figure 2. As is shown in Figure 2(a), the initial gas accumulation in the decreasing order is exhibited by groups #1, #5, #2, #4, and #3. However, for the total fermentation period of 60 days, the maximum gas yield of 6484.6 ml was observed in group #1 and the lowest one (4583.1 ml) in group #3, which corresponded to 29.3%-difference between these groups. The respective values for the remaining three test groups were nearly identical: 5890.8 ml in group #2, 5829.8 ml in group #4, and 5974.2 ml in group #5.

The respective daily biogas production results are depicted in Figure 2(b), where obvious differences in the five groups can be observed. Each of the five groups has two peaks, while the peak values and positions are different. According to the variation curves of the daily biogas production in each group, longer periods of preliminary anaerobic fermentation of FCD resulted in the earlier appearance of the first peak. Thus, test group #4 had the earliest peak corresponding to day 8, while others were arranged as follows: test group #5 (day 9), test group #3 (day 9), test group #2 (day 18), and test group #1 (day 22). The highest value of the first peak, namely, 524.3 ml/d, was observed in test group #4, the remaining ones being equal to 506.5 ml (test group #5), 264.7 ml/d (test group #3), 378 ml/d (test group #2), and 330.3 ml/d (test group #1), respectively.

The anaerobic fermentation cycle is conventionally subdivided into three phases, namely, start-up phase, stable gas production phase, and decline stage. The start-up phase is critical for ensuring a rapid transfer to the stable gas production stage. Its optimization can shorten the fermentation cycle, thus improving the process-cost and labor-efficiency and saving the material resources [28]. Apparently, the start-up time in different groups significantly differs. Test group #1, which corresponds to codigestion of FCD and corn straw, has the longest time of 18 days. The reason is that there are few anaerobic microorganisms in the FCD, which cause the acidification and hinder the fermentation process after FCD is mixed with corn stalks. At this point, it is essential to monitor the pH value of fermentation reactor, to add the buffer or weak alkaline solution after the pH value decline, in order to provide the neutral pH value, which is more suitable for fermentation. In other groups, there exist some microorganisms in the fermentation broth, which came from the anaerobic-digested cow dung and have a self-adjustment ability of abating the acidification. As seen in Figure 2(b), the other test groups have significantly shorter start-up phase, as compared to that of test group #1. The start-up times of test groups #2 and #3 were ten and six days, respectively. Test groups #4 and #5 exhibited the shortest fermentation start-up time of four days, which was 14 days less than that of test group #1 and implied a strong reduction of the anaerobic fermentation cycle. It is expedient to introduce the notion of effective volume loading rate (EVLR) via the formula

$$\text{EVLR} = \frac{\text{Daily biogas production}}{\text{Fermentation reactor volume}}. \quad (1)$$

Since Figure 2(b) shows that the gas production rate was about 30 ml/d, while the fermentation reactor volume was 400 mL, the respective EVLR amounted to approx. 0.075, where value was too low for the industrial implementation. If the fermentation cycle is readjusted based on the EVLR = 0.1, the fermentation cycles for the five test groups will be 53, 42, 45, 37, and 35 days, respectively. This implies the reduction of the 60-day cycle by 7, 18, 15, 23, and 25 days, respectively, where test groups #4 and #5 have the shortest fermentation cycle. For the new fermentation cycle, the total volume of gas production accounted for 95.71, 90.27, 93.44, 93.03, and 92.75% of groups (#1 to #5), as compared to those in the original cycle, so that the biogas production level of 90% was exceeded in all five groups. This preliminary results provide a reference for the further refinement of the appropriate anaerobic fermentation cycle.

*3.2. Organics Degradation.* The degradation rate of organic matter is significant for studying the material transformation

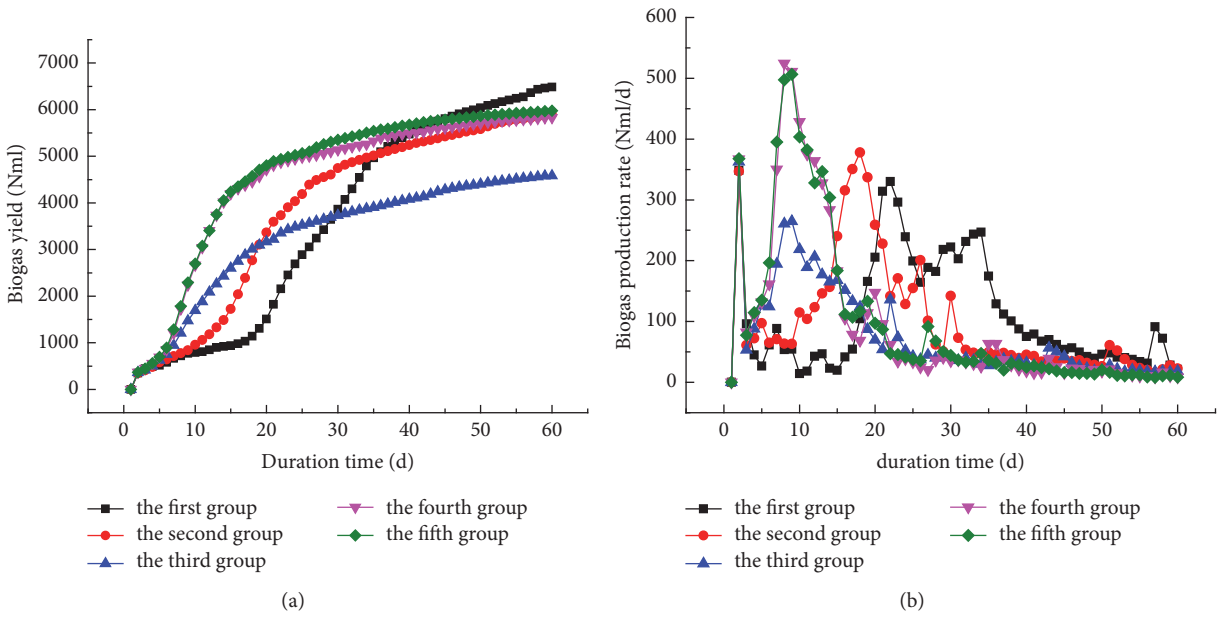


Figure 2: The biogas production of codigestion: accumulative biogas yield (a) and biogas production rate (b).

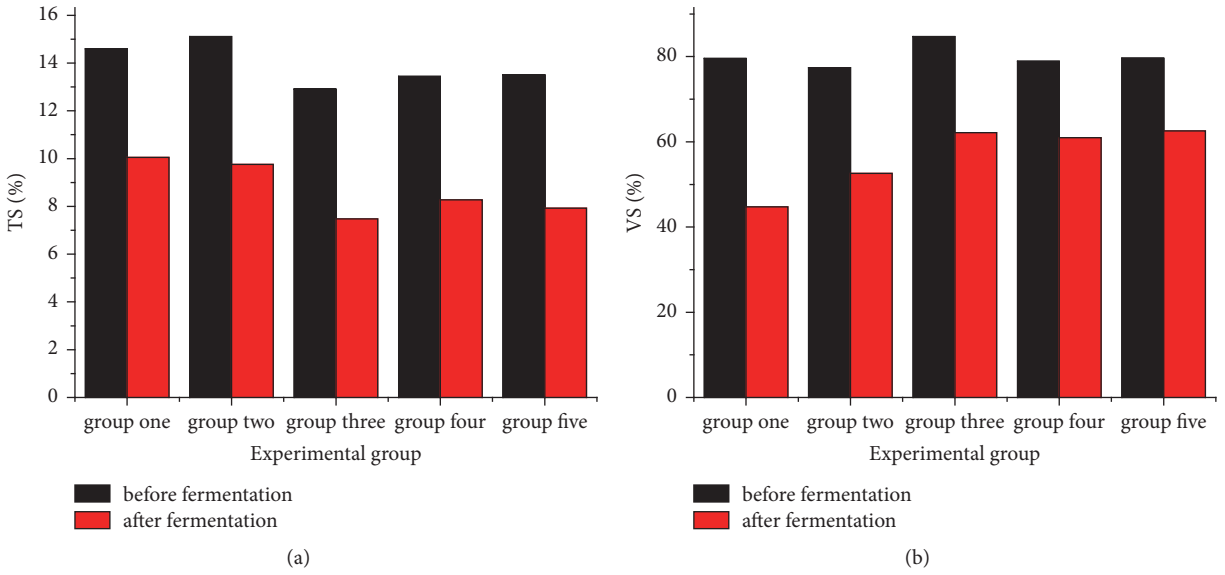


Figure 3: Content variation of TS and VS before and after anaerobic fermentation: (a) TS; (b) VS.

during fermentation, and it can reflect the anaerobic digestion efficiency of fermentation experiments [29]. Figure 3 shows the total solids (TS) and volatile solids (VS) content variation before and after anaerobic fermentation: the above values are nearly identical in all test groups before anaerobic fermentation but exhibit large differences after fermentation, which reflects their different digestion abilities. Figure 3(a) depicts the change of TS before and after fermentation. The TS values before the fermentation were 14.6, 15.11, 12.91, 13.44, and 13.51% for test groups #1 to #5, respectively. Here the TS value of group #2 is the highest, and that of test group #3 is the lowest, while the difference in groups #4 and #5 is quite small. The TS values after fermentation were 10.05, 9.76, 7.48, 8.27, and 7.93%, respectively, whereas test groups #1 and #3 had the highest and lowest values, respectively. According to the TS content variation during fermentation, the degradation of TS in the five test groups was 31.16, 35.41, 42.07, 38.47, and 30.57%, which implies that the degradation increased first and then decreased, test group #3 test (adding corn stalks after 15 days of FCD anaerobic fermentation) has the highest degradation rate of TS, and test group #5 (adding corn stalks after 31 days of anaerobic fermentation of FCD) was the lowest, that is, by 27.34% lower than that of test group #3.

Figure 3(b) depicts the VS variation in test groups before and after fermentation. The VS values of the mixed raw

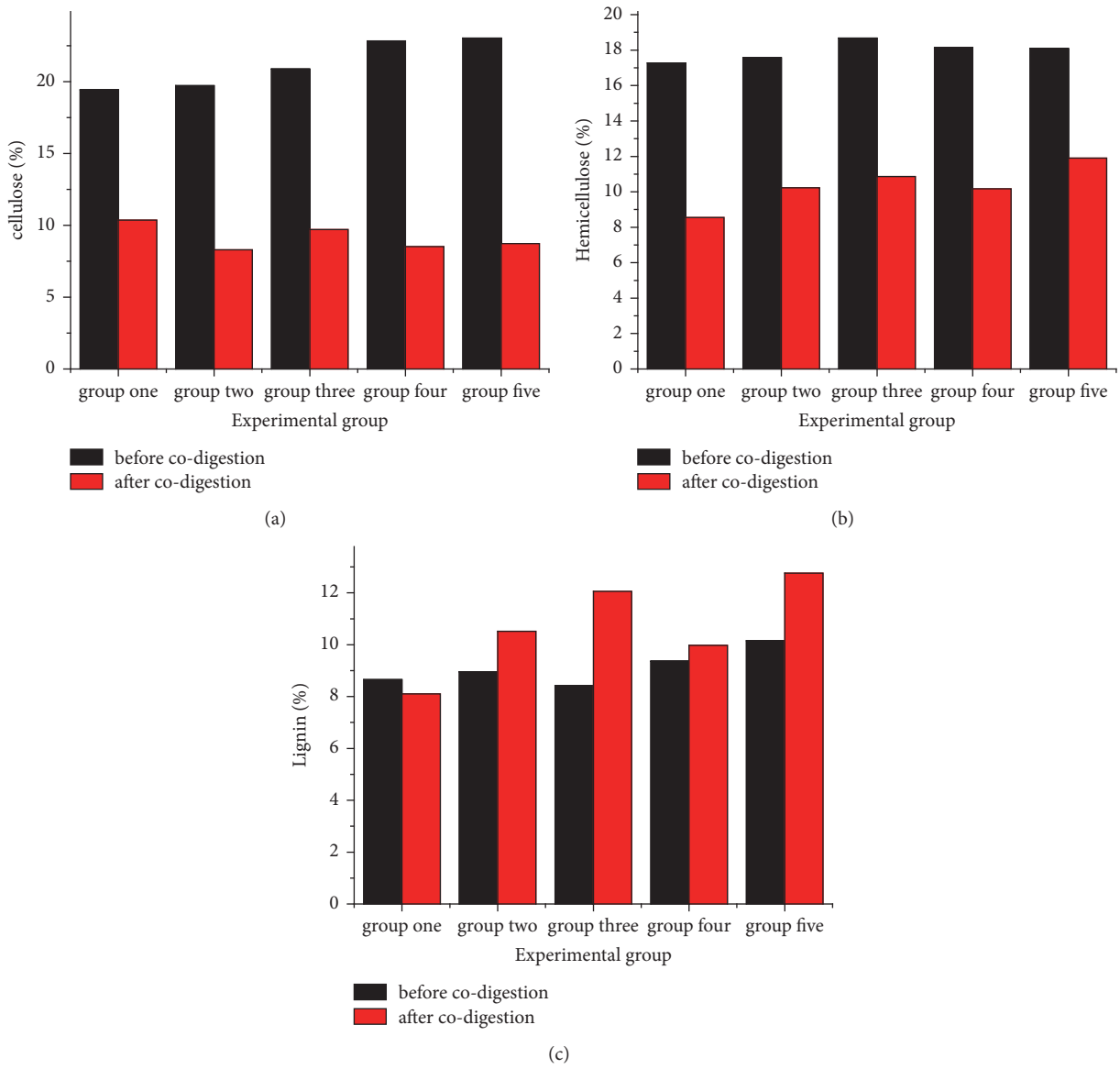


Figure 4: Lignocellulose content variation before and after anaerobic fermentation: (a) cellulose, (b) hemicellulose, and (c) lignin.

materials before fermentation were 79.55, 77.41, 84.7, 78.87, and 79.62%, for the five groups, respectively. The VS content variation of groups is very small, but test group #3 has the highest VS. After fermentation, the VS values in the five groups were 44.76, 52.60, 52.16, 50.96, and 52.58%, respectively. The VS content in test group #1 was the lowest, and nearly identical values were observed in the remaining four groups. According to the VS contents before and after fermentation, the VS removal rates of five groups were 43.73, 32.05, 26.62, 22.71, and 21.4%, respectively. Test group #1 had the highest removal rate, and test group #5 had the lowest one.

Corn straw contains large amounts of lignocellulose, which is composed mainly of cellulose, hemicellulose, and lignin, which are refractory components in straw. Destroying corn straw structure means the disintegration of cell material and the production of humus, while the speed of degradation directly reflects the hydrolysis rate of anaerobic fermentation, which is the most important variation of physical properties in the biological fermentation process.

The contents of lignocellulose before and after anaerobic fermentation are shown in Figure 4. It can be seen from Figure 4(a) that the cellulose content before the fermentation increased gradually with group number: 19.44, 19.73, 20.89, 22.84, and 23.04%, respectively. For the same content of corn straw, the cellulose content variation during cow dung fermentation has affected the total fiber content. Since the same quantities of cow dung broth were added, the longer fermentation time implied the less dry matter. Therefore, the greater the proportion of straw, the higher the cellulose content. After anaerobic fermentation for 60 days, cellulose content in the five groups reduced by different degrees, which were 10.36, 8.30, 9.71, 8.52, and 8.72%, respectively. Thus,

the cellulose content after fermentation was the lowest in test group #2 and the highest in group #1, which implies the cellulose degradation rate of 46.71, 57.93, 53.52, 62.70, and 62.15%, respectively. Since the highest and lowest cellulose degradation rates are observed in groups #4 and #1, respectively, this strongly suggests that cellulose degradation effect of mixed corn straw-cow dung fermentation is the most pronounced when straw is added with 23 days of FCD fermentation, while simultaneous anaerobic fermentation of mixed FCD and corn straw is not beneficial for the cellulose degradation.

Figure 4(b) illustrates the hemicellulose content variation before and after fermentation, where five test groups exhibit similar values before (17.27, 17.56, 18.68, 18.13, and 18.0%) and after anaerobic fermentation (8.55, 10.23, 10.86, 10.17, and 11.90%), respectively. Here test group #1 had the lowest values, and the fifth one had the highest ones. The degradation rates of hemicellulose were 50.49, 41.90, 41.86, 43.91, and 34.22%, respectively, so that the respective parameters of test group #1 (the highest ones) exceeded those of test group #5 (the lowest ones) by 47.55%.

Figure 4(c) depicts the lignin content variation in five groups before and after fermentation. Lignin degradation is extremely hard to achieve in anaerobic fermentation [30, 31]. Lignin content before fermentation was 8.65, 8.95, 8.42, 9.36, and 10.15%, respectively, so that its content in group #5 was the highest. After anaerobic fermentation, the lignin content in five groups was 8.11, 10.52, 12.06, 9.98, and 12.76%, respectively. Once again, the content of lignin in test group #5 was the highest and exceeded that of group #1 (the lowest value) by 57.34%. More detailed analysis of the lignin content variation in five groups before and after the fermentation shows that after fermentation it decreased in test group #1 by 0.54% but increased in the other four groups by 0.57, 3.64, 0.62, and 2.61%, respectively. As compared to the original lignin content before fermentation, the respective variation rates were as follows: −6.21% for group #1; 6.36% for group #2; 43.23% for group #3; 6.62% for group #4; and 25.71% for group #5. Thus, the lignin variation rate in test group #3 was the maximum and its lignin content exhibited the largest increase, while that of test group #1 showed the negative increase.

*3.3. Scanning Electron Microscopy Analysis.* In the process of anaerobic fermentation, the microstructure of corn stalk particles is changed by the action of microorganisms, and damage accumulation and densification of defects can be observed on their surface. The surface morphology of particulate matter reflects the action of particulate matters, microorganisms, and enzymes in the anaerobic fermentation system, eventually, affecting the degradation of organic matters, which constitute corn stalk particles [32, 33].

Figure 5 depicts electron scanning micrographs of the ferment materials, after anaerobic codigestion, where the low-magnification (×1000 or 100 $\mu$m) ones are shown on the left side and the high-magnification ones (×5000 or 20 $\mu$m) on the right side.

Figure 5(a) depicts the electron scanning micrograph of corn stalk after pulverization. The integral structure of the stalk is yet intact and dense, the surface is smooth, and the density is high. Figure 5(b) presents SEM images of corn stalks mixed with fresh cow dung (FCD). The structure is intact, its surface is more coarse compared with pure stalk, and some streaks are observed, but the density is still high. Thus, both stalks have integral structure, which is not prone to the digestion and degradation for microorganisms, which implies low rate and long-term period of anaerobic digestion and stalk degradation.

Figures 5(c)–5(g) are the electron scanning micrographs of corn stalks mixed with cow dung after fermentation. In 100 $\mu$m electron micrographs, the structure of stalks after fermentation, as compared to those before fermentation, is severely damaged and broken up in different degrees, and many ravines appear on their surfaces. In 20 $\mu$m electron micrographs, the surfaces of stalks after fermentation look wrinkled, coarse, and uneven. In Figure 5(d), a crevice appears on the straw surface; in Figure 5(e), the surface is partially lifted and slightly cracked; in Figure 5(f), the surface is sunken in and covered by deep crevices; in Figure 5(g), the surface is full of cracks; in Figure 5(h), the surface exhibits cotton-like irregularity and deep cracks. In general, the degradation degree of stalks fermented by the microorganisms is vividly reflected by the electron micrographs. The rougher the surface, the more obvious the crack and the less the density. After analyzing and comparing the scanning electron micrographs of five test groups, the surfaces of stalks in the first three groups (#1 to #3) are found to have more crevices but possess less damaged structures. In the remaining two groups of electron micrographs (#4 and #5), the surface damage was more intense, the degree of biodegradation was more apparent, and fracture of the stalk integral structure was deeper. The results show that in these two groups (#4 and #5) the degradation of cellulose and hemicellulose was more pronounced than that of the first three groups (#1 to #3).

*3.4. Crystallinity Analysis.* In the anaerobic digestion, because of changes in the degree of interbonding of particles, the change of crystallization degree of cellulosic material, and clean size launch tube, the interior of the particle crystallinity is reduced, while the specific surface area of straws is increased, raising their exposure to microorganisms and their secondary metabolites. Each crystalline substance has a specific crystal structure type, while each unit cell can be represented in terms of its lattice parameters. The X-ray diffraction method is used to determine the crystal structure type of particles, for example, as in the recent study of Zheng et al. [28].

Figure 6(a) presents the XRD diagrams of corn straw and cow dung before and after fermentation. Evident X-ray diffraction peaks are observed at diffraction angles of about 22°, 24°, and 27°. The above three positions correspond to the diffraction intensity peaks of fiber ⟨002⟩ crystal surface ($C_{12}H_{22}O_{11}$), crystalline silica ($SiO_2$), and calcium carbonate ($CaCO_3$), respectively. Silicate substances and calcium carbonate substances are the essential components of straw cell wall strength, while the composition of cellulose and cell wall changes during the fermentation process. The curves in

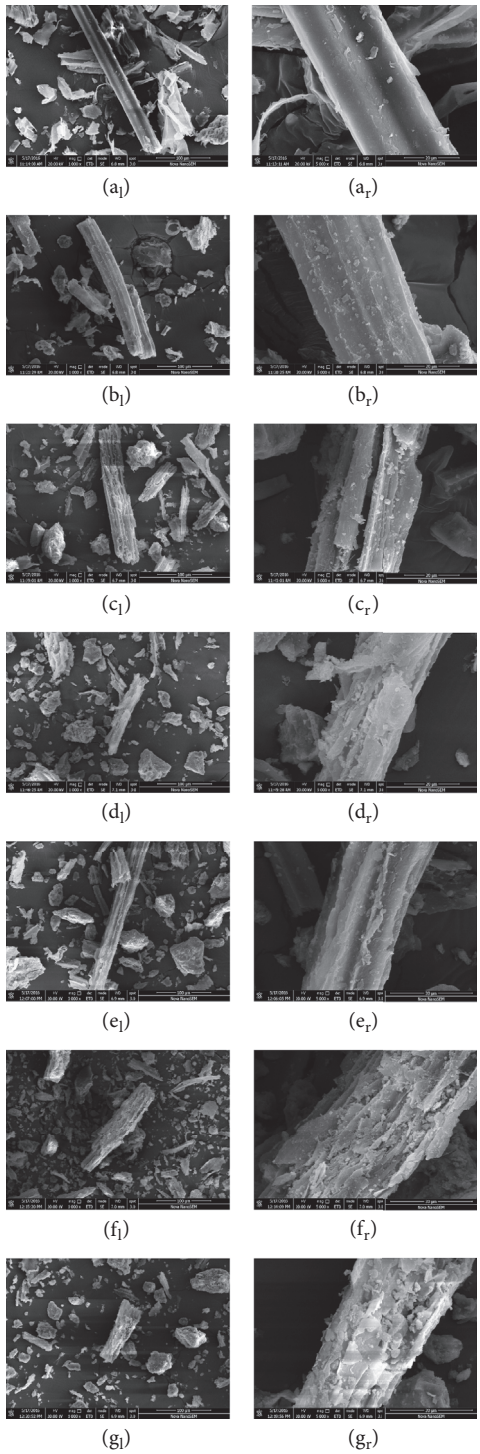


Figure 5: Scanning electron micrographs: magnification of ×1000 (left part) and ×5000 (right part). (a) Pure corn stalk; (b) corn stalk with FCD; (c) test group #1; (d) test group #2; (e) test group #3; (f) test group #4; (g) test group #5.

XRD diagram of corn straw (the upper plot in Figure 6(a)) fluctuate slowly; crests/peaks are not obvious, while burr-type fluctuations are more numerous due to more organic species in corn straw, and there is more interference. The peak appears at about 22°, which corresponds to the diffraction peak of cellulose, while those of silica and calcium carbonate salts are not obvious. In the XRD diagram of cow dung, the crest is obvious, while the burr features are less pronounced, as compared to the corn straw diagram. This may be due to less organic matter and fewer influence factors. The peak

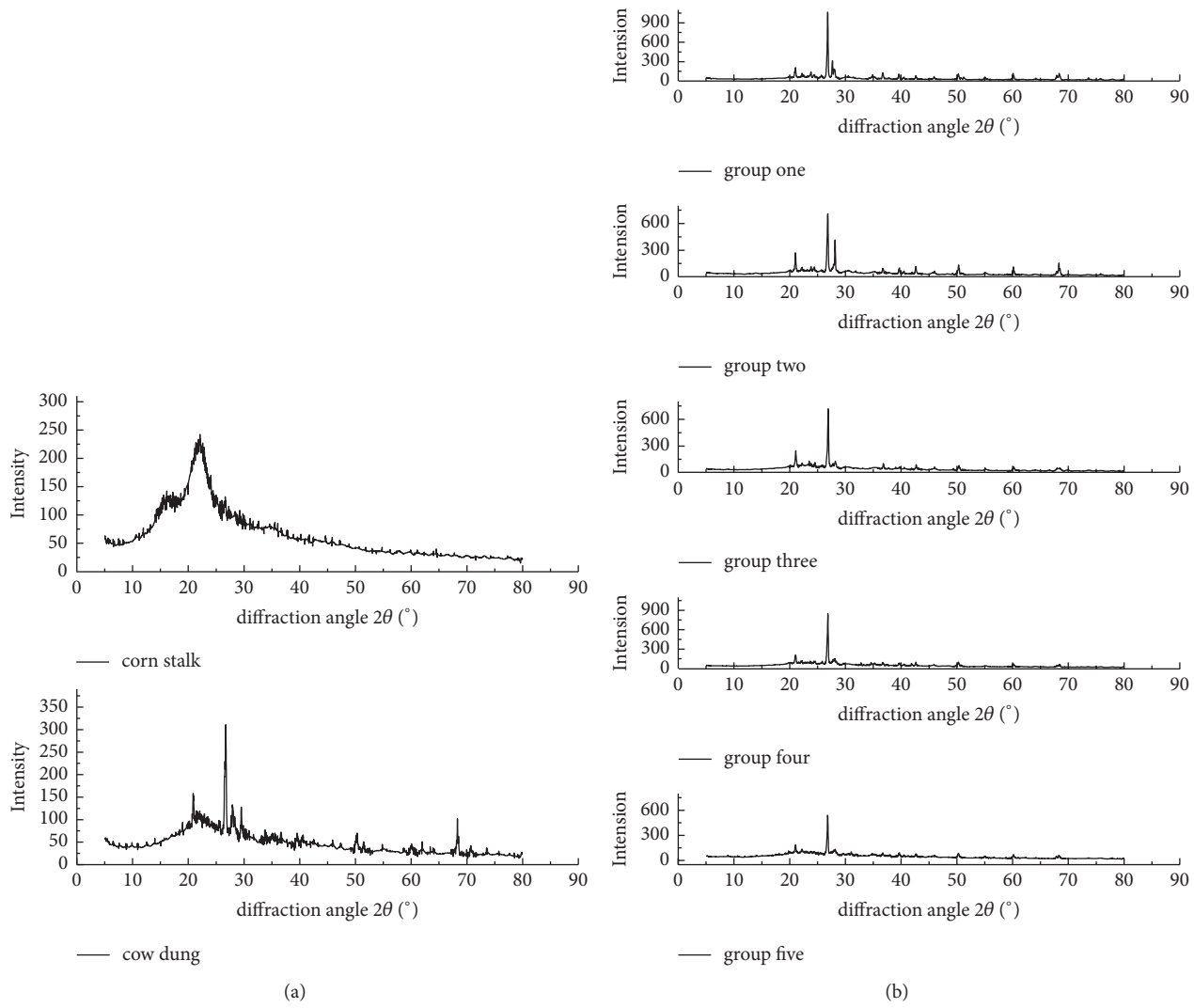


Figure 6: XRD diagram: (a) corn stalk and cow dung and (b) mixed material in five test groups after codigestion.

intensity of cellulose diffraction decreases at 22°; the peaks are obvious, and the highest one corresponds to that of calcium carbonate.

The XRD diagrams of the five test groups are presented in Figure 6(b). The comparative analysis of graphs in Figures 6(a) and 6(b) reveals that, in the latter ones, the burrs are significantly reduced, the wave lines are relatively smooth, and the peaks are more salient, as compared to the former ones. In all five curves of Figure 6(b), the crest is most pronounced near the diffraction angle of 27°, which corresponds to the diffraction peak position of calcium salts. However, cellulose and silica salts diffraction peaks are much less obvious. It means that the intensity of cellulose diffraction peak decreased significantly, as compared to that of raw materials, while the intensity of the calcium carbonate salts was strongly enhanced. This enhancement can be attributed to the fact that the anaerobic fermentation process consumes a lot of organic matter, thus reducing the relative content of the organic material and increasing the relative content of calcium carbonate and silica salts.

The notion of crystallinity is used to express the proportion of crystalline regions in the fiber: the higher the crystallinity, the larger the crystalline area [34]. The crystallinity of raw and cofermented materials can be assessed via the following formula:

$$\mathrm{Cr} = \left( \frac{(I_{002} - I_{am})}{I_{002}} \right) \times 100\%, \quad (2)$$

where Cr is the percentage of relative crystallinity, $I_{002}$ is the maximum intensity of the ⟨002⟩ lattice diffraction angle (the diffraction intensity of the crystalline region), and $I_{am}$ is the scattering intensity of noncrystalline background diffraction with the diffraction angle $2\theta = 18^{\circ}$ [35].

The crystallinity indices of pure corn stalk and FCD were 0.515 and 0.429, respectively, while those of mixed cofermented materials in the five test groups were 0.469, 0.473, 0.357, 0.396, and 0.314, respectively, in which the crystallinity of corn stalk is highest. The crystallinity of the biogas solution after anaerobic fermentation was significantly

lower than that of corn stalks by 8.93, 8.16, 30.68, 23.11, and 39.03% for the five test groups, respectively. It is noteworthy that group #5 exhibited the lowest crystallinity of the biogas solution. This strongly indicates that the codigestion can efficiently reduce the crystallinity of cellulose and destroy the crystallization structure, whose effect is the most pronounced in test group #5.

## 4. Conclusions

This study has demonstrated that the mesophilic (i.e., affected by microorganisms growing in moderate temperature range between 25 and 40°C) codigestion of corn stalk mixed with cow dung can improve the biogas production, enhance the degradation efficiency of organic matter, and reduce the anaerobic fermentation cycle. The highest biogas production rate of 524.3 ml/d was observed on day 8 in test group #4 (the codigestion of cow dung after 23 days of anaerobic digestion with corn stalk). Test groups #4 and #5 exhibited better TS and VS removal rates, destroying effect of straw structure fracture, and crystallinity reduction rates.

## Conflicts of Interest

The authors declare that they have no conflicts of interest.

## Acknowledgments

This work was supported by the National Science and Technology Support Plan of China (no. 2015BAD21B02).

## References

[1] National Bureau of Statistics, *China Statistical Year book*, China Statistics Press, Beijing, China, 2016.

[2] C. Li, S. Strömberg, G. Liu, I. A. Nges, and J. Liu, "Assessment of regional biomass as co-substrate in the anaerobic digestion of chicken manure: Impact of co-digestion with chicken processing waste, seagrass and Miscanthus," *Biochemical Engineering Journal*, vol. 118, pp. 1–10, 2017.

[3] D. Somayaji and S. Khanna, "Biomethanation of rice and wheat straw," *World Journal of Microbiology & Biotechnology*, vol. 10, no. 5, pp. 521–523, 1994.

[4] Z. Zhao, K. Cheng, and J. Zgang, "Advances in pretreatment technology of lignocellulose renewable biomass," *Modern Chemical Industry*, vol. 26, no. 2, pp. 39–42, 2006.

[5] L. Chen, L. Zhao, B. Dong, and et al., "The status and trends of the development of biogas plants for crop straws in China," *Renewable Energy Resources*, vol. 28, no. 3, pp. 145–148, 2010.

[6] Y. Sun, G. Li, F. Zhang, C. Shi, and Z. Sun, "Status quo and developmental strategy of agricultural residues resources in China," *Nongye Gongcheng Xuebao*, vol. 21, no. 8, pp. 169–173, 2005.

[7] L. Zhang, Z. Yang, B. Chen, and G. Chen, "Rural energy in China: Pattern and policy," *Journal of Renewable Energy*, vol. 34, no. 12, pp. 2813–2823, 2009.

[8] V. N. Nkemka and M. Murto, "Biogas production from wheat straw in batch and UASB reactors: The roles of pretreatment and seaweed hydrolysate as a co-substrate," *Bioresource Technology*, vol. 128, pp. 164–172, 2013.

[9] H. B. Møller, S. G. Sommer, and B. K. Ahring, "Methane productivity of manure, straw and solid fractions of manure," *Biomass & Bioenergy*, vol. 26, no. 5, pp. 485–495, 2004.

[10] B. Demirel and P. Scherer, "Bio-methanization of energy crops through mono-digestion for continuous production of renewable biogas," *Journal of Renewable Energy*, vol. 34, no. 12, pp. 2940–2945, 2009.

[11] W. Parawira, J. S. Read, B. Mattiasson, and L. Björnsson, "Energy production from agricultural residues: high methane yields in pilot-scale two-stage anaerobic digestion," *Biomass & Bioenergy*, vol. 32, no. 1, pp. 44–50, 2008.

[12] S. Bayr, M. Ojanperä, P. Kaparaju, and J. Rintala, "Long-term thermophilic mono-digestion of rendering wastes and co-digestion with potato pulp," *Waste Management*, vol. 34, no. 10, pp. 1853–1859, 2014.

[13] G. Silvestre, J. Illa, B. Fernández, and A. Bonmatí, "Thermophilic anaerobic co-digestion of sewage sludge with grease waste: effect of long chain fatty acids in the methane yield and its dewatering properties," *Applied Energy*, vol. 117, pp. 87–94, 2014.

[14] J. Kim and C.-M. Kang, "Increased anaerobic production of methane by co-digestion of sludge with microalgal biomass and food waste leachate," *Bioresource Technology*, vol. 189, pp. 409–412, 2015.

[15] A. Kacprzak, L. Krzystek, K. Paździor, and S. Ledakowicz, "Investigation of kinetics of anaerobic digestion of Canary grass," *Chemical Papers*, vol. 66, no. 6, pp. 550–555, 2012.

[16] H. M. El-Mashad and R. Zhang, "Biogas production from co-digestion of dairy manure and food waste," *Bioresource Technology*, vol. 101, no. 11, pp. 4021–4028, 2010.

[17] W. Mussoline, G. Esposito, P. Lens, G. Garuti, and A. Giordano, "Design considerations for a farm-scale biogas plant based on pilot-scale anaerobic digesters loaded with rice straw and piggery wastewater," *Biomass & Bioenergy*, vol. 46, pp. 469–478, 2012.

[18] J. Ye, D. Li, Y. Sun et al., "Improved biogas production from rice straw by co-digestion with kitchen waste and pig manure," *Waste Management*, vol. 33, no. 12, pp. 2653–2658, 2013.

[19] G. Luo and I. Angelidaki, "Co-digestion of manure and whey for in situ biogas upgrading by the addition of H2: Process performance and microbial insights," *Applied Microbiology and Biotechnology*, vol. 97, no. 3, pp. 1373–1381, 2013.

[20] H. M. Jang, M.-S. Kim, J. H. Ha, and J. M. Park, "Reactor performance and methanogenic archaea species in thermophilic anaerobic co-digestion of waste activated sludge mixed with food wastewater," *Chemical Engineering Journal*, vol. 276, pp. 20–28, 2015.

[21] Z. Zheng, J. Liu, X. Yuan et al., "Effect of dairy manure to switchgrass co-digestion ratio on methane production and the bacterial community in batch anaerobic digestion," *Applied Energy*, vol. 151, pp. 249–257, 2015.

[22] T. V. Fernandes, G. J. Klaasse Bos, G. Zeeman, J. P. M. Sanders, and J. B. van Lier, "Effects of thermo-chemical pre-treatment on anaerobic biodegradability and hydrolysis of lignocellulosic biomass," *Bioresource Technology*, vol. 100, no. 9, pp. 2575–2579, 2009.

[23] G. Qin, R. Liu, and C. Sun, "Effects of different concentrations of NaOH pretreatment on anaerobic digestion of rice straw for biogas production," *Society of Agricultural Engineering*, vol. 227, pp. 59–63, 2011.

[24] R. Li, S. Chen, and X. Li, "Biogas production from anaerobic co-digestion of food waste with dairy manure in a two-phase

digestion system," *Applied Biochemistry and Biotechnology*, vol. 160, no. 2, pp. 643–654, 2010.

[25] J. Gebert and A. Groengroeft, "Passive landfill gas emission - Influence of atmospheric pressure and implications for the operation of methane-oxidising biofilters," *Waste Management*, vol. 26, no. 3, pp. 245–251, 2006.

[26] APHA, *Standard Methods for the Examination of Water and Wastewater*, American Public Health Association, Washington, DC, USA, 2005.

[27] P. J. Van Soest, "Use of detergents in the analysis of fibrous feeds.II.A rapid method for the determination of fiber and lignin," *Journal of the Association of Official Analytical Chemistry*, vol. 46, pp. 829–835, 1963.

[28] M. Zheng, X. Li, L. Li, X. Yang, and Y. He, "Enhancing anaerobic biogasification of corn stover through wet state NaOH pretreatment," *Bioresource Technology*, vol. 100, no. 21, pp. 5140–5145, 2009.

[29] G. Zhen, X. Lu, T. Kobayashi, G. Kumar, and K. Xu, "Anaerobic co-digestion on improving methane production from mixed microalgae (Scenedesmus sp., Chlorella sp.) and food waste: Kinetic modeling and synergistic impact evaluation," *Chemical Engineering Journal*, vol. 299, pp. 332–341, 2016.

[30] A. Hatakka, "Lignin-modifying enzymes from selected white-rot fungi: production and role in lignin degradation," *FEMS Microbiology Reviews*, vol. 13, no. 2-3, pp. 125–135, 1994.

[31] T. W. Jeffries, "Biodegradation of lignin and hemicelluloses," in *Biochemistry of Microbial Degradation*, C. Ratledge, Ed., Kluwer Academic Publishers, Netherlands.

[32] D. S. Himmelsbach, S. Khalili, and D. E. Akin, "The use of FT-IR microspectroscopic mapping to study the effects of enzymatic retting of flax (Linum usitatissimum L) stems," *Journal of the Science of Food and Agriculture*, vol. 82, no. 7, pp. 685–696, 2002.

[33] C. Karlsson, M. Mörgelin, M. Coilin et al., "SufA - A bacterial enzyme that cleaves fibrinogen and blocks fibrin network formation," *Microbiology*, vol. 155, no. 1, pp. 238–248, 2009.

[34] Z. Xiaomei and Y. Sixun, "Research on the silk aging with X-Ray diffraction spectra," *Spectroscopy and Spectral Analysis*, vol. 30, no. 1, pp. 261–265, 2010.

[35] L. Segal, J. Creely, A. Martin, and C. Conrad, "An empirical method for estimating the degree of crystallinity of native cellulose using the x-ray diffractometer," *Textile Research Journal*, vol. 29, no. 10, pp. 786–794, 1959.

Hindawi
BioMed Research International
Volume 2018, Article ID 2158205, 9 pages
https://doi.org/10.1155/2018/2158205

*Research Article*

# Energy Analysis of a Complementary Heating System Combining Solar Energy and Coal for a Rural Residential Building in Northwest China

**Xiaofei Zhen,[1,2,3] Jinping Li,[1,2,3] Yassir Idris Abdalla Osman,[1,2,3] Rong Feng,[4] Xuemin Zhang,[1,2,3] and Jian Kang[1,2,3]**

[1] *Western China Energy & Environment Research Center, Lanzhou University of Technology, Lanzhou 730050, China*
[2] *Key Laboratory of Complementary Energy System of Biomass and Solar Energy, Lanzhou, Gansu Province 730050, China*
[3] *Collaborative Innovation Center of Key Technology for Northwest Low Carbon Urbanization, Lanzhou 730050, China*
[4] *Shaanxi Key Laboratory of Industrial Automation, Shaanxi University of Technology, Hanzhong 723000, China*

Correspondence should be addressed to Jinping Li; 283386515@qq.com

Received 30 November 2017; Accepted 22 January 2018; Published 14 February 2018

Academic Editor: Ningbo Gao



In order to utilize solar energy to meet the heating demands of a rural residential building during the winter in the northwestern region of China, a hybrid heating system combining solar energy and coal was built. Multiple experiments to monitor its performance were conducted during the winter in 2014 and 2015. In this paper, we analyze the efficiency of the energy utilization of the system and describe a prototype model to determine the thermal efficiency of the coal stove in use. Multiple linear regression was adopted to present the dual function of multiple factors on the daily heat-collecting capacity of the solar water heater; the heat-loss coefficient of the storage tank was detected as well. The prototype model shows that the average thermal efficiency of the stove is 38%, which means that the energy input for the building is divided between the coal and solar energy, 39.5% and 60.5% energy, respectively. Additionally, the allocation of the radiation of solar energy projecting into the collecting area of the solar water heater was obtained which showed 49% loss with optics and 23% with the dissipation of heat, with only 28% being utilized effectively.

## 1. Introduction

In rural areas of northern China, the energy consumption for heating buildings has reached $1 \times 10^9$ tce, which occupies a large portion of the 56% of the total energy consumption, of which coal comprises 74% [1]. It is expected that, with the development of the economy in rural areas and the improvement of the living standards of farmers, the energy consumption will increase tremendously in the future, which is detrimental to the sustainable development of a society as a whole. The utilization of the local renewable energy resources that are replacing fossil-fuel energy to meet the heating demands of buildings is becoming an effective method of solving this problem. Therefore, solar energy has long been one of the most abundant alternative resources arousing wide public interest.

*1.1. Literature Review.* It is widely known that there are two major types of solar heating technology, namely, passive and active. Passive solar energy technology is the earliest pattern for heating buildings by the utilization of solar energy, which uses building orientation, glass windows, and other building materials for collecting, storing, and utilizing solar energy to achieve indoor thermal comfort [2, 3]. In 1977, the first passive solar house in China was constructed in Minqin County, Gansu Province. A large number of studies have been performed on the performance improvements of this technology. Barea et al. [4] investigated and calculated the thermal performance of a specific orientation of multiazimuthal windows. They concluded that multiazimuthal windows with an angle of 45° in the side panels reach a multiazimuthal/flat solar gain factor (M/FSGF) daily average value of 1.20, which means 20% more solar gain than the

daily average solar gain of a flat window. In addition, a window with an angle of 90° in the side panels is the best for temperate climates, with daily average solar gains 27% greater than those of flat windows. Tiwari and Sahota [5] presented a review on the energy and economic efficiencies of passive and active solar distillation systems, highlighted by experimental and theoretical detailed work performed in the recent past on passive and active solar technology. Jie et al. [6] studied the indoor temperature of a fenestrated room with PV-Trombe walls. Rempel et al. [7] found that over half of all the energy input into each sunspace originated as diffuse solar radiation. Nguyen and Reiter [8] examined the potential of improving thermal comfort under the climatic conditions of Vietnam resulting from a passive strategy by using a newly developed climate analysis tool. Wang et al. [9] found that a passive solar house equipped with a water thermal storage wall reduced yearly energy consumption by 8.6%. In addition, many recent studies have focused on the phase-change materials integrated in passive solar houses [10–12]. Mazarrón et al. [13] studied the design, installation, and evaluation of a solar water heating system with an evacuated tube collector and active circulation. The results showed that the energy collected can be increased sharply by improving the collector characteristic and reducing the pipes losses. The kang is a primary heating method in rural areas of northwest China. According to the characteristics of a traditional fire-based kang, Jiang et al. [14] presented a theoretical study of a solar-based kang system, the results of which are in accordance with experiment. Bellos et al. [15] suggested an innovative Trombe wall as a passive heating system for a building.

The solar-assisted heat pump is another important active solar heating technology that has attracted much attention. Han et al. [16] proposed a multisource hybrid heat pump system (MSHHPS) with seasonal thermal storage. The composition, operation modes, mathematical model, and transition conditions of the different operating modes of the system were determined. Ma et al. [17] presented an evaluation of the performance of a solar-groundwater heat pump (SGHP) unit associated with radiant floor heating. The results show that the new system has an energy-saving rate of 30.55% compared to a conventional central heating system (CCHS). The floor heating systems can have an energy-saving rate of 18.96% compared to a traditional radiator. Deng and Yu [18] investigated a combined solar/air, dual-source, heat pump water-heater system for domestic water heating applications. The simulation results show the modified direct-expansion solar-assisted heat pump water heaters (M-DX-SHPWHs) system exhibits better performance than that of a conventional direct-expansion solar-assisted heat pump water heaters (DX-SHPWH) system. At a low solar radiation rate of 100 W/m$^2$, the M-DX-SHPWH heating time decreases by 19.8% compared to the DX-SHPWH when the water temperature reaches 55°C. Meanwhile, the COP, on average, increases by 14.1%. Ni et al. [19] projected a phase-change-material- (PCM-) based, solar-assisted air-source heat pump (PCM-SAHP) system consisting of an air-source heat pump (ASHP), a PCM unit, and a solar thermal collector. The experimental findings indicate that in the cooling mode the ambient temperature still has a significant effect on the operating performance of the system. In contrast, it was found that the effect of the chilling water flow rate (throughout the PCM unit) on the system performance is relatively subtle. Fraga et al. [20] addressed the analysis of the potential of a combined solar thermal and heat pump (HP) system on new and existing multifamily buildings in which a numerical simulation as a complement to a monitored study case was proposed. Chen et al. [21] experimentally and theoretically investigated a solar combination system consisting of a solar collector and a $CO_2$ heat pump. The simulated results show that the optimized system can save 14.2% of electricity and improve the solar fraction by 8%, with the solar fraction of the optimized system capable of reaching 71.1%. Kong et al. [22] described a direct-expansion solar-assisted heat pump (DX-SAHP) system that uses R410A as a refrigerant, which can supply domestic hot water over the entire year, and provided a numerical model to estimate the thermal performance of the system.

There have also been many studies related to innovative solar heating systems. Chen et al. [23, 24] designed a nearly net-zero annual energy consumption house in Eastman, Quebec, Canada, utilizing building-integrated thermal mass both in passive and in active forms, and the annual space heating energy consumption of the house was approximately 5% of the national average. A new type of radiant end system with even lower supplying temperature for a solar or solar-assisted space heating system was proposed in Ren et al. [25], and the simulation results showed that the new end system had good prospects for the effective use of local renewable resources. Esen and Yuksel [26] conducted an experimental study to investigate greenhouse heating by biogas, solar, and ground energy in Elazig. Yu et al. [27] proposed a hybrid solar air heating system for building space heating, which included passive and active dual-function solar collectors. Detailed measurements of the auxiliary energy consumption for space heating and domestic hot water preparation in two detached passive houses heated by a solar water heating system and an air-to-water heat pump were reported in [28].

Economic analysis has been performed for solar heating systems as well. Ziemele et al. [29] examined the transition from a conventional district heating (DH) system to a fourth-generation DH (4GDH) system using system dynamics modeling and economic feasibility analysis. The results show how the price of a fossil-fuel influences the share of heat energy production and the balance point between investment at the source and on the heat consumer side. Milani et al. [30] addressed the proposition of the hybridization concept and the simulation of benchmark power plants for a suitable Brazilian site (high direct normal irradiation and low-cost biomass availability). Sonthikun et al. [31] designed and constructed a solar-biomass hybrid for natural rubber sheet drying. The solar-biomass hybrid dryer was tested for drying of 100 natural rubber sheets, and the moisture content of the rubber sheets was reduced from 34.26% to 0.34% (dB) in only 48 h. Mehdaoui et al. [32] presented a parametric study with the help of the TRNSYS program to optimize solar heating

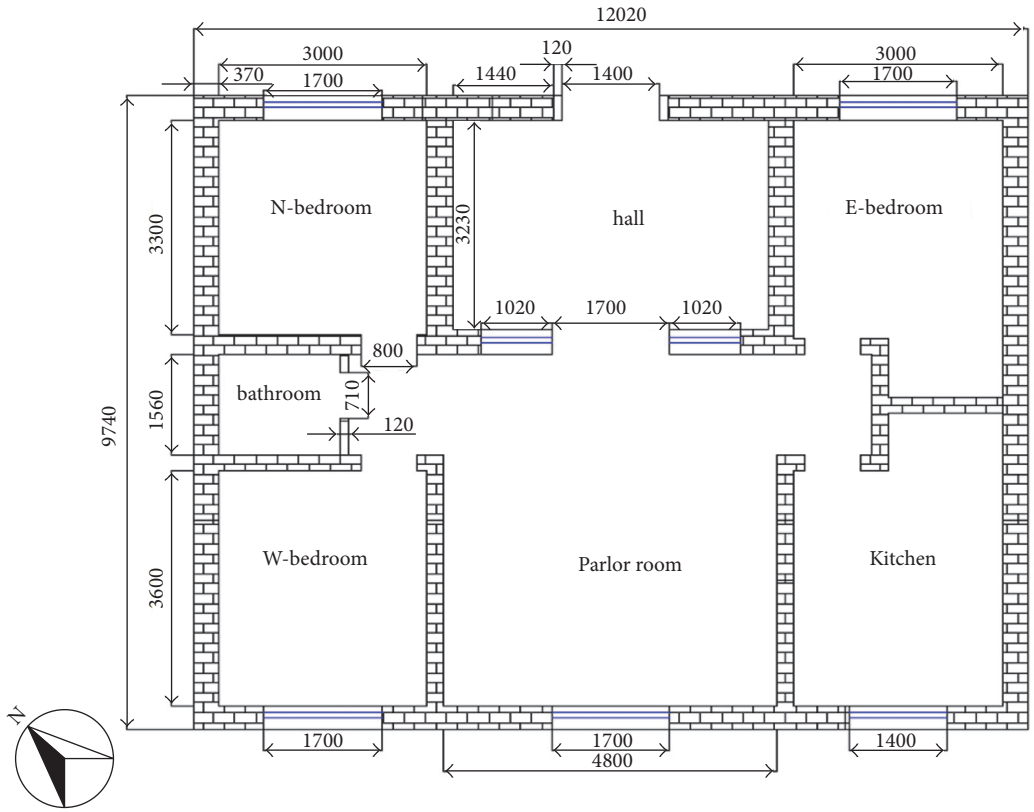


Figure 1: Floor plan of the building (mm).

prototype design parameters, and the program was validated by experiment.

Recently, numerous rural buildings are being built in northwest China; however, the majority of them lack solar heating technology since they are located in areas where coal is still the primary heating resource. Although many renewable systems have appeared, few studies have focused on rural residential buildings in cold regions of northwest China. Those buildings have unique characteristics: scattered distribution and weak energy-conservation performance dominate; however, sufficient space exists for installation of solar energy utilization devices, and it is easy to utilize local biomass energy resources.

## 2. Description of the Rural Household Building and the Complementary Heating System

A complementary heating system combining solar energy and coal for a rural household building has been established in a new socialist countryside called Zhangma, Minqin County, Gansu Province (latitude 38°34′N, longitude 103°3′E). Neither the solar energy utilization device nor the coal stove in the system is highly sophisticated, but they are the easiest to operate and most economical model in practice for the heating of rural household buildings. The experiment on the performance of the system was carried out from December 10, 2014, to March 30, 2015. The aim of the present work was to analyze the efficiency of the energy utilization of the system and to reveal the combined effects of multiple factors on solar energy utilization.

*2.1. Rural Household Energy-Saving Residential Building.* Figure 1 shows the floor plan of the rural household building under study; the building area is approximately 117 $m^2$. The heights of the external walls, the double-glazed windows, and the outer door measurements are 3.3, 1.4, and 3.0 m, respectively. The external wall is constructed of perforated bricks with a thickness of 0.37 m, and the roof is constructed of reinforced concrete with a thickness of 0.15 m. Later, approximately 0.07 m of slag was laid on the roof, as an insulating material. In addition, to decrease the heating loading of the building in winter, extruded polystyrene board (XPS) insulating panels with a thickness of 0.06 m were attached to the outside surface of the external wall, except for the left-side external wall, which is shared with a neighboring structure.

*2.2. Complementary Heating System.* The building's previous heating system was a natural circulation heating system that consisted of a coal stove installed in the kitchen and radiators fixed in other rooms, but not in the hall. Six solar water heaters were added in the new complementary heating system; the existing coal stove and solar water heaters are


(a) Coal-fired stove (b) Solar water heaters

Figure 2: The complementary heating system.

shown in Figure 2. Each solar water heater has a 3.85 $m^2$ collector area (40 all-glass vacuum tubes measuring 0.058 m in diameter and 1.8 m in length) and a 400 L storage tank. The inclination angles of the solar water heaters are all 45°, which is suitable for the optimal inclination angle in local areas. However, the orientation, which is approximately south by west 40°, is not ideal due to the orientation and layout of the building. There are three lines of solar water heaters on the roof of the building, each line consisting of two solar water heaters. After the six solar water heaters were connected in series, they were connected with the coal stove in parallel. A circulation pump was installed in the branch pipe of the series-wound solar water heaters. If the temperature of the water in the storage tank of the solar water heaters is suitable, the circulation pump will deliver the hot water to the radiators to heat the house; the circulation pump will shut down when the temperature of the water is too low to heat the house. The heating system operates like the previous model, with gravity circulation forced by the coal stove.

## 3. Experimental Methods

To analyze the efficiency of the energy utilization of the system, both the input and output energy must be measured or calculated (Using the prototype model, the average thermal efficiency of the furnace is obtained. Based on the measured coal quality, the amount of heat absorbed by the solar energy and released into the room. The energy input to the building is calculated based on the inputs coal and the solar energy.). The intensity of the surface facing south, with an inclined angle of 45° and which receives the maximum solar energy in winter, was measured by a pyranometer. The weight of coal consumed by the stove was also weighed by a platform of the solar radiation on balance every day, and the caloric value of the coal was calculated in the laboratory at Lanzhou University of Technology. The inlet/outlet temperature and the circulation flow rate of the hot water were measured to calculate the energy outputs supplied by the solar water heaters. Moreover, the ambient temperature, the temperature in the five indoor rooms (except the hall), and the temperature of the hot water in one of the storage tanks in the middle line were measured. A solar water heater, used to heat the digester, was employed as a reference that faced south and was not shaded in order to study the influence of the orientation and shade effects on thermal performance. The inlet/outlet temperature, circulation flow rate, and water temperature in the storage tank of the reference solar water heater were also measured. All the measurements were recorded automatically by a data acquisition system (Agilent 349702, Agilent Technologies, USA) every 10 s. The detailed parameters of the measuring instruments used in this study are shown in Table 1.

The energy output supplied by the coal stove was difficult to measure directly, so a prototype model for calculating the thermal performance of the coal stove was set up; it will be described in detail in Section 4.1.

## 4. Results and Discussion

*4.1. Prototype Model for Calculating the Thermal Efficiency of the Coal Stove.* There are several studies that refer to the efficiency of traditional natural circulation coal stoves. Jiang [1] obtained a value of 32% in a field experiment. The results of Yang et al. [33] showed an efficiency of 30–40%. In general, there are two main methods of calculating the thermal efficiency of a coal-fired boiler and stove, namely, the direct balance and indirect balance methods. However, both were unsuitable for this study because the stove was installed in the kitchen. The heat released from the stove's surface cannot be measured directly even though it contributed to space heating. Therefore, a prototype model for calculating the thermal efficiency of the coal-fired stove in this system was proposed.

Chinese National Standard JGJ 132-2001, entitled "Standard for Energy Efficiency Inspection of Heating Residential

Table 1: The detailed parameters of instruments.

| Measured parameters | Measuring instruments | Range | Precision |
|---|---|---|---|
| Temperature | Pt-100 temperature sensor | −50~100°C | ±0.1°C |
| Flow rate for building | LWGY-20 turbine flowmeter | 0.7~7.0 $m^3$/h | ±0.45% |
| Flow rate for digester | LWGY-15 turbine flowmeter | 0.4~4.0 $m^3$/h | ±0.45% |
| Solar radiation | TBQ-2 pyranometer | 0~2000 W/$m^2$ | ±2% |
| Coals weight | Platform balance | - | ±0.2 kg |

Buildings" [34], provided a method of measuring the heat loss of a building, which is expressed by

$$q_{hm} = \frac{Q_{hm}}{A_0} \cdot \frac{t_i - t_e}{t_{ia} - t_{ea}} \cdot \frac{278}{H_r} + \left( \frac{t_i - t_e}{t_{ia} - t_{ea}} - 1 \right) \cdot q_{\mathrm{IH}}, \quad (1)$$

where $q_{hm}$ is the heat loss of a building, in W/$m^2$; $Q_{hm}$ is the total heat entering the building during the experiment, in MJ; $A_0$ is the heating area of the building, 103 $m^2$ (except for the hall); $q_{\mathrm{IH}}$ is the internal heat liberation rate of the building, 3.8 W/$m^2$ [35]; $t_i$ is the designed indoor temperature, 14°C, which is selected according to [36]; $t_e$ is the designed outdoor temperature, −2.6°C [35]; $t_{ia}$ is the average indoor temperature during the experiment, in °C; $t_{ea}$ is the average outdoor temperature during the experiment, in °C; and $H_r$ is the experiment duration, in h (the duration of the experiment, 278, is the conversion factor).

From (1), the calculation for a given building in given region requires all the parameters, which can be calculated by experiment in this study under the condition that the solar water heaters work alone, as follows:

$$Q_{hm,s} = \sum cm \left( T_{\mathrm{in}} - T_{\mathrm{out}} \right) t, \quad (2)$$

where $c$ is the specific heat capacity of water, 4200 J/(kg·°C), $m$ is the circulation flow rate for building heating, in kg/s; $T_{\mathrm{in}}$ is the inlet temperature, in °C; $T_{\mathrm{out}}$ is the outlet temperature, in °C; and $t$ is the time interval of each scan by the Agilent 349702 (the scanning interval is 10 s).

When the coal-fired stove is used for heating only, $Q_{hm}$ marked by $Q_{hm,c}$ can then be calculated using (3), which is transformed from (1). The thermal performance of the coal-fired stove can therefore be obtained:

$$Q_{hm,c} = \left( q_{hm} - \left( \frac{t_i - t_e}{t_{ia} - t_{ea}} - 1 \right) \cdot q_{\mathrm{IH}} \right) \cdot A_0 \cdot \frac{t_{ia} - t_{ea}}{t_i - t_e} \cdot \frac{H_r}{278}. \quad (3)$$

In practice, there are three heating models, namely, (1) using the coal-fired stove as the unique heating source on cloudy days; (2) using the solar water heaters and coal stove together for space heating when it is sunny, but the solar radiation is not sufficient; and (3) using the solar water heaters to supply the total heating energy when the solar energy is sufficient. For model 2, the coal-fired stove is used in the morning and during the time after the solar heating finishes at night. In the daytime, neither the coal stove nor solar water heaters work when the residents leave their home. The solar water heaters begin to provide heat at night according to the practical situation. In order to reduce the impact of the indoor temperature when the sunlight enters the building from the window, five durations are selected from model 2 as shown in Table 2. During the five durations, when the circulating pump starts to work, no sunlight enters the building. Similarly, all seven durations in model 1 are adopted in (3). The detailed durations and results are shown in Table 2. It can be seen in Table 2 that the $q_{hm}$ calculations are within the range 32.3–44.0 W/$m^2$; the corresponding $Q_{hm}$ range for 1 kg of coal is 5.5-MJ/kg. Some factors may lead to errors. First, Chinese National Standard JGJ 132-2001 [34] requires that the duration for an experiment be no less than 168 h; however, the duration in this study cannot satisfy the requirements due to conditionality. Second, it is very difficult to measure the indoor temperature exactly [34]. In addition, the internal heat gain and the ventilation rate were different from the design values. Other possible issues include the passive energy gain and the operating conditions of the coal stove. The stove cannot work at an optimum performance level when the room is empty. Therefore, the average value of each result is selected to be the final result, namely, 38.1 W/$m^2$ for $q_{hm}$ and 6.4 MJ/kg for $Q_{hm}$. Then, the caloric value of the coal is 16.7 MJ/kg, and the average thermal efficiency is 38%, which are close to the above-mentioned results. During the experiment period, the accumulated heat that entered the building was 11619 MJ from solar energy and 7571 MJ from coal, which means that the energy portions are 60.5% and 39.5%, respectively.

*4.2. Heat-Collection Capacity of the Solar Water Heater.* In fact, the heat-collection capacity and the efficiency of the solar water heater are influenced by a series of factors, such as solar radiation, ambient temperature, collecting temperature, and orientation. A relational expression for the determination of the daily heat-collection capacity is provided in Chinese National Standard GB/T 18708-2002, which is

$$Q_s = a_1 H + a_2 \left( T_b - T_a \right) + a_3, \quad (4)$$

where $Q_s$ is the capacity of the daily heat-collection capacity of the storage tank, in MJ; $H$ represents the daily solar radiation on the collecting area of solar water heater, in MJ/$m^2$; $T_b$ relates to the initial water temperature in the storage tank, in °C; $T_a$ is the average ambient temperature, in °C; and $a_1$, $a_2$, and $a_3$ are the coefficients that must be determined by experiment.

The duration for calculating the heat-collection capacity during the daytime is valid when the solar radiation intensity

Table 2: Durations and results for $q_{hm}$ and $Q_{hm}$ for per kg mass of coal.

| $q_{hm}$/W/m$^2$ | | | $Q_{hm}$ for per kg mass of coal/MJ/kg | | |
|---|---|---|---|---|---|
| Duration | $q_{hm}$ | $q_{hm,ave}$ | Duration | $Q_{hm}$/(kg coal) | $Q_{hm,ave}$/(kg coal) |
| 17:00 pm on 12 to 2:30 am on 13 Dec, 2014 | 32.3 | | 9 to 11 Dec, 2014 | 5.2 | |
| 17:30 to 24:00 pm on 2nd Jan, 2015 | 42.1 | | 4 Jan, 2015 | 5.9 | |
| 17:00 to 23:00 pm on 5 Jan, 2015 | 36.1 | 38.1 | 6 Jan, 2015 | 7.2 | |
| 17:00 to 23:00 pm on 5 Jan, 2015 | 44.0 | | 17 Jan, 2015 | 7.5 | 6.4 |
| 19:50 pm on 15 to 1:50 am on 16 Feb, 2015 | 36.1 | | 27 to 28 Jan, 2015 | 7.1 | |
| | | | 31 Jan to 3 Feb, 2015 | 6.5 | |
| | | | 6 Feb, 2015 | 5.5 | |

is higher than 120 W/m$^2$; moreover, the circulation pumps may sometimes work in the duration, given that $T_b$ in this study refers to the average water temperature during the daytime.

As mentioned above, a solar water heater at its best working conditions is employed as a reference, and its thermal behavior will be realized using the same method. For convenience, a single solar water heater used for heating the building was designated SI, and the output energy of each solar water heater is considered to be equal; the reference one was designated SII.

SI and SII are calculated by the following:

$$Q_{\mathrm{SI}} = \frac{\sum_{t_1}^{t_2} cm\left(T_{\mathrm{in}} - T_{\mathrm{out}}\right)t}{6} + cM\left(T_{t_1} - T_{t_2}\right),$$
$$Q_{\mathrm{SII}} = \sum_{t_1}^{t_2} cm'\left(T_{\mathrm{in}} - T_{\mathrm{out}}\right)t + cM\left(T_{t_1} - T_{t_2}\right), \quad (5)$$

where $t_1$ is the time when the solar radiation intensity is greater than 120 W/m$^2$; $t_2$ is the time when the solar radiation intensity is less than 120 W/m$^2$; $T_{t_1}$ is the water temperature in the storage tank at $t_1$; $T_{t_2}$ is the water temperature in the storage tank at $t_2$; $m'$ is the circulation flow rate for the heating digester, in kg/s; and $M$ is the weight of the water in a storage tank, 400 kg.

All the related data were dealt with using multiple linear regression models in Excel. The analytical results are calculated using (6) and (7) below. Figure 3 shows the relationship of heat-collection capacity to the daily solar radiation and the differences in the temperature of the water in and around the storage tank. From these equations and Figure 3, it is obvious that not only is the increasing rate of the heat-collection capacity of SI with daily solar radiation less than that of SII, but its decreasing rate with increasing temperature difference is less as well. Moreover, $R^2$ of SI is less than that of SII, mainly because of the inconsistency of the water temperature in the six storage tanks caused by the shade between them:

$$Q_{\mathrm{SI}} = 2.32H - 0.30\left(t_b - t_a\right) + 5.75, \quad R^2 = 0.633, \quad (6)$$

$$Q_{\mathrm{SII}} = 3.38H - 0.34\left(t_b - t_a\right) + 2.94, \quad R^2 = 0.896. \quad (7)$$

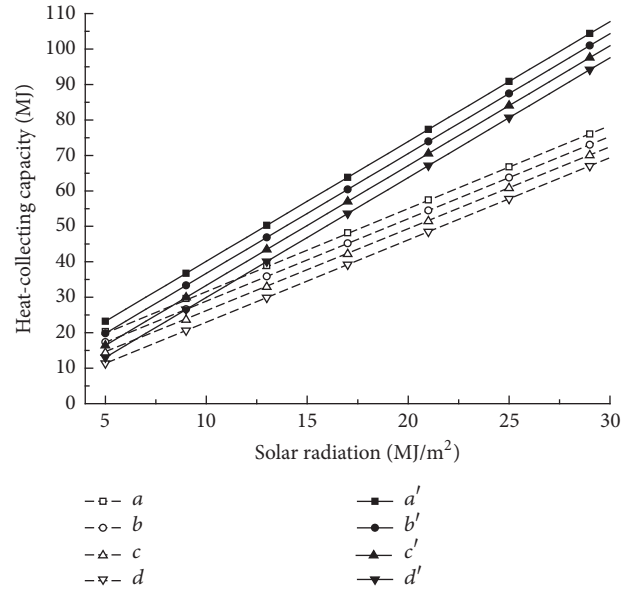


Figure 3: The relationship of heat-collecting capacity between solar radiation and temperature difference. $a$: $t_b - t_{ad} = -10^\circ$C; $b$: $t_b - t_{ad} = 0^\circ$C; $c = t_b - t_{ad} = 10^\circ$C; $d = t_b - t_{ad} = 20^\circ$C; $a$, $b$, $c$, and $d$ were for SI; $a'$, $b'$, $c'$, and $d'$ were for SII.

*4.3. Heat-Loss Coefficient of the Storage Tank.* When solar energy is transformed into thermal energy, a part of it is transported into the building for space heating, but another part is lost to the ambient because the water temperature is always higher than the ambient temperature, so it is important to know the heat-loss coefficient of the storage tank. The Chinese National Standard GB/T 18708-2002 also provides an experimental method for determining the heat-loss coefficient of a storage tank, as follows:

$$U_s = \frac{cM}{\Delta t}\ln\left(\frac{T_i - T_{a,\mathrm{av}}}{T_f - T_{a,\mathrm{av}}}\right), \quad (8)$$

where $U_s$ is the heat-loss coefficient of the storage tank, in W/K; $\Delta t$ is the time interval of experiment, 28800 s; $T_i$ is the initial water temperature, in $^\circ$C; $T_f$ is the final water temperature, in $^\circ$C; and $T_{a,\mathrm{av}}$ is the average ambient temperature, in $^\circ$C.

The following experimental conditions are required by Chinese National Stand GB/T 18708-2002: Static Conditions;

Table 3: The heat loss coefficient of the storage tank.

| Duration | | $U_s$/W/K | $U_{s,av}$/W/K |
|---|---|---|---|
| 2014-12-21 | 0:00–8:00 | 4.17 | 4.10 |
| 2014-12-26 | 0:00–8:00 | 4.70 | |
| 2015-01-30 | 0:00–8:00 | 4.38 | |
| 2015-02-11 | 0:00–8:00 | 3.77 | |
| 2015-02-14 | 0:00–8:00 | 3.59 | |
| 2015-02-15 | 0:00–8:00 | 4.01 | |

that is, the uniform temperature field being kept above 50°C; natural cooling for 8 h and nine uniform temperature points to calculate; and an average wind speed of less than 4 m/s. Six durations in all were in accordance with these conditions, and the results obtained are shown in Table 3.

The calculated values ranged from 3.59 to 4.70 W/K, and the error might have resulted from some unmeasured parameters, such as the wind speed. The average value of 4.10 W/K is therefore taken as the heat-loss coefficient of the storage tank. Otherwise, another Chinese National Standard, GB/T 19141-2011 [37], establishes the rule that the average heat-loss factor ($U_{sl}$) of domestic solar water heating systems must be under 16 W/(m$^3$·K). When transforming the obtained $U_s$ to $U_{sl}$ using (7), the value is 10.25 W/(m$^3$·K), which meets the requirement of the Chinese National Standard GB/T 19141-2011:

$$U_{sl} = \frac{U_s}{V}, \tag{9}$$

where $V$ is the volume of the storage tank, 0.4 m$^3$.

*4.4. Allocation of Solar Energy.* The energy-conservation equation for a single solar water heater can be expressed as follows:

$$Q_{\text{in}} = Q_u + Q_{h,l} + Q_{h,o} + Q_{\text{st}}, \tag{10}$$

where $Q_{\text{in}}$ is the solar energy projected onto the collecting area of a solar water heater, $Q_u$ the heat energy utilized effectively, $Q_{h,l}$ the heat loss, $Q_{h,o}$ the optical loss, and $Q_{\text{st}}$ the energy stored in the water, which can be neglected for the duration of the long-time experiment period. The detailed method of calculating $Q_{\text{in}}$, $Q_u$, and $Q_{h,l}$ is as follows:

$$Q_{\text{in}} = \sum \sum_{t_1}^{t_2} IAt, \tag{11}$$

$$Q_u = \sum cm\Delta \left(T_{\text{in}} - T_{\text{out}}\right), \tag{12}$$

$$Q_{h,l} = \sum U_l \left(T - T_{am}\right) t, \tag{13}$$

where $I$ is the solar radiation intensity, in W/m$^2$, and $T$ is the transient water temperature in the storage tank, in °C. Then, $Q_{h,o}$ can be determined as follows:

$$Q_{h,o} = Q_{\text{in}} - Q_u - Q_{h,l}. \tag{14}$$

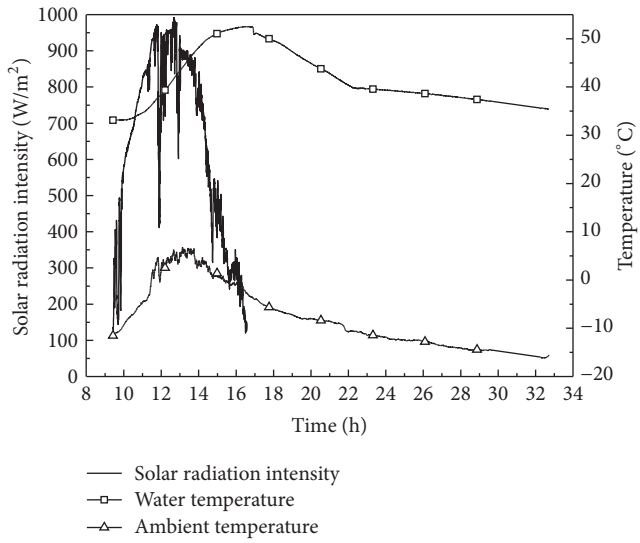


Figure 4: The variations of water temperature, ambient temperature, and solar radiation intensity of a typical duration.

Using the above equations, the allocation of the solar energy projected onto the collector area of a solar water heater for heating the building during the experiment period was obtained. Figure 4 shows the variation of the temperature of the water in the storage tank, the ambient temperature, and the intensity of the solar radiation for a typical duration, which started at $t_1$ on December 14, 2015 and finished at $t_1$ on December 15, 2015. The duration of the sunshine on December 14 was 7.2 h, and the total solar energy radiation projected onto the collector area of a solar water heater was 63.1 MJ. The water temperature in the storage tank was 33.1°C at the beginning and reached its peak point of 52.5°C at 16:45, when the circulation pump started to work. Later, the temperature decreased sharply because of the heat energy not only being transferred into the building, but also being released into the environment. At 22:15 the rate of change decreased gradually, when the circulation pump was shut down and the water temperature was 40°C. Based on (4), (10), and (11), the results were 32.6, 12.5, and 17.9 MJ, respectively, for the aforementioned duration.

The total radiation of solar energy projected onto a solar water heater was 7046 MJ, of which 49% is lost to optics and 23% to heat dissipation, with only 28% being utilized efficiently. When compared to the reference solar water heater, the portion of optical loss was only 33% in the same period, which shows that orientation and shade have the largest influence on the heat-collection capacity of a solar water heater.

In our view, there are two main factors that cause the high heat loss. The first is the location of the storage tank. Although the heat-loss coefficient is lower than that required by the Chinese National Standard, the storage tank always loses heat to the environment because the water temperature is higher than the ambient temperature. The second factor causing the high heat loss is the mismatch between the working temperature of the radiator and the collecting temperature of

the solar water heater. Therefore, when the water temperature is too low to heat the building, the circulation pump will be shut down, and the heat energy cannot then be utilized, but only released to the environment.

## 5. Conclusions and Future Study Recommendations

The energy utilization efficiency of a complementary heating system using solar energy and coal for a rural household building in northwest China was analyzed. The prototype model shows that the average thermal efficiency of the stove is 38%, which means that the portion of energy that enters into the building from solar energy and coal is 60.5% and 39.5%, respectively. A relational expression for the daily heat-collection capacity of the solar water heaters and the heat-loss coefficient of the storage tank was obtained. When compared to the reference solar water heater, it was found that the orientation of the solar water heaters and the shade between them have the largest influence on heat-collecting capacity. Regarding the solar energy projected onto the collecting area of the solar water heater, 49% was lost to optics and 23% to heat dissipation, with only 28% being used effectively. The mismatch between the working temperature of the radiator and the collecting temperature of the solar water heater and the location of storage tanks are considered to be the main factors that led to the high heat loss.

Several items must be considered for a solar heating system applied to rural household buildings in the future. It can be seen from the above analysis that the portion of SI is 16% higher than that of SII, which is caused by the orientation of the solar water heaters and the shade between them. Despite the influence from each of not being distinguished clearly in this research, it is highly recommended to consider a reasonable design of the building originally, especially regarding the layout of solar collectors, as well as for employing the passive technique. On the other hand, the radiant floor heating technology seems to be common feature of new era. Such advanced techniques can decrease the collecting temperature of the solar collectors and improve the collecting efficiency. The work of this paper is of great significance for the next study of the influence of multifactor coupling on the heat-collecting performance of solar collectors. Continuous and stable use of solar energy to meet the user's multilevel energy demand, not only for the improvement of people's livelihood in northwest China and the protection of the ecological environment of great value but also of international renewable energy, has important academic value and significance.

## Conflicts of Interest

The authors declare that they have no conflicts of interest.

## Acknowledgments

This work was funded by the National High Technology Research and Development Program of China (863 Program) (2014AA052801), the National Natural Science Foundation of China (51676094), Major S&T Special Projects of Gansu Province (1502NKDA007), International S&T Cooperation Projects of Gansu Province (1604WKCA009), Natural Science Foundation of China (no. 51706128), Scientific Research Program Funded by Shaanxi Provincial Education Department (Program no. 17JS018), the Natural Science Foundation of Gansu Province (1508RJYA097), the National Natural Science Foundation of China (51166008), and Gansu Construction Science and Technology Project (JK2014-48).

## References

[1] Y. Jiang, in *Annual Report on China Building Energy Efficiency*, p. 56, China Building Industry Press, Beijing, China, 2012.

[2] M. Crosbie, in *The Passive Solar Design and Construction Handbook*, pp. 16–18, Steven Winter Associates, 1997.

[3] E. Mazria, in *Passive Solar Energy Book*, pp. 8–10, Rodale Press, 1979.

[4] G. Barea, C. Ganem, and A. Esteves, "The multi-azimuthal window as a passive solar system: a study of heat gain for the rational use of energy," *Energy and Buildings*, vol. 144, pp. 251–261, 2017.

[5] G. N. Tiwari and L. Sahota, "Review on the energy and economic efficiencies of passive and active solar distillation systems," *Desalination*, vol. 401, pp. 151–179, 2017.

[6] J. Jie, Y. Hua, P. Gang, and L. Jianping, "Study of PV-Trombe wall installed in a fenestrated room with heat storage," *Applied Thermal Engineering*, vol. 27, no. 8-9, pp. 1507–1515, 2007.

[7] A. R. Rempel, A. W. Rempel, K. V. Cashman, K. N. Gates, C. J. Page, and B. Shaw, "Interpretation of passive solar field data with EnergyPlus models: un-conventional wisdom from four sunspaces in Eugene, Oregon," *Building and Environment*, vol. 60, pp. 158–172, 2013.

[8] A.-T. Nguyen and S. Reiter, "A climate analysis tool for passive heating and cooling strategies in hot humid climate based on Typical Meteorological Year data sets," *Energy and Buildings*, vol. 68, Part C, pp. 756–763, 2014.

[9] W. Wang, Z. Tian, and Y. Ding, "Investigation on the influencing factors of energy consumption and thermal comfort for a passive solar house with water thermal storage wall," *Energy and Buildings*, vol. 64, pp. 218–223, 2013.

[10] N. Soares, J. J. Costa, A. R. Gaspar, and P. Santos, "Review of passive PCM latent heat thermal energy storage systems towards buildings' energy efficiency," *Energy and Buildings*, vol. 59, pp. 82–103, 2013.

[11] D. Zhou, C. Y. Zhao, and Y. Tian, "Review on thermal energy storage with phase change materials (PCMs) in building applications," *Applied Energy*, vol. 92, pp. 593–605, 2012.

[12] M. Safari and F. Torabi, "Improvement of thermal performance of a solar chimney based on a passive solar heating system with phase-change materials," *Energy Equipment and Systems*, vol. 2, no. 2, pp. 141–154, 2014.

[13] F. R. Mazarrón, C. J. Porras-Prieto, J. L. García, and R. M. Benavente, "Feasibility of active solar water heating systems with evacuated tube collector at different operational water temperatures," *Energy Conversion and Management*, vol. 113, pp. 16–26, 2016.

[14] Q. Jiang, W. He, J. Ji, and W. Wei, "Study on thermal storage performance of solar KANG and thermal comfort for sleeping

environments," *Journal of University of Science and Technology of China*, vol. 42, no. 4, pp. 335–344, 2012.

[15] E. Bellos, C. Tzivanidis, E. Zisopoulou, G. Mitsopoulos, and K. A. Antonopoulos, "An innovative Trombe wall as a passive heating system for a building in Athens—A comparison with the conventional Trombe wall and the insulated wall," *Energy and Buildings*, vol. 133, pp. 754–769, 2016.

[16] Z. Han, L. Qu, X. Ma, X. Song, and C. Ma, "Simulation of a multi-source hybrid heat pump system with seasonal thermal storage in cold regions," *Applied Thermal Engineering*, vol. 116, pp. 292–302, 2017.

[17] H. Ma, C. Li, W. Lu, Z. Zhang, S. Yu, and N. Du, "Investigation on a solar-groundwater heat pump unit associated with radiant floor heating," *Renewable & Sustainable Energy Reviews*, vol. 75, pp. 972–977, 2017.

[18] W. Deng and J. Yu, "Simulation analysis on dynamic performance of a combined solar/air dual source heat pump water heater," *Energy Conversion and Management*, vol. 120, pp. 378–387, 2016.

[19] L. Ni, D. Qv, Y. Yao, F. Niu, and W. Hu, "An experimental study on performance enhancement of a PCM based solar-assisted air source heat pump system under cooling modes," *Applied Thermal Engineering*, vol. 100, pp. 434–452, 2016.

[20] C. Fraga, P. Hollmuller, F. Mermoud, and B. Lachal, "Solar assisted heat pump system for multifamily buildings: Towards a seasonal performance factor of 5? Numerical sensitivity analysis based on a monitored case study," *Solar Energy*, vol. 146, pp. 543–564, 2017.

[21] J. F. Chen, Y. J. Dai, and R. Z. Wang, "Experimental and theoretical study on a solar assisted CO2 heat pump for space heating," *Journal of Renewable Energy*, vol. 89, pp. 295–304, 2016.

[22] X. Q. Kong, Y. Li, L. Lin, and Y. G. Yang, "Modeling evaluation of a direct-expansion solar-assisted heat pump water heater using R410A," *International Journal of Refrigeration*, vol. 76, pp. 136–146, 2017.

[23] Y. Chen, A. K. Athienitis, and K. Galal, "Modeling, design and thermal performance of a BIPV/T system thermally coupled with a ventilated concrete slab in a low energy solar house: Part 1, BIPV/T system and house energy concept," *Solar Energy*, vol. 84, no. 11, pp. 1892–1907, 2010.

[24] Y. Chen, K. Galal, and A. K. Athienitis, "Modeling, design and thermal performance of a BIPV/T system thermally coupled with a ventilated concrete slab in a low energy solar house: Part 2, ventilated concrete slab," *Solar Energy*, vol. 84, no. 11, pp. 1908–1919, 2010.

[25] J. Ren, L. Zhu, Y. Wang, C. Wang, and W. Xiong, "Very low temperature radiant heating/cooling indoor end system for efficient use of renewable energies," *Solar Energy*, vol. 84, no. 6, pp. 1072–1083, 2010.

[26] M. Esen and T. Yuksel, "Experimental evaluation of using various renewable energy sources for heating a greenhouse," *Energy and Buildings*, vol. 65, pp. 340–351, 2013.

[27] Z. Yu, J. Ji, W. Sun et al., "Experiment and prediction of hybrid solar air heating system applied on a solar demonstration building," *Energy and Buildings*, vol. 78, pp. 59–65, 2014.

[28] J. Rekstad, M. Meir, E. Murtnes, and A. Dursun, "A comparison of the energy consumption in two passive houses, one with a solar heating system and one with an air–water heat pump," *Energy and Buildings*, vol. 96, pp. 149–161, 2015.

[29] J. Ziemele, A. Gravelsins, A. Blumberga, and D. Blumberga, "Combining energy efficiency at source and at consumer to reach 4th generation district heating: economic and system dynamics analysis," *Energy*, vol. 69, pp. 1–12, 2017.

[30] R. Milani, A. Szklo, and B. S. Hoffmann, "Hybridization of concentrated solar power with biomass gasification in Brazil's semiarid region," *Energy Conversion and Management*, vol. 143, pp. 522–537, 2017.

[31] S. Sonthikun, P. Chairat, K. Fardsin, P. Kirirat, A. Kumar, and P. Tekasakul, "Computational fluid dynamic analysis of innovative design of solar-biomass hybrid dryer: An experimental validation," *Journal of Renewable Energy*, vol. 92, pp. 185–191, 2016.

[32] F. Mehdaoui, M. Hazami, N. Naili, and A. Farhat, "Energetic performances of an optimized passive Solar Heating Prototype used for Tunisian buildings air-heating application," *Energy Conversion and Management*, vol. 87, pp. 285–296, 2014.

[33] T. Yang, N. Zhu, et al. "Investigation and analysis on the building energy consumption of small towns in Northern China", National HVAC annual conference proceedings, 2006.

[34] JGJ 132-2001, "Standard for energy efficiency inspection of heating residential buildings" (Chinese).

[35] JGJ 26-2010, "Design standard for energy efficiency of residential buildings in severe cold and cold zones" (Chinese).

[36] GB/T 50824-2013, "Design standard for energy efficiency of rural residential buildings" (Chinese).

[37] GB/T 19141-2011, "Specification of domestic solar water heating systems" (Chinese).